(2)

STRAIN RATE AND STRESS RELAXATION EFFECTS ON PRESSUREMETER TESTING IN CLAYS

FINAL REPORT TO AFOSR PROJECT #F49620-89-C-0090

Prepared by

A. Skandarajah
D. Penumadu
J. L. Chameau

Purdue University
School of Civil Engineering
West Lafayette, IN 47907

UNCLASSIFIED
SECURITY CLASSIFICATION OF THIS PAGE

REPORT DOCUMENTATION PAGE

Form Approved OMB No. 0704-0188

1a. REPORT SECURITY CLASSIFICATION: Unclassified

1b. RESTRICTIVE MARKINGS:

2a. SECURITY CLASSIFICATION AUTHORITY:

2b. DECLASSIFICATION / DOWNGRADING SCHEDULE:

3. DISTRIBUTION / AVAILABILITY OF REPORT: Approved for Public Release; Distribution Unlimited

4. PERFORMING ORGANIZATION REPORT NUMBER(S):

5. MONITORING ORGANIZATION REPORT NUMBER(S):

6a. NAME OF PERFORMING ORGANIZATION: School of Civil Engineering, Purdue University

6b. OFFICE SYMBOL (If applicable):

7a. NAME OF MONITORING ORGANIZATION: AFOSR/NA Bolling AFB DC 20332-6448

6c. ADDRESS (City, State, and ZIP Code): W. Lafayette, IN 47907

7b. ADDRESS (City, State, and ZIP Code): AFOSR/NA Bolling AFB DC 20332-6448

8a. NAME OF FUNDING / SPONSORING ORGANIZATION: Air Force Office of Scientific Research

8b. OFFICE SYMBOL (If applicable): AFOSR/NA

9. PROCUREMENT INSTRUMENT IDENTIFICATION NUMBER: F49620-89-C-0090

8c. ADDRESS (City, State, and ZIP Code): Bolling AFB DC 20332-6448

10. SOURCE OF FUNDING NUMBERS

PROGRAM ELEMENT NO.	PROJECT NO.	TASK NO.	WORK UNIT ACCESSION NO.
61102F	2302	CS	

11. TITLE (Include Security Classification): Final Technical Report (Unclassified) "Strain Rate and Stress Relaxation Effects on Pressuremeter Testing in Clays"

12. PERSONAL AUTHOR(S): A. Skandarajah, D. Penumadu, J. L. Chameau

13a. TYPE OF REPORT	13b. TIME COVERED	14. DATE OF REPORT (Year, Month, Day)	15. PAGE COUNT
Final	FROM 8/1/89 TO 12/31/91	March, 1992	265

16. SUPPLEMENTARY NOTATION: Bound attachement volume relevant to this report.

17. COSATI CODES		
FIELD	GROUP	SUB-GROUP

18. SUBJECT TERMS (Continue on reverse if necessary and identify by block number): Strain Rate and Stress Relaxation Effects on Pressuremeter Testing in Clays

19. ABSTRACT (Continue on reverse if necessary and identify by block number)

This research was undertaken to answer issues related to cavity expansion and in-situ testing using the pressuremeter. Emphasis of the research was placed upon validating the fundamental concepts underlying the cylindrical cavity expansion theory.

Test were performed in a cuboidal shear device (CSD) at strain rates of 0.01%, 0.05%, 0.10%, 0.50%, 1.00% and 5.00% per minute on artificially sedimented specimens of kaolin clay and a kaolin-ground silica mixture with a plasticity index in the range similar to most clays. It was found from the experiments that the normalized shear strength (with respect to 0.01%/min) increases linearly with the logarithm of strain rate. The increase in undrained shear strength in the pressuremeter stress path is about 14.3% per log cycle for kaolin clay and 15.3% for the kaolin-silica mixture. The undrained shear strength in the conventional triaxial test was found to increase about 8 to 10% for a tenfold increase

(cont'd. overleaf)

20. DISTRIBUTION / AVAILABILITY OF ABSTRACT: ☐ UNCLASSIFIED/UNLIMITED ☒ SAME AS RPT. ☐ DTIC USERS

21. ABSTRACT SECURITY CLASSIFICATION: Unclassified

22a. NAME OF RESPONSIBLE INDIVIDUAL: MARTIN LEWIS, MAJ, USAF

22b. TELEPHONE (Include Area Code): (202) 767-6963

22c. OFFICE SYMBOL: NA

DD Form 1473, JUN 86 Previous editions are obsolete.

SECURITY CLASSIFICATION OF THIS PAGE

UNCLASSIFIED

in strain rate. Therefore, it can be concluded that the undrained shear strength increases about 40-50% more in pressuremeter stress path tests than in the triaxial stress path tests.

A new state variable, ψ, indicative of the fabric of clays is introduced. Based on these concepts and a general failure criterion, a simple model to predict failure parameters of anisotropic clays for many commonly encountered stress paths was developed. The model capability to interpret in situ strength measured under a given stress path and transfer it to another stress path was illustrated. Finally, the ability to obtain failure parameters for any stress path using data from a single CIUC test was demonstrated.

The model developed based on cavity expansion theory is able to incorporate the influence of decreasing strain rate within the surrounding soil mass. The findings from the strain rate test for the pressuremeter were used in the model to estimate the difference in the interpretation of the undrained shear strength. Even though the actual undrained shear strength increases with the strain rate, the interpreted undrained shear strength from the pressuremeter expansion curve shows a higher strain softening behavior for the higher value obtained for the pressuremeter stress path. From the parametric studies, it was determined that the level of upper yield does not have any significant influence on the predicted strength.

From the pressuremeter test (PMT) simulated in the CSD it was found that for kaolin clay, irrespective of the initial strain level or strain rate, the relaxation time was about 200 to 250 minutes for undrained and drained conditions. Theoretical models have been included to show how to obtain creep/relaxation parameters from PMT creep/relaxation tests conducted in a borehole. Several correlations are also identified in order to obtain relaxation parameters from creep parameters and empirically from the plasticity index. These creep/relaxation parameters are required to predict the time dependent behavior of soil.

Model pressuremeter expansion in the calibration chamber (CC) is numerically simulated using the Finite Element Method (FEM). The elasticity based FEM model was developed using a commercially available program ANSYS. The elasticity based analysis was helpful to further investigate the boundary effects in chamber testing.

The test data from the CSD and CC have been used to train a three layer feed forward neural network using a back propagation algorithm. The potential for use of artificial neural networks for incorporating strain rate effects in pressuremeter testing and for similar applications in the area of computational mechanics has been evaluated.

TABLE OF CONTENTS

LIST OF TABLES

LIST OF FIGURES

Figure Page

Figure Page

Figure Page

Figure Page

APPENDIX

Figure Page

Figure Page

Figure Page

ABSTRACT

The research was undertaken to answer issues related to cavity expansion and in situ testing using the pressuremeter. Emphasis of the research was placed upon the fundamental concepts underlying the cylindrical cavity expansion theory.

Tests were performed in a cuboidal shear device (CSD) at strain rates of 0.01%, 0.05%, 0.10%, 0.50%, 1.00% and 5.00% per minute on artificially sedimented kaolin clay and kaolin-silica mixture whose plasticity indices range similar to the most of the clays. It was found from the experiments that the normalized shear strength (with respect to 0.01%/min) increases linearly with the logarithm of strain rate. The increase in undrained shear strength in the pressuremeter stress path is about 14.3% per log cycle for kaolin clay and 15.3% for kaolin-silica mixture. The undrained shear strength in the conventional triaxial test was found to increase about 8 to 10% for a tenfold increase in strain rate. Therefore, it can be concluded that the undrained shear strength increases about 40-50% more in pressuremeter stress path tests than in the triaxial stress path tests.

A new state variable, ψ, indicative of the fabric of clays is introduced. Based on these concepts and general failure criterion a simple model to predict failure parameters of anisotropic clays for many commonly encountered stress paths is developed. The model capability to interpret in situ strength measured under a given stress path and transfer it to another stress path is illustrated. Finally, the ability to obtain failure parameters for any stress path using data from a single CIUC test is demonstrated.

The model developed based on cavity expansion theory is able to incorporate the influence of decreasing strain rate along the surrounding soil mass. The findings from

the strain rate test for the pressuremeter was used in the model to estimate the difference in the interpretation of the undrained shear strength. Even though the actual undrained shear strength increases with the strain rate, the interpreted undrained shear strength from the PMT expansion curve shows a higher strain softening behavior for the higher value obtained for PMT stress path. From the parametric studies it was determined that the level of upper yield does not have any significant influence on the predicted strength.

From the PMT simulated in the CSD it was found that for kaolin clay, irrespective of the initial strain level or strain rate, the relaxation time was about 200 to 250 minutes for undrained and drained conditions. Theoretical models have been included to show how to obtain creep/relaxation parameters from PMT creep/relaxation tests conducted in a borehole. Several correlations are also identified in order to obtain relaxation parameters from creep parameters and empirically from plasticity index. These creep/relaxation parameters are required to predict the time dependent behavior of soil.

Model pressuremeter expansion in calibration chamber (CC) is numerically simulated using Finite Element Method (FEM). The elasticity based FEM model was developed using commercially available program ANSYS. The elasticity based analysis was helpful to further investigate the boundary effects in chamber testing. Numerical simulation of pressuremeter testing using critical state finite element program CRISP will be performed and its validity will also be evaluated.

The test data from the CSD and CC are used to train a three layer feed forward neural network using a back propagation algorithm. The potential of artificial neural network will then be evaluated for incorporating strain rate effects in pressuremeter testing and for similar applications in the area of computational mechanics.

CHAPTER 1

INTRODUCTION

The geotechnical engineering profession today is increasingly using in situ devices to determine soil parameters. In situ testing is intended to reduce disturbance and stress-relief associated with sampling and laboratory testing. A major drawback of most in situ devices is that the boundary conditions are poorly defined, as a result, the test data are usually interpreted empirically to correlate the soil properties. Of all the in situ tests now in use, the pressuremeter offers the greatest possibility to interpret the test results analytically because of its well defined boundary conditions. Furthermore, load deformation relation is directly obtained from the test, and this information may with proper interpretation yield the constitutive relationship for the soil and, in situ horizontal stress, deformability modulus and in some cases, the consolidation characteristics of the soil.

However, in spite of the tremendous potential of the pressuremeter, it has encountered several problems. One of the major problem was that the pressuremeter test (PMT) predicts higher undrained shear strength and modulus values. There are also inconsistencies in the results obtained by different user, mainly because of differences in rate of probe expansion, probe advancing techniques, and interpretation methods. Unfortunately, there are no formal standards for performing pressuremeter tests.

One of the major difference between the PMT and laboratory tests, for example, triaxial test, is the rate of straining the soil specimen. Other differences between the PMT and laboratory tests include the stress-relief and stress relaxation, which is not a

usual concern in the standard laboratory testing. The main target of the research undertaken is to study how the time dependent factors affect pressuremeter tests. Emphasis is given to quantifying the strain rate effect in the PMT, and studying the influence of stress relief and stress relaxation in the PMT by simulating pressuremeter stress path in cuboidal shear device, as well as conducting model pressuremeter test in calibration chamber.

Chapter 2 describes computer controlled calibration chamber equipment to perform model pressuremeter tests. A control system having electro-pneumatic control and differential pressure transducer has been developed to maintain the same internal and external cell pressures throughout the K_o consolidation phase. This assures a rigid system in the horizontal direction. Other developments such as automatic data acquisition and reduction, improved slurry preparation technique, and an effective piezometer design are also described among other details including some experimental results. The calibration chamber apparatus is used to perform model pressuremeter tests.

A detail description of the cuboidal shear device, slurry preparation technique, properties of the soils used, servo-controlled system to perform K_o consolidation and strain controlled tests are provided in Chapter 3. Simulation of pressuremeter test strain path in the cuboidal shear device is discussed in Chapter 4. The main thrust of this chapter is to compare various strain rate related tests with the strain rate tests in pressuremeter test. Major conclusions are made from the extensive experimental program. A numerical scheme is developed to incorporate the strain rate effect in pressuremeter test and the influence of several parameters that affect the shear strength are also studied in Chapter 5.

Chapter 6 discusses the effect of stress relief and stress relaxation in pressuremeter test. Tests were conducted in cuboidal shear device to study the stress relaxation and normalization period. Theoretical models have been included to show how

to obtain creep/relaxation parameters from PMT creep/relaxation tests conducted in a borehole.

The main conclusions of the research are re-evaluated in the final chapter. Appendix A contains a listing of the technical papers and discussions already published or in preparation on the results of this research.

CHAPTER 2

MODEL PRESSUREMETER TESTING USING AN AUTOMATED FLEXIBLE WALL CALIBRATION CHAMBER

2.1 Introduction

An automated control and data logging system has been developed to perform model pressuremeter tests in clays using a flexible wall calibration chamber. Several of the important questions related to cavity expansion and pressuremeter testing in clays are being investigated using the newly developed calibration chamber test set up. Methods for slurry preparation and consolidation under K_o conditions are presented. Special considerations have been given to prepare high quality specimens and perform pore pressure measurements. Preliminary test results indicate successful performance of the system.

A series of one eighth scale model pressuremeter tests are being conducted to evaluate the effects of strain rate and stress disturbance in cavity expansion of cohesive soils. The initial phase of the research involved the development of an automated control and data logging system to perform model pressuremeter tests in a double wall calibration chamber. The calibration chamber built for a previous research study (Huang, 1986) was modified to work with the new set up.

The test set up includes a double wall calibration chamber, a slurry consolidometer, differential piston pump, model pressuremeter, piezometer, electro-

pneumatic control, data acquisition system and control panels. The flexible wall calibration chamber system and the procedure involved in preparing uniform specimens obtained by consolidating a slurry of kaolin or kaolin-silica mix, are described. The performance of newly designed piezometers is also discussed. Using the same soils, tests were performed in a cuboidal shear device to simulate pressuremeter stress paths, with strain rates varying from 0.01% per minute to 5.0% per minute. The experimental data indicated an increase in undrained strength of 15% for each tenfold increase in strain rate (Skandarajah et al., 1991). One of the main objectives of this research is to confirm the strain rate effects measured in the true triaxial simulation. Calibration chamber test results will also be used to calibrate the anisotropic model developed for the study.

2.2 Strain Controlled Pressuremeter Tests in a Calibration Chamber

Most of the scaled in situ tests using a calibration chamber has been performed in granular soils. In the past, pressuremeter tests in calibration chamber were performed in granular soils by Jewell et al., 1980 and in cohesive soils by Huang et al., 1988. A calibration chamber provides a controlled environment to perform this type of testing with the unique capability of subjecting soil samples to known stress history and boundary conditions. It also makes it possible to work with uniform and reproducible samples.

The calibration chamber approach for pressuremeter testing in cohesive soils has been used by Huang, 1986 prior to this research. Other studies concentrated field pressuremeter tests and comparison with conventional laboratory tests on samples from the same site. It is believed that calibration chamber technique for cohesive soils is a desirable alternative.

The two types of calibration chambers used in practice are the rigid-wall and flexible wall chambers. A rigid-wall chamber has a rigid wall that ensures no lateral strain. The main disadvantage in a rigid-wall chamber is that, to avoid boundary effects,

the size of the chamber must be much larger than the in-situ device that is being calibrated. This makes the testing expensive and time consuming. In a flexible wall chamber, it is possible to have independent control on vertical and lateral stresses, which makes the simulation of field tests possible with relatively small samples. The flexible wall chamber used in the current research has two walls, the inner wall being slightly thinner than the outer one so that if the cell pressure at some stage exceeds its yield value, it would burst inward ensuring the safety of the working environment. The two types of boundary conditions used are BC1: Constant vertical stress and zero lateral strain, and BC2: Constant vertical stress and constant lateral stress. It can accommodate a specimen of size 200 mm in diameter and 367 mm in height. The design allows for K_o consolidation as well as pressuremeter testing on that specimen at the end of consolidation. In the flexible wall chamber, the sample is hydraulically confined around a soft membrane which makes it possible to have independent control on lateral and vertical stresses. In order to make the consolidation and testing time manageable, the specimen dimensions were scaled down to the above mentioned values. The following sections give a detailed account of the salient features of the test set up, techniques of sample preparation, chamber consolidation, and strain controlled model pressuremeter testing.

2.2.1 Chamber Top Platen

The chamber top platen is shown in Fig. 2.1. It is a 28 mm thick aluminum platen and 200 mm in diameter. The model pressuremeter is attached to it at its center through 1/4" NPT. Piezometers are also attached to this platen. They are arranged diagonally opposite at 20 mm, 27 mm, and 44 mm respectively. It is thus possible to obtain two porepressure readings at the same distance from the center of the probe. The chamber top platen becomes the bottom platen of the slurry consolidometer. The tips of the piezometers extend approximately to the center of the probe. The chamber platen provides connectors for back pressuring and also for initial flushing. The pore and probe

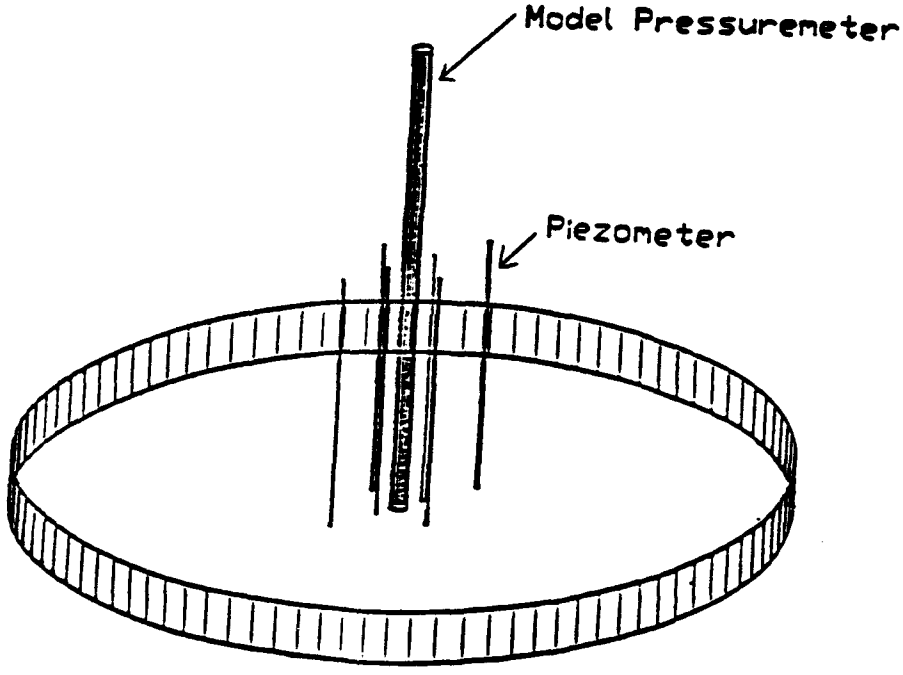

Fig. 2.1 Isometric View of Chamber Top Platen

pressures are measured using high sensitivity Model AB type pressure transducers (Data Instruments, Inc.) and the chamber top platen has all the mounting adapters attached to it. Prior to using the platen in the slurry consolidometer, all the piezometers and model pressuremeter are filled with deaired distilled water and thoroughly flushed to remove any entrapped air bubbles. The model pressuremeter has a custom made 9.5 mm ID, 0.8 mm thick latex membrane. Since light has detrimental effect on latex, when not in use, the platen is stored in a dark place.

2.2.2 Piezometers

Evaluating pore pressures is an important and integral part of calibration chamber test and is essential to the success of undrained testing. It is important to saturate the piezometers completely so that negative pore pressures resulting from cavitation are avoided. However, excess positive pore pressure should also be avoided. The piezometer shown in Fig. 2.2 was designed based on these considertions. The piezometer is typically made of 19 gauge stainless steel hypodermic needle. The needle is attached to the 1/8" pipe union through brass solder. The total length is 160 mm and the tip is plugged with fine polyethylene porous plastic having a mean pore size of 10 to 20 microns. At the end of each test, porous plastic plugs are removed using 0.56 mm plain steel acoustic string. The small diameter of the pressure sensitive area makes it ideal for instantaneous response. Initial test results indicate their acceptable performance and authors are considering to improve their performance by using silicone oil instead of water for initial saturation of the piezometers.

2.2.3 Slurry Tank

The slurry preparation procedurc must be systematically followed to obtain uniform and reproducible specimens. The slurry preparation involves three phases: slurry mixing, slurry vacuuming, and transfer to consolidometer. A tank shown in Fig. 2.3 has been designed to perform the these tasks. It is 343 mm in diameter and 559 mm

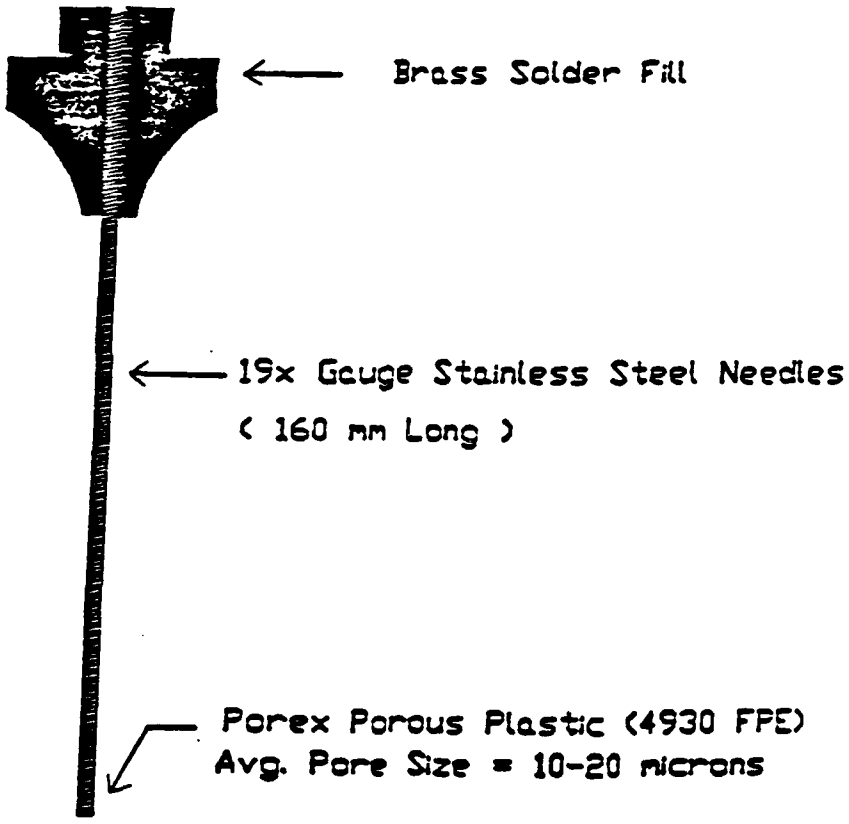

Fig. 2.2 Cross-Section of Piezometer

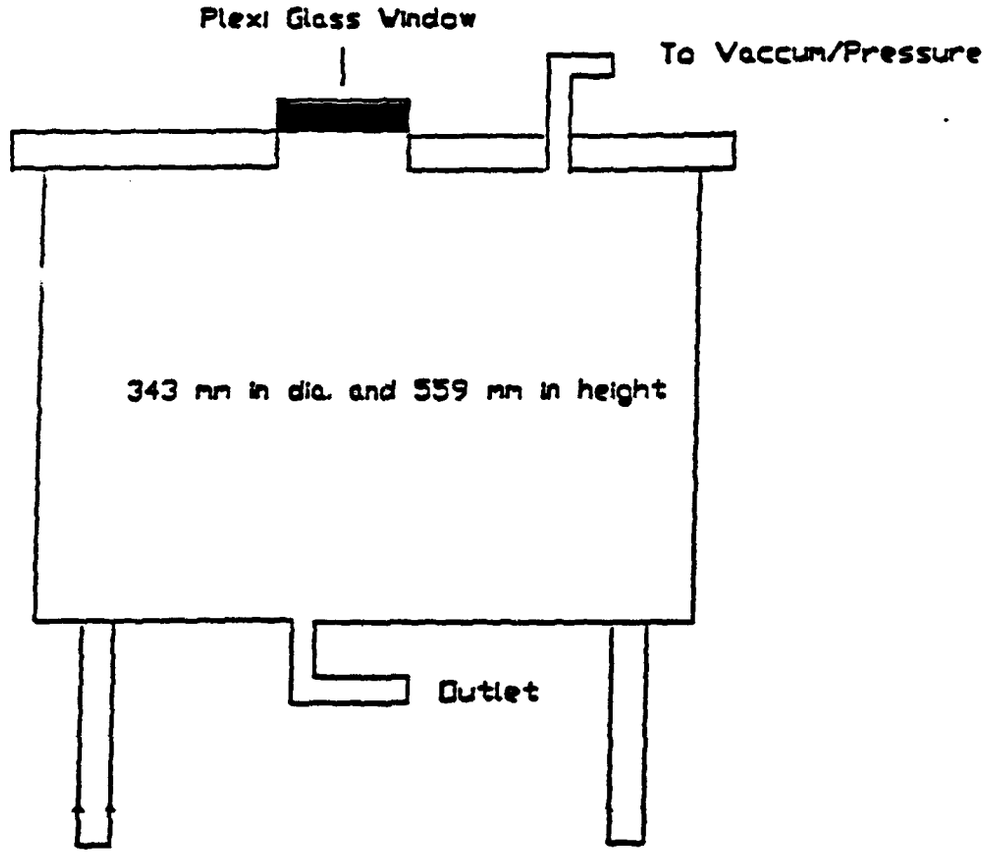

Fig. 2.3 Cross-Section of Slurry Tank

in height. Known amounts of water and kaolin-silica mix are added to the tank and are thoroughly mixed using conventional heavy duty mixer with 1/3 H.P. motor and type 316 stainless steel blades, at 1725 rpm, until a uniform mix is obtained. Subsequently, the mix is subjected to full vacuum for a period of six hours by which time the air entrapped during mixing is removed. A pressure of 5 psi is applied to the surface of the mix to transfer the slurry slowly into the consolidometer through 25.4 mm tygone flexible tubing. The mix is placed gradually from bottom to top in the consolidometer and the chances of air entrapment are minimized. Since very viscous mixing is involved, it is important to properly select the suitable motor and blades for obtaining a uniform slurry.

2.2.4 Slurry Consolidometer

The soils used for testing to date are Georgia Kaolin and crushed ottawa silica. Deionized and deaired water added to the soil and uniform slurry mix is obtained using the technique mentioned above. The water content corresponds to twice the liquid limit of the soil. The slurry is then transferred to the slurry consolidometer shown in Fig. 2.4. The device is used to consolidate the slurry from an initial height of 800 mm to a final height of approximately 350 mm. The slurry consolidometer has 2 steel pipe compartments having an inside diameter of 200 mm. The chamber top platen becomes the bottom platen for this device, with all the piezometers and model pressuremeter attached to it. A porous stone is attached to the piston and the slurry is consolidated by 207 kPa air pressure applied to the piston. Double drainage is allowed for the slurry to consolidate under K_o conditions. It takes approximately 12 days for the completion of primary consolidation. The lower compartment has same height as the soil sample. It is split longitudinally in two halves and bolted together. The interior is lined with sandpaper which is required to prevent slippage of the membrane caused by adhesion between clay and the membrane during the process of consolidation. The additional space for the slurry during the initial phase of the consolidation is provided by the upper compartment which is bolted to the lower one. The 0.64 mm thick custom made latex membrane for the specimen extends out of the lower compartment and provides a seal

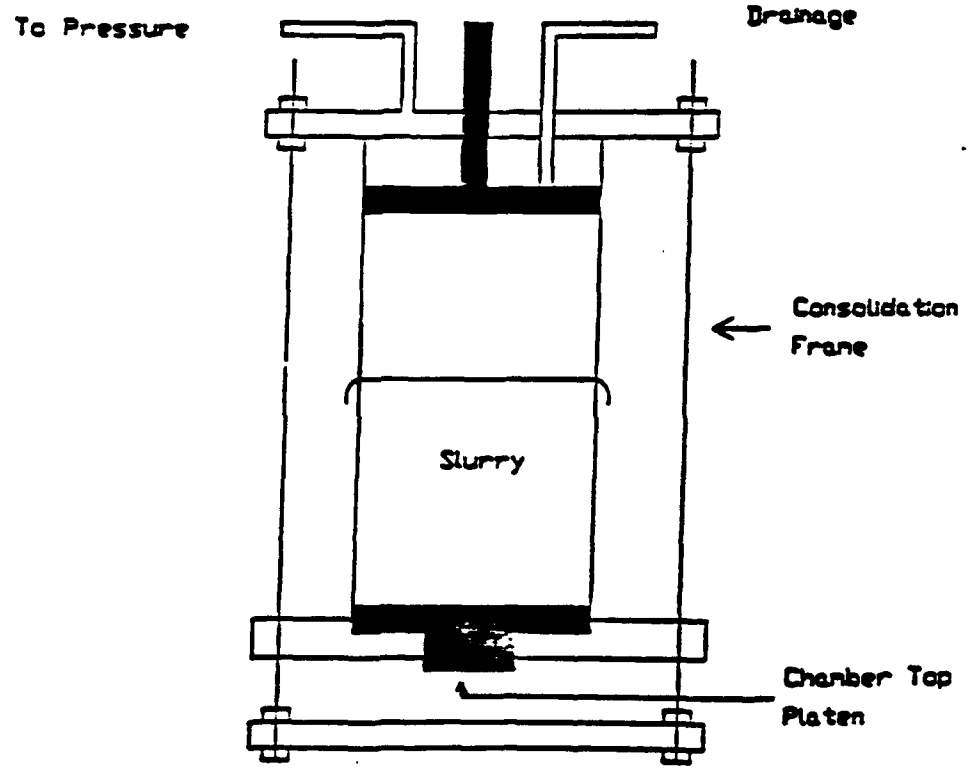

Fig. 2.4 Cross-Section of Slurry Consolidometer

between the two cylinders (Fig. 2.4). This completes the first phase of the consolidation process. The sample confined in the lower compartment and encased in the latex membrane is then transferred to the calibration chamber with the split mold. Since the sample is transported without touching it, and no mechanical extrusion is involved, disturbance is essentially eliminated.

2.2.5 Differential Piston Pump

A differential piston pump is used to expand the probe at a constant rate of strain (Fig. 2.5). It has two pistons of diameters 12.738 mm and 9.525 mm, respectively. They are attached to stepper motor and a DCDT. Through the stepper motor control box, four different speeds are preset with a switch box. By controlling the rate of movement of the stepper motor and with the input valve closed, the volume of water injected to the probe can be regulated at a constant rate. Thus, with the preset switch box, it is possible to obtain four constant strain rates for the probe expansion. A device of this accuracy is necessary because a radial strain of 12% for the model pressuremeter corresponds to a differential piston movement of only 37 mm.

2.2.6 Electro-pneumatic Control

During the second phase of consolidation inside the calibration chamber it is essential to create a rigid system with no lateral deformation in the horizontal plane. To ensure this, the cell and wall pressures are balanced throughout the consolidation process. A differential pressure transducer monitors the pressure difference between cell and wall, sends the resulting voltage signal to an electro-pneumatic transducer which converts the input voltage to an appropriate output pressure which is applied to the annular space between the internal and external walls. This electro-pneumatic control assures a zero lateral deformation condition, which is essential for successful K_o consolidation.

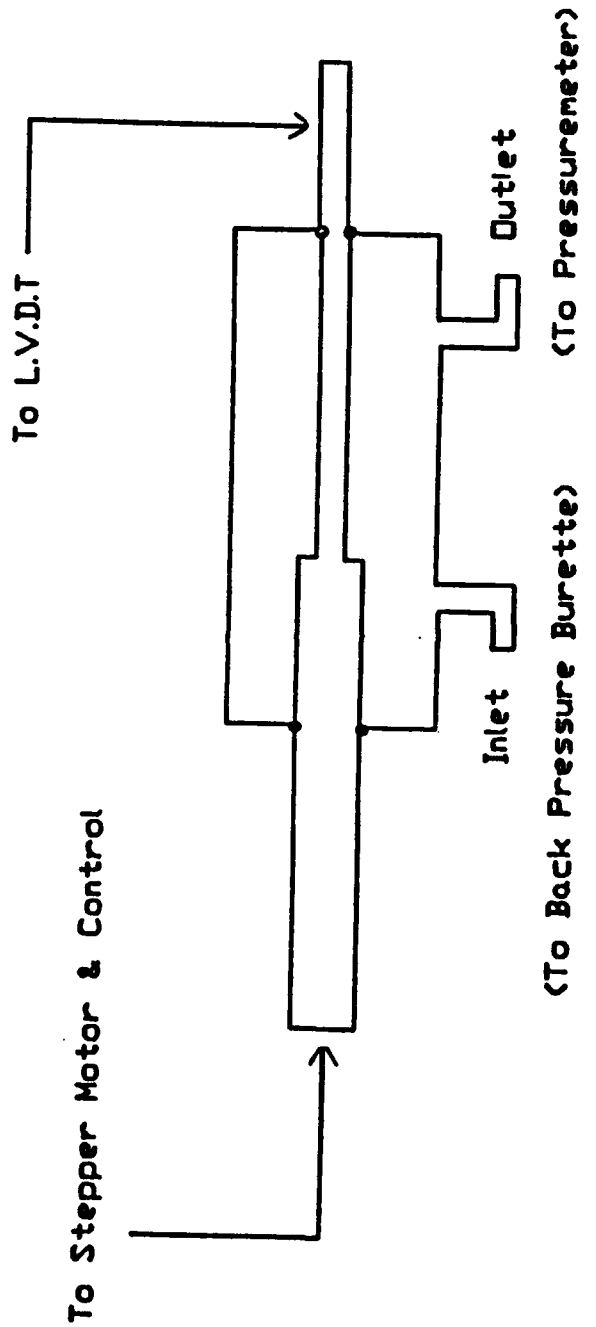

Fig. 2.5 Cross-Section of Differential Piston Pump

2.2.7 Flexible Wall Calibration Chamber

The schematic of the flexible wall calibration chamber is shown in Fig. 6 (after Huang, 1986). Upon completion of the slurry consolidation in the consolidometer, the sample confined in the lower compartment (bolted split mold) is transferred to the chamber and placed upside down. The bottom platen of the slurry consolidometer becomes the chamber top platen. During the transfer operations it is critical to center the sample on the piston of the calibration chamber before placing it. Once it is supported on the piston platen, it is very difficult to re-align it without disturbing the sample. The piston providing the vertical stress inside the chamber has the same diameter as that of the sample and has a maximum vertical travel of 62 mm. Since the sample is encased in a membrane and is attached to top and bottom platens with two 158 mm o-rings, both ends of the sample are isolated from the cell water. Hence the stresses in horizontal direction through cell pressure, and vertical direction through piston pressure, can be independently controlled. By balancing the pressure between cell and wall, and by maintaining constant piston pressure and preventing volume change in the cell-water system, conditions simulating K_o consolidation are obtained. The sample at the end of the first phase of the consolidation process in the slurry consolidometer does not have uniform water contents along the vertical direction due to friction between clay and rigid wall. By subjecting this sample to a second phase of K_o consolidation and avoiding rigid boundary, a very uniform sample is obtained. Fig. 7 shows the three dimensional profile of the variation of water contents for a typical kaolin-silica mix specimen. Porous discs are placed at both ends of the sample to permit double drainage. During K_o consolidation, loss of sample volume is replaced by the piston movement, therefore allowing displacements in the vertical direction only. K_o consolidation under an effective vertical stress of 276 kPa was performed using a single load increment method proposed by Campanella and Vaid, 1972.

In summary, the five step procedure that accomplishes chamber K_o consolidation is made of the following steps:

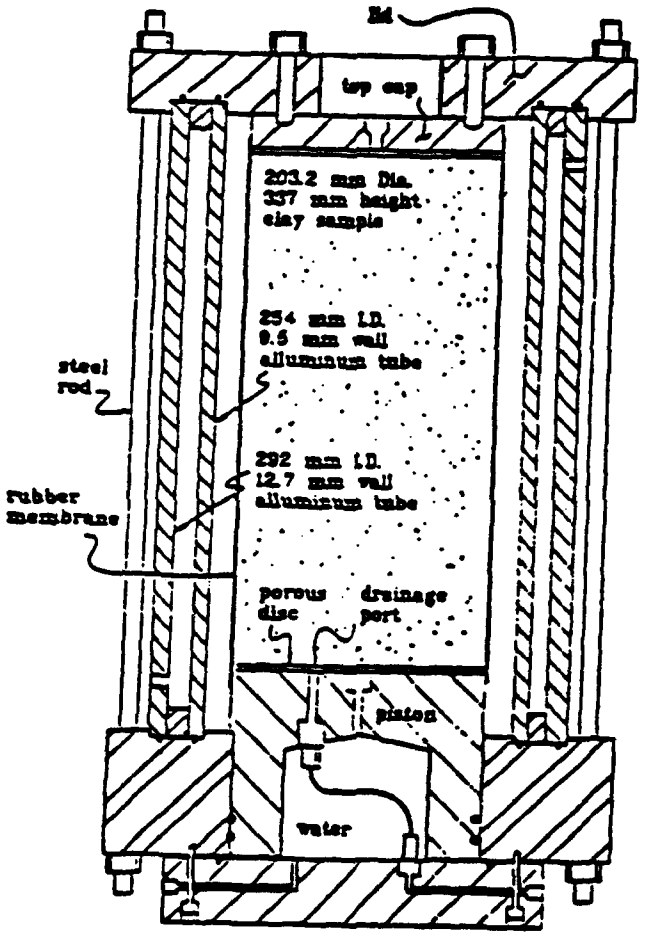

Fig. 2.6 Cross-Section of Calibration Chamber
(After Huang, 1986)

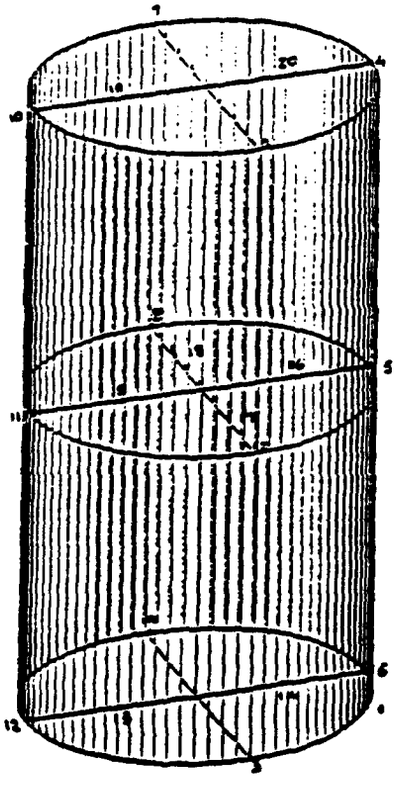

Location	Water Content (%)
1	28.53
2	28.32
3	27.04
4	28.52
5	28.10
6	27.14
7	28.63
8	28.52
9	27.06
10	28.79
11	27.93
12	27.65
13	28.33
14	28.47
15	28.58
16	28.57
17	28.47
18	28.65
19	28.74
20	28.90

Fig. 2.7 Variation of Moisture Content

1) Close the pore water drainage lines.
2) Increase cell and axial pressures to back pressure + effective consolidation pressure (690 kPa + 276 kPa) simultaneously.
3) Maintain a constant cell-water system.
4) Open the drainage lines and permit drainage against high back pressures.
5) Monitor axial deformation and cell pressure changes, and electro-pneumatically control the wall pressure.

Because of the limited vertical movement of the piston, very soft samples could not be tested using the present calibration chamber.

2.3 Boundary Effects

The sample is eighteen times larger than the diameter of the pressuremeter probe. In order to evaluate the radial distance at which stress increase diminishes to zero a simple elasticity based approach can be used. The equation of equilibrium for a cylindrical cavity is (tension being positive):

$$\frac{d\sigma_r}{dr} - \left(\frac{\sigma_\theta - \sigma_r}{r}\right) = 0 \qquad 2.1$$

Introducing compatibility and plane strain conditions, the variation of radial and circumferential stresses are:

$$\sigma_r = -p_1 - \frac{(p_1 - p_2)}{\left(\frac{a^2}{b^2} - 1\right)} + \frac{(p_1 - p_2)}{\left(\frac{1}{b^2} - \frac{1}{a^2}\right)} \left(\frac{1}{r^2}\right) \qquad 2.2$$

$$\sigma_\theta = -p_1 - \frac{(p_1 - p_2)}{\left(\frac{a^2}{b^2} - 1\right)} - \frac{(p_1 - p_2)}{\left(\frac{1}{b^2} - \frac{1}{a^2}\right)} \left(\frac{1}{r^2}\right) \qquad 2.3$$

For a maximum probe pressure of 1173 kPa (ϵ_r = 12%) and a cell pressure of 830 kPa, elasticity based analyses indicate that the stress increase is essentially negligible at a

radial distance equivalent to 9 times the probe radius (Fig. 8). Numerical analysis by Carter et al. (1979) have shown that in a soil mass which extends laterally to infinity, the stress increase diminishes to essentially zero at approximately 20 times the cavity radius as radial strain reaches about 25%. In the chamber pressuremeter tests, maximum radial strain was limited to 12%. Elasticity based arguments coupled with the numerical analysis by Carter et al., 1979, thus indicate that the size of the probe to soil specimen ratio is satisfactory within the strain rate of interest.

2.4 The Model Pressuremeters

Based on the design concept of a single cell lateral load tester made by Oyo Corporation, Tokyo, Japan (Suyama et al., 1982), one eighth scaled water inflated model pressuremeters were built as a part of an earlier research program. The probe has a diameter of 11.1 mm and is 112 mm long. Custom made 0.8 mm thick, 9.5 mm I.D. latex membranes are used as the probe membrane. The fluid pressure is measured at the center of probe, accounting for the head loss. Strain controlled pressuremeter tests are performed by injecting constant amount of fluid, using the differential piston pump. Details of the model pressuremeter are shown in Fig. 9 (after Huang, 1986).

2.5 Strain-Controlled Testing

The complete control system involved in the strain-controlled probe expansion is shown in Fig. 10. Initial calibration chamber tests using the model pressuremeter have been performed in a 50/50 blend of kaolin and very fine crushed silica. The slurry was K_o consolidated under a pressure of 207 kPa around the model pressuremeter and six piezometer needles, and then transferred to the calibration chamber. The performance of the piezometers was evaluated during the B parameter check. After saturation, the specimen was subjected to a second phase K_o consolidation in the chamber under an effective vertical stress of 276 kpa against a back pressure of 690 kPa. A strain controlled pressuremeter test was performed at the end of chamber consolidation. All

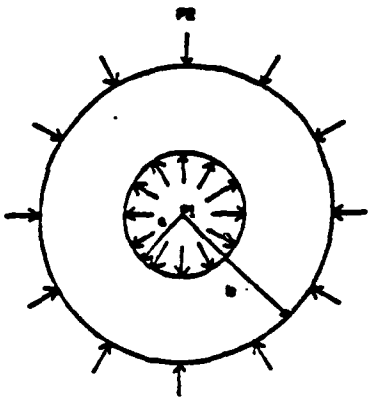

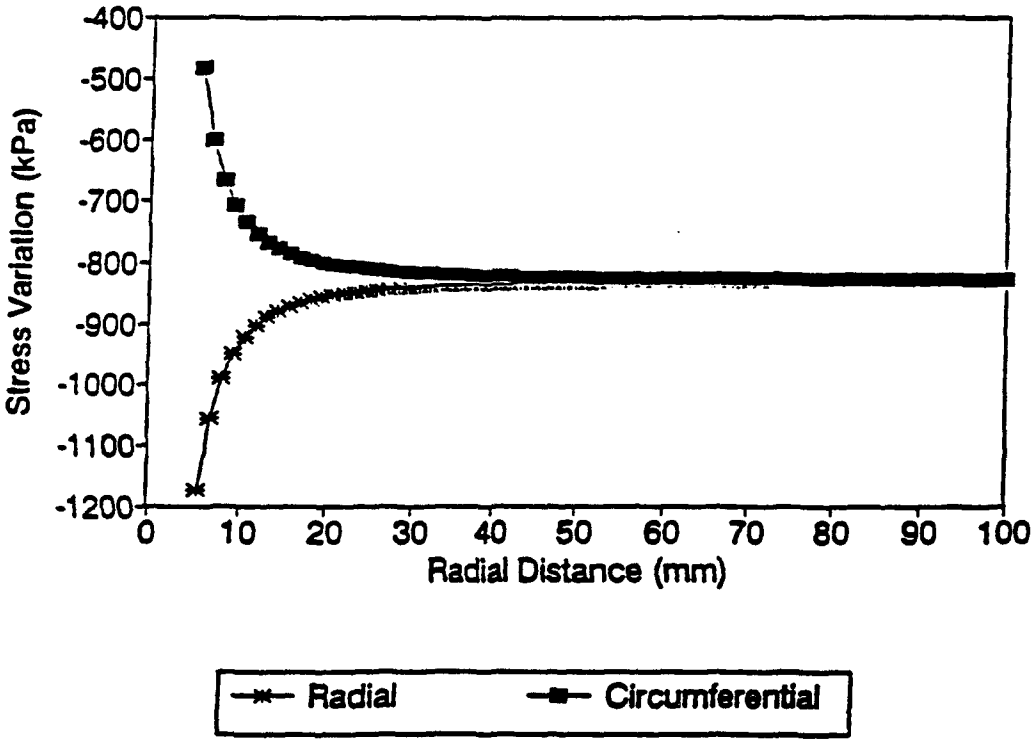

Fig. 2.8 Calibration Chamber Stress Variation

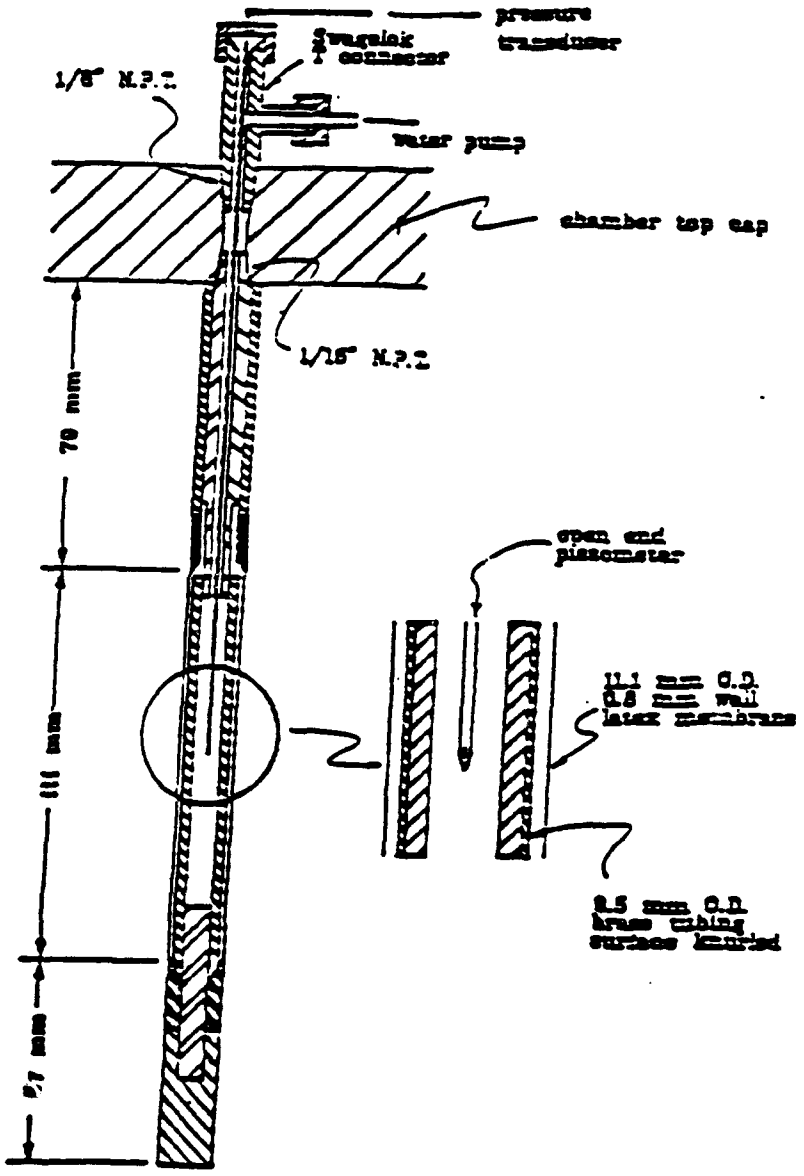

Fig. 2.9 Cross-Section of Model Pressuremeter
(After Huang, 1986)

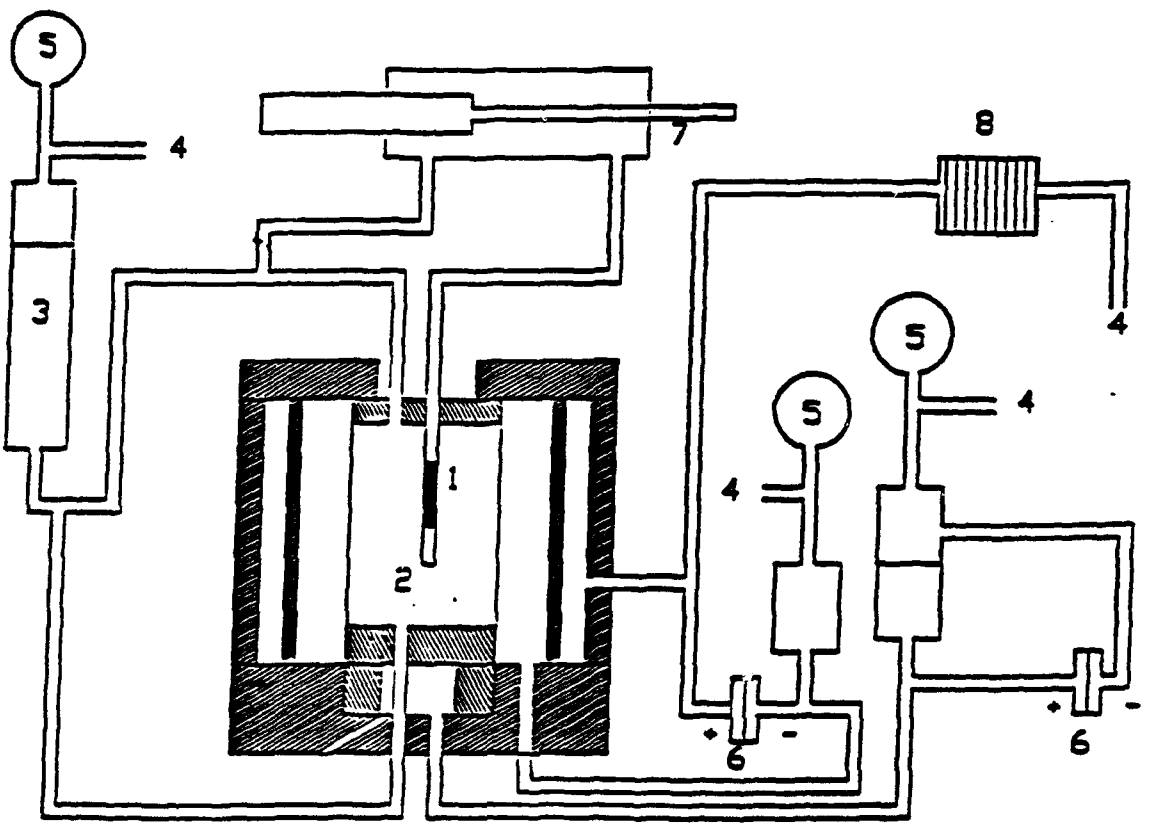

1) Model Pressureneter

2) Soil Sample

3) Back Pressure Burette

4) Air Pressure

5) Pressure Gage

6) Differential Pressure Transducer

7) Differential Piston Pump

8) Electro-Pneumatic Control

Fig. 2.10 Calibration Chamber Control System

the control and acquisition during the testing was performed by a Keithly series 500 data acquisition system. The probe expansion curve obtained at the end of the test represents the combined effect of system compliance, membrane stiffness and the soil resistance. The system compliance was measured by inserting the model pressuremeter in a tight-fitting thick walled brass tube. The membrane stiffness was evaluated by performing the pressuremeter test in an empty chamber with cell pressure equal to horizontal stress obtained at the end of chamber consolidation. The net pressuremeter curve is obtained from probe expansion curve by subtracting the system compliance and the membrane stiffness.

The results indicate that small radial strains occurred before exceeding the true soil lateral stress which is the chamber cell pressure at the end of K_o consolidation. Hence with reasonable accuracy, true "lift-off" point can be evaluated using the model pressuremeter under controlled conditions. Essentially elastic behavior was observed for the unload-reload cycle.

A typical model pressuremeter expansion curve for kaolin-silica mix is shown in Fig. 2.11. The compliance curve and the membrane stiffness are also shown in the same figure. The variation of probe pressure with respect to radial strain,reported in Fig. 2.11, was not very smooth and has step response. This was found to be due to the limitation on resolution of A/D converter in the data acquisition system used. Hardware gain was added to the existing system for subsequent testing and much better response was observed for kaolin samples (Fig. 2.12). The variation of pore pressure for kaolin-silica mix during chamber K_o consolidation is shown in Fig. 2.13. The excess pore pressure developed during pressuremeter expansion is as shown in Fig. 2.14 for kaolin specimens.

From the net pressuremeter curve obtained using the raw data for kaolin-silica mix specimen, shown in Fig. 2.11, horizontal stress was interpreted as 820 kPa and the true horizontal stress was observed to be 830 kPa. From Fig. 2.12, the lateral stress

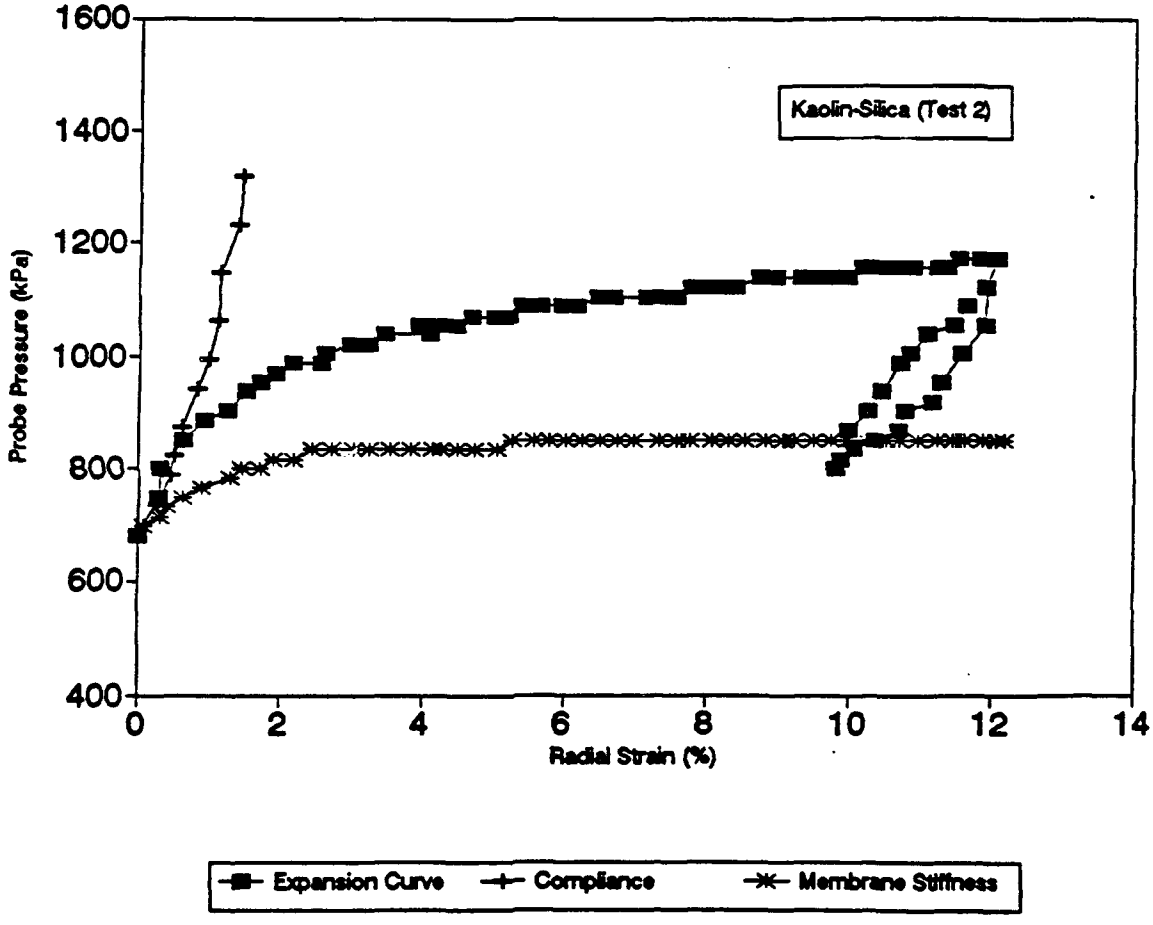

Fig. 2.11 Pressuremeter Expansion Curve - Test 2 (Kaolin-Silica)

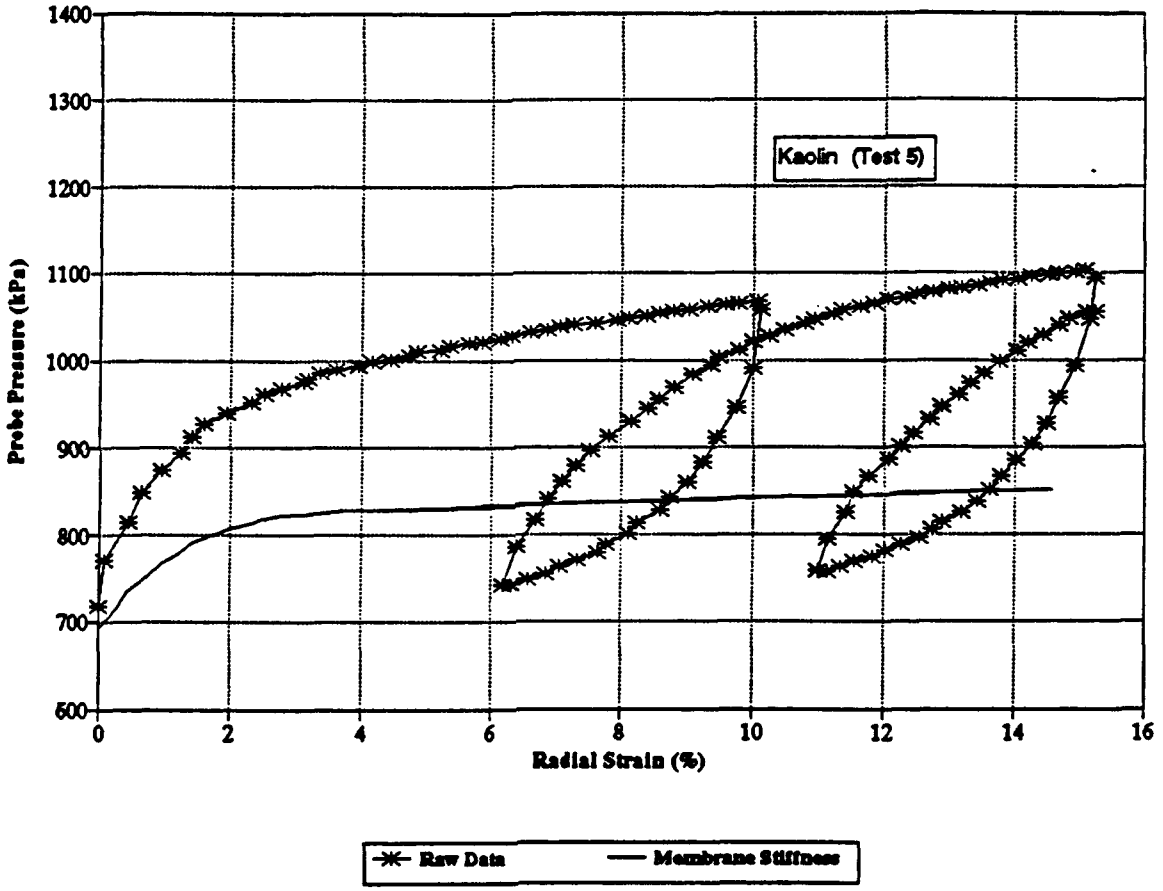

Fig. 2.12 Pressuremeter Expansion Curve - Test 5 (Kaolin)

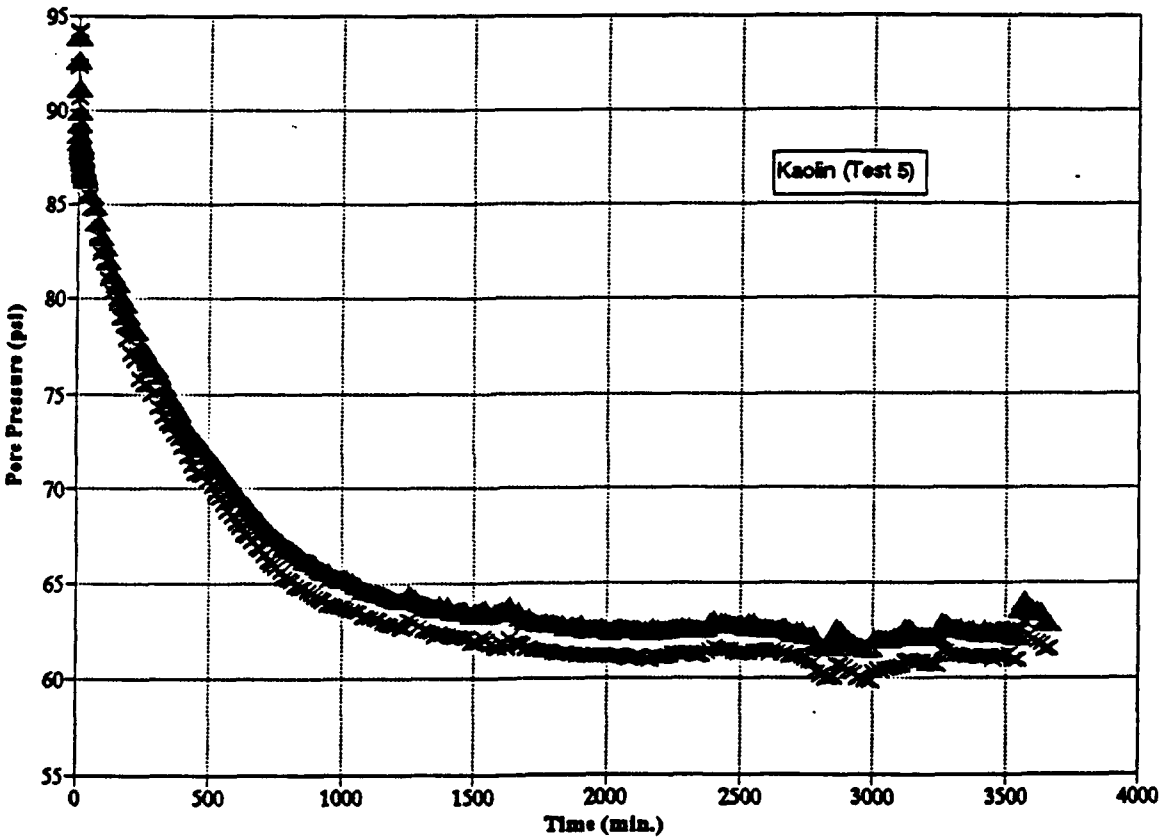

Fig. 2.13 Pore Pressure Dissipation During Chamber K_o Consolidation (Test 5, Kaolin)

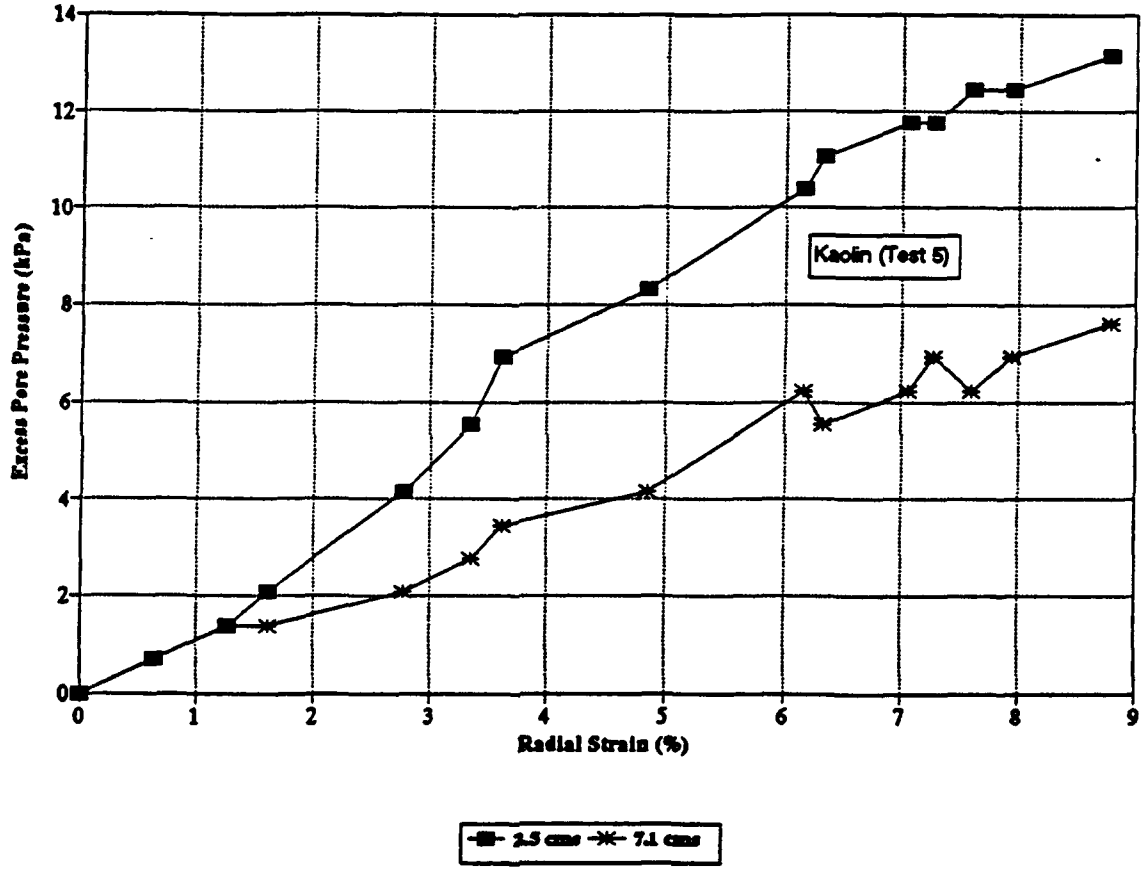

Fig. 2.14 Excess Pore Pressure Developed During Model Pressuremeter Expansion (Test 5, Kaolin)

was interpreted for the kaolin specimen to be 815 kPa and the true lateral stress (cell pressure after K_o consolidation) was 820 kPa. Hence excellent lateral stress predictions were obtained using a model pressuremeter test in the calibration chamber which further validate the immense potential of pressuremeter to predict true lateral stresses when performed with no disturbance. The pore pressure dissipation observed in two piezometers while consolidating the kaolin specimen under K_o cosolidation is shown in Fig. 2.13 and the variation of pore pressure observed on two different piezometers is quite similar and validates their funcitoning. Excess pore pressures were observed during the probe expansion for kaolin sample (Fig. 2.14) and conclusive results on pore pressure behavior can made after additional calibration chamber testing. This pore pressure data is very important for validating many of the existing numerical models and good quality test data in the related area is not available.

2.6 Summary

An automated calibration chamber system which includes a double wall chamber, slurry consolidometer, piezometers, electro-pneumatic control, model pressuremeter, data acquisition and control system has been developed. From the testing done so far, the following are concluded:

a) By employing standard slurry preparation techniques and two phase consolidation process, a very uniform sample can be obtained.

b) True lateral stress predictions can be made using pressuremeter. This also reflects the disturbance free state obtained at the end of chamber consolidation.

Currently model pressuremeter testing using the calibration chamber is being performed. Conclusive results on several aspects related to pressuremeter testing will be made after performing statistically admissible number of tests. Since only couple of tests at the maximum can be performed for each month, more time is required to perform additional testing. Detailed account of results and conclusions based on calibration chamber testing will thus be reported at a later date.

CHAPTER 3

LABORATORY TESTING USING CUBOIDAL SHEAR DEVICE

3.1 Introduction

By simulating pressuremeter stress path tests in the cuboidal shear device the strain rate effects, stress relaxation time, oversize probe and disturbance effects in the pressuremeter test were studied.

A slurry consolidometer was used to prepare 102 mm cubical samples from artificially sedimented mix. The cubical specimens were reconsolidated one dimensionally in the cuboidal shear device to simulate the field condition and then to perform pressuremeter test with various strain rates. The measurements were made automatically using a data acquisition system. This chapter describes the slurry consolidometer, cuboidal shear device, measurement systems, membrane preparation, properties of the soils used, and experimental procedures for various tests performed. The experimental results of the strain rate effects, error in pressuremeter test interpretation due to strain rate, and stress relaxation effects are presented and discussed in Chapters 4, 5 and 6, respectively.

3.2 Slurry Consolidometer

A slurry consolidometer made of plexiglass was used to prepare 102 mm cubical specimens by sedimentation and consolidation under K_o condition from the powdered soil-water mix. An isometric view of the slurry consolidometer is depicted in Fig. 3.1.

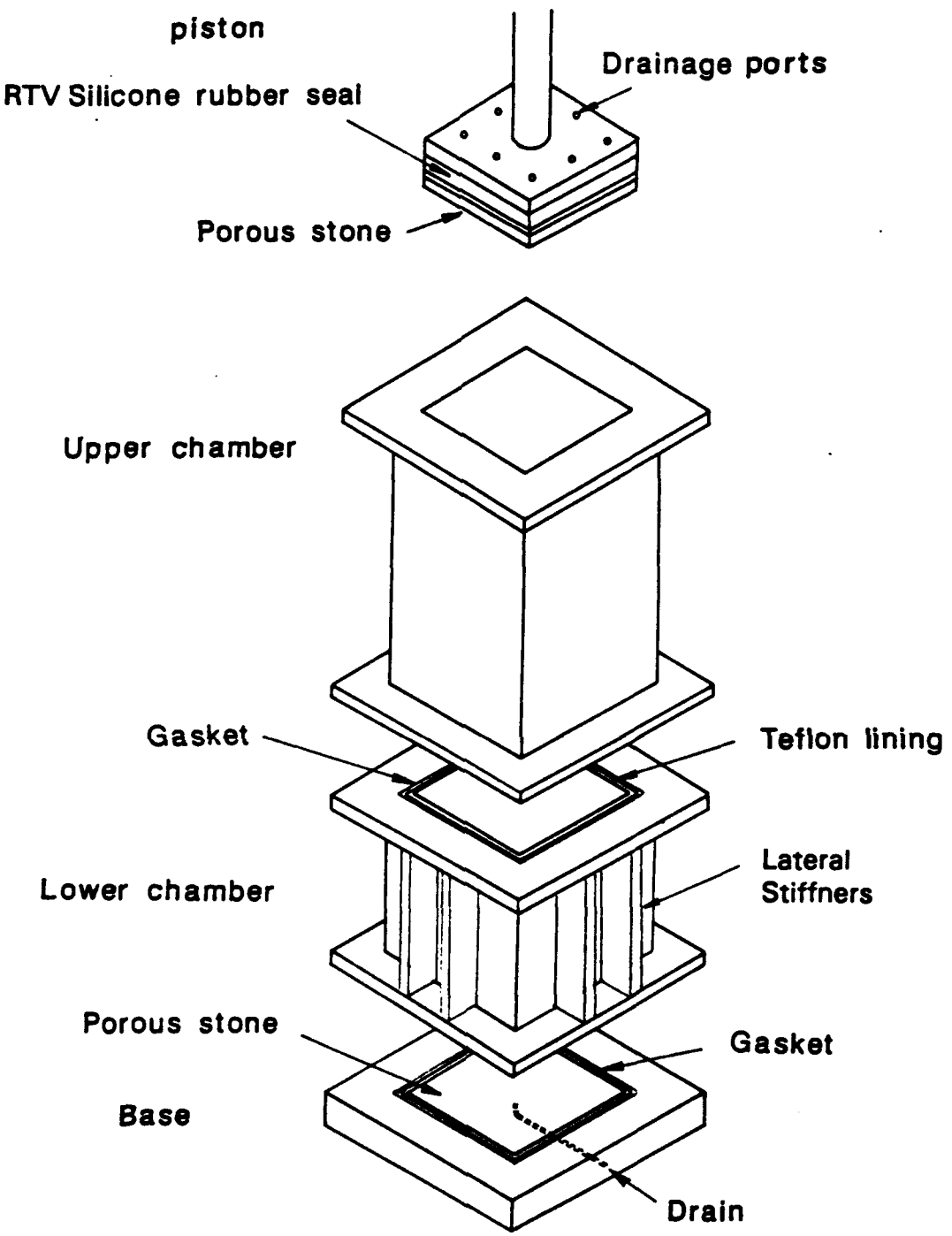

Fig. 3.1 Isometric View of Slurry Consolidometer (Modified from Sivakug, 1987)

The cross-sections of the upper and lower chambers are shown in Figs. 3.2 and 3.3, respectively.

The consolidometer consists of two chambers, a piston and a base. The internal cross-section of the chambers is a 102 mm x 102 mm square. The heights of the upper and lower chambers are 229 mm and 102 mm, respectively. The walls of the lower chamber are externally reinforced in order to minimize lateral deformation and to assure that the sample obtained was consolidated one dimensionally under K_o condition. The interior surface of the lower chamber is lined with teflon in order to minimize the wall friction in the sedimentation, consolidation and extrusion stages. The consolidation load is applied through a plexiglass piston (Fig. 3.4) consisting of a 32 mm diameter 292 mm long rod and a 32 x 102 x 102 mm base. A 6.35 mm thick sintered bronze porous stone is attached to the bottom of the piston to facilitate drainage through the top of the sample. There are 16 holes 3.2 mm in diameter connecting the porous stone to the top of the piston. An RTV silicone rubber seal is attached to the middle of the piston to avoid the slurry from being squeezed up between the piston and the chamber walls during the early stages of the consolidation. Another identical porous stone is embedded in the base of the consolidometer (Fig. 3.5) to allow bottom drainage. Provision of drainage at the bottom and top reduces the drainage path by half and thus reduce the consolidation time by four times.

3.3 Cuboidal Shear Device

Under field conditions, the soil is subjected to three-dimensional states of stress. Hence, for appropriate simulation of the field conditions and for predictions based upon sophisticated constitutive models, it is desirable to test soil specimens under truly triaxial states of stress. The cuboidal shear device is such an apparatus where three stresses can be applied independently under any stress path.

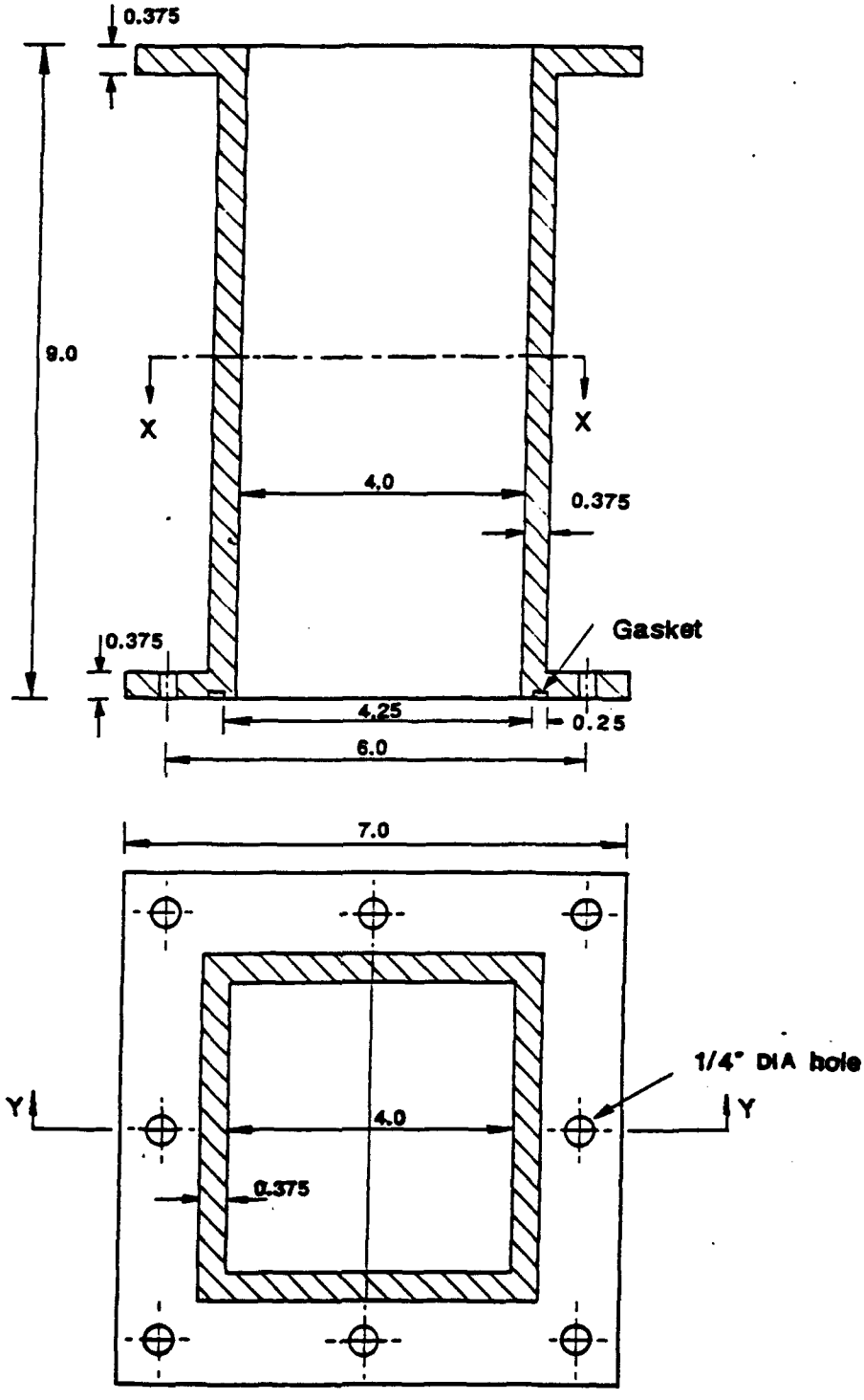

Fig. 3.2 Cross-Section of Upper Chamber of the Consolidometer (Modified from Sivakugan, 1987)

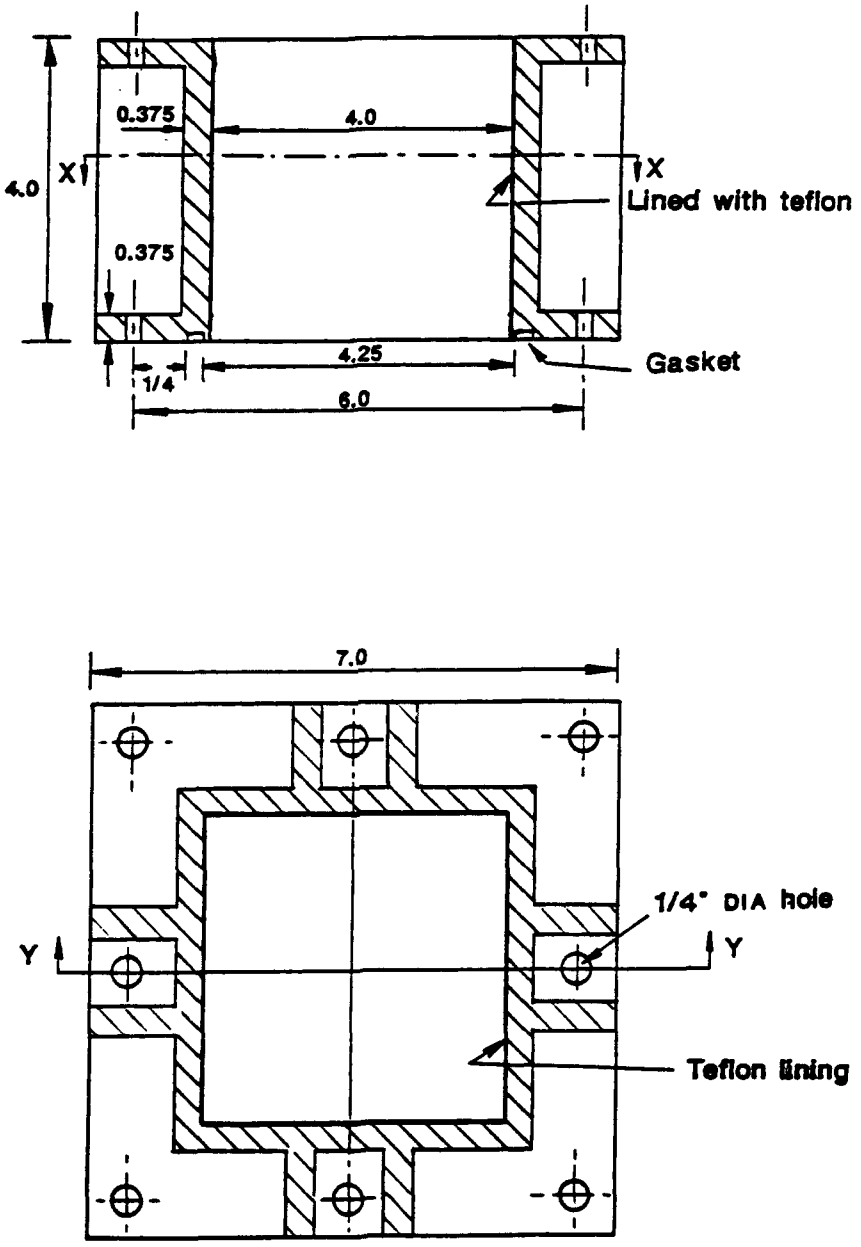

Fig. 3.3 Cross-Section of Lower Chamber of the Consolidometer (Modified from Sivakugan, 1987)

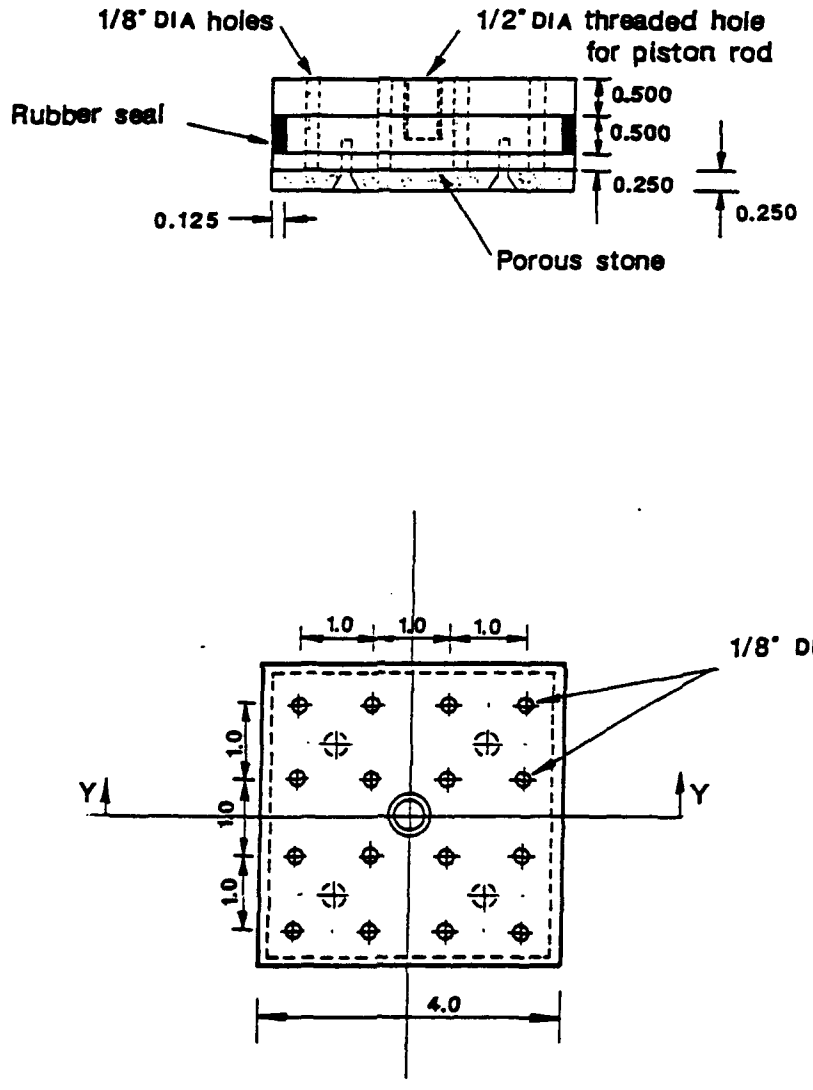

Fig. 3.4 Cross-Section of Piston (After Sivakugan, 1987)

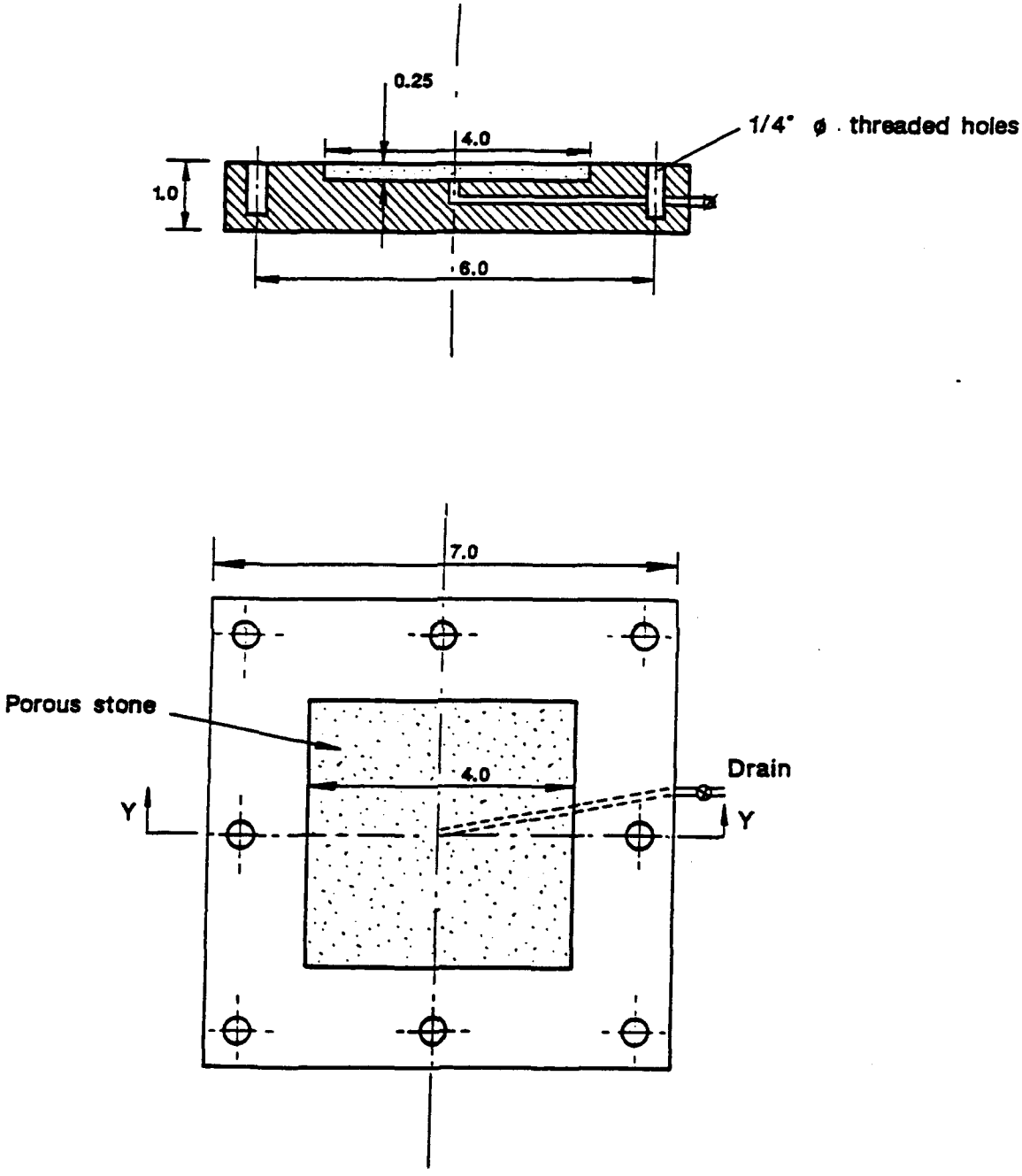

Fig. 3.5 Cross-Section of Base of the Consolidometer (After Sivakugan, 1987)

The boundary stresses can be applied to a cuboidal-shaped specimen either via rigid flat platens or flexible membranes, or a combination of both. The first attempt to test sand in a cubical triaxial apparatus by Kjellman (1936) and then by Jakobson (1957) using a segmental rigid platen had limited applicability due to basic mechanical difficulties. Later on, the mechanical problems were overcome and the non uniform stresses induced in the rigid platen loading were minimized by using layers of silicone grease (Green, 1971), and flexible rubber membranes on each of the three pairs of faces for tests on sand (Ko and Scott, 1967). Green (1971) and Sture and Desai (1979) have described in detail the subsequent developments of flexible boundaries and the various combinations of flexible and rigid, and rigid-lubricated boundaries on two pairs of faces. A comparison of the merits and drawbacks of the three types of boundary conditions used in true triaxial apparatus is given in Table 3.1 (after Sture and Desai, 1979).

Loads/pressures applied through rigid boundaries assure strain controlled conditions, and uniform strains which can be measured precisely, at the expense of non uniform stresses induced in the sample. The major issue with this type of equipment is the interference of loading platens. Several creative techniques were proposed (Pearce, 1971) to overcome this problem, however they consist of complicated and expensive mechanical systems.

The flexible membranes can be used for stress controlled tests where uniform stress distribution is possible, however the uniformity of large strains is difficult to maintain. The interference of flexible membranes can be avoided with proper precautions (Sture and Desai, 1979). Plain strain or any other strain controlled test can be performed with flexible boundary loadings through stepwise corrections using a trial and error approach.

TABLE 3.1 A Comparison of Three Types of Boundary Conditions in a Multiaxial Cubical Test Apparatus (Sture and Desai, 1979)

Advantages

Strain Controlled; All Rigid Boundaries	Stress Controlled; All Flexible Boundaries	Mixed (Rigid and Flexible) Boundary Condition
(a) Strains can be measured accurately	(a) normal, principal stresses assured on the loading faces	(a) boundary interference is usually avoided by assigning the rigid boundary as the compressive deviator and stress-controlled flexible boundary as extension deviator direction
(b) Uniform strains are possible	(b) uniform stress distribution over all faces is possible	(b) pore water pressure and other facilities are easily accommodated
(c) Large uniaxial strains can be achieved	(c) large strain can be achieved in three dimensions without significant boundary interference	(c) stress or strain paths can be easily followed if a predetermined selection of specimen orientation with respect to apparatus axes is allowed
(d) Complicated and predetermined strain paths can be readily modeled	(d) complicated and predetermined stress paths can be readily followed	(d) plane strain tests can be modeled
(e) Pressure cells and pore water pressure instrumentation can easily be accommodated in the loading platens	(e) shear distortions are possible and measurable	

Table 3.1 (Continued)

Disadvantages

Strain Controlled; All Rigid Boundaries	Stress Controlled; All Flexible Boundaries	Mixed (Rigid and Flexible) Boundary Condition
(a) The uniformity of stresses induced is difficult to verify	(a) interference at boundaries can occur if proper precautions are not taken	(a) complicated predetermined stress or strain paths are difficult or impossible to follow
(b) Apparatus will not accommodate or allow shear distortions	(b) the uniformity of large strains can be difficult to maintain if proper lubrication is not performed	(b) uniformity of stress and strain fields in directions normal to rigid and flexible boundaries difficult to ascertain
(c) Loading platen interference occurs at large multiaxial strain states	(c) difficult to follow predetermined strain paths	(c) heterogeneous stress and strain fields occur near boundaries
(d) Difficult to follow predetermined stress paths	(d) plane strain experiments can only be achieved through stepwise corrections of stress state normal to plane	(d) apparatus is usually large and unwieldy
(e) Apparatus is usually large and unwieldy	(e) pore water pressure facilities are not easily accommodated	(e) operation is usually extremely complicated
(f) Operation is usually complicated		(f) apparatus will not allow shear distortions

The mixed boundary apparatuses avoid the boundary interference but heterogeneous stress and strain fields occur near the boundaries. Usually they are large devices with complicated test operations. However, there is not any one type of apparatus most suitable for testing all types of soil over a large range of stress and strain levels and paths.

The true triaxial apparatus used for this research is of the flexible boundary type, based on the design by Sture and Desai (1979). A detailed description of the device was given by Sivakugan (1987) and Sivakugan et al. (1988). An isometric view of the CSD is shown in Fig. 3.6. The dimensions and a cross sectional view of the space frame are shown in Figs. 3.7 and 3.8, respectively.

The space frame and the cylindrical casings of the cuboidal shear device were machined from solid forged billet of aluminum. A 102 mm cubical sample "floats" in the 114 mm cubical cavity of the space frame and is confined within six identical silicone rubber membranes. The specimen is loaded by compressed air or compressed nitrogen applied to the membranes through the cylindrical casings. A thin coating of silicone oil is always applied on the surfaces of the membrane and space frame in order to minimize the friction between the sample and the membrane, and between the membrane and the space frame. In the absence of friction, the three pairs of orthogonal stresses are principal stresses.

The cylindrical pressure casings contain the linear variable differential transformers (LVDTs) and the pressure transducers as shown in Fig. 3.9. They also serve as holders of the flexible membranes. The casings on opposite sides are connected together by stainless steel tubings and thus equal pressures can be applied on opposite sides of the specimen. All three directional pressures can be controlled independently, either manually through pressure regulators or automatically through servo-controlled solenoid valves.

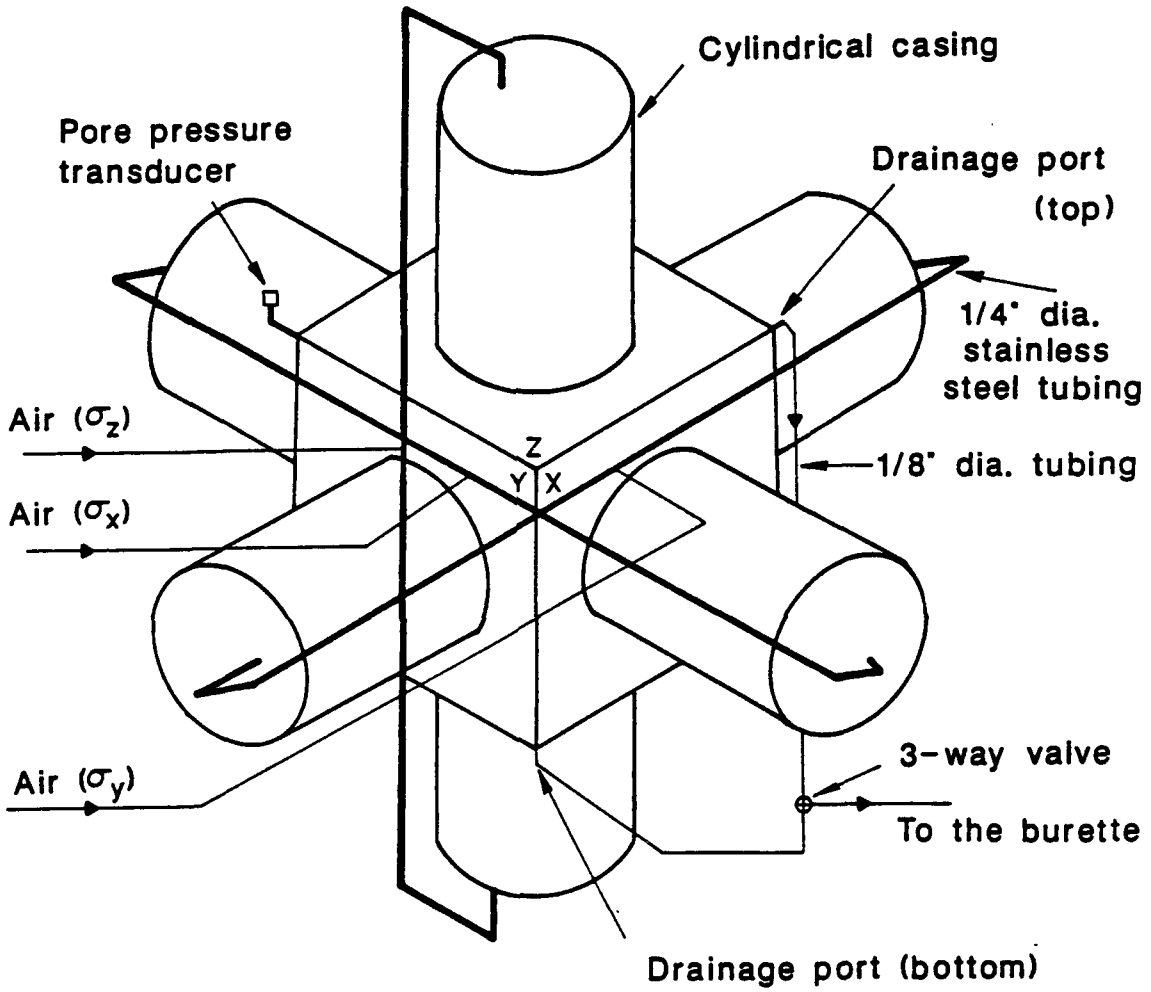

Fig. 3.6 Isometric View of Cuboidal Shear Device (After Sivakugan, 1987)

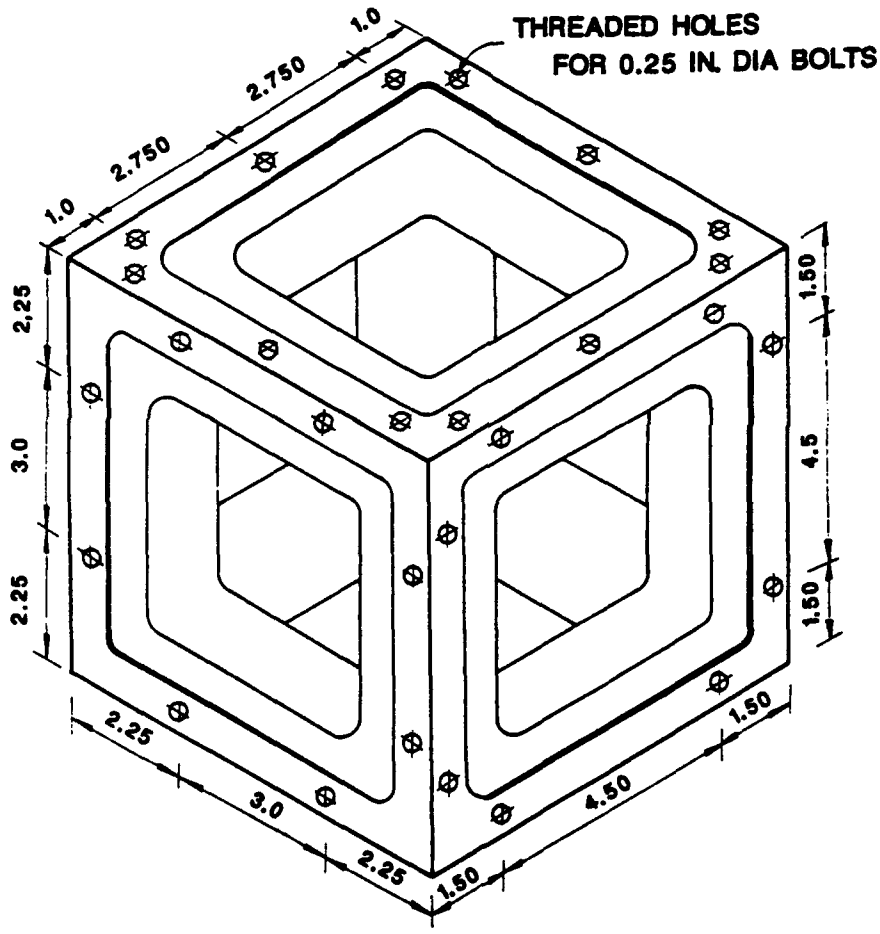

Fig. 3.7 Dimensions of Space Frame (After Sivakugan, 1987)

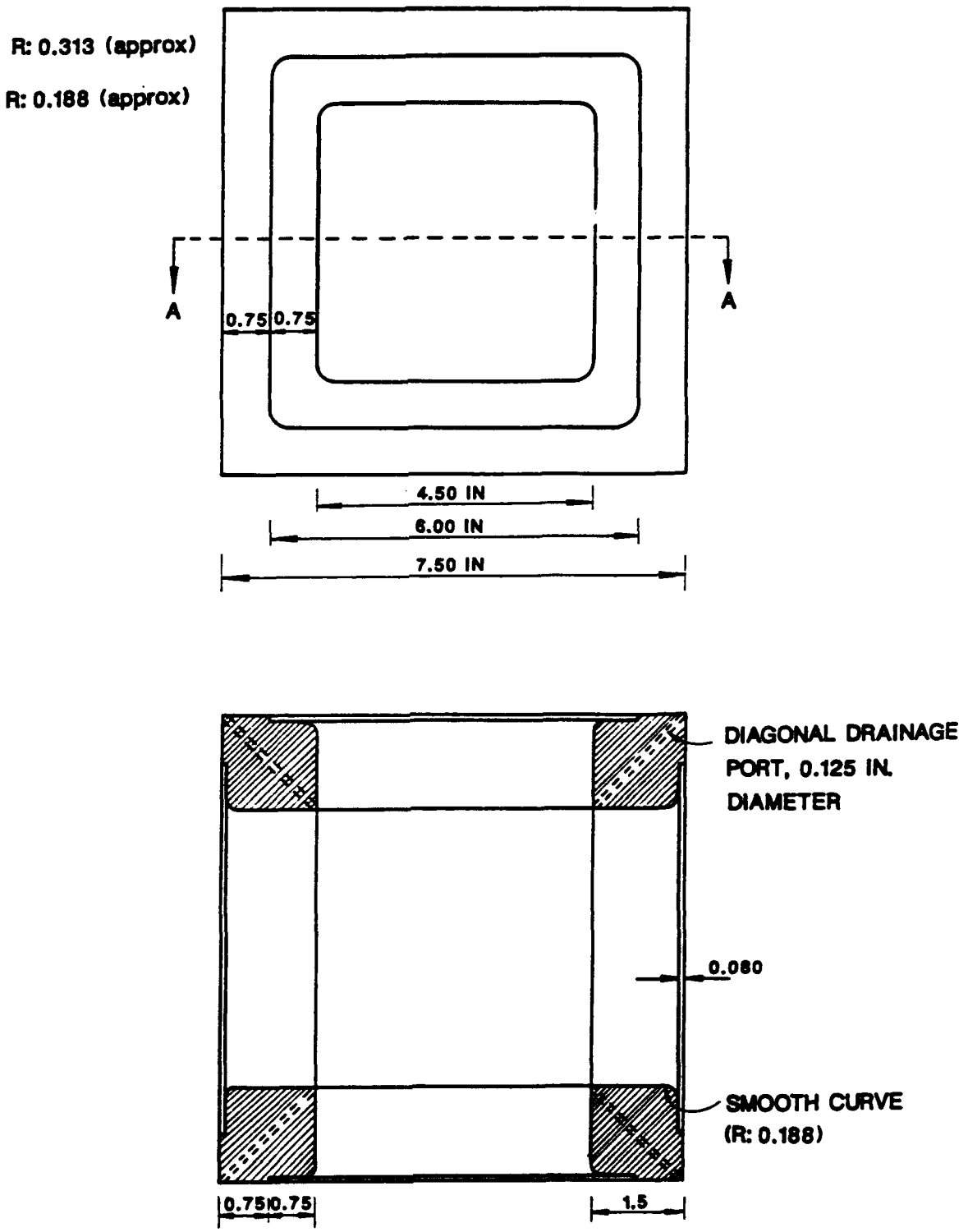

Fig. 3.8 Cross-Sectional View of the Space Frame (After Sivakugan, 1987)

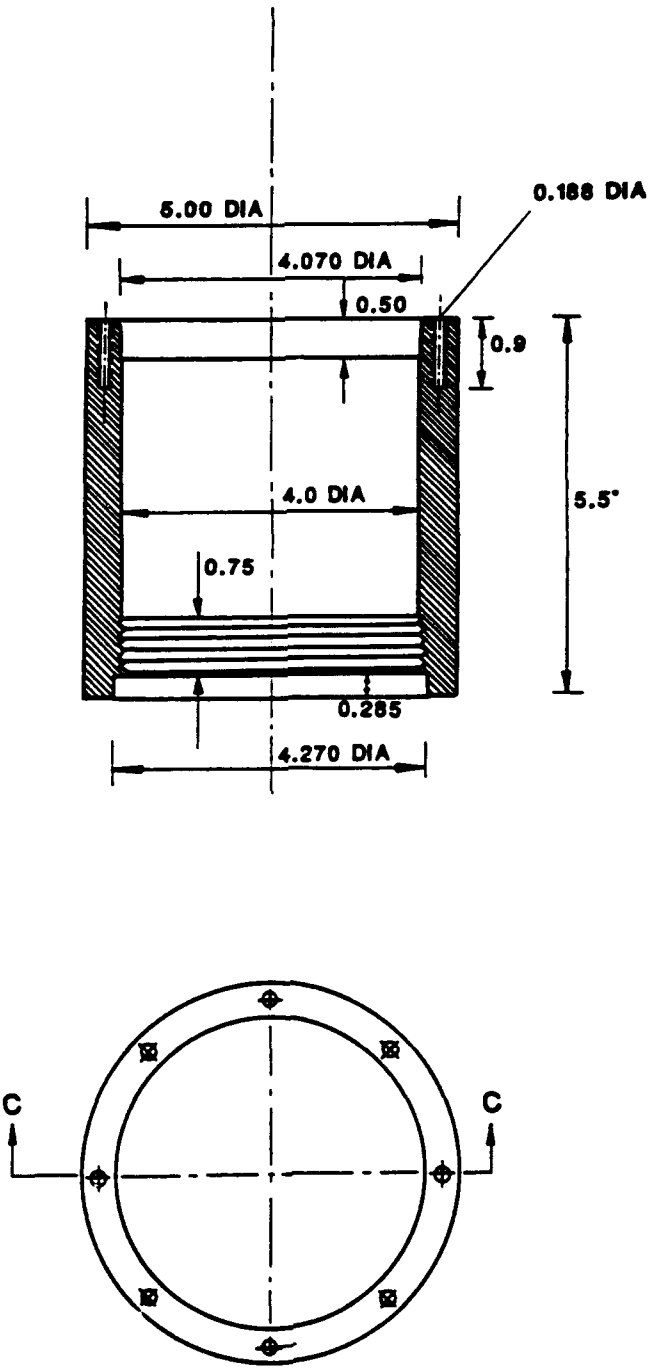

Fig. 3.9 Cross-Section of Pressure Casing (After Sivakugan, 1987)

3.3.1 Total and Pore Pressure Measurement

Pressures are applied through the pressure casings to the flexible membranes, using "in house" compressed air up to 100 psi and "bottled" compressed nitrogen to achieve higher pressures. The pressures in the casings (and on the membranes) are measured by pressure transducers attached on the base plate of each casing of the three pairs. The pressure transducers are made by Data Instruments, Inc. of Lexington, MA. They are model AB type with a pressure range of 200 psi and a maximum signal output of 100 mV.

Pore pressure at the center of the specimen is measured by custom made "needle" piezometer. A thin needle (0.820 mm OD) is inserted through a bottom diagonal port into the specimen. At the tip of the needle several small holes were drilled for the first centimeter, and the tip was covered with a No. 200 wire mesh to prevent clogging of the tube. This technique worked well except in one or two tests out of about a hundred tests the needle got clogged. The piezometer needle is connected to a pressure transducer of model AB. The pore pressure response is immediate and very accurate. The needle is cleaned after every test using compressed air to prevent drying of kaolin particles in the needle. Before starting the test, the needle is flushed thoroughly with deionized deaired water, saturated and then connected to the pressure transducer.

All four transducers are connected to a multiplexer MUX1 with a gain of 50.0, and then to the analog-to-digital (A/D) convertor. Data received from the A/D convertor are processed by the microprocessor. According to the instructions given to the computer and microprocessor, measurements from the LVDTs and the pressure transducers are analyzed and decisions made. Based on these decisions, directions are passed to the relay board to activate or inactivate the appropriate relays. This enables opening or closing the solenoid valves and thereby automatically regulating the pressures in all three directions independently. The schematic diagram of the servo control interfacing is shown in Fig. 3.10.

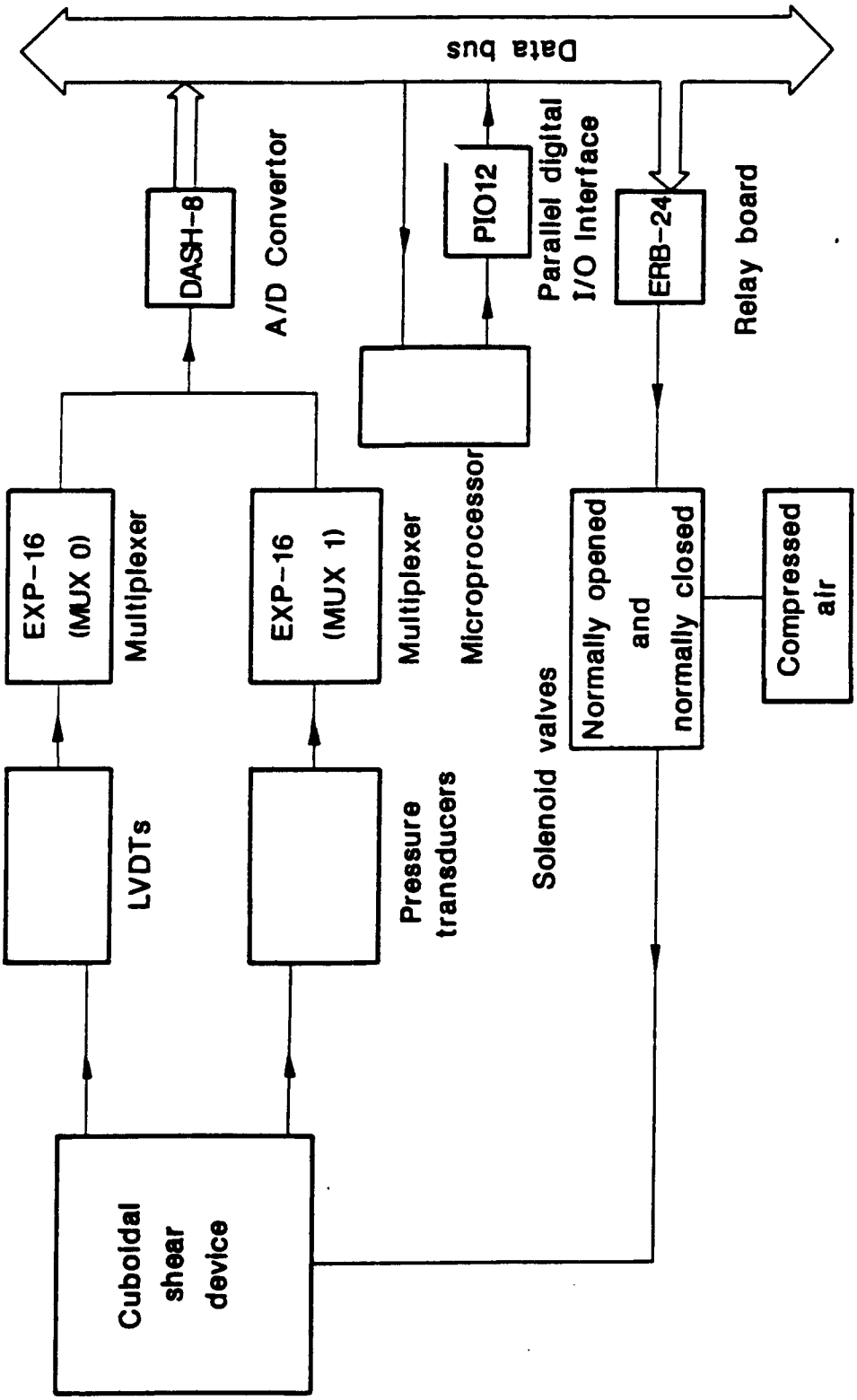

Fig. 3.10 Schematic Diagram of Hardware Interfacing (After Sivakugan, 1987)

3.3.2 Deformation Measurement

The deformations of the specimen are measured using the linear variable differential transformers. The LVDTs are fixed on the front plate of the pressure casing, contained within the casing, and the leads are taken through the end cap to the A/D convertor, the DASH-8 board. The LVDTs are DC operated and have a nominal linear range of ± 0.250 inches. The LVDTs used are manufactured by Schaevitz Engineering (GCD/GPD-121-250 type), and are hermetically sealed and spring loaded. The sensitivity of the LVDTs is 1.6 volt/mm. A ± 15V DC external power supply provides power to all LVDTs. The outputs of the LVDTs are taken to the multiplexer MUXO. As already described in section 3.3.1 the readings from LVDTs are analyzed in the microprocessor and the proper instructions are sent to the solenoid valves to regulate the pressure. By regulating these pressures, either stress controlled tests or strain controlled tests can be performed.

A total of eight LVDTs are used in the deformation measurement, one each in all six sides of the cube and two more on a lateral side. This arrangement is to check and confirm the planar deformation of each face. The three LVDTs located staggeredly on one side yielded essentially the same readings for all tests, thus conforming to planar displacement. Teflon disks of 12.7 mm diameter with a slight convexity are attached to the tips of the LVDTs in order to reduce the contact pressure on the membrane and the sample.

Since the LVDTs have a limited linear range (maximum of 0.5 in), the initial position of the LVDTs is adjusted depending on the strain path in order to utilize the LVDTs maximum linear range. For example, a LVDT would be placed in its maximum compressed level where a compressive deformation would be measured on that side. On the other hand, initial position of an LVDT will be set with fully extended position of rod where it will measure a maximum extensive deformation of the sample.

3.4 Properties of Soils Used

Two different soils were utilized in the testing program. One is Georgia kaolinite clay in dry powdered form, obtained from Akrochem Corporation, Akron, Ohio under the trade name Akrochem SC-25 (soft clay #25). The other soil used is ground silica obtained from U.S. Silica Company, Ottawa, Illinois under the commercial name Sil-Co-Sil #270.

The Atterberg limits and specific gravity of the soils are given in Table 3.2, and their particle size distributions are shown in Fig. 3.11.

Table 3.2 Properties of the Kaolinite and Kaolin-Silica Mix

Soil	Liquid Limit	Plastic Limit	Specific Gravity
Kaolinite	63	33	2.60
Kaolin-Silica	37	22	2.65

Additional characteristics of the kaolinite and ground silica are given in Appendix D.

3.5 Slurry Preparation

A proper slurry preparation method is an important factor to obtain a high quality uniform specimen. This includes an appropriate water content, proper mixer and a vacuuming system. According to Sheeran and Krizek (1971), samples prepared from the higher water content slurry will not be influenced by the techniques adopted to place the slurry into the slurry consolidometer. However, higher water content slurries requires a larger equipment, longer piston and larger loading frame. From their experiments, Sheeran and Krizek found out that a water content of 2 to 2.5 times the liquid limit of the soil would be an ideal amount.

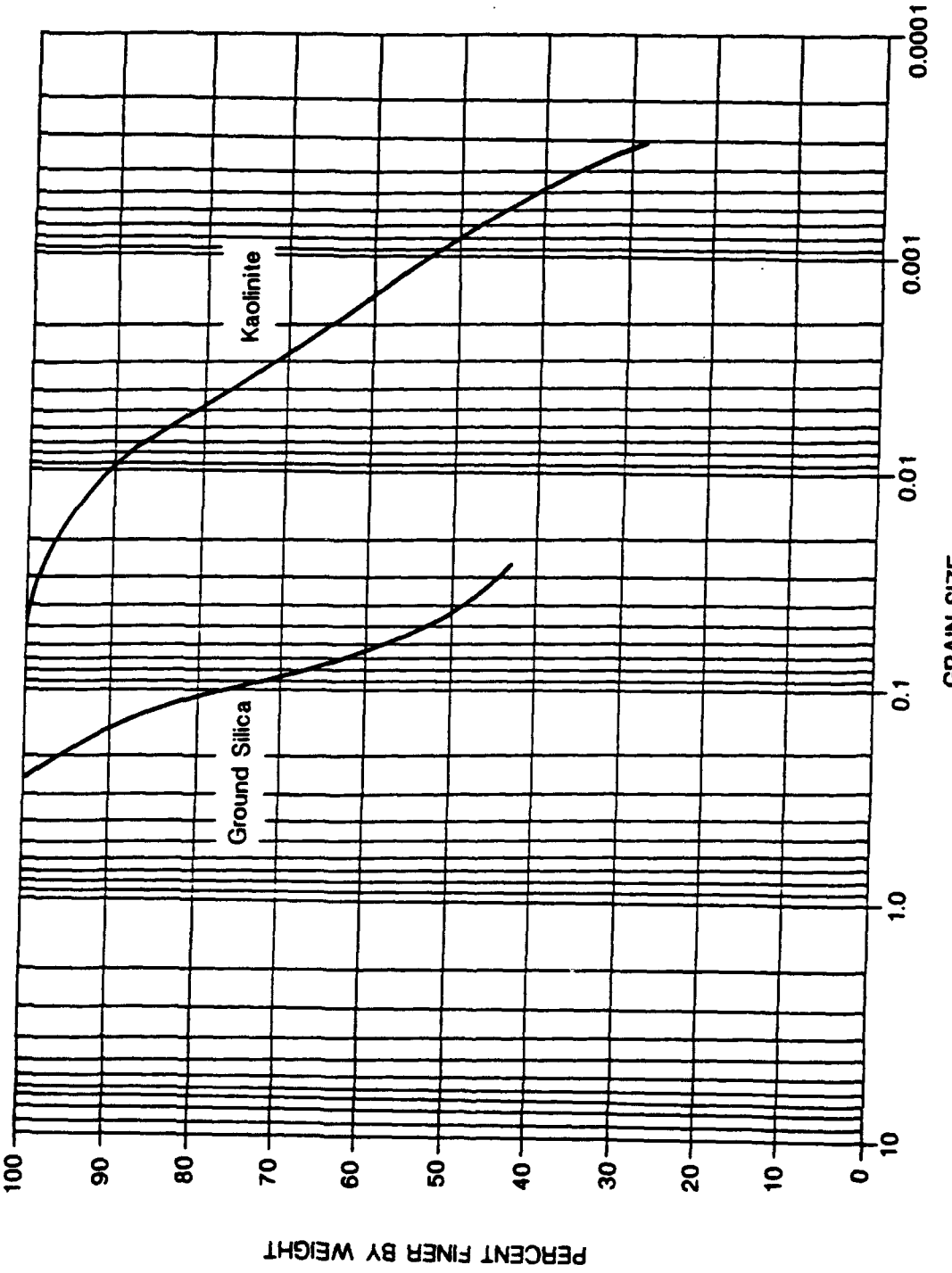

Fig. 3.11 Particle Size Distribution of Kaolinite and Ground Silica

To obtain kaolin specimens, 1700 g dry powdered kaolin was added to 2380 g (140% water content) deionized and deaired water, and mixed thoroughly by a hand held mixer for about 10 minutes. [Note: If the clay is put first in the vessel and then water is added, clay sticks to the bottom and wall and it is very difficult to mix because of clay lumps.] Then the slurry was subjected to a vacuum of about 650 mm mercury by an aspirator for about 4 hours. After the vacuuming, soil particles were separated from water, and therefore the mix was stirred by a spatula slowly and gently but thoroughly without inducing any air into the slurry, until it became a smooth homogeneous mix. Before the slurry was poured into the consolidometer (as shown in Fig. 3.1), silicone oil was applied to the inner wall in order to reduce the wall friction. Wet filter papers were placed in between the slurry and porous stones (on the base and under the piston). Gaskets were provided in between the upper and lower chamber, and lower chamber and base to avoid leaks. A rubber seal was attached around the sides of the piston to capture any squeezing of slurry between the piston and the walls.

3.6 *Consolidation in the Slurry Consolidometer*

Initially a small pressure of 3 psi is applied to the piston for a day. This prevents any leak between the compartments or between the piston and walls and the slurry becomes semi-solid. After the semi-solid cake is formed closer to the porous stones, there will not be any leak even at high pressures. The second pressure increment of 18 psi is applied for another day to complete the slurry consolidation.

From the c_v values of the soils tested it was estimated the primary consolidation would be over within a day. Thus, for both soils, two days were allowed to complete the consolidation. The 16 holes of ⅛" diameter drilled through the piston for top drainage also help to remove the piston without suction. The lower chamber is reinforced externally to obtain exactly a four inch cube sample.

After the slurry consolidation, the consolidometer is removed from the loading

frame, and the water collected on the top is poured into a sink. After removing the screws fastening the upper and lower chambers, the chambers are separated slowly using a flat screwdriver, allowing enough time to equalize the internal pressure to atmospheric. The excess consolidated cake is cut with a wire cutter and the top surface of the sample is trimmed to the exact size with a sharp straight edge. A wet 4x4 filter paper was placed on the top surface. The lower chamber with the specimen was removed from the base and the bottom surface of the sample was covered with a filter paper and transported to an extrusion jack. A teflon block was used to extrude the sample and after extruding all other four sides were covered with wet filter papers. Then the sample was taken to the space frame with the teflon block.

The wall friction plays an important role on the deposition, sedimentation and consolidation of the slurry. Deschamps (1991) found that the water content varied about 15% from top to bottom of a sample consolidated from a montmorillonite slurry, and from empirical correlations estimated that stress differences of 25% existed between the top and bottom. To minimize frictional effect in the lower compartment of the slurry consolidometer where the test specimen is collected, the walls are lined with teflon sheets. In addition, silicone oil is applied to the teflon surface before the slurry is poured into. To check the efficiency of this method in reducing wall friction, a four inch cube sample from a consolidated slurry was cut into 64 one inch cubes, numbered as shown in Fig. 3.12, and the water contents of the 64 samples were determined (Fig. 3.13). The water content distribution is almost uniform throughout the sample. The overall variation is only of $\pm 0.8\%$ of the mean, indicative that the effect of wall friction is almost negligible.

3.7 Placing, Flushing and Back Pressure Saturation

Before the sample which is covered with wet filter paper is transferred to the space frame, the following steps are followed. The tip of the piezometer needle is covered with 200 wire mesh cloth. Then the needle is thoroughly flushed and filled with

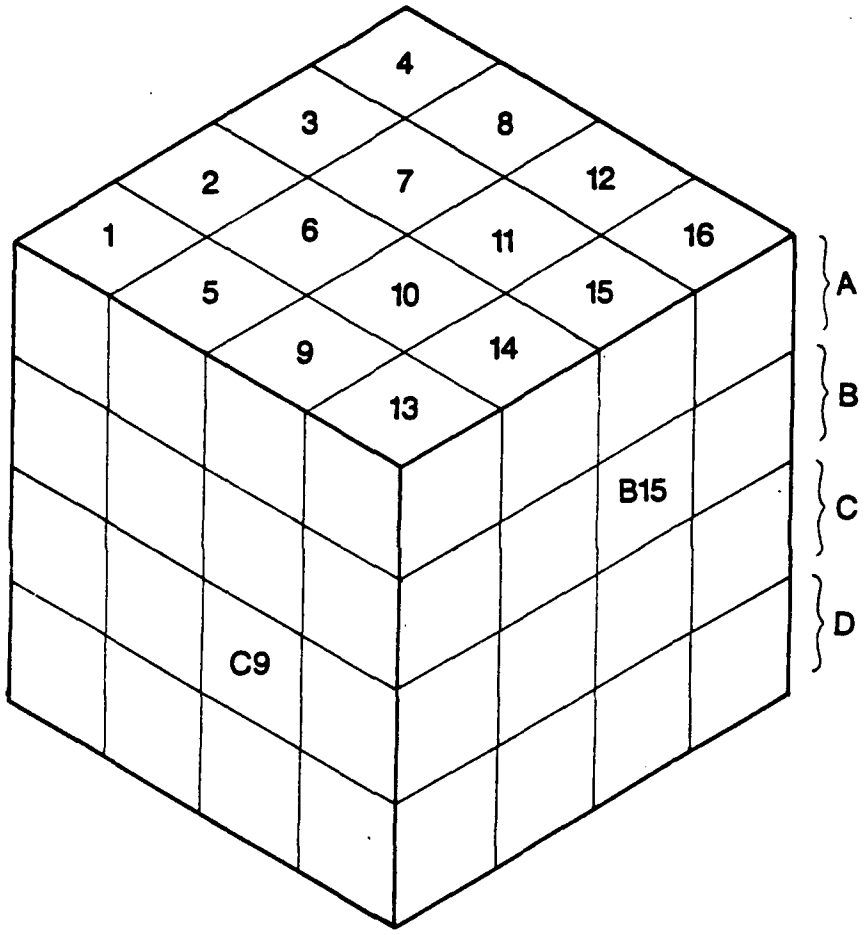

Fig. 3.12 Cubical Specimen for Water Content Determination

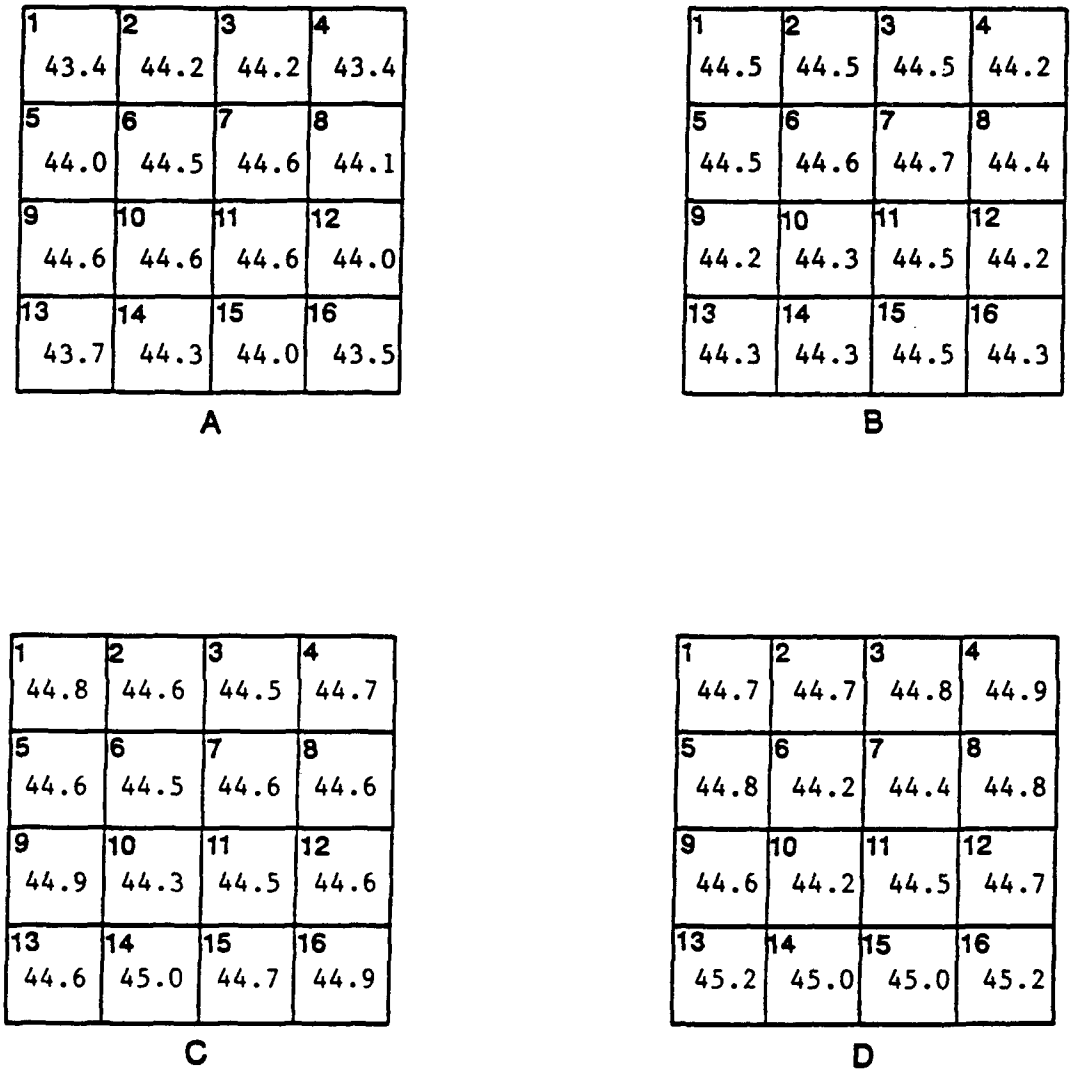

For Kaolin Soil After Slurry Consolidation of 17 psi

Fig. 3.13 Water Content Distribution within Cubical Specimen

water, and the pressure transducer is attached carefully without any air bubble entrapped. To minimize friction during the testing, silicone oil is applied to the space frame and to the membranes. A very small pressure is applied to the bottom membrane, just enough to carry the self weight of the sample and the teflon block. The sample is brought to the space frame with the teflon block and placed through the top opening. The teflon block is carefully slipped out and the sample adjusted exactly at the center. The bottom spaghetti tube is left beneath the sample at the center, and the top spaghetti tube is placed on the top center of the sample. These spaghetti tubes are used for flushing, back saturation, back pressurizing and for draining during the consolidation phase. The piezometer needle (attached with the pressure transducer) is inserted through a diagonal port in the bottom and guided to penetrate diagonally through the sample such that the tip reaches the center of the sample. All five sides of the specimen are covered by the membranes and the pressure casings are fixed tightly to hold the membranes in place. To measure the deformations, LVDTs had already been placed inside the casings and their positions adjusted according to the type of test to be run, in order to use their *maximum range*.

The ¼" stainless steel tubings are connected to the opposite pressure casings, and to the outlets of normally closed and normally opened solenoid valves. After all the connections were tightened, the computer program "stress.bas" (given in Appendix E) is loaded and executed, to measure the pressures and deformations and then to record the data.

In order to expel the air entrapped in between the sample and the membranes a small pressure of 5 psi is applied in all directions. The outlet tubing for flushing is kept in a beaker with water so that the expulsion of air can be monitored. After the air bubbles have stopped, the valve for back pressure saturation is opened and a small water pressure is applied through the burette. By closing and opening the flushing valve most of the air pockets are removed. Remaining air is dissolved in the water during the back pressure saturation stage. The all around pressures and the back pressure are increased

slowly and simultaneously by 5 psi. The sample is left for one day under that pressure (10 psi cell and 5 psi back pressure). The cell pressure and the back pressure are then increased to 30 psi and 25 psi, respectively, and left for another day. After checking the B-parameter, all pressures are increased by another 20 psi and kept for another day. The difference between the all around cell pressure and back pressure are always kept at 5 psi. The pressure increments are applied steadily and slowly at about 2 psi per minute, allowing enough time for pore pressure to stabilize and not allowing to prestress the sample during the saturation. The applied back pressure is maintained throughout the whole testing procedure. At the end of saturation, B-values were found greater than 0.98 in all tests.

3.8 1-D Consolidation in the Cuboidal Shear Device

Although the data in Fig. 3.13 indicate that uniform specimens are obtained (moisture content variation of less than 0.8% from the mean) by minimizing friction in the lower chamber where the specimen is consolidated, the disturbance during the leveling, extruding, handling during transferring and placing could have some effect on the specimen. To overcome this, after ensuring saturation the specimen was consolidated one dimensionally using the flexible membrane boundaries and the servo controlled system to higher stresses (55 psi vertical and about 35 psi horizontal) than subjected during slurry consolidation. It has been shown (Sivakugan, 1987) that after such consolidation in the CSD, uniformity of water content throughout the specimen had improved to $\pm 0.5\%$ of the mean.

One dimensional consolidation in the cuboidal shear device is achieved by increasing simultaneously to 100 psi all the pressures in all three directions, keeping the same back pressure of 45 psi at the end of saturation phase with the drainage valve closed. Since the B-parameter was close to 1.0, the pore pressure has to increase by the same amount (i.e. by 50 psi, to 95 psi). The pore pressure dropped by 2 to 3 psi and remained constant after 10 minutes. After the pore pressure is stabilized, the drainage

valve is opened and the sample allowed to consolidate one-dimensionally by decreasing the lateral stresses through the servo-controlled system maintaining very little deformations in lateral directions. The flow chart for the servo controlled one dimensional (K_o) consolidation is given in Fig. 3.14. A tolerance of 0.0005 inch is permitted for the zero lateral deformations. Eighty percent of the primary consolidation was basically over within 80 minutes in all tests. This is apparent from the typical pore pressure vs time curves and settlement vs time curves for kaolin and kaolin-silica mix in Figs. 3.15 to 3.18. The primary consolidation was completely over within 24 hours. The main reason for the fast consolidation is the shorter drainage path provided by the filter papers surrounded all six sides.

3.9 Stress Controlled and Strain Controlled Tests

One of the main advantages of the cuboidal shear test is the ability of achieving any kind of stress/strain path. All three stresses can be applied independently, and combined with the servo-controlled system it is possible to perform both stress controlled and strain controlled tests. The one dimensional (K_o) consolidation test CSD is a typical example of a strain controlled test, with the lateral strains maintained at zero.

The flexible membrane boundary condition is ideal for applying uniform stress on to the specimen. In the CSD, air pressures can be directly applied to the membranes and controlled through the regulators and thus stress controlled tests can be easily performed. On the other hand strain controlled tests can be executed directly by rigid platen at the expense of non uniform stress distribution. In the CSD, strain controlled condition is achieved indirectly with the aid of the servo-controlled system. A small pressure increment is applied and the deformation is measured and checked against the condition given. If the deformation is found higher than the required value, the pressure is decreased using normally closed solenoid valve, and if it is less than the required, an additional pressure increment can be applied through the normally opened solenoid valve. The response is immediately checked again and readjustments made. This iteration

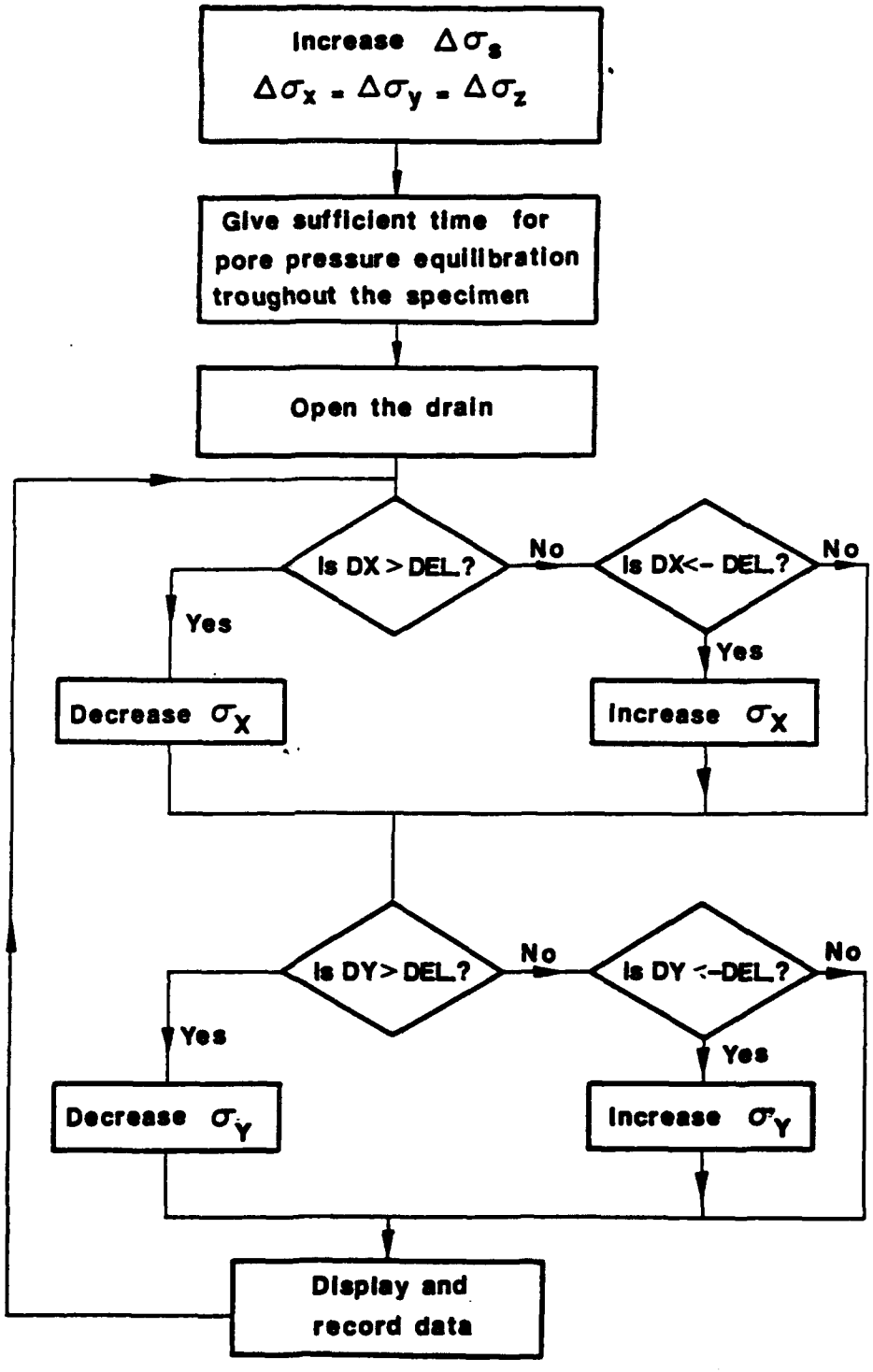

Fig. 3.14 Flow Chart for K_o-Consolidation

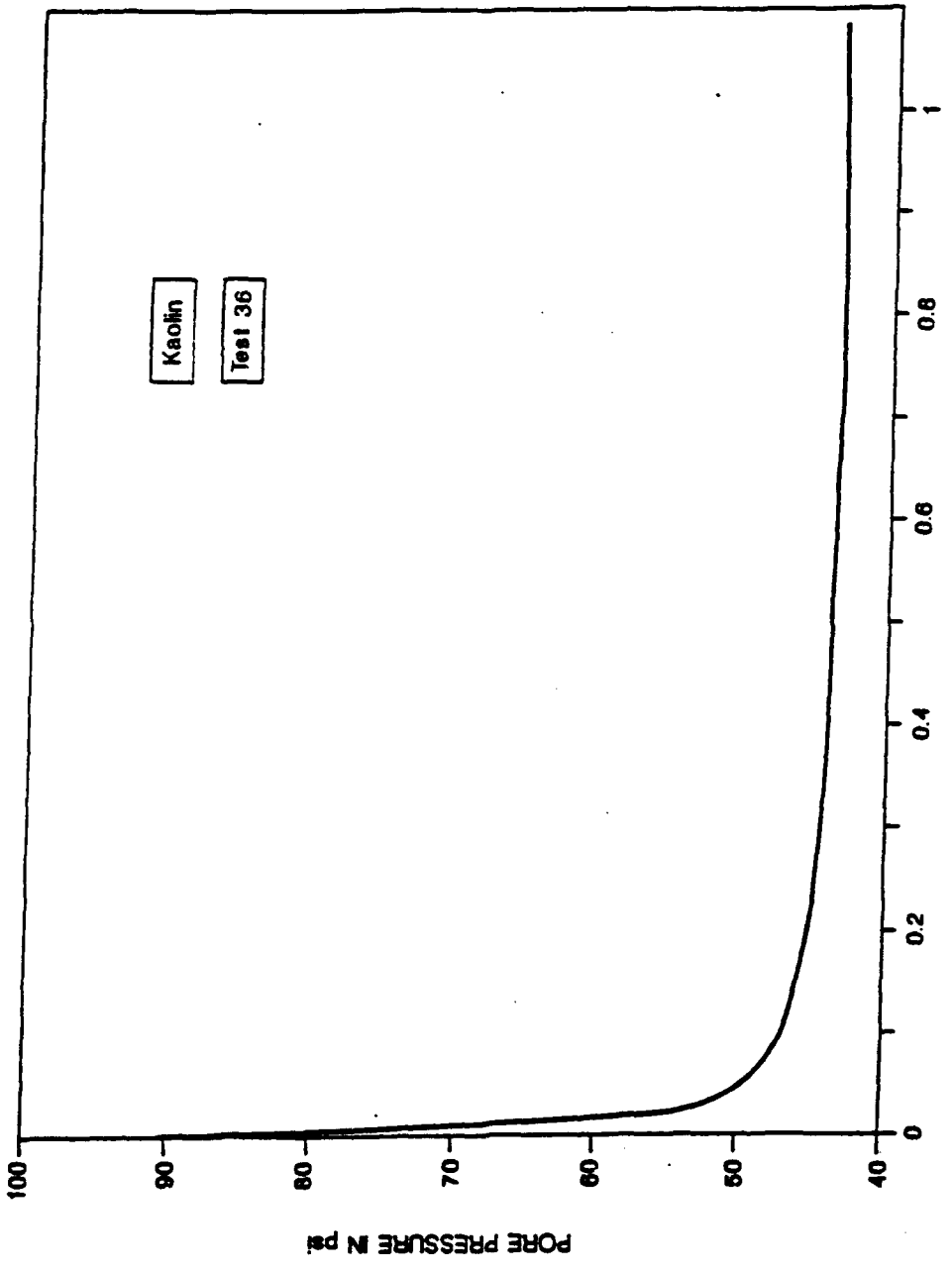

Fig. 3.15 A Typical Pore Pressure Versus Time Curve for Kaolin During 1-D Consolidation

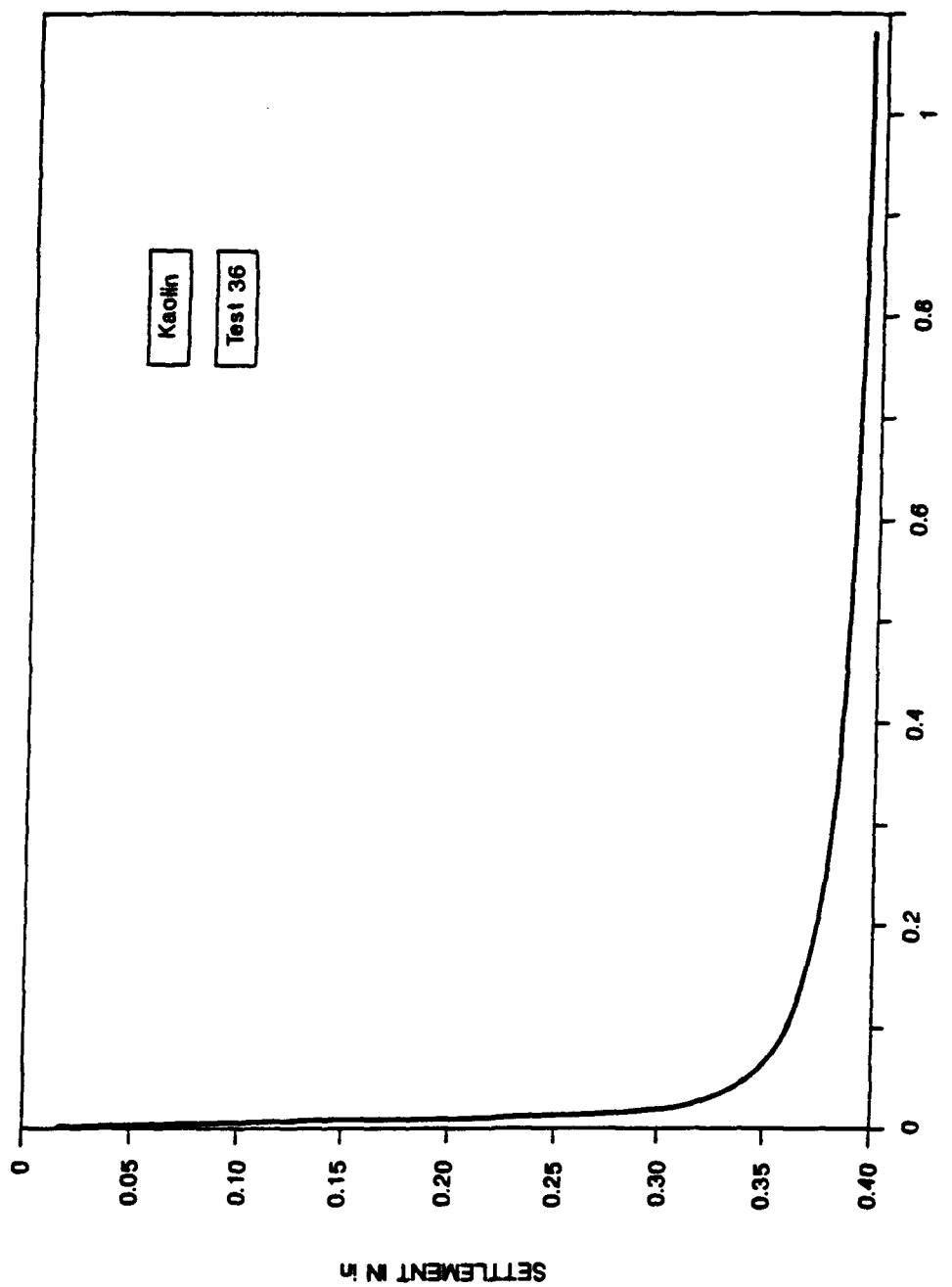

Fig. 3.16 A Typical Settlement Versus Time Curve for Kaolin During 1-D Consolidation

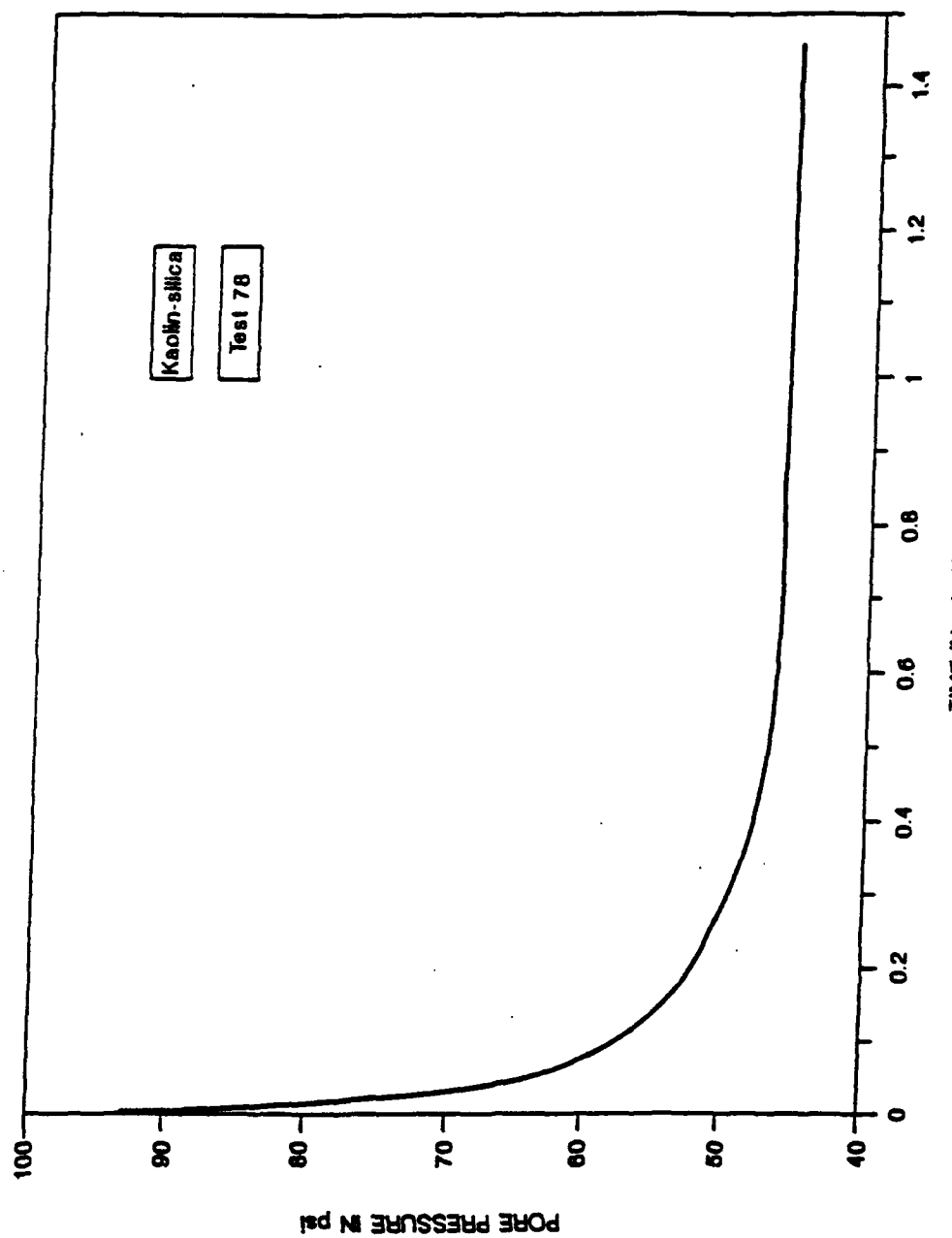

Fig. 3.17 A Typical Pore Pressure Versus Time Curve for Kaolin-Silica During 1-D Consolidation

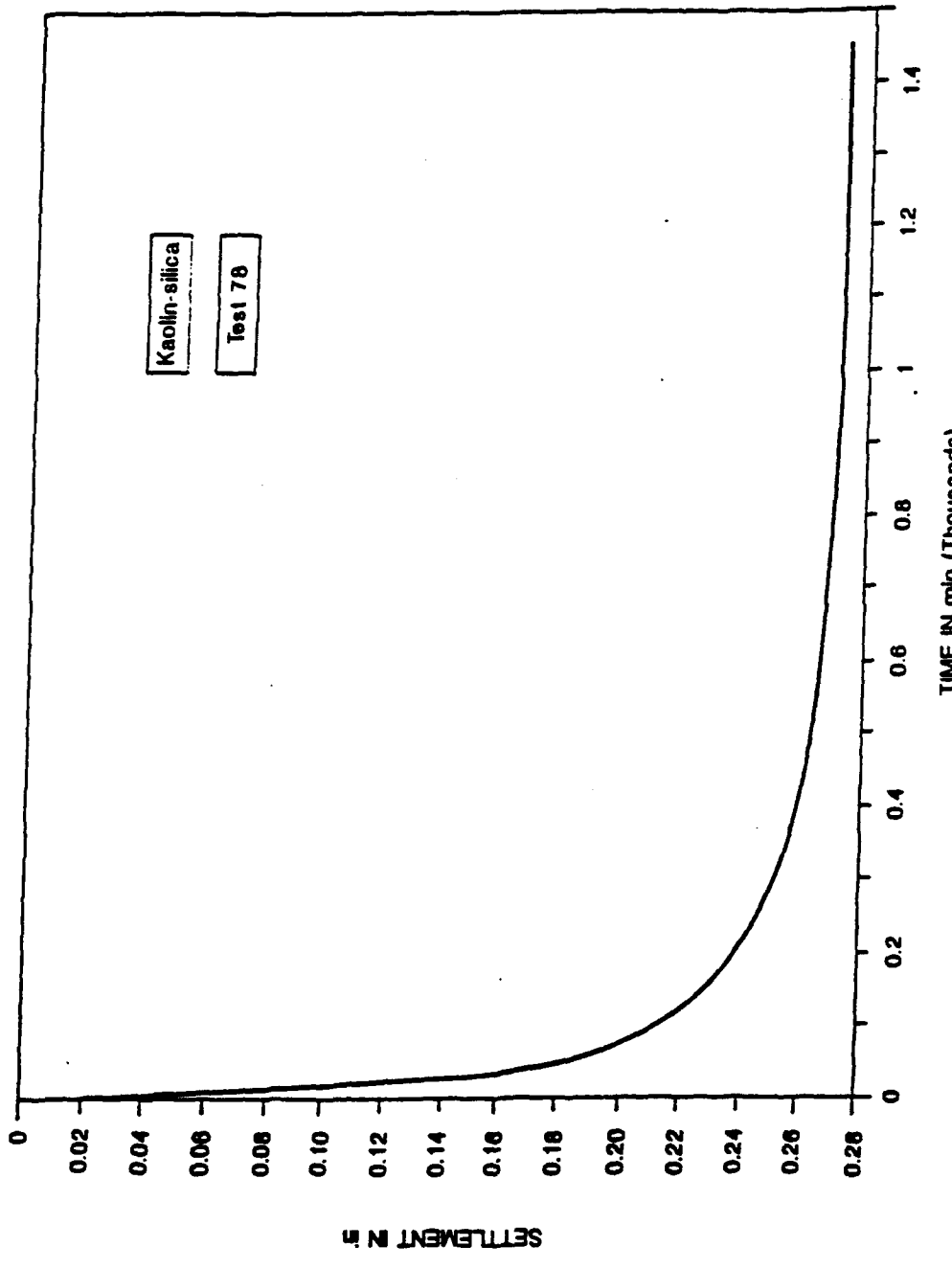

Fig. 3.18 A Typical Settlement Versus Time Curve for Kaolin-Silica During 1-D Consolidation

process continues until the required condition is achieved, and can be independently and simultaneously performed for all three directions. A flow chart for strain controlled loading is shown in Fig. 3.19.

For example, to perform tests under various strain rates, the deformation measured is divided by the time interval and checked with the prescribed strain rate and the iteration continues until both strain rates are equal. To achieve plane strain condition and K_o consolidation the strain is maintained to zero using the same above procedure.

The speed of the data acquisition was increased by several fold by using Turbo Basic compiler and the compiled version of the coupled program.

3.10 Summary

The servo-controlled cuboidal device is an inexpensive but well versatile equipment in which almost any stress path can be achieved. With the flexible boundary loading and minimized friction between the membrane and frame using silicone oil, a uniform principal stress can be applied. The boundary conditions are well defined and the pressure and deformation measurements are obtained accurately and quickly. Using the servo-control system, accurate K_o consolidation, strain controlled loading and any type of stress path tests can be performed in the cuboidal shear device.

Exactly same procedures were adopted to prepare the test specimen, to make sure that the different results obtained were only due to the variation in the test procedures. The uniformity of the specimen was verified by the moisture content profile (indirect measurement of void ratio) after the slurry consolidation and before performing pressuremeter test. The variation of the moisture content improved from $\pm 0.8\%$ of the mean after the slurry consolidation to $\pm 0.5\%$ of the mean after reconsolidation in the CSD. This moisture content variation is so small and it can be assumed that the specimen preparation method is satisfactory and it yields uniform samples.

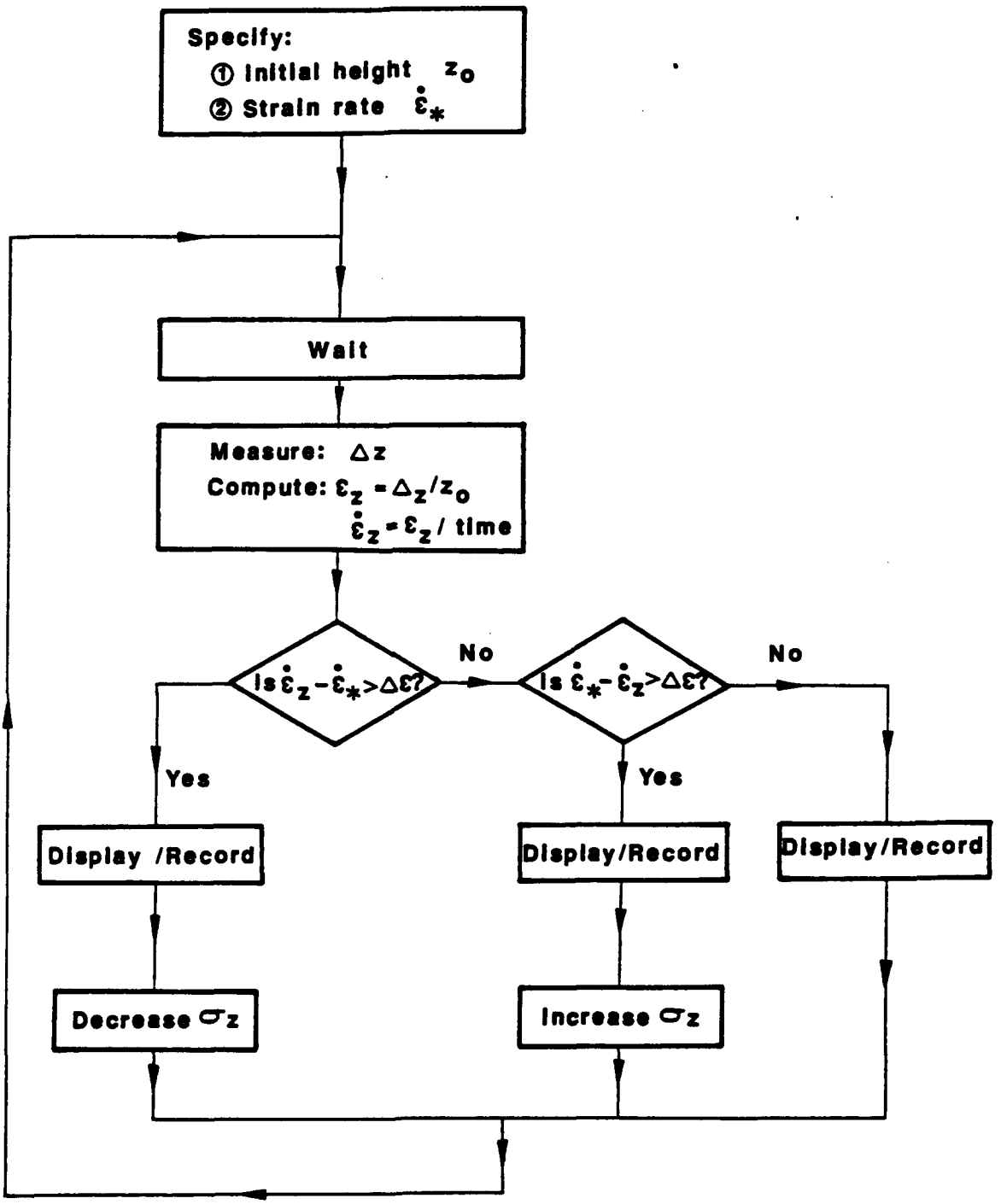

Fig. 3.19 Flow Chart for Strain Controlled Test (After Sivakugan et al., 1988)

CHAPTER 4

STRAIN RATE EFFECTS ON PRESSUREMETER TESTING

4.1 Introduction

Even though the shear strength of a soil can be interpreted from a pressuremeter test, one can not expect the same value from a triaxial test because the tests follow different stress paths. The pressuremeter consistently yields high undrained shear strength, as high as 100% more than the triaxial test. This difference was attributed to the speed of the test, because the strain rate in the pressuremeter (about 1%/min) is about 100 times higher than the strain rate in conventional triaxial tests (about 0.01%/min). However, stress path effects also contribute to these differences.

The influence of the strain rate in triaxial testing has been thoroughly studied, however only a few experiments have been performed to study strain rate effects in pressuremeter tests, and they were nonconclusive. Therefore, this study was undertaken to quantify strain rate effects in pressuremeter testing.

4.2 Effect of Rate of Strain in Triaxial Tests

Shear strength and deformation behavior of clays are time dependent. Several researchers (e.g., Casagrande and Wilson, 1951; Crawford, 1959; Perloff and Osterberg, 1963; Richardson and Whitman, 1963) have shown that the undrained shear strength determined from laboratory tests depends on the speed of testing. From the undrained triaxial compression tests on the plastic clay from Drummen (Norway), Bjerrum (1972)

concluded that the shear strength was increasing about 10% for every ten fold increase of strain rate.

Vaid and Campanella (1977) performed conventional constant rate of strain shear, constant stress creep and various other tests on a local undisturbed clay (called Haney clay). Their tests showed a linear increase in undrained shear strength with the log of strain rate in the higher strain rate regions. However, in the lower strain rate domain, the undrained strength reached a limit (called upper yield), and a further reduction in rate did not result in additional loss of strength. On the other hand, Bjerrum's test results did not show this upper yield limit although his lowest strain rate is less than that of Vaid and Campanella.

Nakase and Kamei (1986) investigated the influence of strain rate on undrained shear characteristics of K_o-consolidated cohesive soils by performing triaxial compression and extension tests. They used Kawasaki clay (PI = 30) and two reconstituted soils of Toyura sand and Kawasaki clay with PI of 15 and 10. Prapaharan et al. (1989) combined all the above results and plotted them together using shear stress at a strain rate 0.01% as the normalized value (Fig. 4.1). The upper yield strength was assumed to occur at a strain rate of 0.001%/min and after that the shear strength increases by 8-10% for a tenfold increase in strain rate. All these results were based on conventional triaxial tests performed on various types of soils.

4.3 Effect of Rate of Strain in Pressuremeter Test

The strain rate used in the pressuremeter test is commonly one to two orders of magnitude larger than that used in laboratory tests. Furthermore the strain rate varies inversely with the square of the radius in the soil mass around the probe during the test (Wroth, 1975).

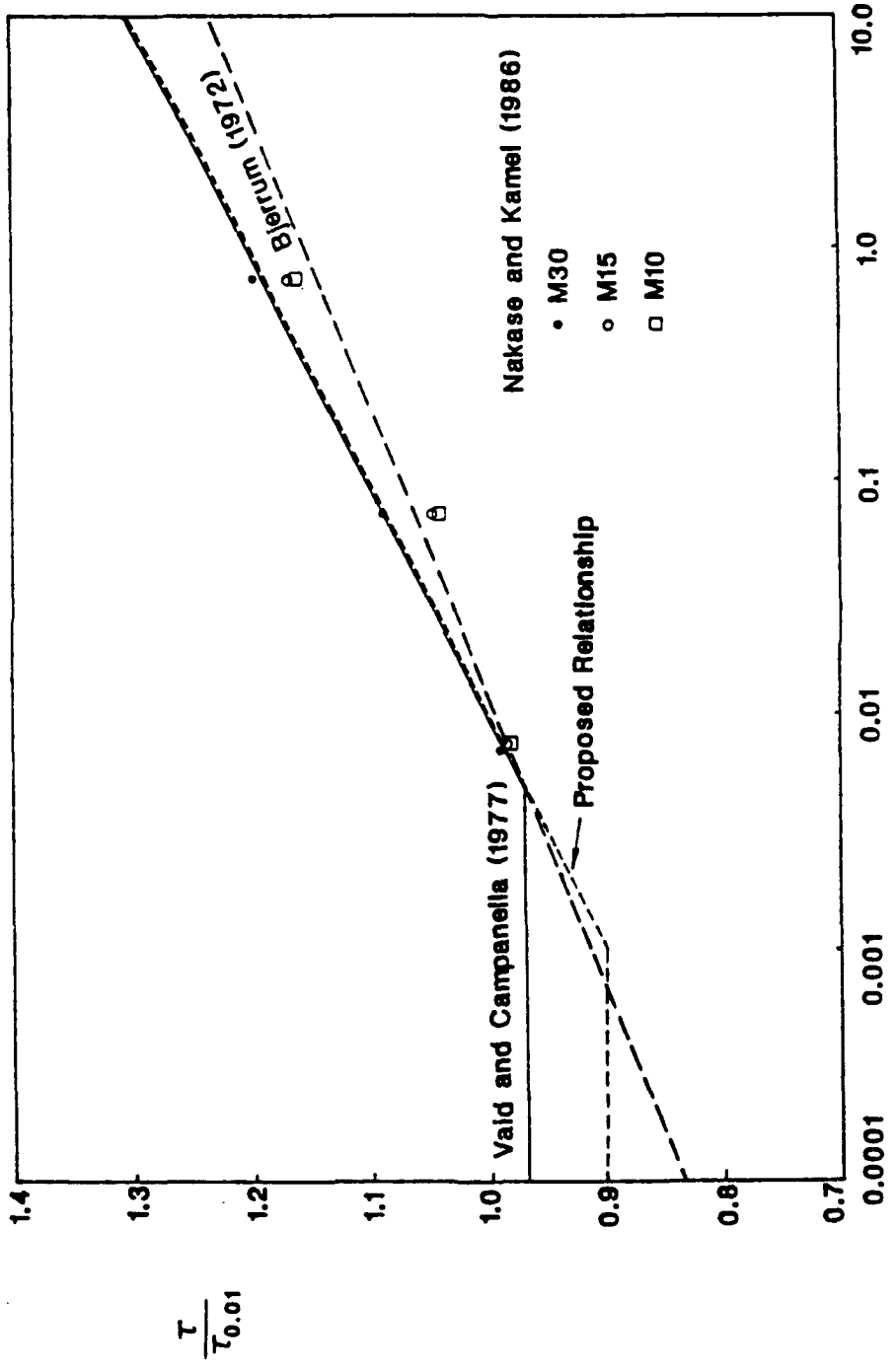

Fig. 4.1 Normalized Shear Strength Versus Strain Rate from Triaxial Tests (After Prapaharan et al., 1989)

There are basically three types of pressuremeters available: (1) pressuremeters used in pre-drilled borehole, e.g., Menard pressuremeter, Lateral Load Tester (LLT), Elastmeter 100, and TEXAM pressuremeter (Briaud et al., 1986); (2) self boring pressuremeters, e.g., PAF (Jazequel, 1982), Camkometer (Wroth and Hughes, 1973), Offshore pressuremeters such as Push in Pressuremeter (PIP) (Fyffe et al., 1986), and PAM (Brucy and LeTirant, 1986); and (3) displacement type such as full-displacement pressuremeter (Hughes and Robertson, 1985) and cone pressuremeter (Withers et al., 1986 and 1989). Generally the pre-drilled pressuremeter tests are stress controlled tests where the pressure is applied in increments, each increment being held for a specified period of time. During this holding time some consolidation and creep will inevitably occur around the expanding probe. The assumption of undrained behavior, therefore, is questionable.

Winter (1982) suggested a procedure for pre-drilled pressuremeter testing in both granular and cohesive soils. It recommends to apply pressure in equal steps until the expansion of the probe during one load increment exceeds about one fourth of the original probe volume (typically 200 cm^3 for a 800 cm^3 probe). The load increments should be selected in such a manner that about ten load increments are required to reach the maximum loading. Generally, 20-, 50-, 100-, or 200-kPa pressure steps are used. The volumetric readings are taken 15, 30, and 60 seconds after the load is applied. This practice is followed in order to take care of creep effects and to dissipate the pore pressures generated due to the probe expansion.

Briaud et al. (1986) suggest both pressure and volume controlled tests, either increasing the probe pressure or its volume in equal increments. From field tests, they found that the recommended pressure and volume increment procedures could be used interchangeably. The test should be performed by doubling the initial size of the probe in 10 minutes. There are merits and drawbacks to both the pressure and volume increment procedures. The disadvantage of the pressure increment procedure is that the limit pressure p_L must be estimated before running the test, on the other hand this is the

advantage of the volume increment procedure where no estimate of p_L is required. The disadvantage of the volume increment procedure is that, if the volume increments are not small enough, the modulus part of the curve may not be defined by enough points. This is the merit of the pressure increment procedure where the modulus is well defined. Considering these aspects, Briaud et al. (1986) recommended ten one minute increments equal to $p_L/10$ for the pressure increment procedure, and forty 15 seconds increments equal to $V_o/40$ for the volume increment procedure where V_o is the deflated volume of the probe.

The effects of consolidation and creep on stress controlled pressuremeter tests have been studied experimentally and numerically by Pyrah et al. (1985) and Anderson et al. (1987). They performed undrained pressuremeter tests in a modified triaxial cell so that hollow cylindrical specimens 150 mm OD and 150 mm high with a 25 mm diameter cylindrical cavity (Fig. 4.2) could be subjected to internal pressure increments simulating expansion of a borehole during a pressuremeter test. The numerical study used the finite element program CAMFE (Carter, 1978), based on a Biot type consolidation and the modified cam clay model with solutions obtained from an incremental, time-marching technique that can deal with both material and finite deformation nonlinearity.

These studies showed that the effect of both consolidation and creep is to reduce the deduced modulus values, but that the consolidation around the probe tends to produce higher deduced undrained shear strengths, while creep tends to have the opposite effect, i.e. give a lower deduced strength. Soil parameters derived from a stress-controlled test are thus dependent on the relative effect of consolidation and creep, and for stress-controlled tests the effect of creep appears to be more critical.

Generally the self boring type pressuremeter tests are performed by increasing the probe volume at a constant rate of volume increase, thus they are strain controlled tests. Pyrah et al. (1988) and Huang et al. (1991) have studied strain controlled pressuremeter

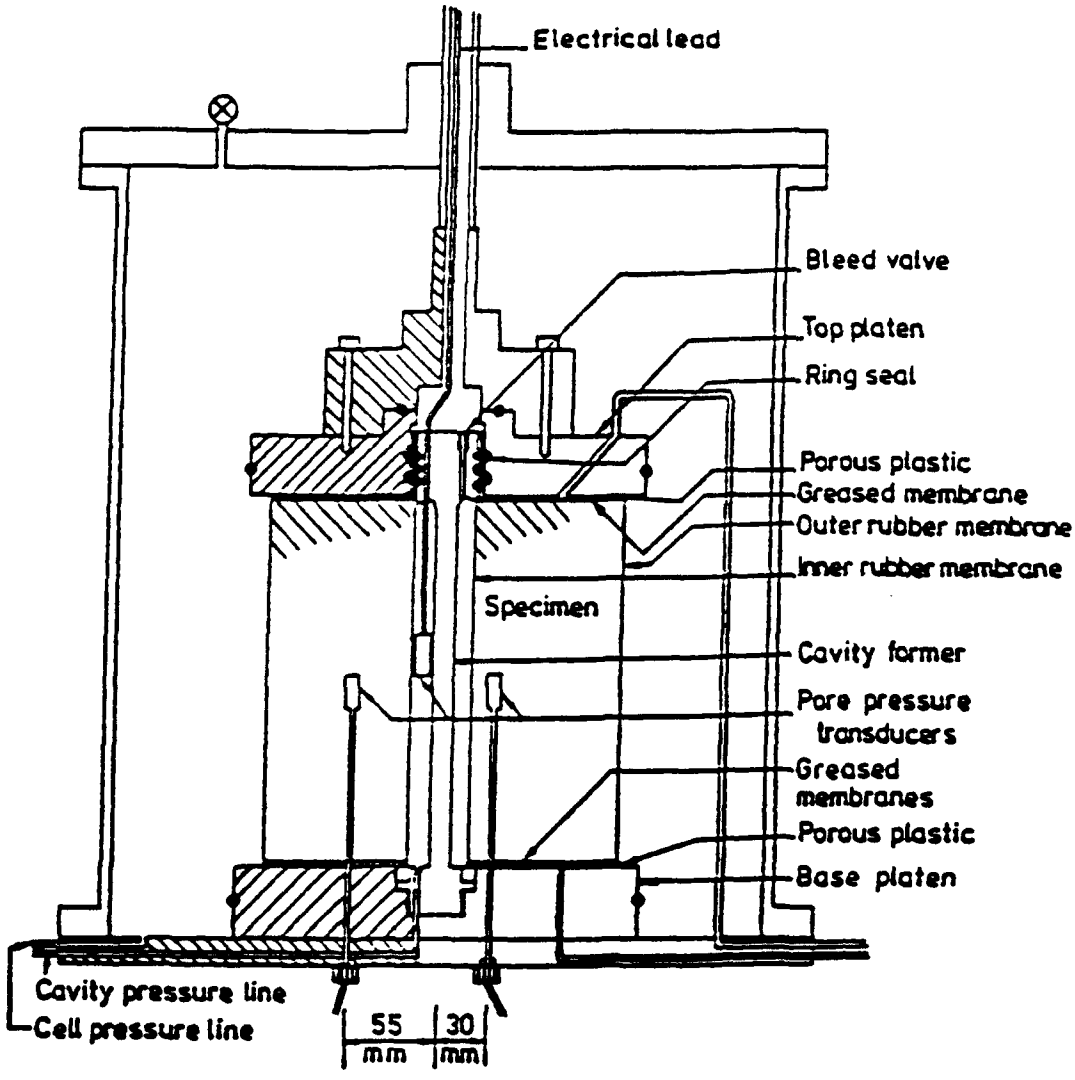

Fig. 4.2 Cross-Section of Hollow Cylinder Triaxial Apparatus (After Anderson et al., 1987)

tests. Similar to the stress controlled tests, Pyrah and Anderson simulated the strain controlled pressuremeter test in the modified triaxial apparatus using hollow cylindrical samples (Fig. 4.2). They carried out series of tests on two clays (kaolin and pottery clay) with radial strain rates ranging from 0.2% to 4.0% per minute. The creep effects were studied incorporating Singh and Mitchell (1968) creep model into the CAMFE program. The strain controlled test was simulated by adopting displacement defined type of loading at the inner boundary. Constant stress was assumed at the outer boundary simulating the in situ horizontal stress in a pressuremeter test. The numerical simulations using CAMFE were performed for strain rates ranging from 0.2% to 4.0% per minute, and maximum expansion of the cavity was taken as 20% radial strain.

By considering consolidation as the sole time-dependent phenomenon in the analysis (consolidation only), the simulated expansion curves for tests at different strain rates are shown in Fig. 4.3. For comparison purposes, Pyrah et al. (1988) simulated an undrained test using a very fast strain rate (40% per minute) with little time allowed for consolidation. It can be noticed from the curves that the slower strain rate tests show higher limit pressure which could be the result of consolidation taken place and subsequent strength gain of the soil around the cavity. Pyrah et al. used Palmer (1972) method to generate stress-strain curves from the expansion curves. The derived stress-strain curves for different strain rates are shown in Fig. 4.4. As expected the faster rate tests gave higher strength at the beginning but the slower rate tests gained strength with strain (i.e. with duration) due to consolidation. Faster strain rate tests show significant amount of strain softening.

With creep also included in the analysis (consolidation and creep), the simulated expansion curves and the interpreted stress-strain curves are shown in Figs. 4.5 and 4.6. These curves clearly show that the strength values increase with the strain rate. From this comparison (consolidation alone and consolidation with creep), creep phenomenon is the main factor to yield smaller strength values at lower strain rates.

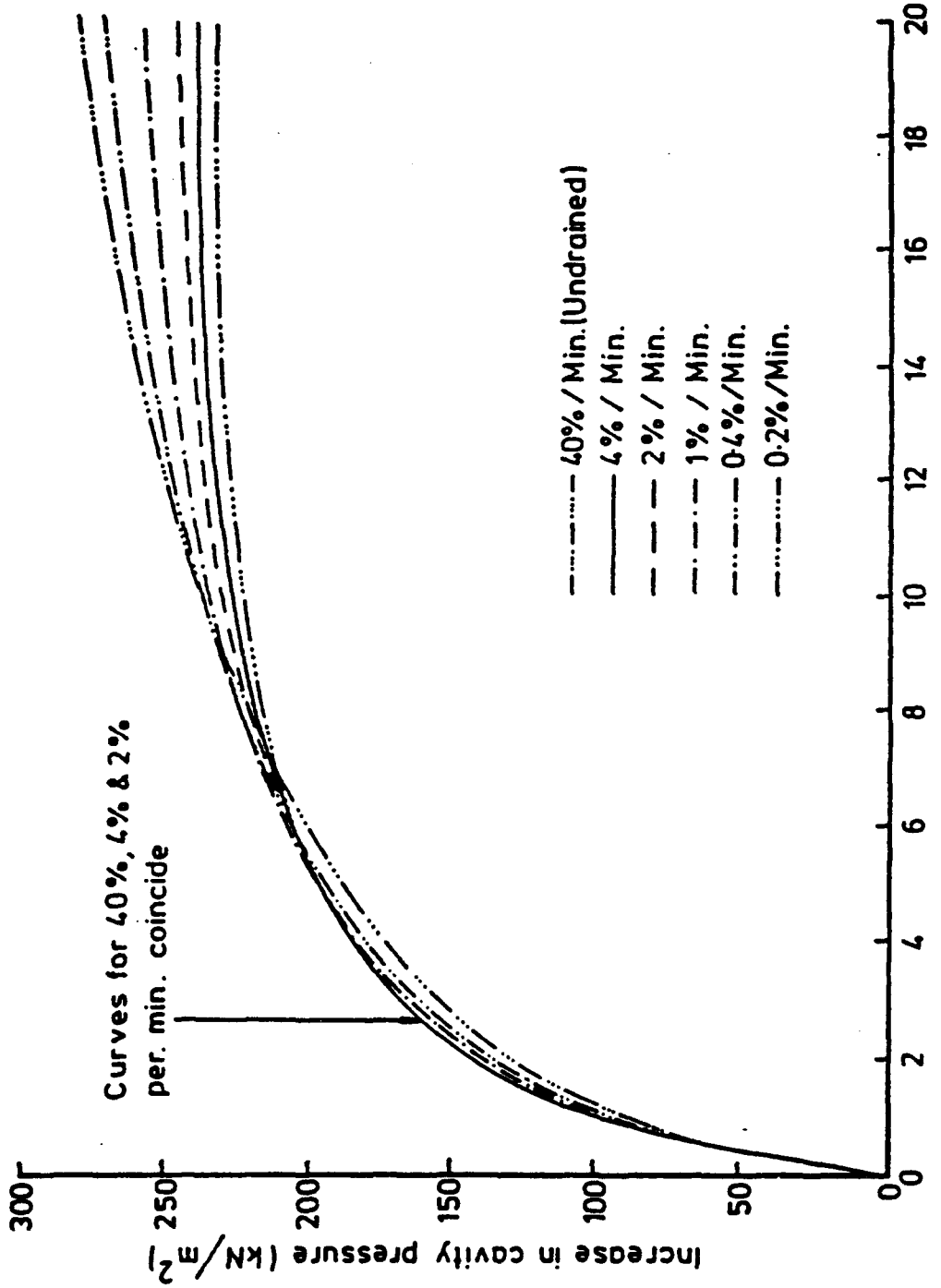

Fig. 4.3 Simulated Expansion Curves for Different Rates of Strain (Consolidation Only) (After Pyrah et al., 1988)

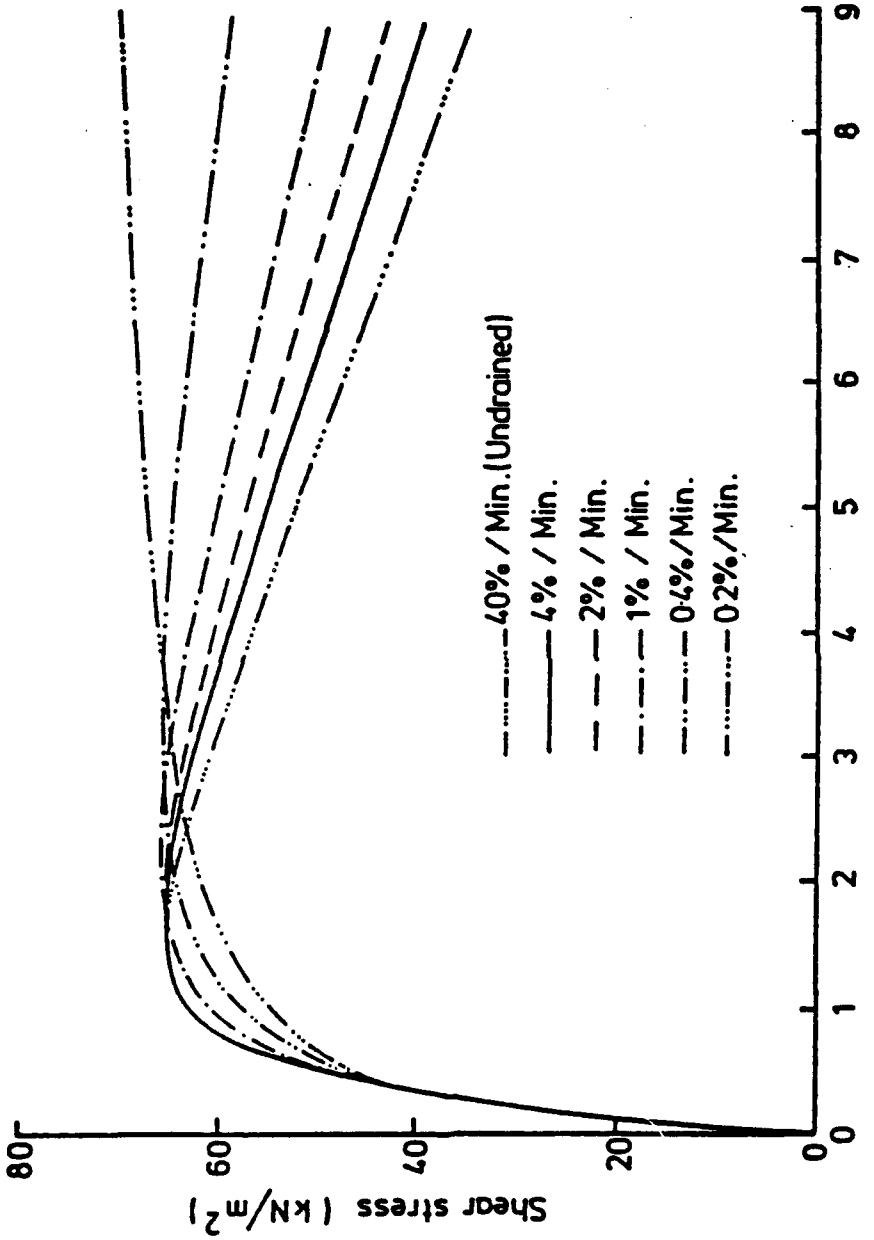

Fig. 4.4 Derived Stress-Strain Curves for Different Rates of Strain (Consolidation Only) (After Pyrah et al., 1988)

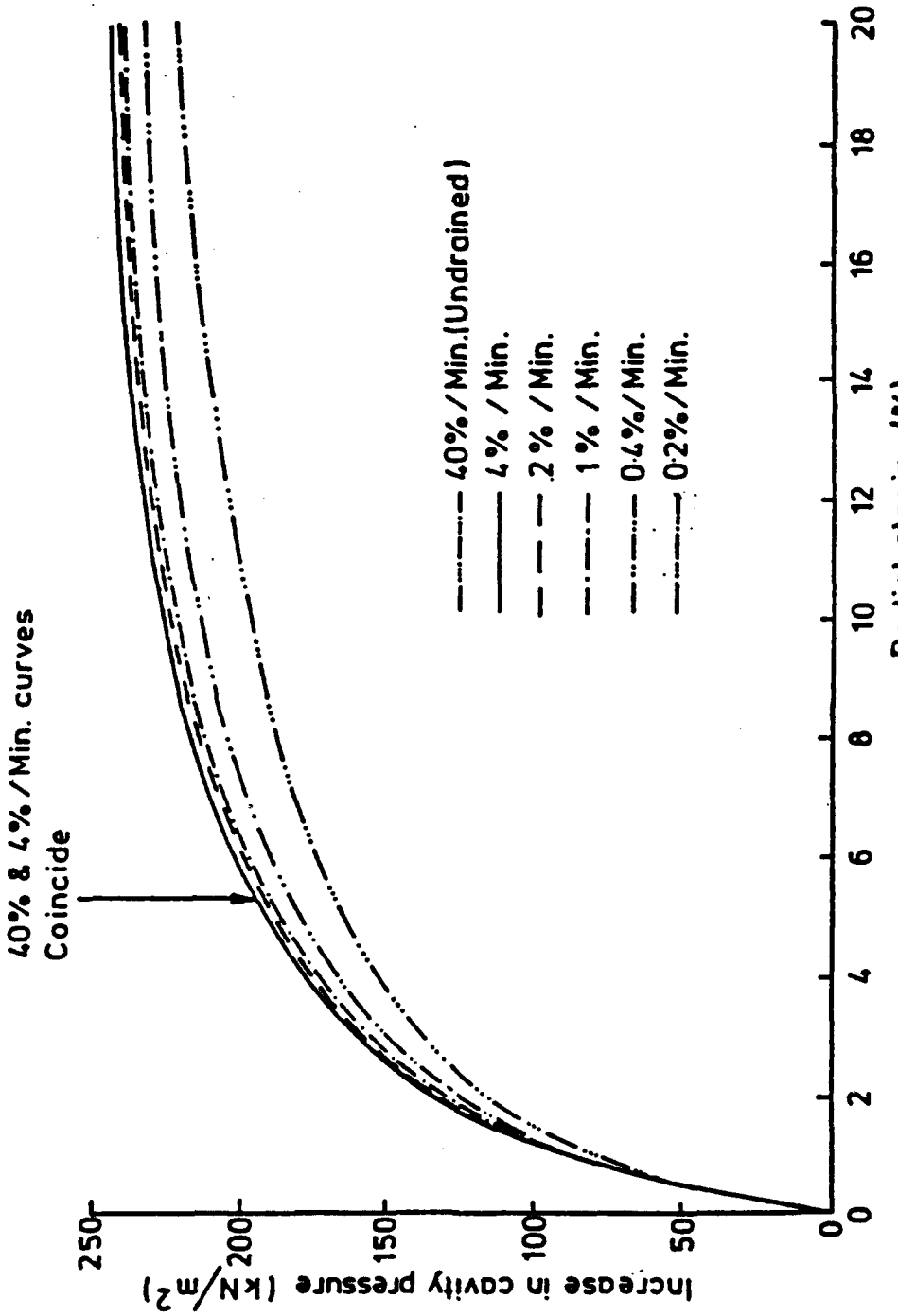

Fig. 4.5 Simulated Expansion Curves for Different Rates of Strain (Consolidation and Creep) (After Pyrah et al., 1988)

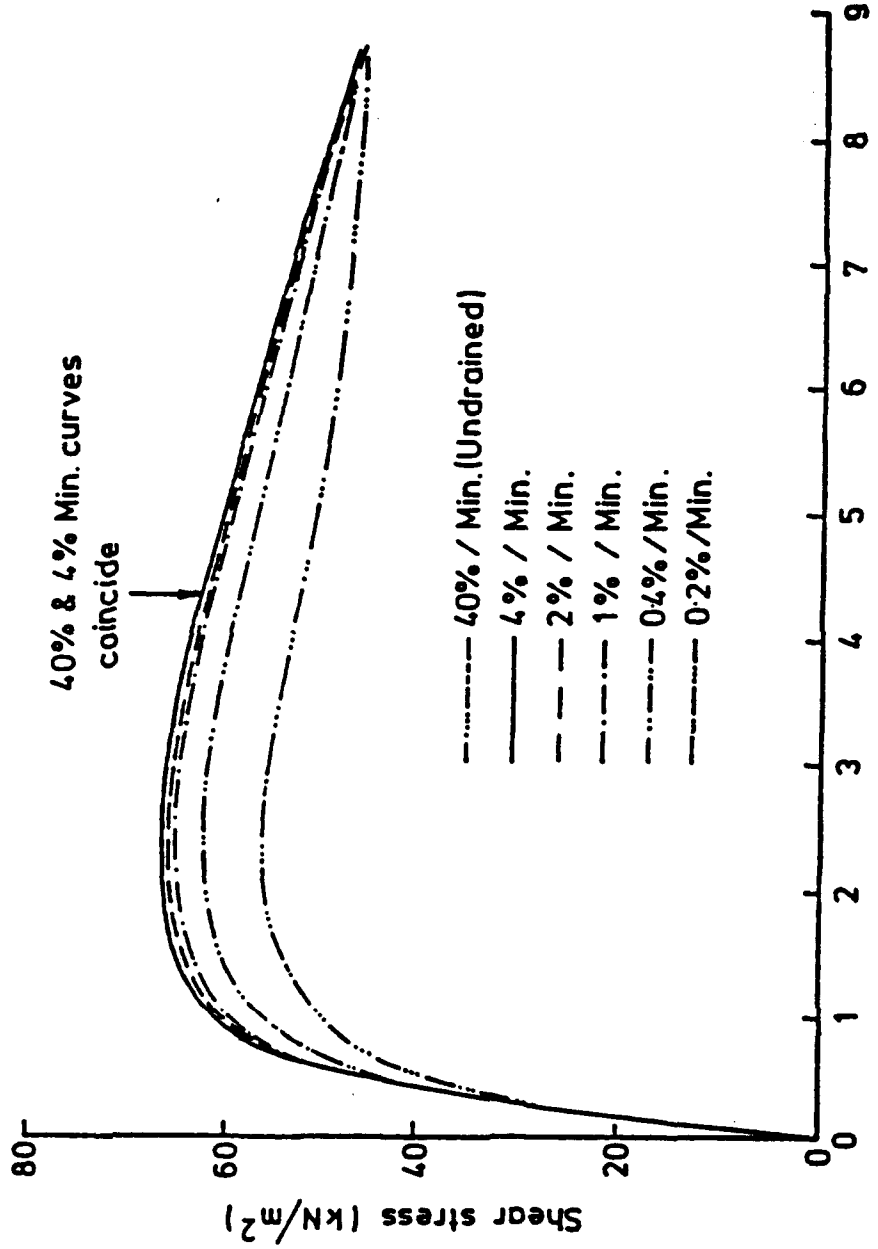

Fig. 4.6 Derived Stress-Strain Curves for Different Rates of Strain (Consolidation and Creep) (After Pyrah et al., 1988)

Unfortunately, the laboratory tests (Fig. 4.7) conducted by Pyrah et al. (1988) did not support the results of numerical simulation. With the exception of the fastest test (4% per minute), which gives the highest strength at the beginning, the other tests show a very irregular pattern. This erratic behavior can be due to the experimental procedure such as the possibility of partial drainage. Pyrah et al. concluded that creep is the more significant time-dependent phenomenon in stress controlled test, while it is of minor importance in a strain controlled test creep is where consolidation is predominant. However, the numerical studies and the triaxial test results (Section 4.2) contradict their conclusion.

The only other experimental study on strain rate effect on pressuremeter test by strain controlled method was carried out by Huang (1986) and Huang et al. (1991). Huang performed a series of strain-controlled model pressuremeter tests in cohesive soils inside a calibration chamber to study the strain rate effects on pressuremeter expansion curve and on derived shear strength. The strain-controlled pressuremeter tests were performed with radial strain rates of 0.1% to 4.4% per minute. Two types of soils namely, kaolinite (K100) and kaolinite and silt mixture (K50) were used in the calibration chamber test. A typical comparison of the expansion curves (i.e. probe pressure, P_r, versus radial strain, ϵ_r) and the deduced principal stress differences (σ_r-σ_θ) for normally consolidated K50 soil are shown in Fig. 4.8 and 4.9, respectively. A summary of the derived parameters for all the strain rate tests is given in Table 4.1. The results indicate that for normally consolidated clays (Fig. 4.8) the initial shear modulus, G_i, increased approximately five times as strain rates varied from 0.75% to 4.4% per minute. The change in G_i for tests in over- consolidated clays was insignificant (Table 4.1). The data further indicated the limit pressure P_L is relatively insensitive to the strain rate.

The numerical studies performed by Anderson, Pyrah and their co-workers and the influence of strain rate in strength measurement by triaxial tests (Section 4.2) suggest that the shear strength (peak) increases with the strain rate. However, similar to Pyrah et al.'s (1988) experiments, Huang's (1986) experiments did not show an increase in

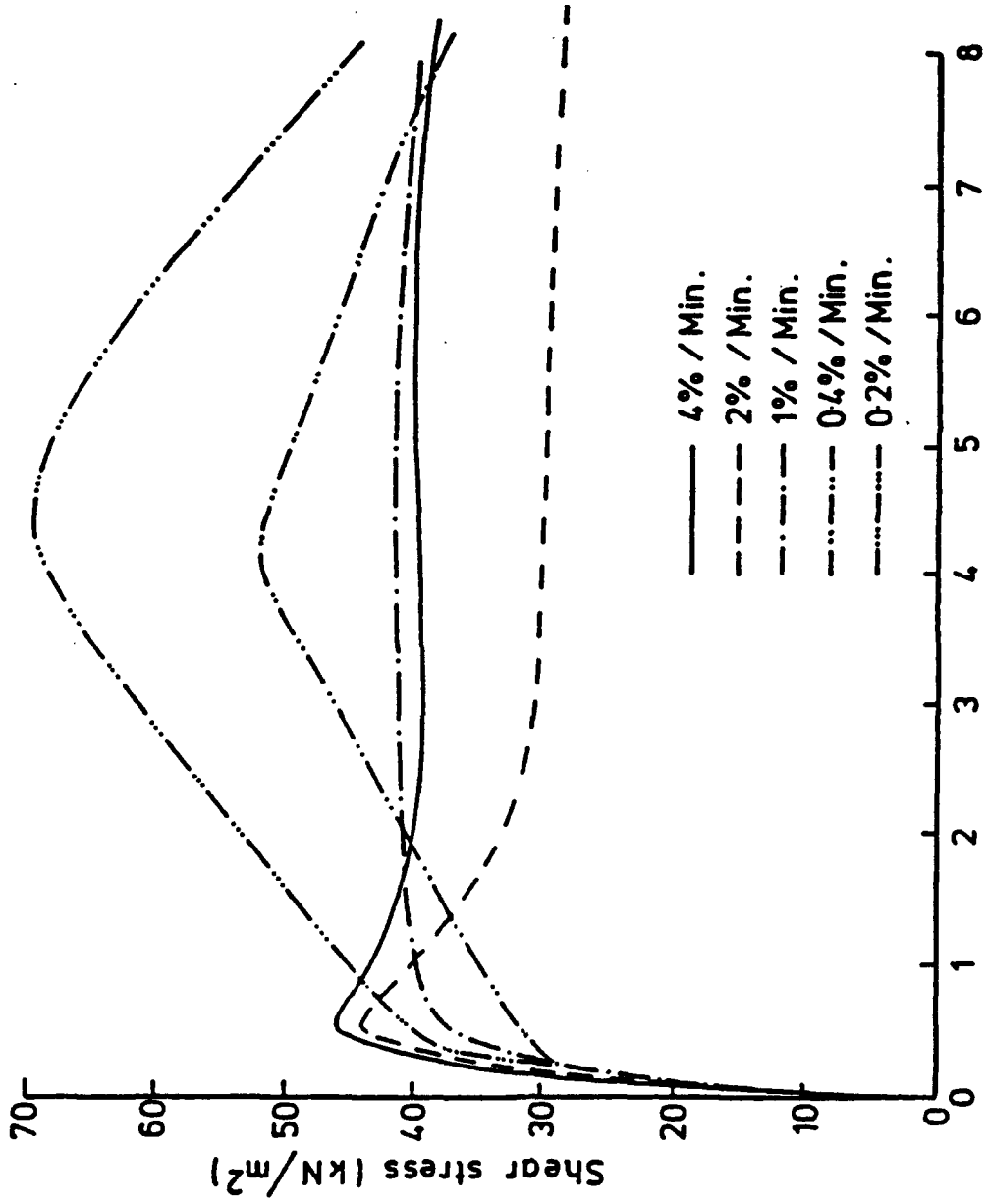

Fig. 4.7 Derived Stress-Strain Curves from Laboratory Hollow Cylinder Tests (After Pyrah et al., 1988)

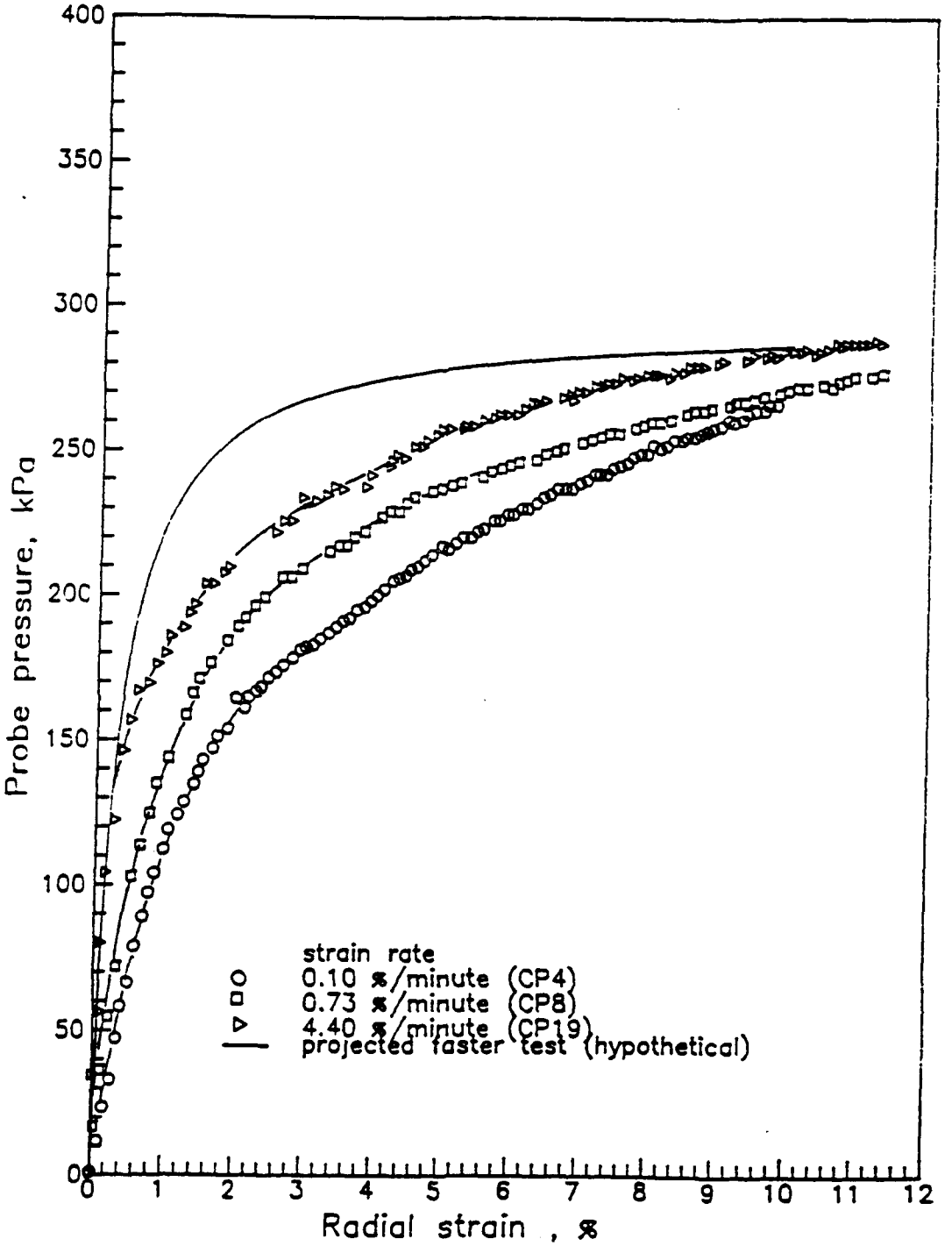

Fig. 4.8 Perfect Pressuremeter Tests in N.C. K50 Soil (After Huang et al., 1991)

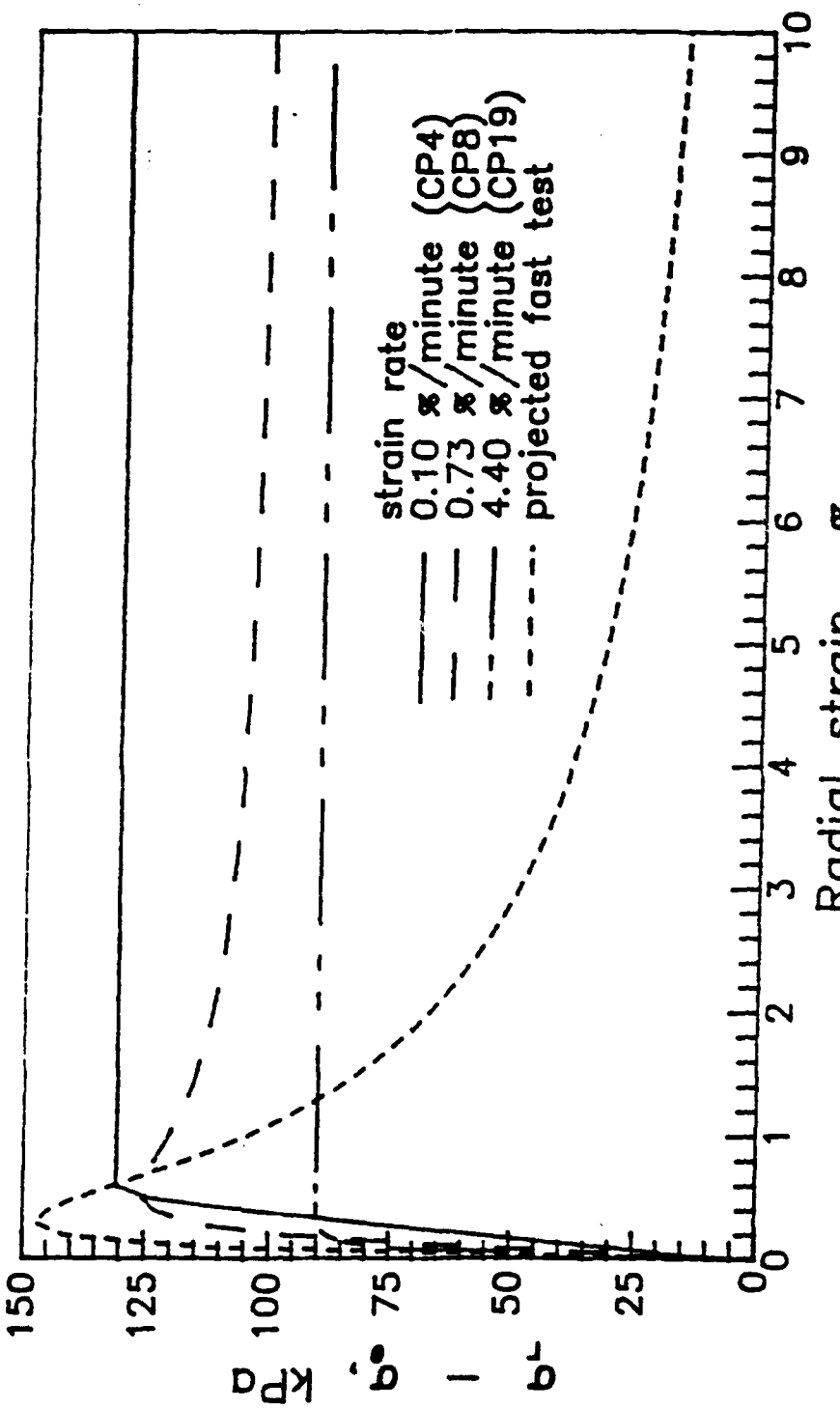

Fig. 4.9 Simplex Interpretation of Tests in N.C. K50 Soil (After Huang et al., 1991)

TABLE 4.1 Interpretation of Perfect PMT with Variable Strain Rates (Huang et al., 1991)

Test number	Soil type	Over Consolidation Ratio	Strain rate (%/min)	S_u^{PMT} (kPa)	G_i (MPa)	E_u^{PMT}/S_u^{PMT}	P_L (kPa)	ϵ_{rf}
CP4	K50	1	0.10	65	7.5	346	260	0.53
CP8	K50	1	0.73	63	20.1	957	260	0.54
CP19	K50	1	4.40	45	112.0	7,476	280	0.54
CP6	K100	1	0.73	62	13.2	639	280	0.82
CP18	K100	1	4.40	43	55.0	3,837	260	0.25
CP23	K50	10	0.73	46	14.0	913	230	-
CP25	K50	10	4.40	42	17.7	1,264	230	-
CP16	K100	10	0.73	41	11.0	805	210	0.22
CP20	K100	10	4.40	54	25.0	1,388	200	0.87

undrained shear strength with strain rate. In fact, the shear strength decreased with the strain rate in most of the tests performed with the exception of two tests (CP16 and CP20, Table 4.1). To clarify this contradiction and to quantify the effect of strain rate on pressuremeter testing an extensive laboratory study was undertaken as described in Section 4.5.

4.4 Simulation of Pressuremeter Test in Laboratory

Since the pressuremeter is a large in situ device (about 40 in long), it is difficult to perform full scale testing to study the influence of various factors that affect its results. Another problem in field tests is that the influence of natural soil variation is unknown. To overcome these problems the PMT is simulated and studied in the laboratory in known soils by several ways such as expansion of hollow cylindrical sample, using model (small scale) pressuremeter, and using a true triaxial apparatus to simulate stresses on an element around the pressuremeter probe.

4.4.1 Simulation of PMT in Thick Hollow Cylinder Test

The cylindrical cavity expansion has been studied theoretically, numerically and experimentally. Some of the geotechnical applications include bearing capacity of piles (e.g., Vesic, 1977, and Sayed and Hamed, 1987), pullout resistance of anchors (Vesic, 1971) and interpretation of pressuremeter tests (e.g., Baguelin et al., 1972, Ladanyi, 1972, Palmer, 1972 and Vesic, 1972).

Pressuremeter tests were simulated in the laboratory by expanding cylindrical cavities of thick hollow samples by Anderson and his co-workers at the University of Sheffield (Anderson and Pyrah, 1986, Anderson et al., 1987, Pyrah et al., 1988 and Anderson and Pyrah, 1989). A triaxial cell was modified, as shown in Fig. 4.2, so that hollow cylindrical specimens with a 150 mm OD and approximately 150 mm high, and a 25 mm diameter cylindrical cavity could be subjected to internal pressure increments

simulating expansion of a borehole during a pressuremeter test. Stress controlled tests were performed on three different clays, pottery clay, Barnsley-clay and kaolin by applying pressures in increments and using different holding times (30 sec, 1 min, 2 min and until creep ceased). Strain controlled pressuremeter tests were simulated to study the strain rate effects on two clay soils (kaolin and pottery clay) with radial strain rates ranging from 0.2% to 4% per minute. Numerical simulation using finite element technique was also performed to simulate the above tests and effects of consolidation and creep were studied both separately and combined. The results were presented and discussed in the previous section.

4.4.2 Simulation of PMT by Model Pressuremeter

Gangopadhyay and Nasr (1986), and Nasr and Gangopadhyay (1988) used a model pressuremeter of 1.5 cm diameter in a 15 cm diameter and 10 cm high artificially sedimented kaolin specimen (Figs. 4.10 and 4.11). To avoid the disturbance during the insertion of the probe, the probe was placed first and kaolin slurry was consolidated around the probe. A series of 17 pressuremeter model tests were performed using different maximum vertical pressures and overconsolidation ratios of 1, 2, 4 and 8. The undrained shear strength of the laboratory pressuremeter model samples were predicted for each test by the interpretation methods proposed by Menard in 1957 (Baguelin et al., 1978), Gibson and Anderson (1961), Baguelin et al. (1972), Ladanyi (1972), Palmer (1972), Prevost and Hoeg (1975), and Denby and Clough (1980). A wide range in shear strength values obtained with the different interpretation methods was observed for the same test, and the difference increased with the OCR. Prevost's method gave the best agreement with the results of triaxial test.

Huang (1986), Huang et al. (1988) and Huang et al. (1991) performed a series of strain controlled model pressuremeter tests in cohesive soils [kaolin (K100) and kaolin-silt mix (K50)] inside a calibration chamber (Figs. 4.12 and 4.13). Their study showed that the initial shear modulus G_i and undrained shear strength are sensitive to both strain

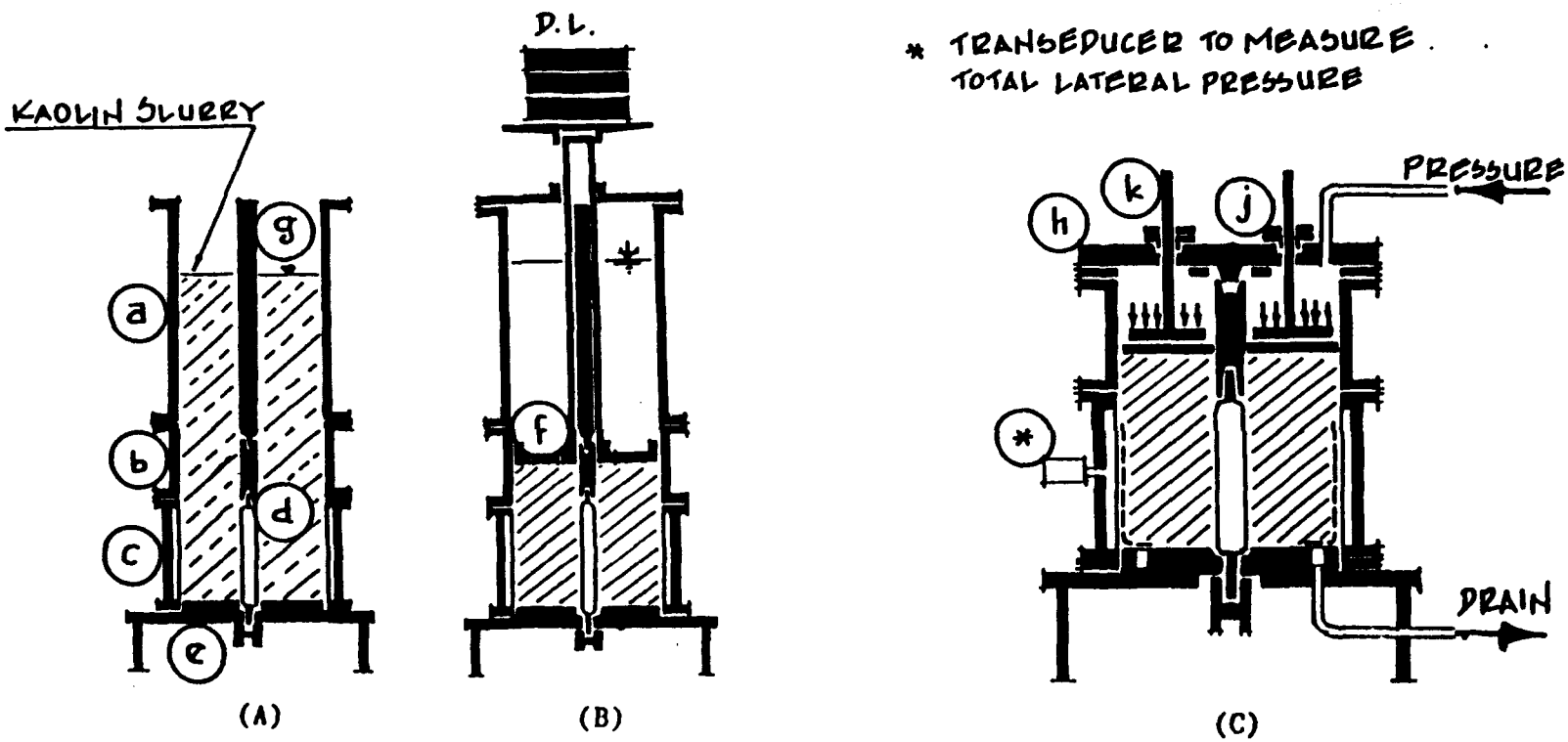

Fig. 4.10 Sample Preparation for Model PMT (A) & (B) Sedimentation Stage (C) Consolidation Stage (After Gangopadhyay and Nasr, 1986)

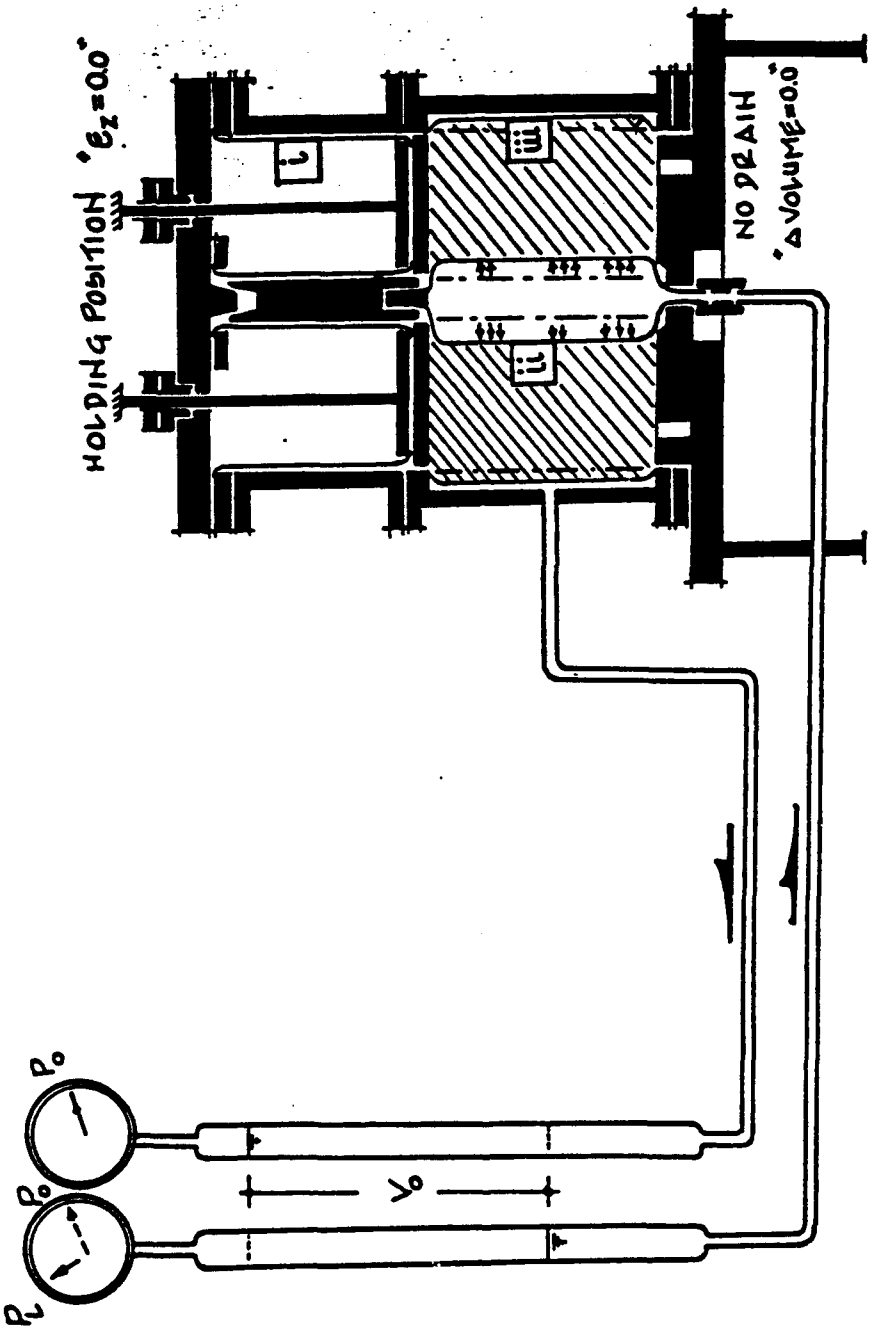

Fig. 4.11 Shear Stage of PMT (Field Test Simulation) (After Gangopadhyay and Nasr, 1986)

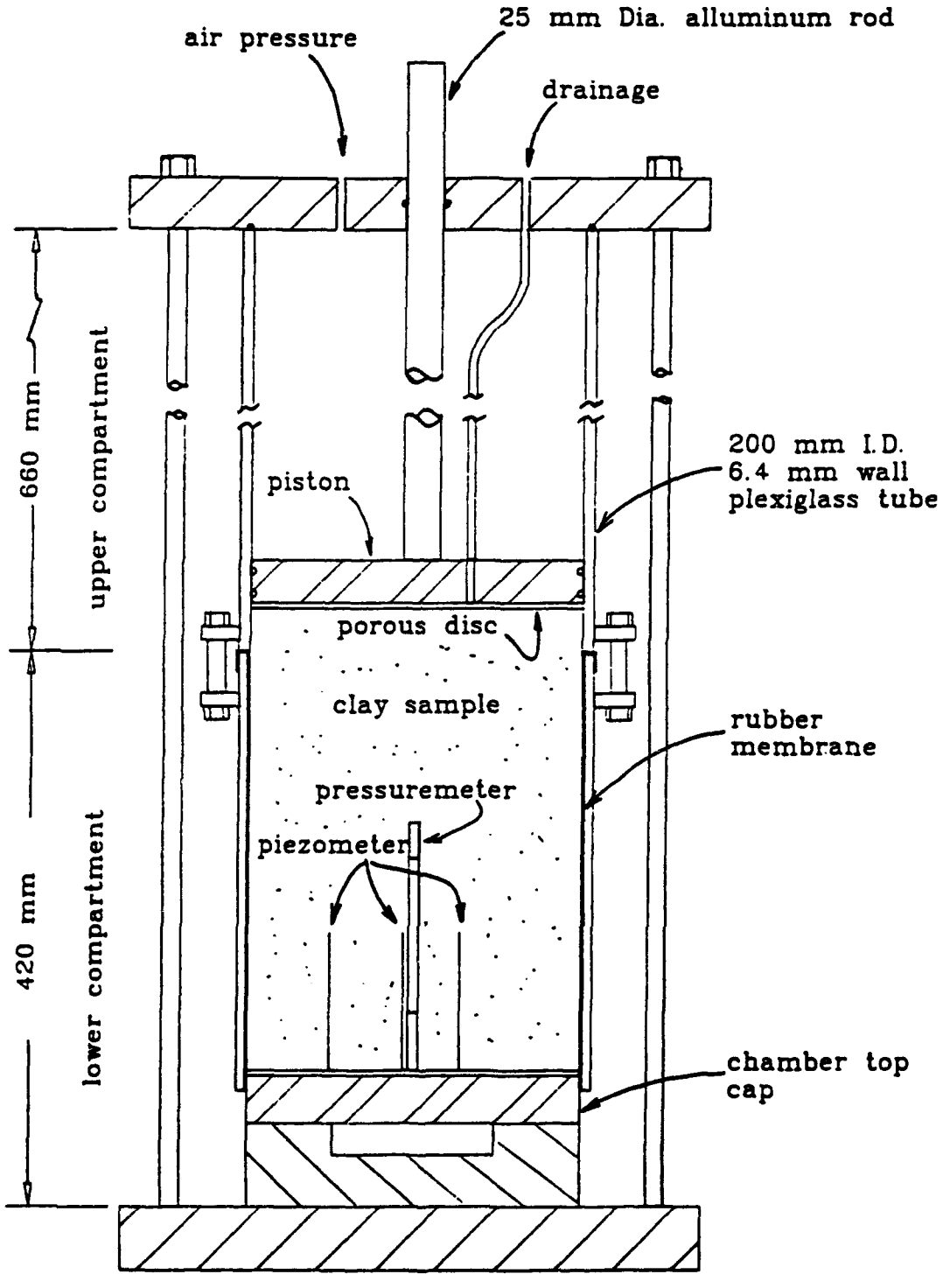

Fig. 4.12 Cross-Section of Chamber Slurry Consolidation (After Huang et al., 1988)

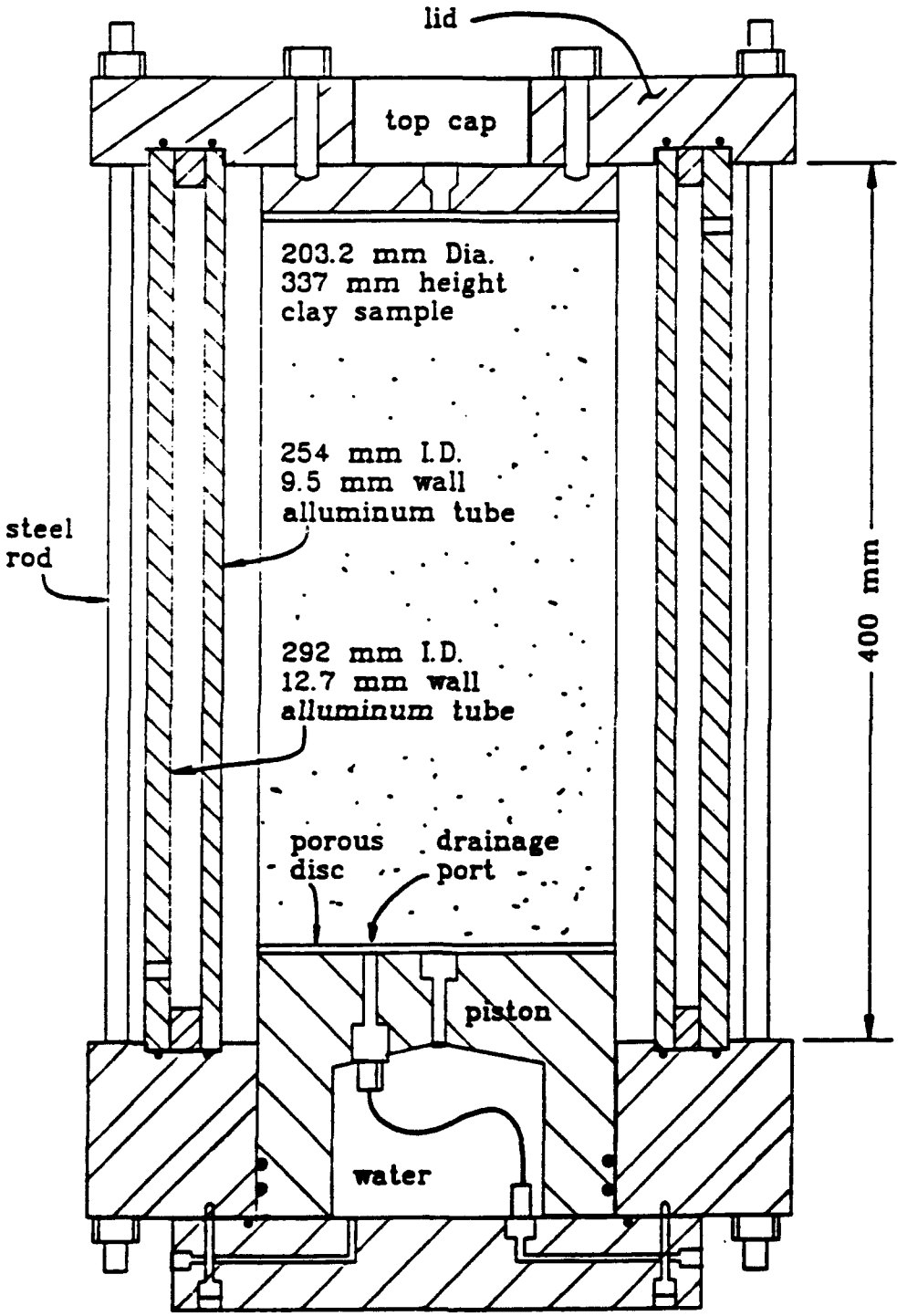

Fig. 4.13 Cross-Section of Double Wall Calibration Chamber (After Huang et al., 1988)

rates and soil disturbance. For the N.C. K100 and K50 clays, G_i increases by four to five times as strain rates vary from 0.73% to 4.4% per min. But for the O.C. clays the strain rate effects on G_i are less dramatic. As Gangopadhyay and Nasr (1986) obtained, Huang et al. (1991) also found out that the undrained shear strength values interpreted from the model pressuremeter test by Prevost's (1979) method were very close to the triaxial values.

4.4.3 Simulation of PMT in True Triaxial Test

Wood and Wroth (1977) simulated pressuremeter expansion tests in the laboratory by testing single elements of soil in a true triaxial device. The strain path of the PMT on an element involves one dimensional consolidation (to simulate the field condition) followed by shearing under conditions of plane strain, at constant volume, in the plane perpendicular to the direction of consolidation. True triaxial devices are the only types of apparatus that can apply this complete strain path in one continuous operation without the need for unloading, trimming and reorientating the sample (Wroth, 1984). Wood used the Cambridge true triaxial apparatus (Hambly, 1969), i.e. the rigid platen type where the strain controlled tests can be performed easily. Large deformations can be achieved because each of the sides of the cuboidal sample can be independently varied between 70 and 130 mm (a maximum strain of 30%).

The clay used for the laboratory tests by Wood and Wroth was Spestone kaolin (LL = 72, PL = 40). The kaolin was mixed as a slurry at a water content of 160%, then pumped into the true triaxial apparatus, and given the required history of 1-D consolidation and unloading. The value of K_o obtained from the 1-D consolidation was about 0.7. By consolidating kaolin in an oedometer with measurement of horizontal stress, Nadarajah (1973) obtained a value of 0.64 for K_o. Sketchley (1973) using the biaxial plane strain apparatus found a value of 0.63. Skandarajah et al. (1991) obtained K_o values of 0.62 after 1-D consolidation in the cuboidal shear device for Georgia kaolin (LL = 63 and PL = 33).

Wood and Wroth (1977) presented stress-strain curves and total and effective stress paths for pressuremeter tests simulated in the true triaxial apparatus on three different clays at different overconsolidation ratios. Patterns of behavior observed in the ground and in the laboratory are compared and the validity of some of the assumptions made in interpreting the pressuremeter test results is assessed in the light of these comparisons.

4.4.4 Full Size PMT in the Laboratory (in Calibration Chamber)

Bellotti et al. (1989) used a SBPM and reported extensive data obtained from 47 tests performed in a large calibration chamber using pluvially-deposited silica sand, and from 25 tests performed in situ in a natural deposit of relatively clean silica sand of the River Po, Italy. Based on the results of these experiments a method to correct the measured unload-reload shear modulus from SBPM tests in sands was proposed to account for the variations in stress and strain levels. The ENEL-CRIS calibration chamber (Fig. 4.14) was designed to calibrate and evaluate different in situ testing devices in sands. The equipment consists of a double-wall chamber, a loading frame, a mass sand spreader for sand deposition and a saturation system. The chamber can test a cylindrical sample of sand 1.2 m in diameter and 1.5 m in height. The cylindrical probe of the SBPM was the Camkometer Mark VIII type 82 mm in diameter and 490 mm long (L/D is about 6).

Anderson and Pyrah (1989) carried out full scale 80 mm dia. SBPM tests in clay in a triaxial calibration chamber (Fig. 4.15). A rigid cylinder 1.7 m high and 0.8 m in diameter was filled with kaolin slurry mixed at 1.5 times LL, which was consolidated one dimensionally using top and bottom drainage. When the height of the slurry had reduced to about 1.0 m, the rigid cylinder was removed and an outer membrane was fitted. The SBPM was bored into the soil and the clay consolidated again around it using equal vertical and horizontal stresses. This attempted to simulate perfect insertion of the SBPM with minimal disturbance. They found a time lag between the pore pressure

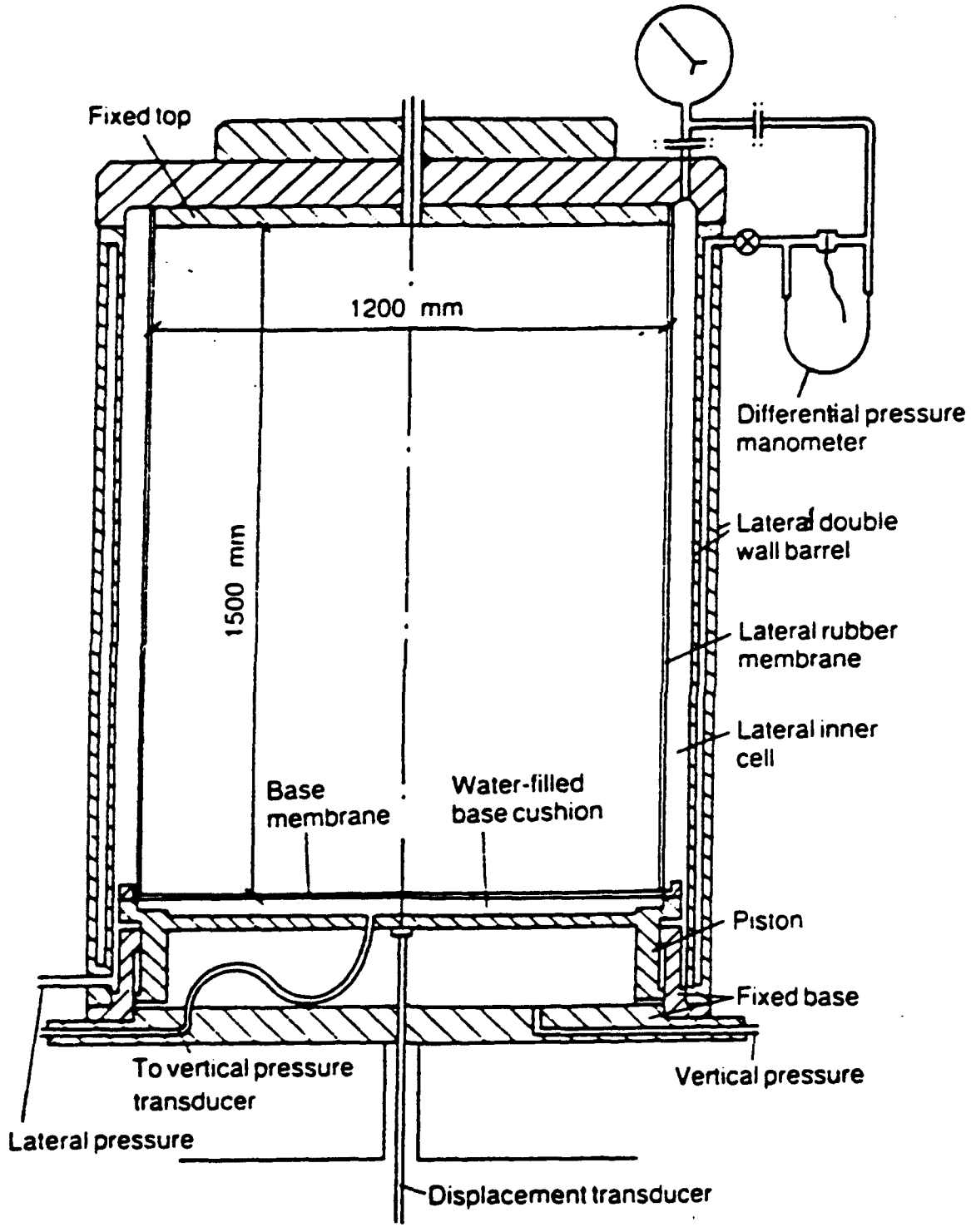

Fig. 4.14 Cross-Section of ENEL-CRIS Calibration Chamber (After Bellotti et al., 1989)

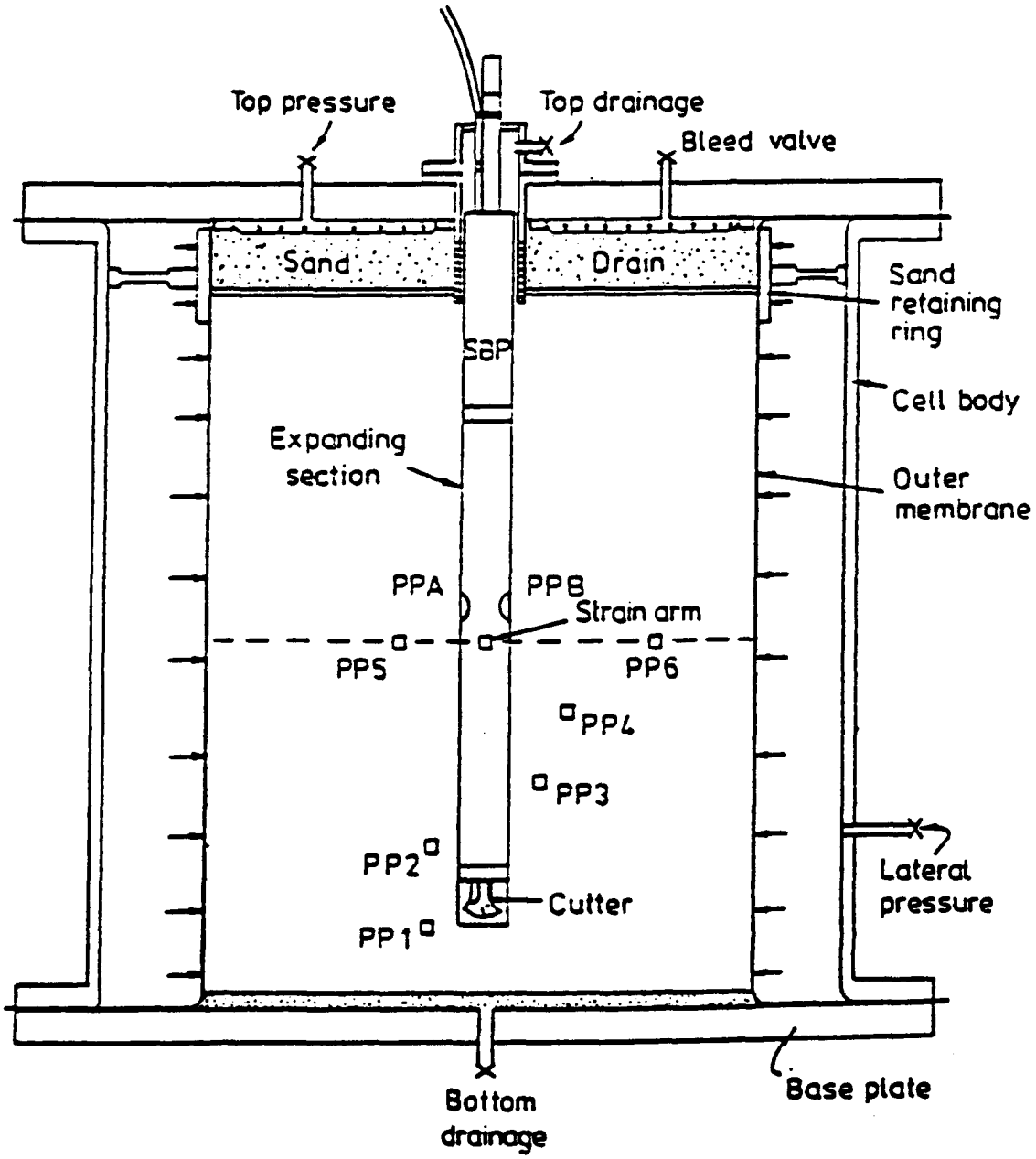

Fig. 4.15 Cross-Section of Calibration Chamber with SBPM in Position (After Anderson and Pyrah, 1989)

transducers placed in the soil and the SBPM pore pressure cells, casting doubt on the validity of the pore pressures measured by current commercially available pressuremeters. Furthermore, the pressuremeter tests carried out in the calibration chamber confirmed the influence of time dependent phenomena such as consolidation and creep, and also suggested the possibility of vertical consolidation away from the mid-height of the pressuremeter.

4.4.5 Full Scale Self-Boring Pressuremeter Testings in Soft Clay

Benoit and Clough (1986) conducted 32 SBPM tests in soft San Francisco Bay Mud wherein key parameters were varied one at a time to isolate their influence. The parameters considered included: expansion rate, cutter position, cutting rate, and cutting shoe dimension. Furthermore, they determined lateral earth pressure, shear strength, stress-strain behavior, and in some cases, coefficient of consolidation, from the probe expansion data.

The strain rate or rate of membrane inflation is one of the major factors influencing undrained shear strength from SBPM tests. It could be due to the possible drainage during the test and to the effects of rheologic parameters. In the pressuremeter test, these factors are bound together and are difficult to isolate. Benoit and Clough (1986) carried out seven SBPM tests on Bay Mud to study the influence of strain rate in the shear strength. Young Bay Mud exhibits the typical rheological behavior for clays in undrained conditions, wherein the strength increases with rate of loading (Lacerda, 1976). On the other hand, Jain (1985) determined from finite element analysis and laboratory tests on Bay Mud that if drainage occurs in the pressuremeter test for a contractive soil like Bay Mud and the results are interpreted assuming undrained conditions, the strength will be underestimated.

Membrane expansion rates used in the SBPM tests were varied from 1.7 to 47.6 $kN/m^2/min$ (0.24-6.90 psi/min) as opposed to the normal rate of 6.9 $kN/m^2/min$ (1 psi/min). The result of their tests is shown in Fig. 4.16 where the shear strengths

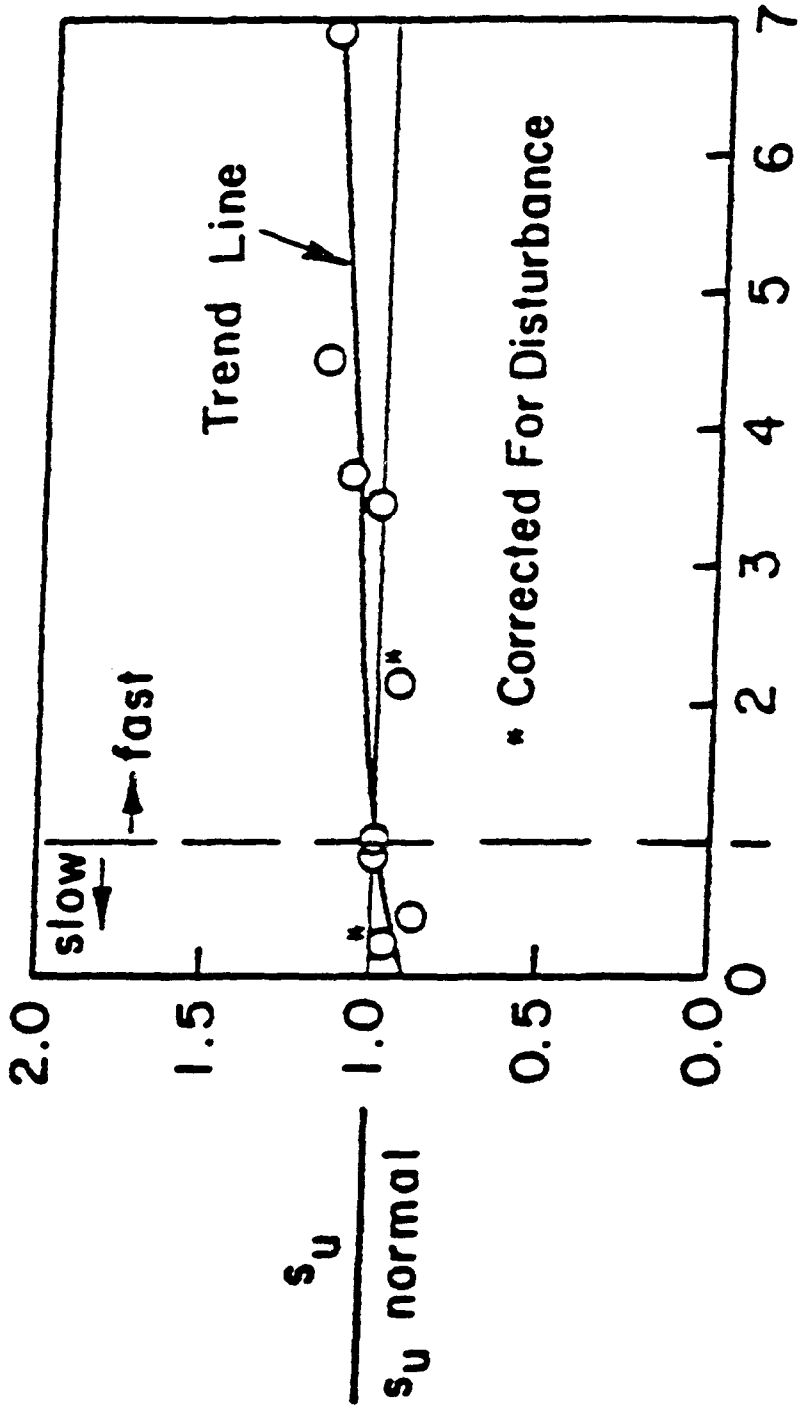

Fig. 4.16 Comparison of Shear Strengths Obtained at Various Inflation Rates (After Benoit and Clough, 1986)

obtained from the tests are normalized by dividing each strength by the corresponding value of strength determined in the normal tests at that depth, and the membrane inflation rate is normalized by the normal rate (1 psi/min). From the normalized strength versus inflation rate ratio plot (Fig. 4.16), it is observed that the shear strength increases steadily by about 10-15% per seven fold strain rate increase.

4.5 Simulation of Pressuremeter Test in the Cuboidal Shear Device

As described in the previous section, the PMT can be simulated several ways in the laboratory, as expansion of cylindrical cavity of a thick hollow cylindrical sample in a modified triaxial cell, small scale or full scale PMT in a calibration chamber or in a modified triaxial cell, or by testing a single element of a soil in a true triaxial apparatus subjecting to PM strain path. Out of all these techniques, testing an element in a true triaxial apparatus is the easiest and most versatile method.

As shown in Fig. 4.17, a small cylindrical element around the cavity is simulated as a cube element. Before the cavity expansion, the vertical stress, σ'_z, is the major principal stress, σ'_1, and the radial and hoop stresses, which are equal, $\sigma'_r = \sigma'_\theta$, are the minor principal stresses, $\sigma'_2 = \sigma'_3$. When the cavity is expanded by applying a pressure on the cavity wall (by probe pressure) the radial pressure increases and hoop pressure decreases and the total vertical pressure remains constant. At one point the radial pressure becomes more than the vertical pressure and thus rotation of principal stress direction occurs.

The pressuremeter test is simulated in the cuboidal shear device (Chapter 3) in the following sequence. Test specimens are prepared in a slurry consolidometer from the slurry at about 2.5 times the LL water content. The four inch cube specimen is transferred to the CSD and reconsolidated one dimensionally to a higher pressure to overcome disturbance effects. Up to this consolidation phase exactly the same procedure is followed for all tests. Since the pressuremeter probe is very long, plane strain condition can be assumed in the plane perpendicular to the direction of consolidation.

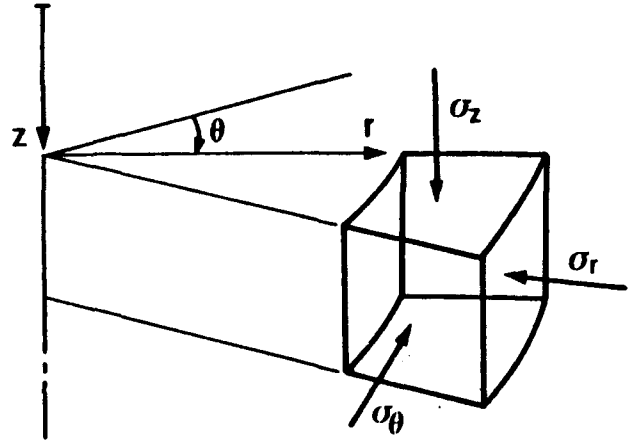

Cylindrical co-ordinates of stress components in the pressuremeter testing

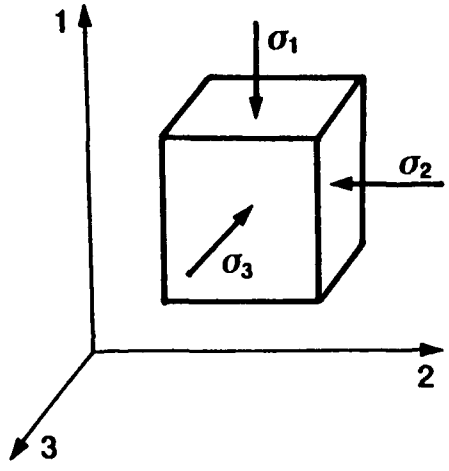

Cartisian co-ordinates of stress components in the true triaxial testing

Fig. 4.17 Simulation of Curvilinear Element to Cubic Element

This condition is implemented in the CSD by maintaining no deformation in the vertical direction, i.e. $\epsilon_z = 0$. The pressuremeter test is usually performed very fast, so undrained condition can be assumed in clays. Therefore, during the pressuremeter expansion, the sharing occurs at constant volume. This condition is enforced in the CSD by closing the drainage valves and maintaining $\epsilon_\theta = -\epsilon_r$. Since there is no volume change and the axial strain is zero, equating the volumes:

$$(1 + \epsilon_r)(1 + \epsilon_\theta) = 1$$

yields $\epsilon_\theta = -\epsilon_r$, neglecting higher order terms. A computer program was written to incorporate the above conditions ($\epsilon_z = 0$ and $\epsilon_\theta = -\epsilon_r$) by adjusting remotely σ_x, σ_y and σ_z through solenoid valves.

4.6 Strain Rate Tests Varying from 0.01%/min to 5.00%/min

As described in Section 3.9 various strain rate tests were performed using a strain controlled method. The strain rate can be prescribed for every test and a tolerance of 0.05 times the strain rate was used. The tolerance for no deformation ($\epsilon_z = 0$) was given as 0.0005 inch.

After the 1-D consolidation in the CSD, the stress path of the pressuremeter testing was simulated in the CSD and the samples were sheared at different strain rates. The pressures were servo-controlled to achieve the required strain path and strain rates. At least three tests were performed at each strain rate (at 0.01%, 0.05%, 0.10%, 0.50%, 1.00% and 5.00% per min). In general the undrained shearing was carried out until the applied pressures reached 200 psi (maximum capacity of the pressure transducers) or until the strains reached 15%. Very good agreement was observed between tests performed at the same strain rate. Hence, under controlled conditions the CSD testing yields very repeatable results. It was noticed after the test that the edges of the specimen

remained in position, showing that the floating type boundary conditions minimize the edge effects.

4.7 Results and Discussion

The frequency of data recording was selected depending on the speed of the test (i.e., strain rate of shearing). For example, for the fastest test (strain rate = 5.00%/min), readings were recorded every 3 seconds (every reading), and for the slowest test (strain rate = 0.01% per min) readings were taken every 15 seconds at the beginning (one in 5 readings), and at about 5 minutes interval (one in 100) after the stress reached the plateau. This procedure was adopted in order to avoid storing too much data without losing accuracy.

In the flexible membrane CSD, strain controlled tests are performed indirectly. As described in section 3.9, strain controlled loading is a trial and error iteration process, thus there is a time lag in the reaction of the soil and the measurement. Even if the speed of data acquisition system is increased, the solenoid valves take some time to react (delay in the mechanical opening and closing system) and thus slower response compared to the measurement speed. So, there is noise in the readings, particularly in the shear stress data, because it is the difference of σ_x and σ_y readings, which are not always completely synchronized.

To obtain a smoother curve, a regression program was written to fit the data points into a 3rd, 4th and 5th order polynomials. The best polynomial was selected for each test. For the same data set (e.g. Test 49), third, fourth and fifth order polynomials are shown in Figs. 4.18-4.20, respectively. Out of these three polynomials, a fifth order polynomial fit was selected because it had the lowest variation and it is consistent with other similar tests, i.e. strain softening behavior. For another test (Test 58), the best suited fifth order polynomial regression curve is shown in Fig. 4.21. Using the above

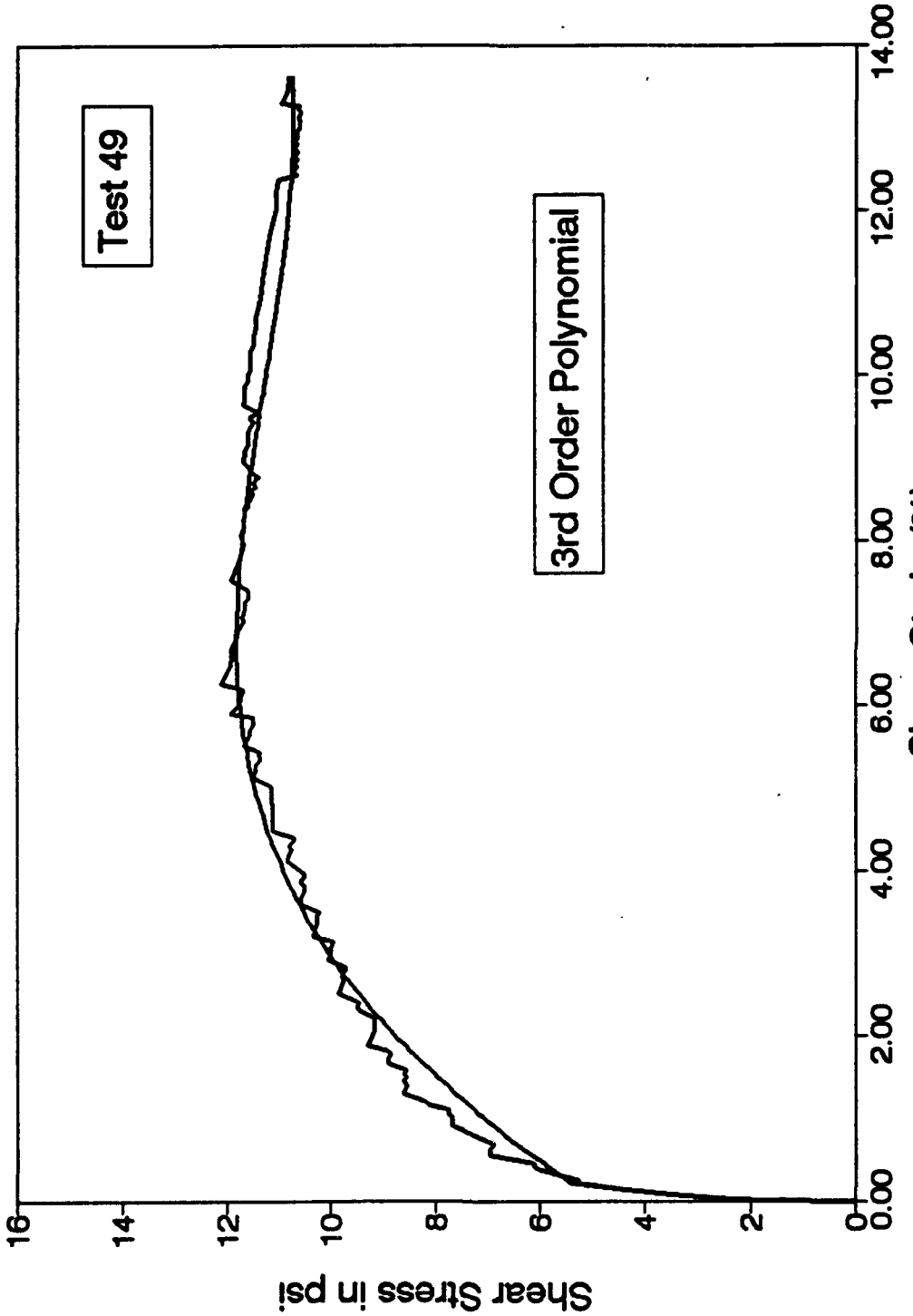

Fig. 4.18 Curve Fitting by Regression Analysis - 3rd Order Polynomial - Test 49

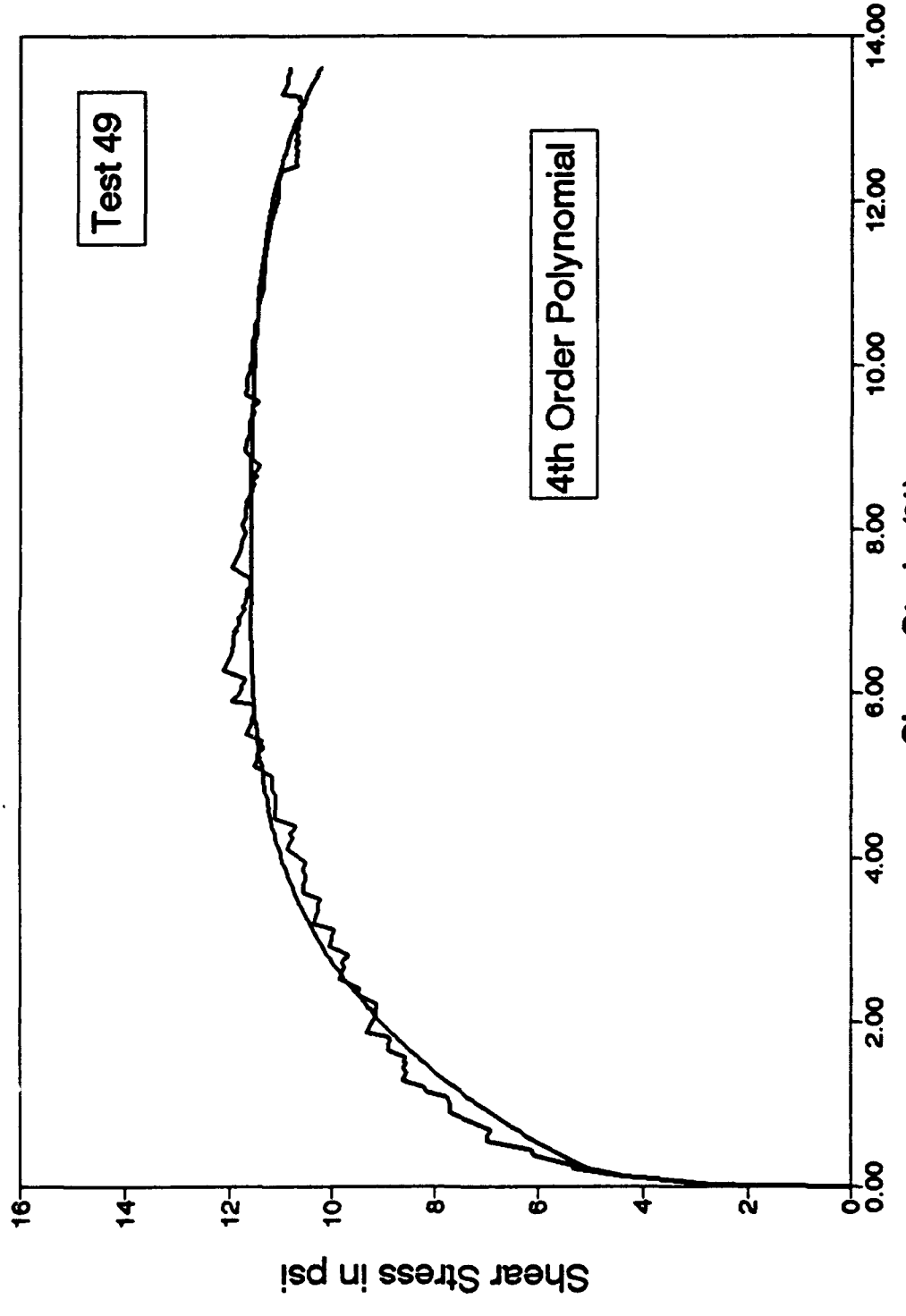

Fig. 4.19 Curve Fitting by Regression Analysis - 4th Order Polynomial - Test 49

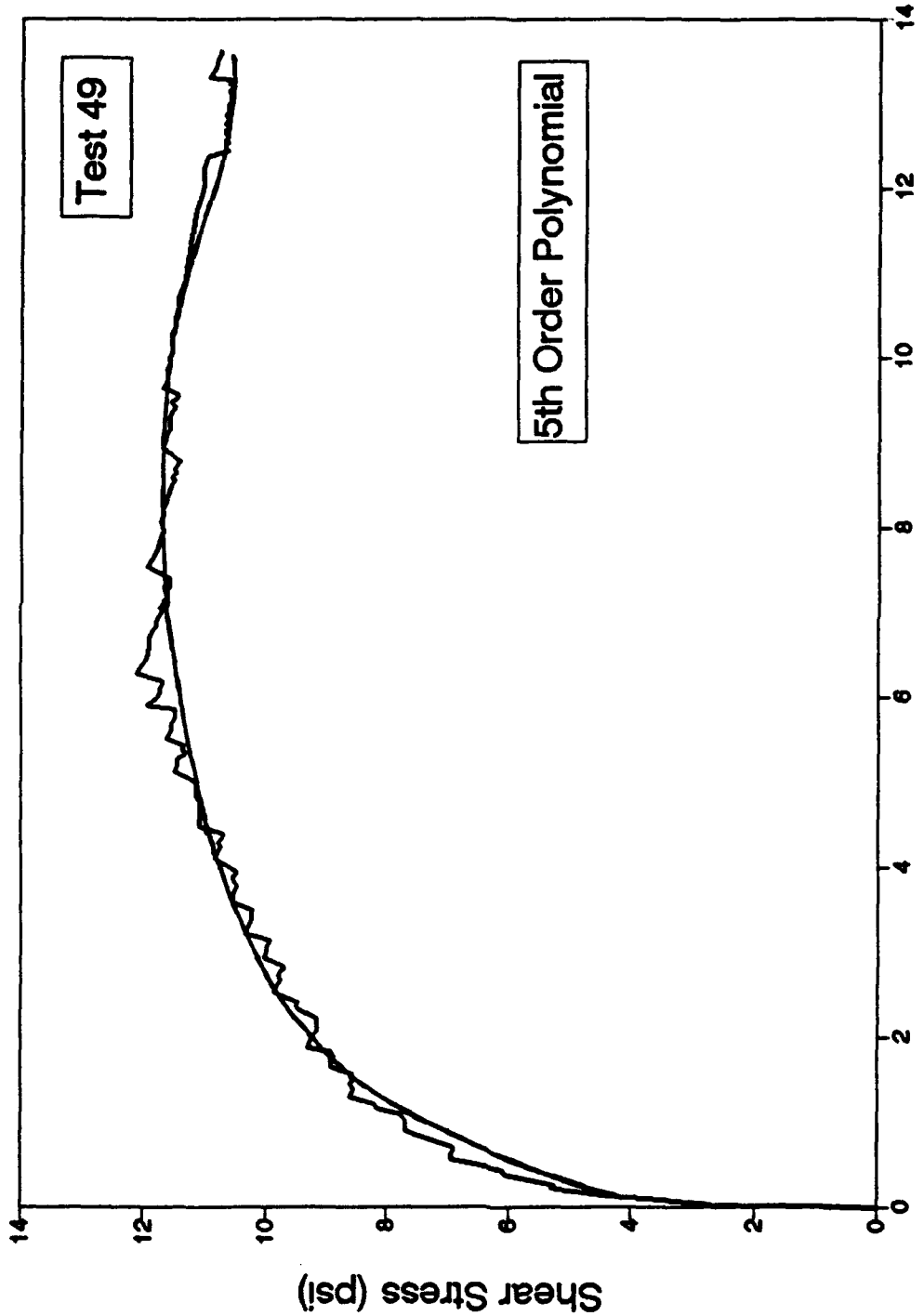

Fig. 4.20 Curve Fitting by Regression Analysis - 5th Order Polynomial - Test 49

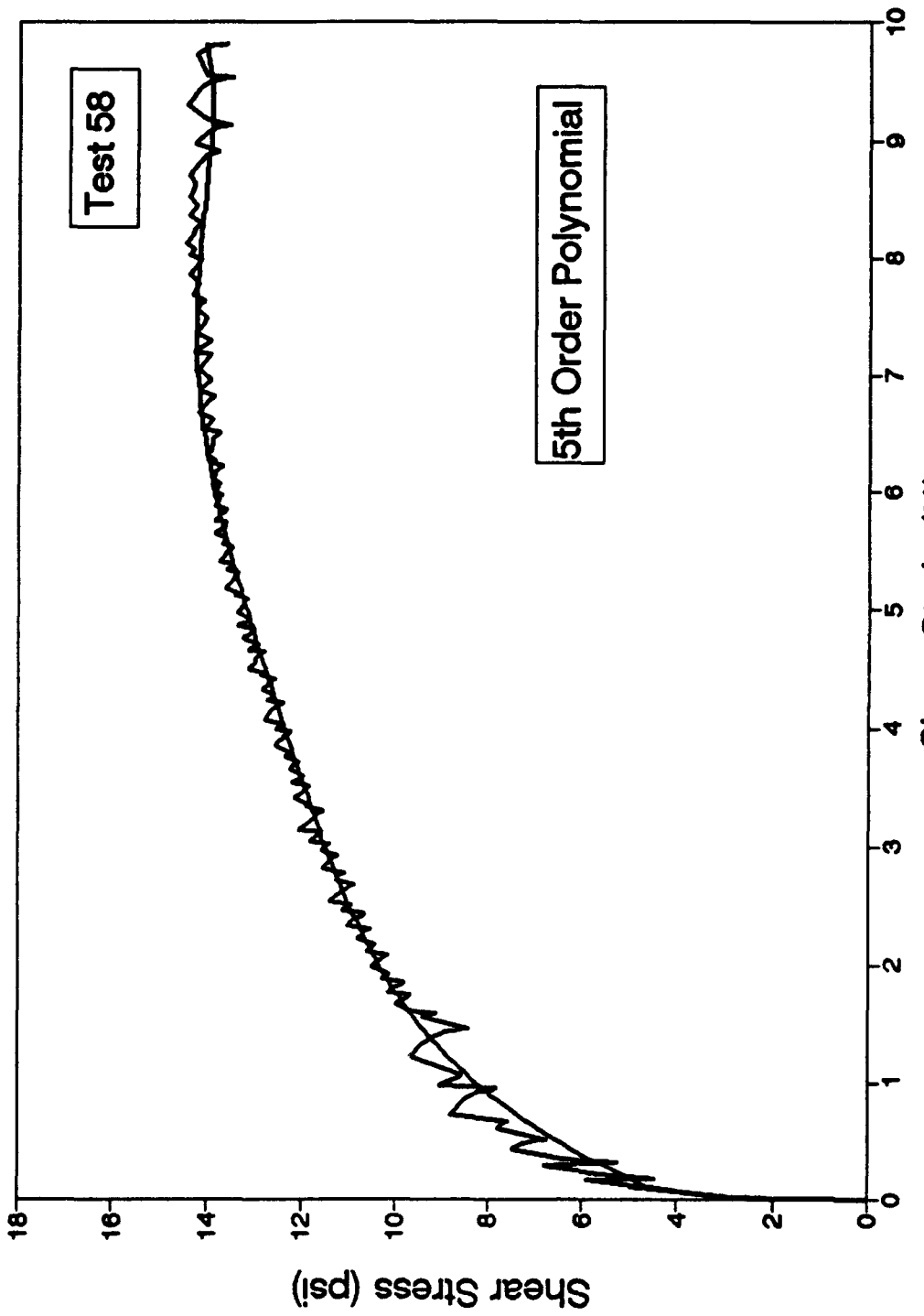

Fig. 4.21 Curve Fitting by Regression Analysis - 5th Order Polynomial - Test 58

regression method all experimental curves were smoothened and are given in Appendix B.

Some typical results are shown in Fig. 4.22 and Fig. 4.23 for kaolin clay and kaolin-silica mix soil, respectively. In order to compare the test results with various strain rates they are plotted together, but only three curves are shown in each figure to avoid congestion. The horizontal axis represents the compression strain in the x direction of the CSD which simulates the radial strain in the pressuremeter test. The vertical stress represents the shear stress which is obtained from the half of the difference between the radial and hoop stresses ($\frac{1}{2}$ (σ_x-σ_y)).

The stress-strain curves are very consistent. They show clearly the increase of tangent modulus values and shear strength values with the increase of strain rate. The kaolin specimens (Fig. 4.22) show a slight strain-softening while the kaolin-silica specimens (Fig. 4.23) exhibit strain-hardening effects.

The summary of the peak shear strength versus strain rate test results are given in Tables 4.2 and 4.3 for kaolin and kaolin-silica, respectively. The corresponding stress-strain curves are attached in Appendix B. The shear strength values at various strain rates were normalized by the average shear strength at 0.01% per minute, in order to compare the test results (for pressuremeter) with the previously published results (e.g., Prapaharan et al., 1989). The normalized shear strength values are plotted with logarithmic of strain rates and shown in Figs. 4.24 and 4.25 for kaolin and kaolin-silica, respectively.

From the plots (Figs. 4.24 and 4.25) and the regression analysis, the slopes of the curves were found as 14.3% and 15.3% for kaolin and kaolin-silica, respectively. For the tests performed in kaolin clay, the strength values fall very closely to the straight line (with r^2 = 0.98, standard error of estimation only 0.02 and standard error of coefficient of 0.0048), whereas for kaolin-silica tests the variation is higher (r^2 = 0.64, standard

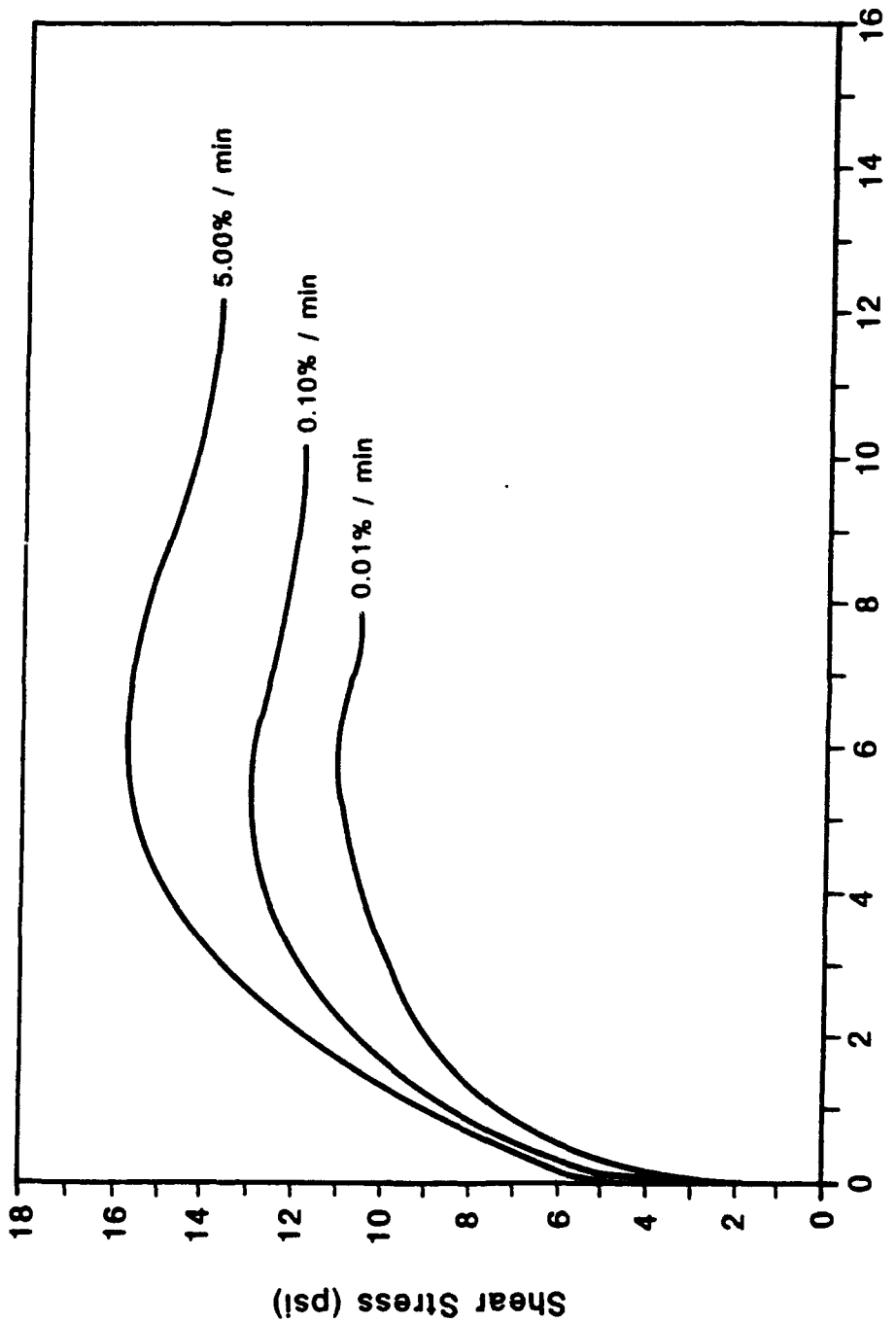

Fig. 4.22 Strain Rate Effect on Stress-Strain Characteristics for Kaolin Clay

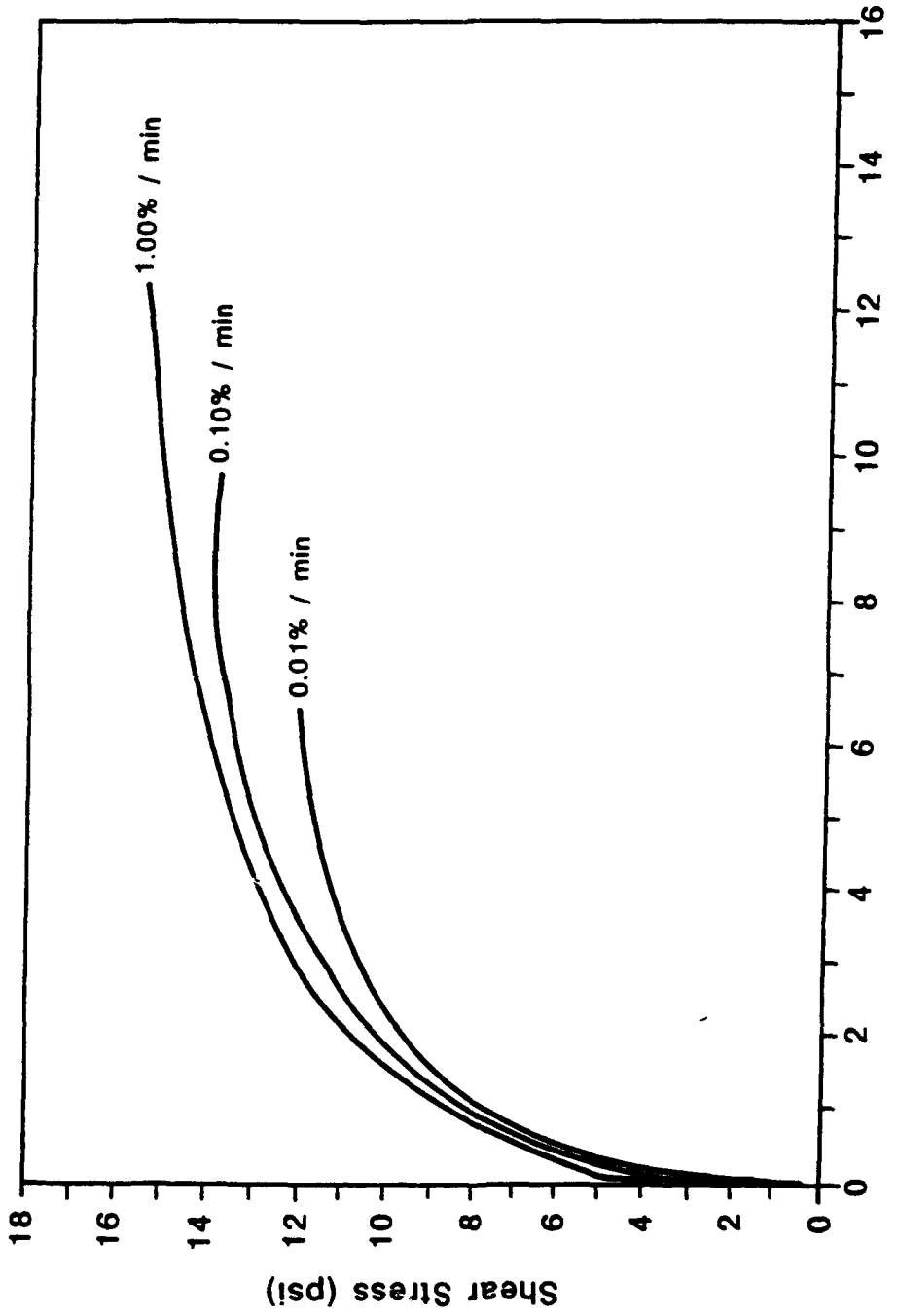

Fig. 4.23 Strain Rate Effect on Stress-Strain Characteristics for Kaolin-Silica Mixture

Table 4.2 Shear Strength Normalized with Respect to 0.01% per min Versus Strain Rate for Kaolinite Clay

Test No.	Strain Rate (% per min)	$\tau_{xy} = \frac{\sigma_x - \sigma_y}{2}$ (psi)	$\frac{\tau_{xy}}{(\tau_{xy})_{0.01\%/min}}$
35	0.01	11.3	0.998
47	0.01	11.5	1.015
48	0.01	11.4	1.007
52	0.01	11.1	0.980
49	0.05	12.2	1.071
51	0.05	13.0	1.148
32	0.10	13.2	1.166
33	0.10	13.2	1.166
34	0.10	13.15	1.161
44	0.10	13.0	1.148
50	0.50	14.2	1.254
36	1.00	14.8	1.307
37	1.00	14.4	1.271
38	1.00	14.5	1.280
39	1.00	14.9	1.316
40	5.00	15.9	1.404
41	5.00	15.65	1.382
43	5.00	15.60	1.377

Table 4.3 Shear Strength Normalized with Respect to 0.01% per min Versus Strain Rate for Kaolin-Silica Mixture

Test No.	Strain Rate (% per min)	$\tau_{xy} = \frac{\sigma_x - \sigma_y}{2}$ (psi)	$\frac{\tau_{xy}}{(\tau_{xy})_{0.01\%/min}}$
55	0.01	11.7	0.946
56	0.01	12.1	0.979
64	0.01	13.15	1.064
78	0.01	12.5	1.011
61	0.05	16.0	1.294
71	0.05	14.5	1.173
77	0.05	12.8	1.035
58	0.10	14.4	1.165
59	0.10	17.0	1.375
60	0.10	17.0	1.375
74	0.10	16.0	1.294
66	0.50	16.7	1.351
67	0.50	17.5	1.416
72	0.50	16.5	1.335
75	0.50	14.0	1.133
53	1.00	15.9	1.286
54	1.00	15.7	1.270
62	1.00	16.4	1.327
79	1.00	15.5	1.254
57	5.00	18.5	1.497
68	5.00	18.4	1.488

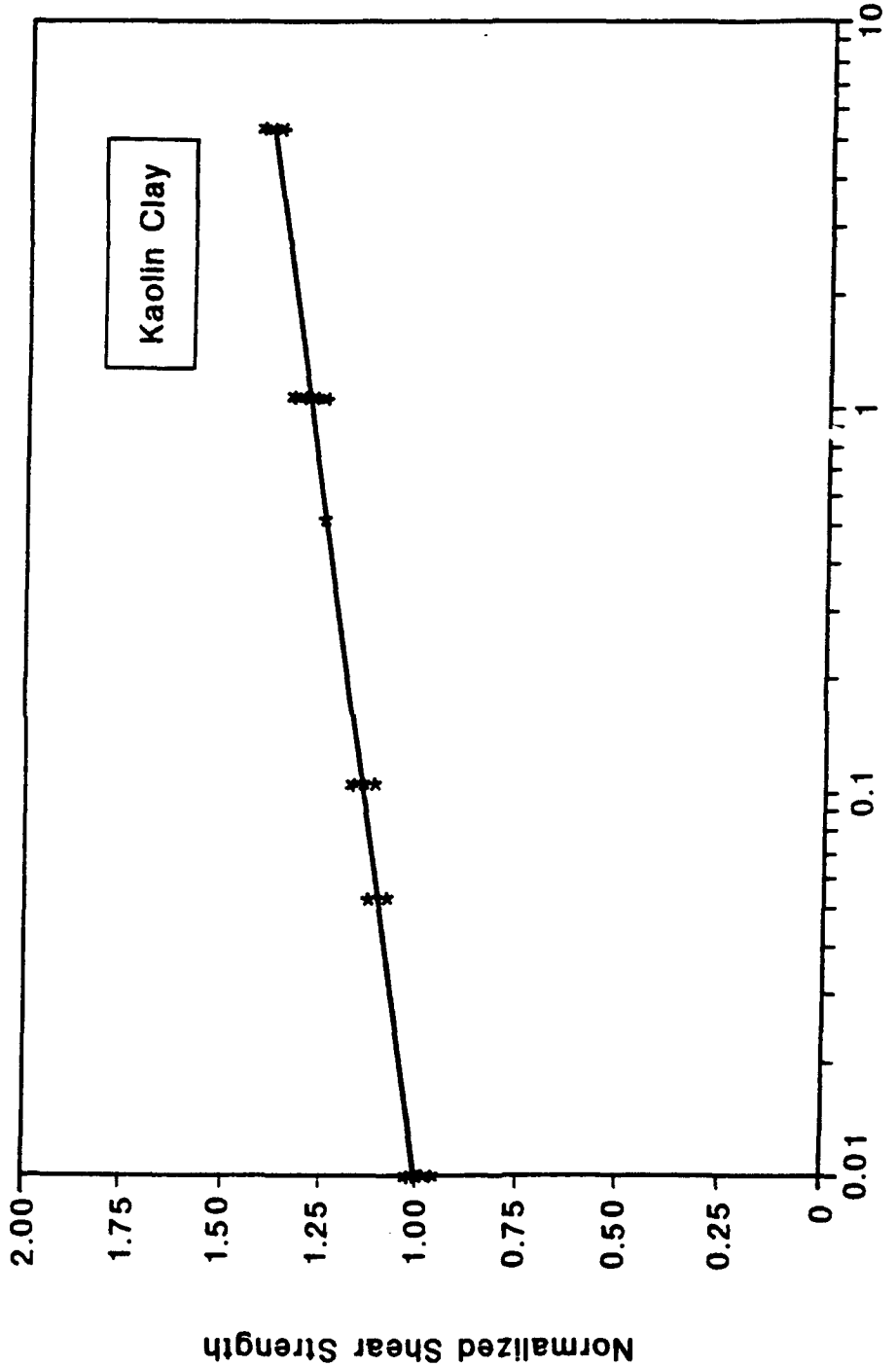

Fig. 4.24 Normalized Shear Strength with Respect to 0.01%/min Versus Strain Rate Plot for Kaolin Clay

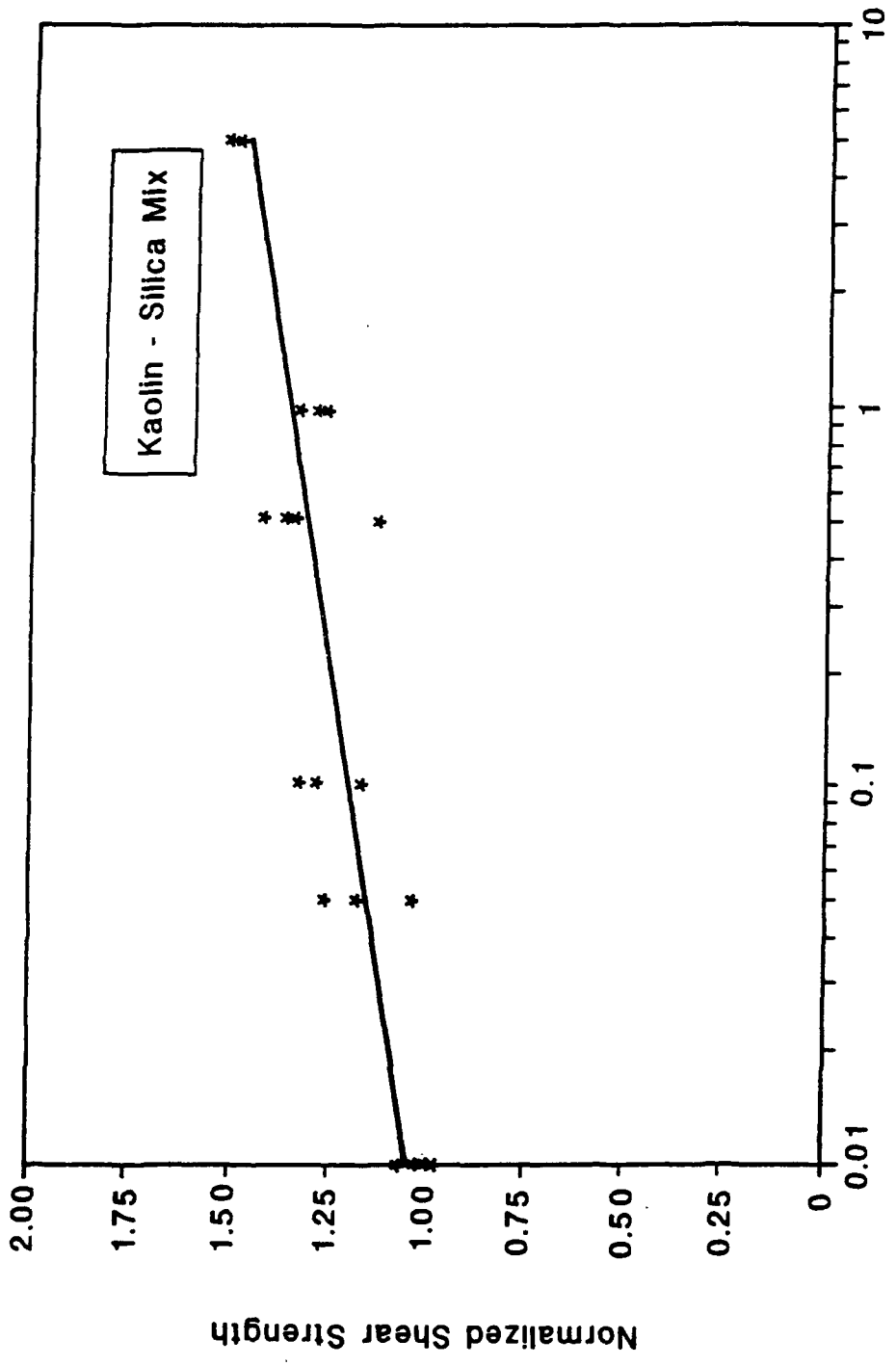

Fig. 4.25 Normalized Shear Strength with Respect to 0.01%/min Versus Strain Rate Plot for Kaolin-Silica Mixture

error of estimation = 0.10 and standard error of coefficient = 0.0262). The reason for this difference could be related to the heterogeneous property of the mixture of two entirely different soils and/or the difficulty to pin point exactly the peak strength for kaolin-silica curves because they were strain hardening type (Fig. 4.23). On the other hand, kaolin clay is a very uniform homogeneous soil with a flaky structure, which can be rearranged along the slip plane and be the cause for yielding strain softening behavior (Fig. 4.22).

The straight line relationship obtained for kaolin (Fig. 4.24) and kaolin-silica (Fig. 4.25) are superimposed on the plots (Fig. 4.1) developed by Prapaharan et al. (1989) and shown in Fig. 4.26. Since the curves in Fig. 4.1 based on triaxial tests are also normalized using the shear strength value at 0.01% per min strain rate, it is possible to superimpose and compare the pressuremeter stress path tests with the triaxial tests. As can be noticed from Fig. 4.26, the undrained shear strength predicted by the pressuremeter tests are more sensitive to the strain rate than the triaxial tests. On the average, it can be concluded that the shear strength increases about 15% for every ten fold of strain rate in pressuremeter tests and about 10% in triaxial tests. This result is consistent with the full scale SBPM tests (Benoit and Clough, 1986) conducted on San Francisco Bay Mud where the normalized strength increases about 15% (Fig. 4.16).

It is encouraging to notice that the test results from the CSD (simulating PMT) are very consistent, and the undrained shear strength increases with strain rate, similar to the triaxial tests (section 4.2). These results are consistent with the numerical studies performed by Pyrah et al. (1988), which included consolidation and creep effects (Fig. 4.6). But the laboratory tests performed in thick hollow cylinder by Pyrah et al. (1988) and in model pressuremeter in a calibration chamber by Huang et al. (1991) did not give any conclusive results (already discussed in section 4.3).

Even though the model pressuremeter test in a calibration chamber and the hollow cylinder test may be expected to physically represent the actual pressuremeter test better

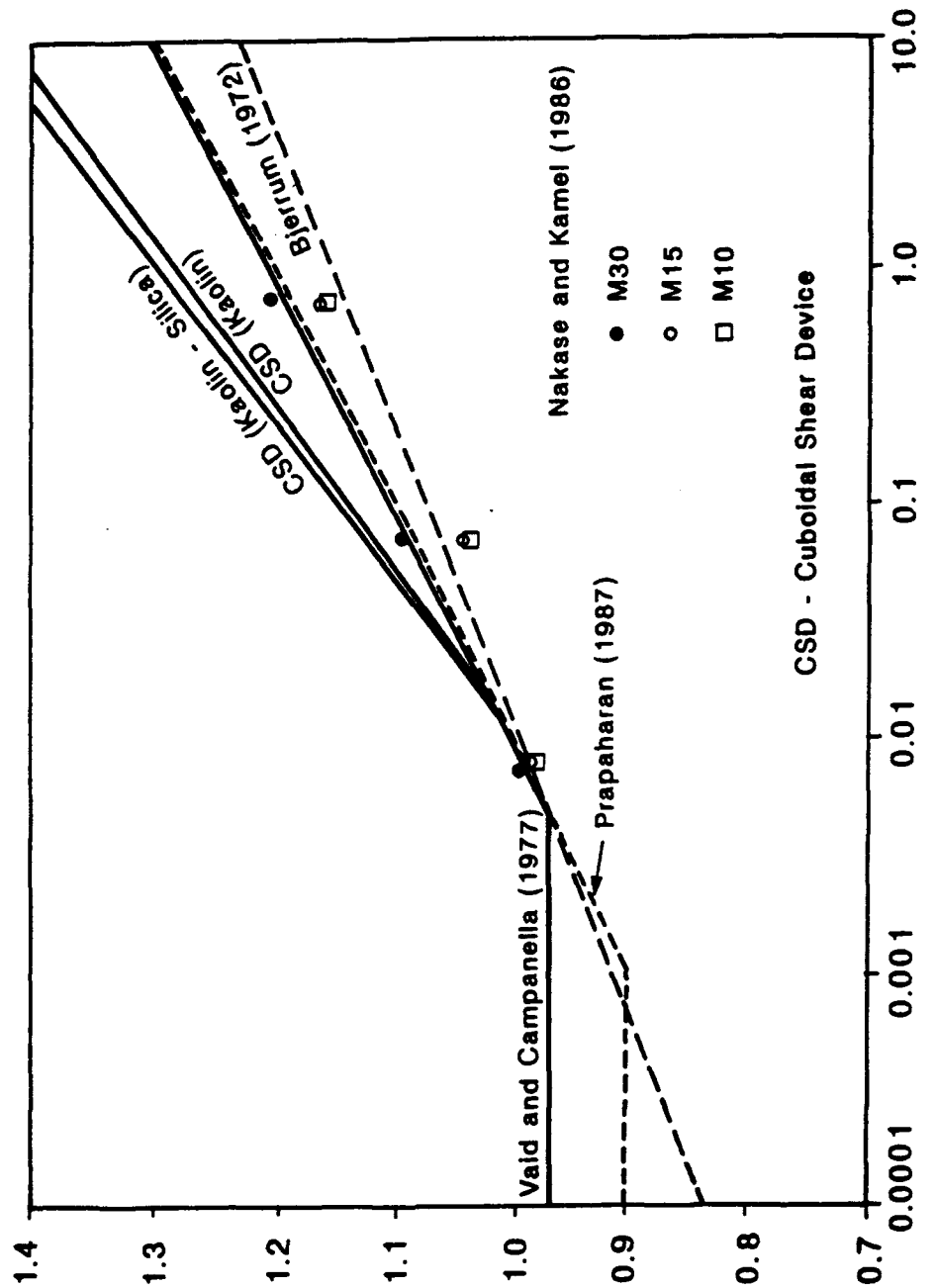

Fig. 4.26 Normalized Shear Strength Versus Strain Rate

than the simulation of pressuremeter strain path in a cuboidal shear device, the latter test had better control in the simulation of undrained condition and better measurement system. From the erratic nature and odd shapes of some curves in Fig. 4.7, it is very clear that testing procedures must have been a problem in the thick hollow cylindrical tests performed by Pyrah et al. (1988). As Huang et al. (1991) indicates in their paper, the partial drainage between the model pressuremeter probe and surrounding soil was an inevitable problem in the calibration chamber testing. Therefore, the results from the simulation in cuboidal shear device and the numerical studies appear more definite and consistent than that of previous studies.

4.8 Conclusion

The shear strength and deformation behavior of clays are time dependent. Usually the faster the load applied the higher the strength of soil. This phenomenon is mainly due to the creep in between the soil particles. When a load is applied slowly, it has more time to sustain the load hence it creeps more and looses its strength. On the other hand, when the load is applied quickly, the soil has less time to creep and it shows higher strength.

From the compression and extension tests performed in the conventional triaxial tests on various soils, it has been found that the undrained shear strength increases about 10% for every tenfold of strain rate. There is no influence in shear strength below a strain rate of 0.001% per min. Since the pressuremeter test follows a different stress path than a triaxial test, it was anticipated that the strain rate would have a different influence in the pressuremeter test.

Anderson, Pyrah and their co-workers studied the effects of consolidation and creep in pressuremeter testings by both experimentally using thick hollow cylindrical soil specimens and numerically using a finite element program CAMFE (Carter, 1978) for both stress controlled and strain controlled conditions. Unfortunately, the experimental

tests did not yield any conclusive results, but the numerical studies shed some light. These studies showed that the effect of both consolidation and creep is to reduce the deduced modulus values, but that the consolidation around the probe tends to produce higher shear strengths, while creep tends to have the opposite effect, i.e., give a lower deduced strength. Soil parameters derived from a stress-controlled test are thus dependent on the relative effects of consolidation and creep, and the effect of creep appears to be more influential.

The same conclusions were reached for the strain controlled pressuremeter tests. When only the consolidation is considered, slower strain rate tests show higher limit pressure which could be the result of consolidation taking place and subsequent strength gain of the soil around the probe. The faster strain rate tests gave higher strength at the beginning but the slower rate tests gained strength with duration due to consolidation. Faster strain rate tests show significant amount of strain softening. With creep also included in the numerical analysis (consolidation and creep), the strength values increased with the strain rate. From this comparison (consolidation alone and consolidation with creep), creep phenomenon is the main factor to yield smaller strength values at lower strain rates. These numerical studies show trends similar to that of triaxial tests, with the deduced undrained shear strength increasing with strain rate, however, the increase could not be quantified because the range of strain rate analyzed was only one magnitude wide (from 0.2% to 4% per min).

Similar to Pyrah et al.'s (1988) experiments, Huang's (1986) model pressuremeter tests in a calibration chamber also did not show an increase in shear strength with strain rate. His tests suffered by the partial drainage along the probe-soil interface.

The pressuremeter strain path was simulated in a cuboidal shear device, conforming to plane strain condition in vertical direction and undrained condition was implemented by closing the drainage valve and maintaining the expansion in the y-direction equal to the compression in the x-direction to satisfy no volume change. From

more than forty well controlled tests, it has been found that the undrained shear strength increases about 15% for every ten fold of strain rate increase. From the seven full scale SBPM tests conducted on San Francisco Bay Mud, Benoit and Clough (1986) found out that the undrained shear strength steadily increased by about 10-15% for an increase of seven times faster than the normal inflation rate of membrane. The consistency of the results from the laboratory tests and field tests enhance the conclusion that the shear strength increases about 15% per log cycle.

The next chapter discusses how to incorporate the strain rate variation in the radial direction in the cavity expansion theory and quantitatively estimate the overprediction of shear strength in the pressuremeter test.

CHAPTER 5

ERROR IN PRESSUREMETER TEST INTERPRETATION DUE TO STRAIN RATE EFFECT

5.1 Introduction

The effects of strain rate on triaxial tests and pressuremeter tests have been discussed in Chapter 4. The undrained shear strength increases with strain rate, about 10% and 15% per every ten fold of strain rate for triaxial and pressuremeter tests, respectively. During the probe expansion in the PMT, the strain rate varies radially across the soil mass surrounding the probe. Theoretically, the strain rate in the probe-soil boundary is the same as the strain rate of probe expansion and the strain rate is zero at infinity. Prapaharan et al. (1989) showed that at a distance of about ten radius of the probe the strain rate is very small and can be neglected.

Since the strain rate varies hyperbolically (shown later), the total effect of the variation of strain rate has to be obtained by integrating the effect in each small element. The purpose of this chapter is to evaluate quantitatively the combined effect of higher strain rate adopted in the PMT and the variation of strain rate within the soil mass on the undrained shear strength derived from pressuremeter tests.

5.2 Expansion of Cylindrical Cavity - Brief Review

Initially the cylindrical cavity expansion was studied in metals because of its application to pressure vessels and gun barrels (Hill, 1950). The expansion of a

cylindrical cavity in soil mass was theoretically studied by Gibson and Anderson (1961) assuming the soil as elastic-perfectly plastic with a Tresca yield criterion, to derive the pressuremeter expansion curve for undrained tests in clays.. Displacements were calculated assuming zero volume change during plastic flow, i.e. the soil was assumed to behave as a rigid-plastic incompressible solid in a plastic zone surrounding the cavity, and as a linear elastic solid beyond that zone. The effect of volume change in the plastic region was not considered. Using experimentally determined stress-strain and volume change-strain relationships, Ladanyi (1963) introduced the volume change effects in the cavity expansion analysis.

In 1972, Baguelin et al., Ladanyi and Palmer independently presented simple interpretation methods for pressuremeter test, removing the rheological restrictions inherent in the elastic-perfectly plastic analysis, implicitly imposed by Gibson and Anderson (1961). The only restrictive assumption was that of deformation under undrained conditions.

Vesic (1972) presented general solutions for the problems of expansion of cylindrical and spherical cavities in soil having both cohesion and friction. He used a linear elastic-plastic model and considered compressive volumetric strains during the plastic phase. However, the elastic-plastic model is unable to take into account volumetric strains due to shear (Baguelin et al., 1978). Nor can the model consider decreases in shear strength with strain. In other words dilatancy and sensitivity are ignored.

Prevost and Hoeg (1975) proposed different equations for strain hardening and strain softening soils. Using those equations in association with equilibrium considerations and plasticity theory, they derived expressions for pressuremeter expansion curves.

Prapaharan (1987) found that even though the modified Prevost and Hoeg method

(Ladd et al., 1980) was the most promising since it could closely fit a curve while having a theoretical background, it did not fit theoretical pressuremeter expansion curves with sufficient accuracy. Therefore, Prapaharan proposed an alternative equation which gave a better fit for theoretical pressuremeter expansion curves.

When more sophisticated constitutive models are used to represent the stress-strain relationships, cavity expansion problems cannot be solved analytically. In such instances numerical methods are used to solve the complicated equations (e.g. Carter et al., 1979). Most classical solutions for stress and strain distribution around an expanding cavity which is so far assumed in pressuremeter test interpretation, have been based essentially on a small strain assumption. Soulie et al. (1986) presented a finite element method solution for large strain problems, based on an incremental formulation for the problem of an expanding cylindrical cavity.

5.3 Formulation of Cavity Expansion with Strain Rate

The following section uses the formulation and assumptions from Prapaharan et al. (1989):

1. Cavity expansion is taking place under undrained condition.
2. Cavity expansion is axisymmetric and taking place under plane strain conditions.
3. Tensile strains are positive.

Fig. 5.1(a) shows the initial in situ stress state of a cavity, with center O and initial radius a_o. The point B represents a generic material point in the soil mass, located at a distance (r-u). During the cavity expansion, the cavity radius increases from a_o to $a_o + u_o$, and the generic point moves from (r-u) to r (point B' in Fig. 5.1(b)). Since the deformation takes place under undrained conditions, the volume of soil displaced in the annulus between A and A' should be equal to the volume of material in the annulus

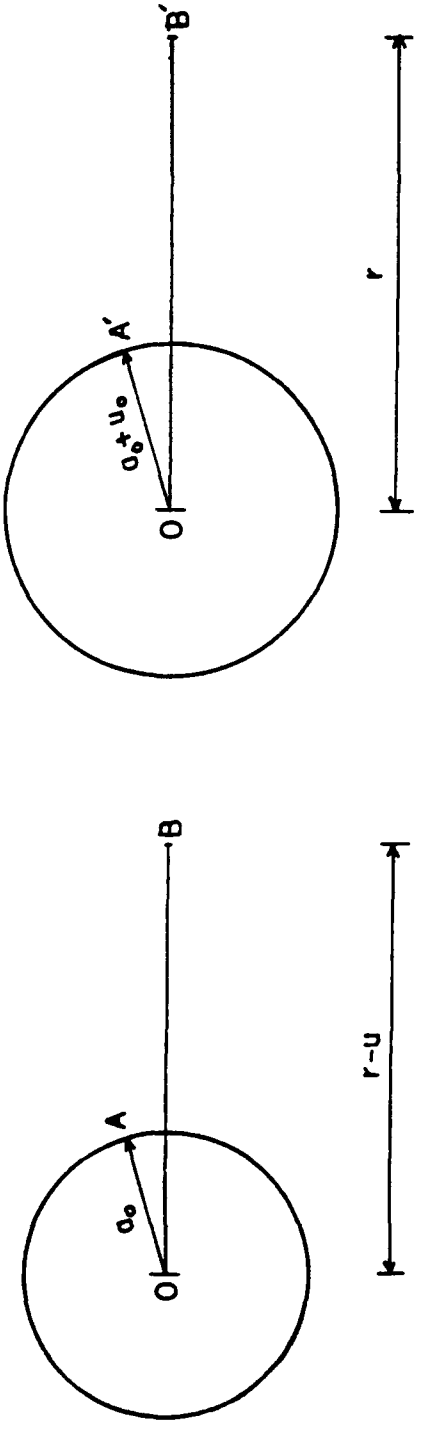

(a) Before Cavity Expansion (Initial In Situ State)

(b) After Cavity Expansion

Fig. 5.1 Expansion of Cylindrical Cavity

between B and B'. By equating these volumes:

$$\pi [(a_o + u_o)^2 - a_o^2] = \pi [r^2 - (r - u)^2] \qquad 5.1$$

After simplification:

$$u = r - [r^2 - (2au_o + u_o^2)]^{1/2} \qquad 5.2$$

The positive root is neglected because u can not be larger than r. The circumferential strain ϵ_θ is tensile everywhere and defined as:

$$\epsilon_\theta = \frac{u}{r - u} \qquad 5.3$$

Substituting for u from Eq. 5.2:

$$\epsilon_\theta = -1 + [1 - u_o(2a_o + u_o)/r^2]^{-1/2} \qquad 5.4$$

The equilibrium equation in the cylindrical system requires:

$$\frac{\partial \sigma_r}{\partial r} + \frac{\sigma_r - \sigma_\theta}{r} = 0 \qquad 5.5$$

The difference between the radial and circumferential effective stresses is given as a function of the circumferential strain ϵ_θ, and the strain rate $\dot{\epsilon}_\theta$. Therefore:

$$\sigma'_r - \sigma'_\theta = \sigma_r - \sigma_\theta = q\ (\epsilon_\theta, \dot{\epsilon}_\theta) \qquad 5.6$$

Substituting Eq. 5.6 in Eq. 5.5:

$$\frac{\partial \sigma_r}{\partial r} = -\frac{1}{r}\, q\ (\epsilon_\theta, \dot{\epsilon}_\theta) \qquad 5.7$$

As r tends to infinity, the radial stress tends to the in situ horizontal stress σ_h, which is independent of time. At the cavity boundary, σ_r is equal to the applied pressure which is a measured quantity $P(\epsilon_0, \dot{\epsilon}_0)$, a function of the circumferential strain ϵ_0 at the

cavity wall and strain rate $\dot{\epsilon}_0$ for strain controlled expansion. By integrating Eq. 5.7 from infinity to the cavity boundary (i.e., at $r = a_o + u_o$):

$$\int_{[\sigma_r]_{r=\infty}}^{[\sigma_r]_{r=a_o+u_o}} d\sigma_r = \int_{\infty}^{a_o+u_o} -\frac{1}{r}\, q(\epsilon, \dot{\epsilon})dr$$

$$P(\epsilon_0, \dot{\epsilon}_0) - \sigma_h = \int_{\infty}^{a_o+u_o} -\frac{1}{r}\, q\,(\epsilon, \dot{\epsilon})dr \qquad 5.8$$

To simplify the notation, the circumferential strain ϵ_θ will be represented by ϵ from here onwards. Using Eq. 5.4 the integration variable r is transformed to ϵ:

$$1 - \frac{u_o(2a_o + u_o)}{r^2} = \frac{1}{(1+\epsilon)^2}$$

$$\frac{1}{r^2} = \left[1 - \frac{1}{(1+\epsilon)^2}\right] \frac{1}{u_o(2a_o + u_o)} \qquad 5.9$$

Differentiating Eq. 5.9:

$$\frac{dr}{r^3} = -\frac{d\epsilon}{(1+\epsilon)^3}\, \frac{1}{u_o(2a_o + u_o)} \qquad 5.10$$

Dividing Eq. 5.10 by Eq. 5.9:

$$\frac{dr}{r} = -\frac{d\epsilon}{\epsilon(1+\epsilon)(2+\epsilon)} \qquad 5.11$$

Substituting Eq. 5.11 in Eq. 5.8:

$$P(\epsilon_o, \dot{\epsilon}_o) - \sigma_h = \int_{o}^{\epsilon_o} \frac{q(\epsilon, \dot{\epsilon})}{\epsilon(1+\epsilon)(2+\epsilon)} d\epsilon \qquad 5.12$$

If the function $q(\epsilon, \dot{\epsilon})$ is known, the Eq. 5.12 can be numerically integrated to obtain the strain rate dependent pressuremeter curve. In conventional interpretation

methods, the strain rate effect is not included, i.e., $q(\epsilon, \dot{\epsilon}) = q(\epsilon)$. In this case, differentiating Eq. 5.12 gives:

$$q(\epsilon_o) = \epsilon_o(1 + \epsilon_o)(2 + \epsilon_o)\frac{dP}{d\epsilon_o} \qquad 5.13$$

which is the same as the equation derived by others (e.g. Baguelin et al., 1972, Ladanyi, 1972, and Palmer 1972).

5.4 Variation of Strain Rate within the Soil Mass

In Section 5.3, the generic point in the initial state (B) was taken at distance (r-u) and after deformation that point (B') moved to r. This step was taken in order to compare the results with Palmer's (1972) results. In order to make the differentiation possible, to get an expression for strain rate in terms of distance, r should be referred to the initial state. See Fig. 5.2 for the new distances of the generic point, before and after the deformation. When the cavity expands from the initial radius a_o to $a_o + u_o$, the material generic point B moves from r to point B' at r+u. Following the same procedure as in Section 5.3, equating the volumes before and after the deformation:

$$\pi\,[(a_o + u_o)^2 - a_o^2] = \pi\,[(r + u)^2 - r^2] \qquad 5.14$$

which leads to

$$u = -r + [r^2 + u_o(2a_o + u_o)]^{1/2} \qquad 5.15$$

The negative root is neglected because u is positive during probe expansion. The strain ϵ_θ results from Eq. 5.15:

$$\epsilon_\theta = \epsilon = \frac{u}{r} = -1 + \left[1 + \frac{u_o(2a_o + u_o)}{r^2}\right]^{1/2} \qquad 5.16$$

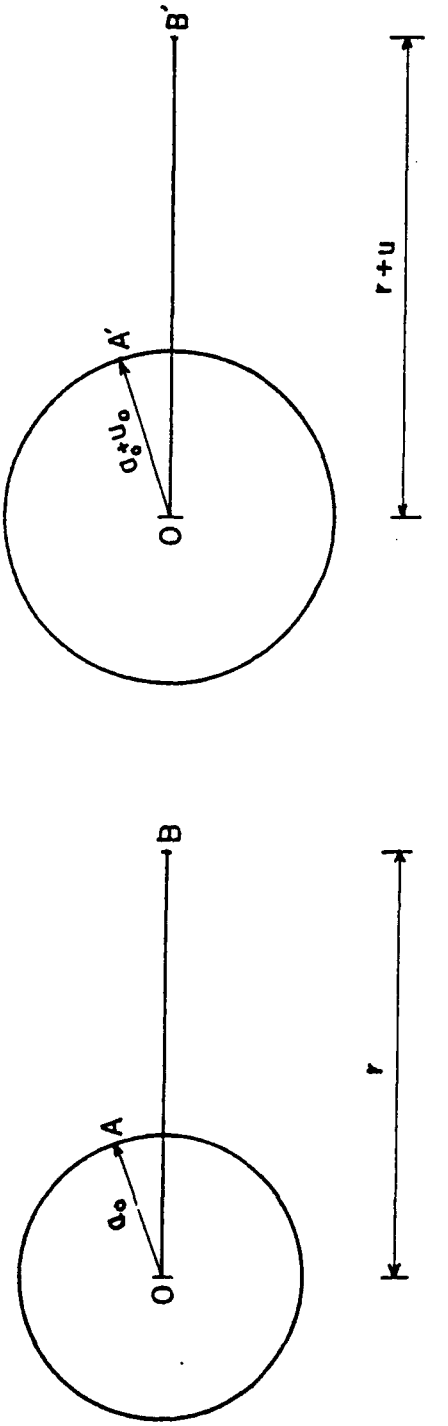

Fig. 5.2 New Notation for the Material Generic Point

Substituting $\epsilon_o = \frac{u_o}{a_o}$ in Eq. 5.16:

$$\epsilon = -1 + \left[1 + (\frac{a_o}{r})^2 \epsilon_o(2 + \epsilon_o)\right]^{1/2} \qquad 5.17$$

Differentiating strain with respect to time:

$$\dot{\epsilon} = \frac{1}{2}\left[1 + \left(\frac{a_o}{r}\right)^2 (2+\epsilon_o)\epsilon_o\right]^{-1/2}\left[\left(\frac{a_o}{r}\right)^2 \{\epsilon_o(\dot{\epsilon}_o) + (2+\epsilon_o)\dot{\epsilon}_o\}\right] \qquad 5.18$$

Substituting Eq. 5.17 in Eq. 5.18:

$$\dot{\epsilon} = \frac{1}{2}\,\frac{1}{1+\epsilon}\left(\frac{a_o}{r}\right)^2 2\dot{\epsilon}_o(1 + \epsilon_o) \qquad 5.19$$

To eliminate r from Eq. 5.19, $\left(\frac{a_o}{r}\right)^2$ is obtained from Eq. 5.17:

$$\left(\frac{a_o}{r}\right)^2 = \frac{(1 + \epsilon)^2 - 1}{\epsilon_o(2 + \epsilon_o)} = \frac{\epsilon(2 + \epsilon)}{\epsilon_o(2 + \epsilon_o)} \qquad 5.20$$

Substituting Eq. 5.20 in Eq. 5.19:

$$\dot{\epsilon} = \dot{\epsilon}_o\,\frac{(1 + \epsilon_o)}{\epsilon_o(2 + \epsilon_o)}\,\frac{\epsilon(2 + \epsilon)}{(1 + \epsilon)} \qquad 5.21$$

The equation 5.21 gives the variation of strain rate within the soil mass for a given strain ϵ_o, and strain rate $\dot{\epsilon}_o$ at the cavity wall. Figures 5.3 and 5.4 show typical variations of strain and strain rate, respectively, with distance from the center of the cavity that were obtained using equations 5.17 and 5.21. The strain and strain rate

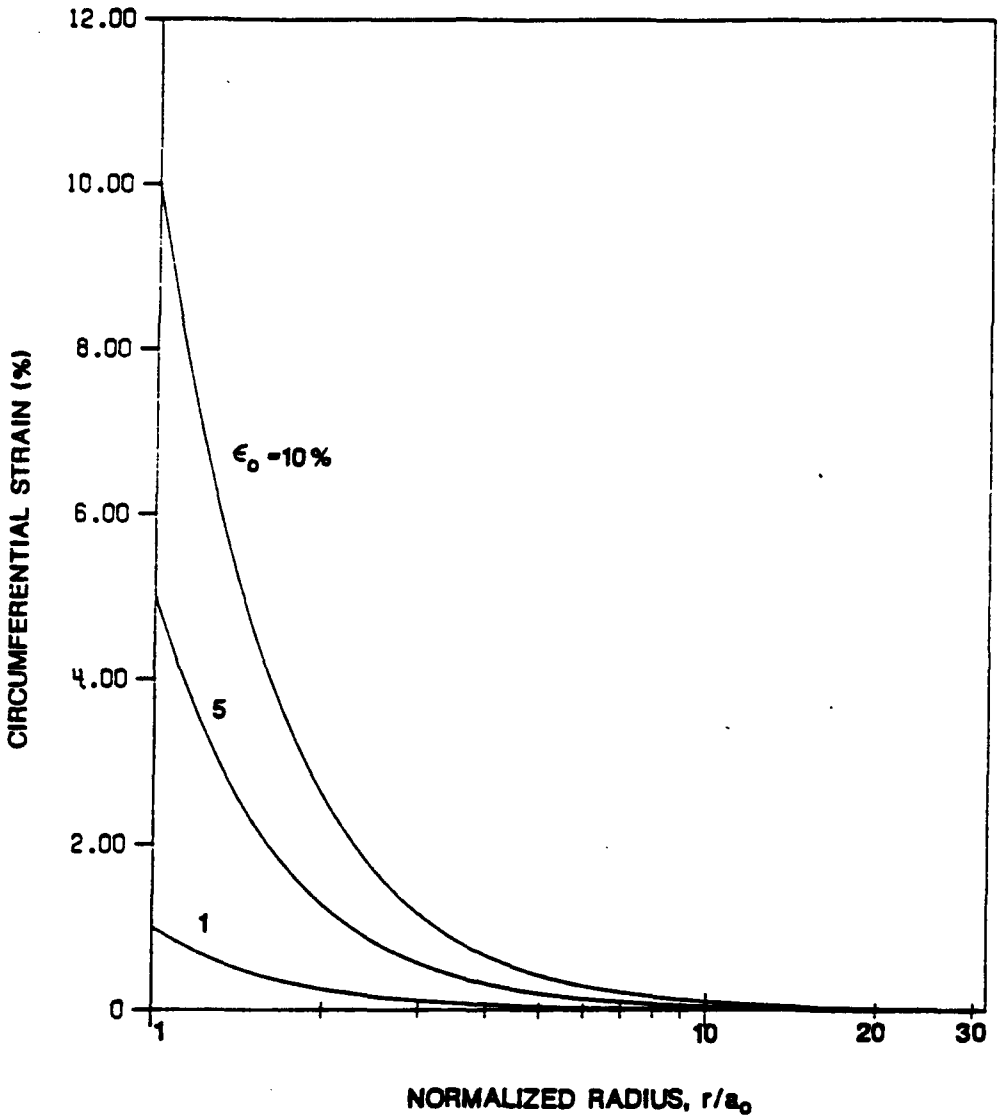

Fig. 5.3 Variation of Strain with Normalized Distance from the Center of Cavity (After Prapaharan et al., 1989)

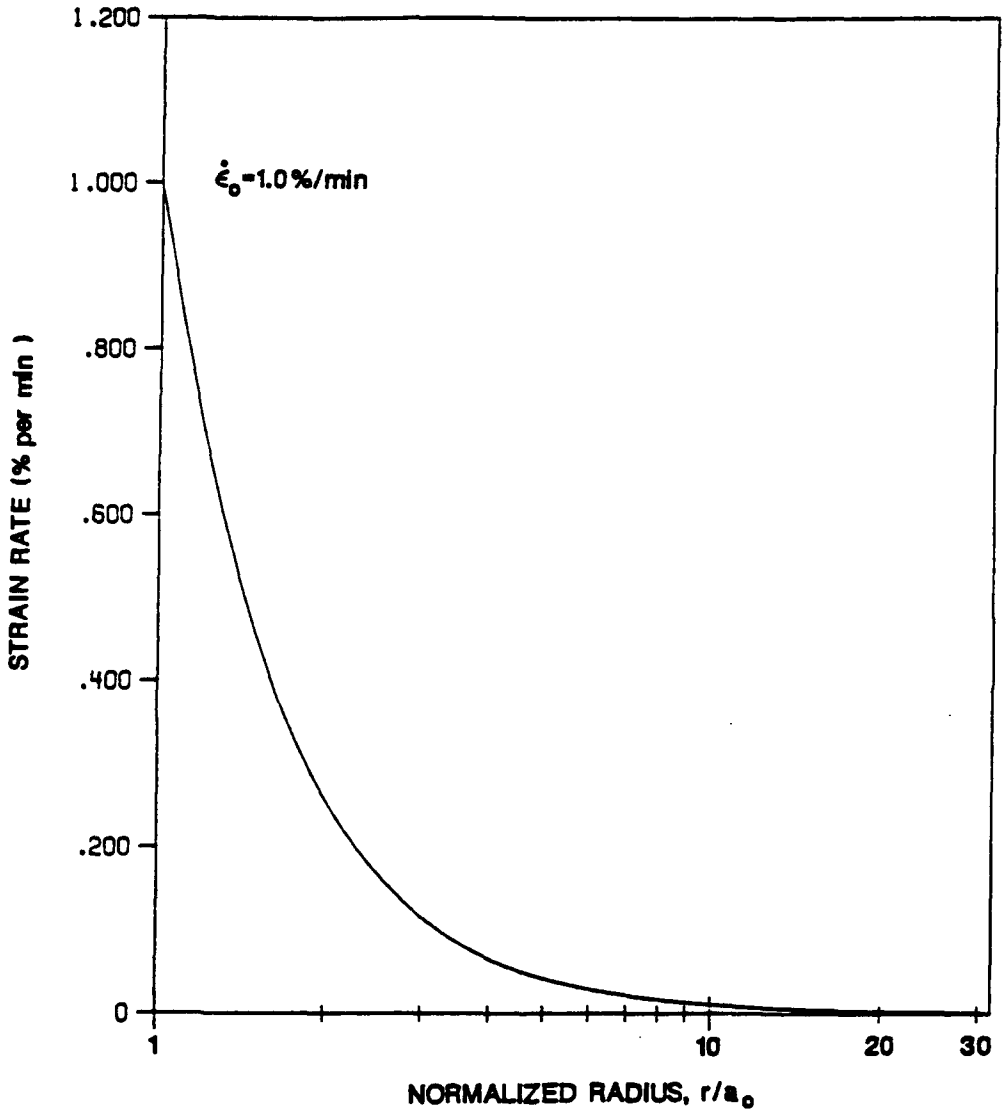

Fig. 5.4 Variation of Strain Rate with Normalized Distance from the Center of Cavity (After Prapaharan et al., 1989)

decrease with distance and are essentially negligible at a distance equal to ten times the radius of the cavity.

5.5 Stress-Strain Modeling Including Strain Rate

The variation of undrained shear strength with strain rate has been discussed in Chapter 4. Based on triaxial tests conducted on various soils with strain rate varying from 0.0001% per min to 10% per min, Prapaharan et al. (1989) proposed a bilinear model to describe the variation of undrained shear strength with strain rate (Fig. 4.1). From the tests performed in CSD simulating pressuremeter strain path, the influence of strain rate in pressuremeter tests was studied and the outcome was included in the same plot and shown in Fig. 4.26.

Prapaharan et al. (1989) proposed the following relationship between undrained strength and strain rate:

$$q_u = q_\alpha \left(1 + \beta \log_{10}\left(\frac{\dot{\epsilon}}{\alpha}\right)\right) \qquad 5.22$$

where q_u is the shear strength at a strain rate $\dot{\epsilon}$, q_α is the strength at a reference strain rate α and β is slope of strength against logarithm of strain rate curve.

From Fig. 4.26, it can be obtained as $\beta = 0.10$ for triaxial tests and $\beta = 0.15$ for pressuremeter tests.

Assume a hyperbolic model to express the stress-strain behavior of a true strain hardening soil:

$$q(\epsilon) = \frac{\epsilon}{D + \epsilon} q_u \qquad 5.23$$

where q_u is the ultimate strength and D is a constant.

Combining Eqs. 5.22 and 5.23:

$$q(\epsilon, \dot{\epsilon}) = \frac{q_\alpha(1 + \beta \log_{10}(\dot{\epsilon}/\alpha))}{(D + \epsilon)} \epsilon \qquad 5.24$$

Substituting Eq. 5.24 in Eq. 5.12:

$$P(\epsilon_o, \dot{\epsilon}_o) - \sigma_h = \int_o^{\epsilon_o} \frac{q_\alpha(1 + \beta \log_{10}(\dot{\epsilon}/\alpha))}{(1 + \epsilon)(2 + \epsilon)(D + \epsilon)} d\epsilon \qquad 5.25$$

The strain rate $\dot{\epsilon}$ in Eq. 5.25 is a function of strain, ϵ, and can be calculated from Eq. 5.21. Eq. 5.25 can be integrated numerically to obtain the pressuremeter expansion curve which includes the strain rate effect. Eq. 5.13 can be used to develop the stress-strain curve from the pressuremeter curve which ignores the strain rate variation in the soil mass. By comparing the derived stress-strain curve $q(\epsilon_o)$ - which does not include the strain rate, against the "true" stress-strain curve $q(\epsilon_o, \dot{\epsilon}_o)$ - which includes the strain rate, error involved in neglecting the strain rate in soil mass can be estimated.

The "true" pressuremeter expansion curves can be developed from Eq. 5.25. The parameters needed are q_α, α, $\dot{\epsilon}_o$, β and the constant D which describes the stress-strain curves for strain hardening soils. The values chosen to these parameters and constants are:

q_α: The derived stress-strain curve is normalized with respect to the reference strength q_α. Therefore, for strain hardening soils, in Eq. 5.25, the term q_α will be cancelled out and the absolute value is not needed.

α: The reference strain rate α is taken as 0.01% per min as it is the standard strain rate used in laboratory tests.

$\dot{\epsilon}_o$: Two strain rates are used: (i) 1.0% per min, the strain rate recommended by Baguelin et al. (1978) to be used in the PMT, and (ii) 0.1% per min for comparison purposes.

β: The slope of the shear strength versus strain rate curve. From Fig. 4.26, the slope for the PMT (from CSD tests) is about 0.15.

The constant D which describe the stress-strain curves for strain hardening soils can be obtained from empirical relationships or from experimental data.

(i) From empirical relationship

The assumed hyperbolic relationship to represent the strain hardening soil is (Eq. 5.23):

$$q = \frac{q_u}{D + \epsilon}\,\epsilon$$

$$\frac{dq}{d\epsilon} = \frac{D\,q_u}{(D + \epsilon)^2} \qquad 5.26$$

As ϵ tends to zero, the slope tends to q_u/D (Eq. 5.26). That is, the slope of the stress-strain curve at zero strain is equal to q_u/D. This slope can be related to the shear modulus. The shear modulus is defined as:

$$G = \frac{\tau}{\gamma}$$

where $\tau = q/2$ and $\gamma = \epsilon_r - \epsilon_\theta = 2\epsilon$ (for small strains).

Therefore:

$$G = \frac{q}{4\epsilon}$$

Hence:

$$\text{Initial slope} = \frac{q}{\epsilon} = \frac{q_u}{D} = 4G$$

Therefore:

$$\frac{1}{D} = \frac{4G}{q_u}$$

The shear modulus G is related to the elastic modulus:

$$G = \frac{E}{2(1 + \nu)}$$

For undrained conditions in clays, it can be assumed that the Poisson's Ratio ν is equal to 0.5. Therefore:

$$G = \frac{E}{3} \quad and \quad \frac{1}{D} = \frac{4E}{3q_u}$$

Since E/q_u values for most clays fall between 250 and 750 (Bjerrum, 1972), 1/D will range from 300 to 1000. For example, a value of 1/500 was selected for by Prapaharan et al. (1989) in their analysis.

(ii) Determination of D from the experimental curves

From the simulated pressuremeter tests in the CSD (Chapter 4), it was found that the kaolin-ground silica soil behaved like strain hardening soils (Fig. 4.23). The behavior of strain hardening soils can be simulated with an hyperbolic relationship (Eq. 5.23):

$$q(\epsilon) = \frac{\epsilon}{D + \epsilon} q_u$$

$$\sigma_1 - \sigma_3 = \frac{\epsilon}{D + \epsilon} q_u \qquad 5.27$$

Rearranging the terms:

$$\frac{\epsilon}{\sigma_1 - \sigma_3} = \frac{1}{q_u}\epsilon + \frac{D}{q_u} \qquad 5.28$$

From the experimental data (Table 4.3), $\frac{\epsilon}{\sigma_1 - \sigma_3}$ versus ϵ curves are plotted (Fig. 5.5-5.8, a few examples in each strain rate) and using the linear regression the slope and the intercept are determined and the calculated D is presented in Table 5.1. An average value of 1/D = 160 for kaolin-silica was used in the present numerical analysis for strain hardening soil.

5.6 Procedure for Numerical Simulation

The relationship derived for the applied pressure on the cavity wall as a function of strain and strain rate for strain hardening soil is (Eq. 5.25):

$$\frac{P(\epsilon_o, \dot{\epsilon}_o) - \sigma_h}{q_\alpha} = \int_0^{\epsilon_o} \frac{1 + \beta\log(\dot{\epsilon}/\alpha)}{(1+\epsilon)(2+\epsilon)(D+\epsilon)}\, d\epsilon \qquad 5.29$$

Since q_α is the strength at a reference strain rate α, it is a known quantity and a constant. Therefore, it can be separated from the integral and brought to the left hand side of the equation, which is in the normalized form.

Method I: Numerical Integration by Incremental Approach

Numerical integration for a complex function can be performed using an incremental method such as Simpson's Rule. Any function can be approximated by a higher order of polynomial and the increment width approximated to the variation of the function. For Simpson's Rule the range [a,b] is divided into n equal parts where n is an even integer. Then, according to Simpson's Rule, the integral can be approximated by:

$$\int_a^b f(x)\, dx = \frac{\Delta x}{3}\left(y_o + 4y_1 + 2y_2 + \ldots + 2y_{n-2} + 4y_{n-1} + y_n\right) \qquad 5.30$$

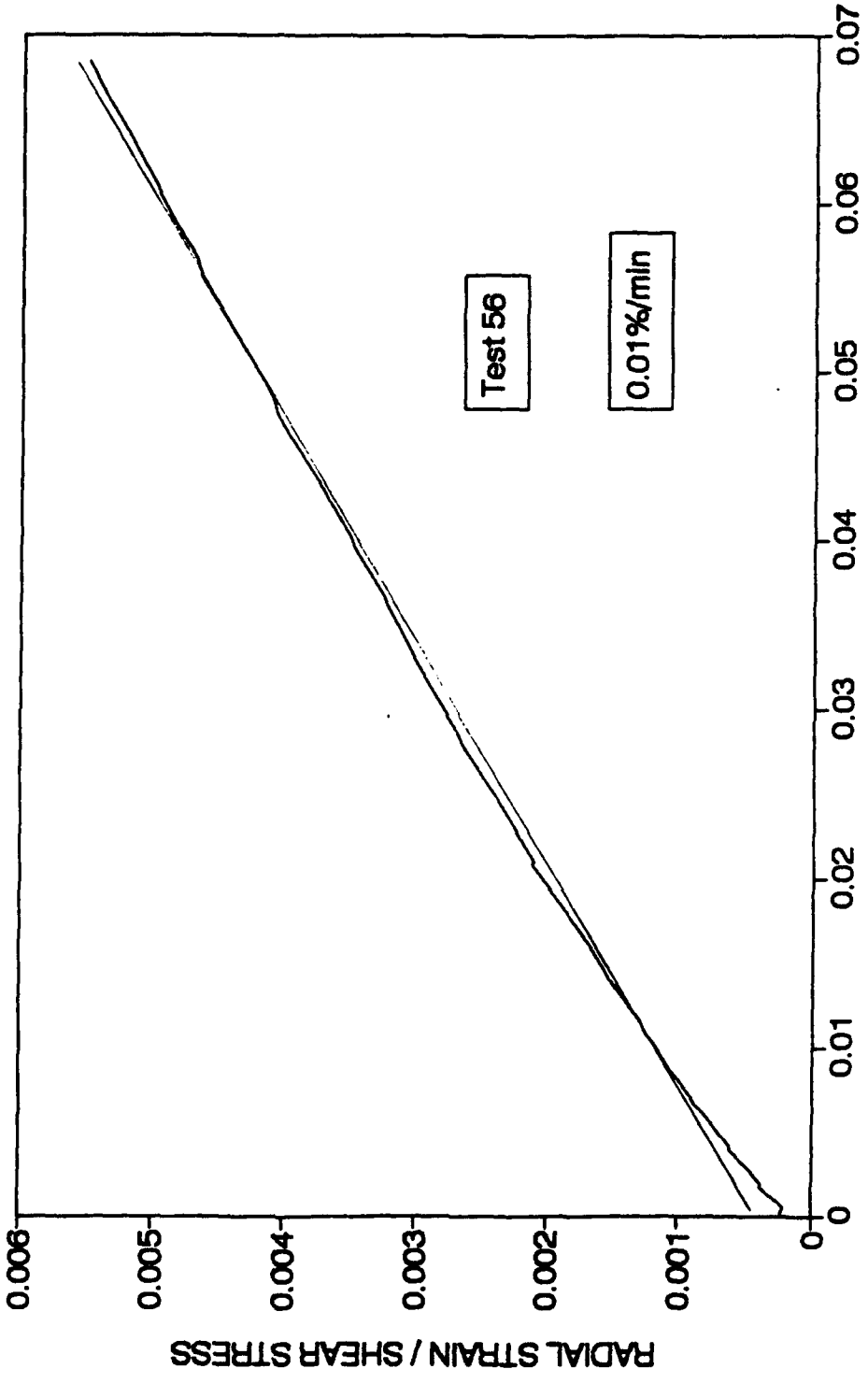

Fig. 5.5 Linear Conversion of Hyperbolic Curve for 0.01%/min

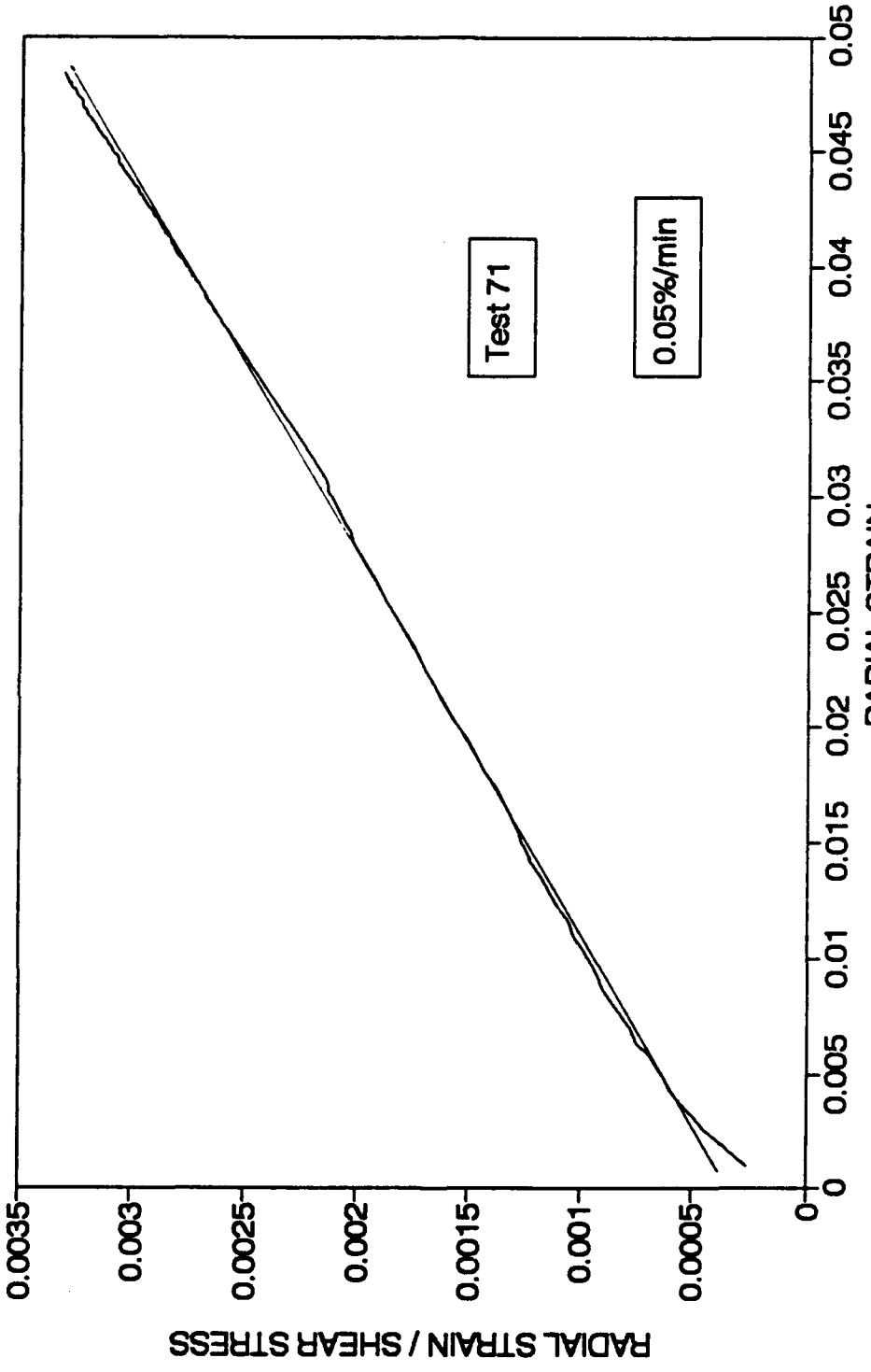

Fig. 5.6 Linear Conversion of Hyperbolic Curve for 0.05%/min

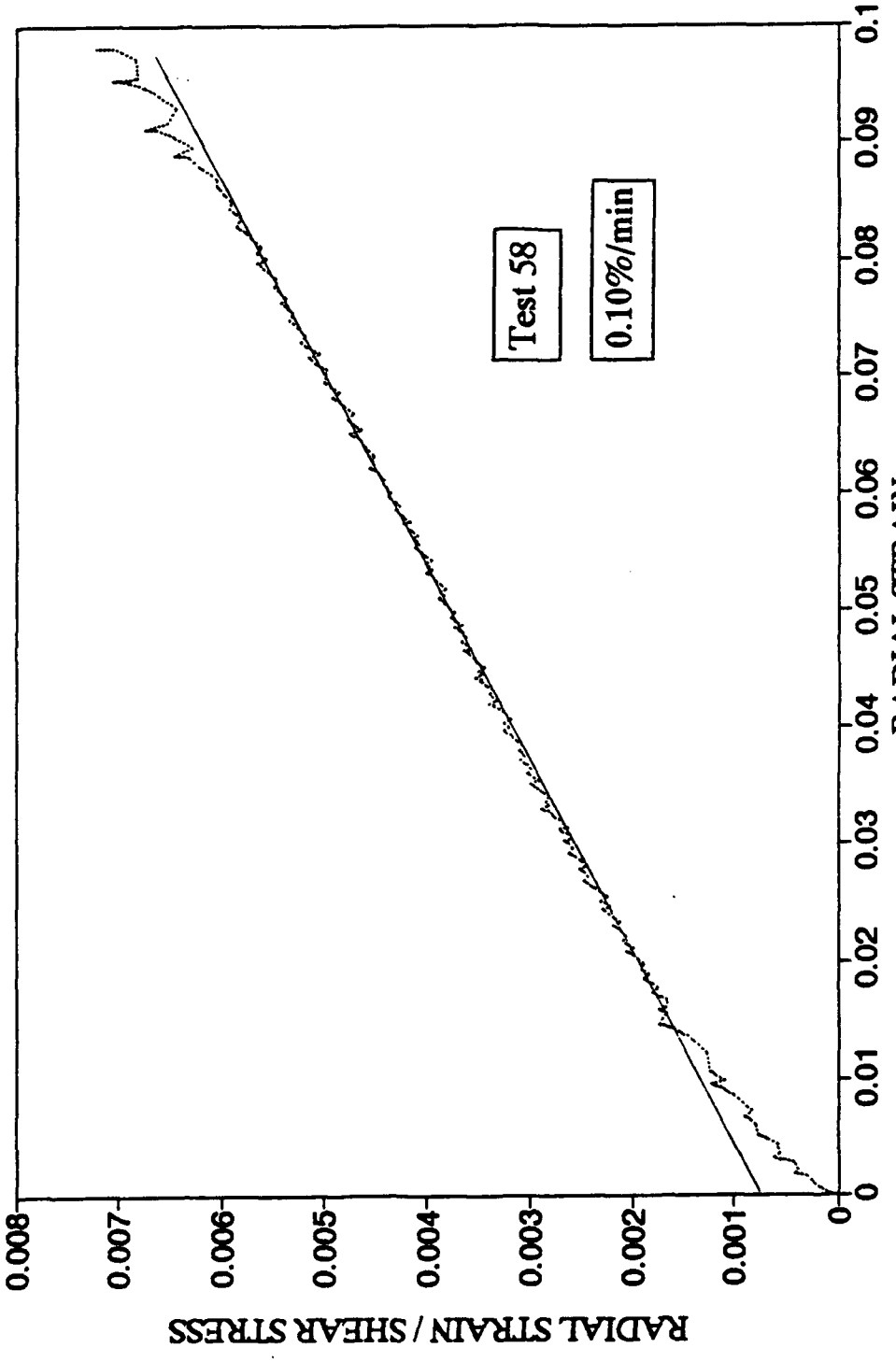

Fig. 5.7 Linear Conversion of Hyperbolic Curve for 0.10%/min

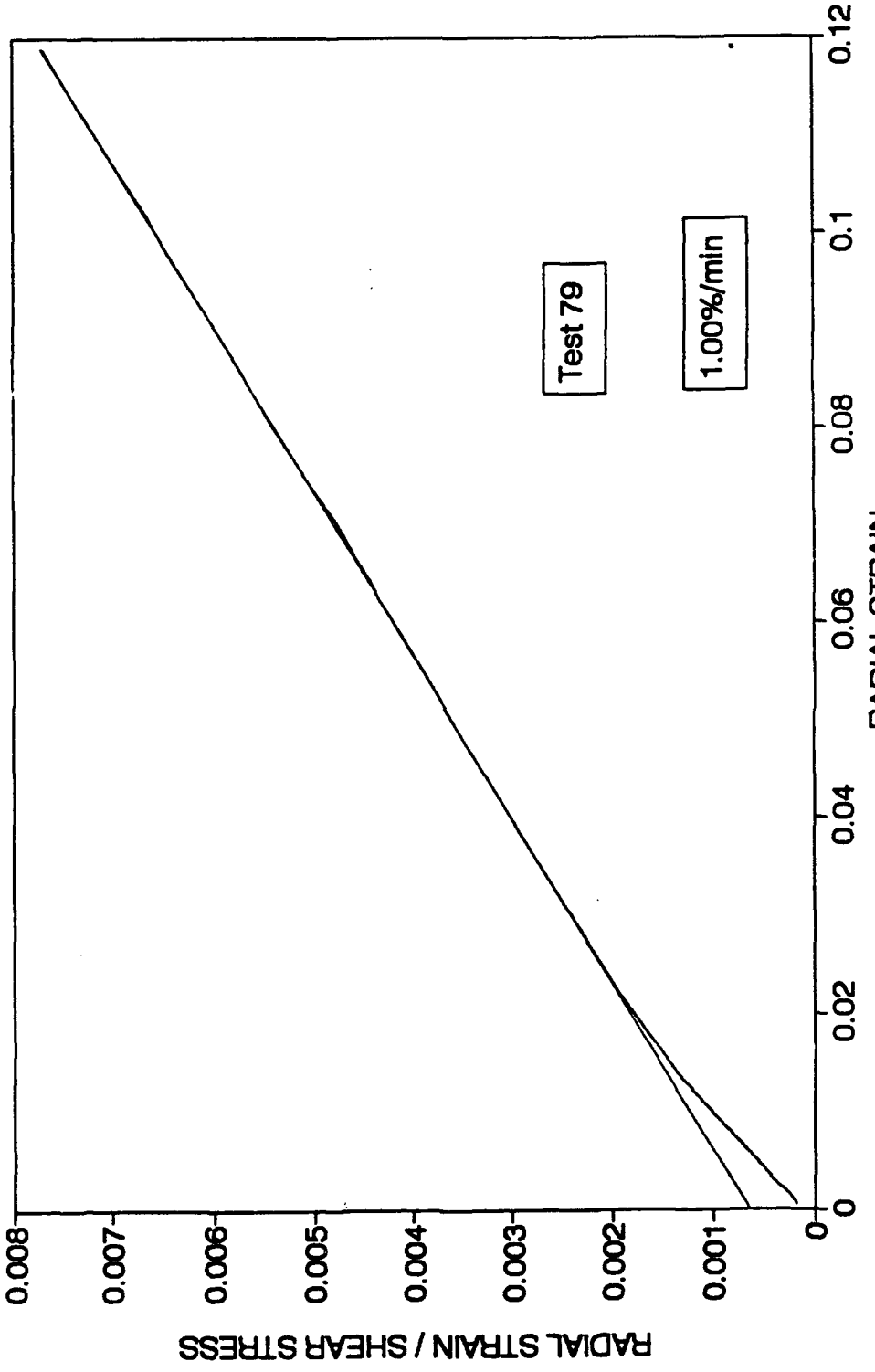

Fig. 5.8 Linear Conversion of Hyperbolic Curve for 1.00%/min

Table 5.1 Value of D from Experimental Data (Kaolin-Silica Soil) Using Hyperbolic Equation

Test No.	Strain Rate (% per min)	Slope $1/q_u$	Intercept D/q_u	q_u (psi)	D	1/D
55	0.01	0.09947	0.000235	10.05	0.0024	423
56	0.01	0.077548	0.000344	12.90	0.0044	225
64	0.01	0.067787	0.000578	14.75	0.0085	117
78	0.01	0.076991	0.000410	12.99	0.0053	188
61	0.05	0.058840	0.000366	17.00	0.0062	161
71	0.05	0.061464	0.000320	16.27	0.0052	192
77	0.05	0.078682	0.000730	12.71	0.0092	108
58	0.10	0.064341	0.000569	15.54	0.0088	113
59	0.10	0.059322	0.000317	16.86	0.0082	122
60	0.10	0.057194	0.000460	13.48	0.0080	124
74	0.10	0.056327	0.000137	17.75	0.0024	410
66	0.50	0.053702	0.000796	18.62	0.0148	68
67	0.50	0.052052	0.000713	19.61	0.0137	73
72	0.50	0.056422	0.000659	13.32	0.0117	86
75	0.50	0.067192	0.001872	14.88	0.0239	36
53	1.00	0.060274	0.000361	16.59	0.0060	167
54	1.00	0.062041	0.000367	16.12	0.0059	169
62	1.00	0.053690	0.001198	18.63	0.0223	45
79	1.00	0.062670	0.000333	15.96	0.0053	188
57	5.00	0.054226	0.000259	18.44	0.0048	209
68	5.00	0.052261	0.000366	19.13	0.0070	143

where $\Delta x = (b - a)/n$.

When n = 2, the Simpson's Rule becomes:

$$\int_a^b f(x)\,dx = \frac{b-a}{6}\left[f(a) + 4f\left(\frac{a+b}{2}\right) + f(b)\right] \qquad 5.31$$

Now the whole integral can be obtained by adding the divided areas as shown in Fig. 5.9:

$$I = \int_a^{a+\Delta x} f(x)\,dx + \int_{a+\Delta x}^{a+2\Delta x} f(x)\,dx + \ldots + \int_{a+(m-1)\Delta x}^{b} f(x)\,dx \qquad 5.32$$

Step 1 Step 2 Step m

In the analysis reported herein each step is repeated 201 times (i.e., n = 201) and 1000 steps were taken (i.e., m = 1000). These values of n and m were found adequate for the function considered. The integral in equation 5.29 is a function of strain and strain rate:

$$I_1 = \int_0^{\epsilon_o} f(\epsilon, \dot{\epsilon})\,d\epsilon \qquad (5.33)$$

The strain rate is related to strain by Eq. 5.21:

$$\dot{\epsilon} = \dot{\epsilon}_o \frac{(1+\epsilon_o)}{\epsilon_o(2+\epsilon_o)} \frac{\epsilon(2+\epsilon)}{(1+\epsilon)} \qquad (5.34)$$

where $\dot{\epsilon}$ varies with cavity strain ϵ_o. A variation of 0% to 10% cavity strain is considered in the numerical analysis.

In Step 1, a = 0, a + Δx = 0.1/201 and $\int_0^{\Delta\epsilon_o}$ is splitted into m = 1000 points to evaluate the integral numerically. The strain rate $\dot{\epsilon}$ is evaluated at every step 0,

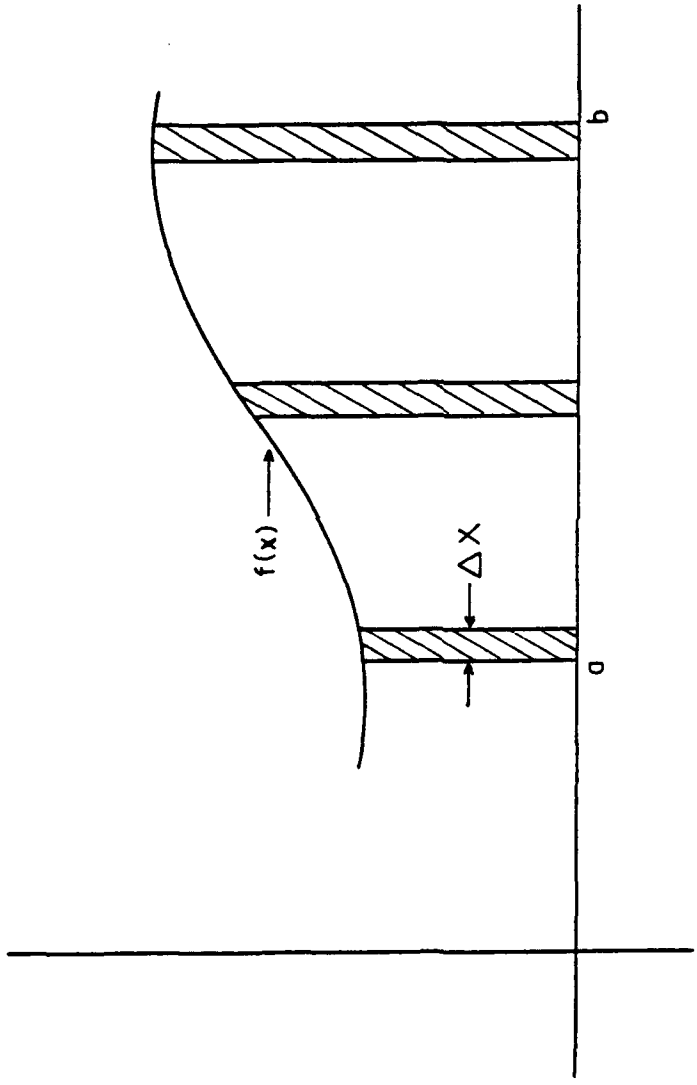

Fig. 5.9 Integration of a Function

$\Delta\epsilon_o/1000$, $2\Delta\epsilon_o/1000$ ... $\Delta\epsilon_o$ and $f(\epsilon, \dot{\epsilon})$ is also evaluated at those steps. Then, using Simpson's Rule (Eq. 5.31):

$$\int_0^{2\frac{\Delta\epsilon_o}{1000}} f(\epsilon, \dot{\epsilon})\, d\epsilon, \quad \int_{2\frac{\Delta\epsilon_o}{1000}}^{4\frac{\Delta\epsilon_o}{1000}} f(\epsilon, \dot{\epsilon})\, d\epsilon \text{ ... and so on}$$

can be calculated and the sum of the above integrals will give the integration in Eq. 5.29, and $(P\ (\epsilon_o, \dot{\epsilon}_o) - \sigma_h)/q_\alpha$ can be calculated for all ϵ_o varies from 0 to 0.1. This gives a pressuremeter expansion curve which includes the variation of strain rate in the soil mass around the probe. Then the pressuremeter curve is differentiated numerically using Gauss functions with Eq. 5.13 in order to obtain $q(\epsilon_o)$.

The above method is called the "incremental approach". A computer program was written in Quick Basic and the source code is annexed in Appendix V. The results are discussed in Section 5.7.

Method II: Numerical Integration Consistent with the Derivation of the Formulation

In Section 5.3, the applied pressure $P(\epsilon_o, \dot{\epsilon}_o)$ on the cavity wall was found by integrating the equilibrium equation in cylindrical coordinate system (Eq. 5.5) and using the boundary conditions, as r tends to infinity, the radial stress tends to the horizontal stress σ_h and at the cavity boundary $r = a_o + u_o$, σ_r is equal to $P(\epsilon_o, \dot{\epsilon}_o)$, the applied pressure is related to the shear stress of the soil (Eq. 5.8). When the domain of integration was switched from dr to $d\epsilon$ (by using Eq. 5.11), the boundary conditions were also externally forced such that at $r = a_o + u_o$, $\epsilon = \epsilon_o$ and at $r = \infty$, $\epsilon = 0$, however this was not implicitly included or enforced anywhere in the formulation. This will induce errors in Method I as shown later. In Method I, without implying the transformation of boundary condition, the integral was numerically calculated by simply finding $\Delta\epsilon_o$ by incremental approach and adding the area under the function.

Method II is performed as follows:

For cavity strain ϵ_o changing from 0% to 10%, i.e. ϵ_o = 0.0 to 0.1 (as earlier), using 201 steps $\Delta\epsilon_o$ = (0.1 - 0)/201. Then,

$$I_1 = \int_0^{\Delta\epsilon_o} f(\epsilon, \dot{\epsilon})\, d\epsilon$$

Split this integral into n steps (say n = 1000 as earlier) and evaluate $\dot{\epsilon}$ at each of $\Delta\epsilon_o$/n points and calculate $f(\epsilon, \dot{\epsilon})$ at these points. Then, calculate $I_1 = \epsilon dI$, using Simpson's Rule. This gives one point in the $P(\Delta\epsilon_o)$ vs $\Delta\epsilon_o$ curve. Similarly, $I_2 = \int_0^{2\Delta\epsilon_o} f(\epsilon, \dot{\epsilon})\, d\epsilon$ can be calculated using repeat of this process up to 201 times and finally, $I_{201} = \int_0^{201\Delta\epsilon_o} f(\epsilon, \dot{\epsilon})\, d\epsilon$ can be calculated. Each numerical integral is performed using n = 1000 points.

The major difference between this method and the previous method (incremental approach) is that the integration is carried out every time starting from 0 and ending up with cavity strain, i.e. the entire soil mass is considered in every small increment of strain. It could be argued that if the same number of integration points (n = 1000) is used for smaller increment such as $\int_0^{\Delta\epsilon_o}$ and the larger increment such as $\int_0^{201\Delta\epsilon_o}$, it might affect the accuracy of the integration. To verify this aspect, n was increased by 100 for every iteration up to 20,100 points and it was found that the results were not improved by increasing the number of integration points (Fig. 5.10). Hence, n = 1000 (points) was found to be a reasonable number of integration points and was used in the subsequent numerical integration.

A computer program was written in Quick Basic to perform the numerical integration and differentiation (using Gauss functions) in order to calculate q (ϵ_o). The

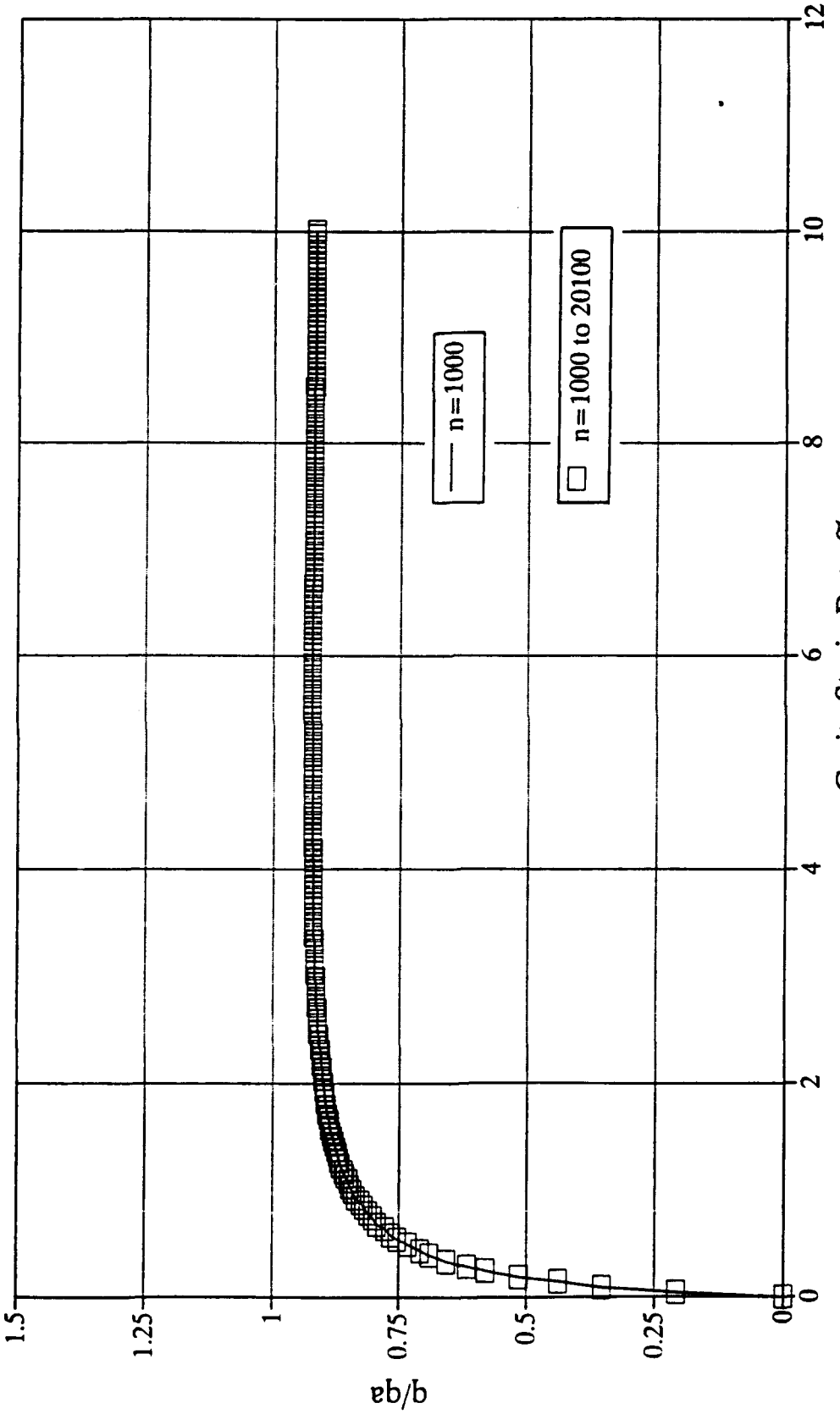

Fig. 5.10 Verification of Number of Integration Points in the Numerical Integration to Simulate Pressuremeter Test

source code is given in Appendix E. The results are discussed in the next section.

5.7 Results and Discussion

The following values are used to check the numerical integration with previously published results (Prapaharan et al., 1989):

α = Reference strain rate = 0.01%/min

β = Parameter for strain rate effect = 0.10

D = 1/500 and

$\dot{\epsilon}_o$ = 0.1%/min and 1.0%/min

Fig. 5.11 shows the effect of strain rate on undrained shear strength derived from pressuremeter test for strain hardening soils (Prapaharan et al., 1989). The solid lines represent the so-called true material stress-strain curves obtained from the assumed strain hardening relationship (Eq. 5.23) for different strain rates (0.001, 0.01, 0.1 and 1.0%/min). The dashed lines show the stress-strain curves derived from the pressuremeter exansion curves obtained for two different expansion rates (0.1%/min, and 1.0%/min). These stress-strain curves were derived using Eq. 5.13 from the pressuremeter curves obtained with Eq. 5.26. The difference between the derived curve and the true material curve for the same strain rate is an indication of strain rate effect induced by the pressuremeter test condition.

Using the computer program developed for Method I, the pressuremeter curves are obtained by numerical integration procedure described in Section 5.9 using Eq. 5.25 and the stress-strain curves are derived from Eq. 5.13 and shown in Fig. 5.12. As can be noticed, the stress-strain curve derived using the Method I (Incremental Approach) coincided exactly with the "true" material stress-strain curve as in Fig. 5.11. This means that the incremental approach did not reflect the pressuremeter test condition and the algorithm or to be exact, the interpretation of the boundary condition is not correct. Even though mathematically there is nothing wrong in the numerical integration by the

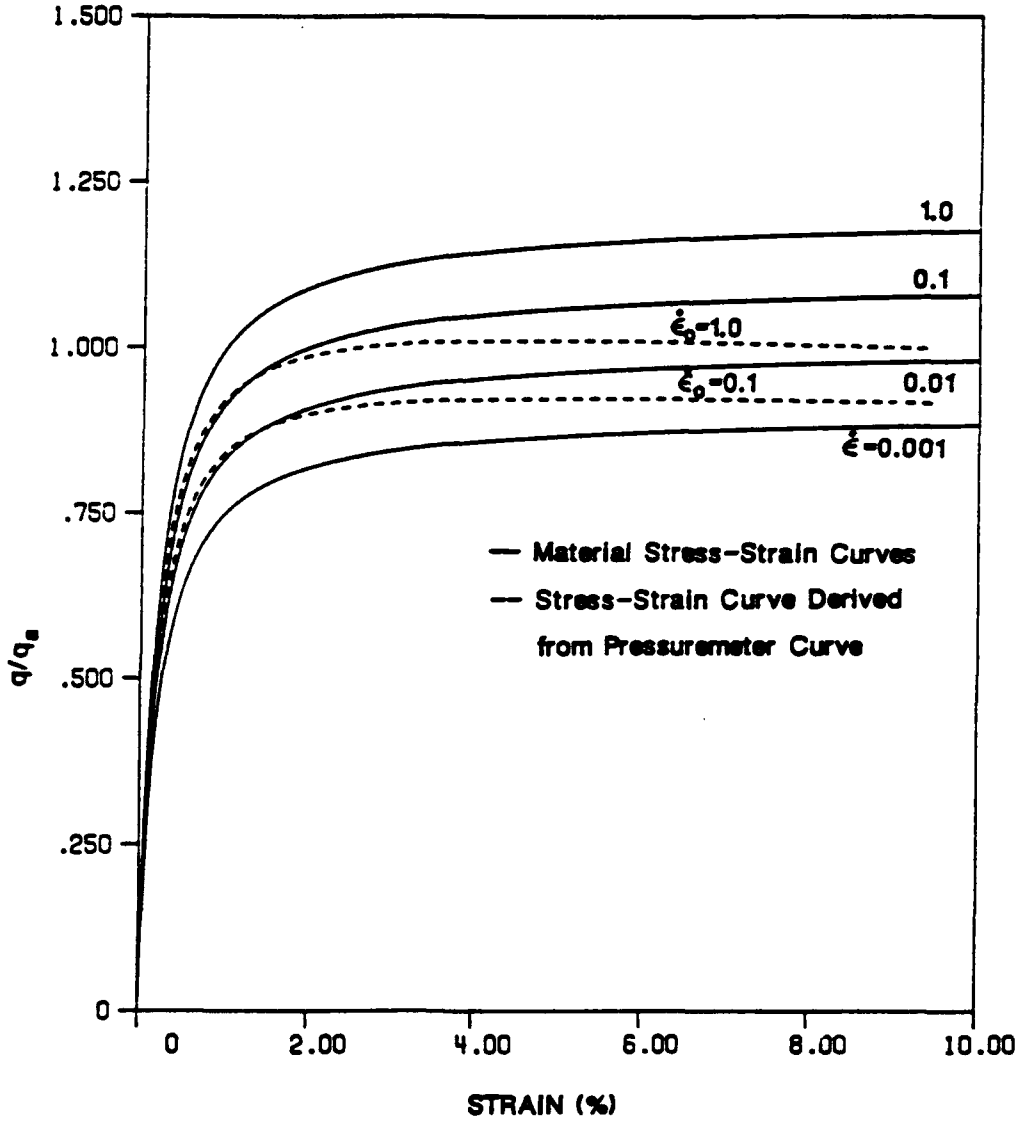

Fig. 5.11 Effect of Strain Rate on Undrained Strength Derived from Pressuremeter Test: Strain Hardening Soils (D = 1/500) (After Prapaharan et al., 1989)

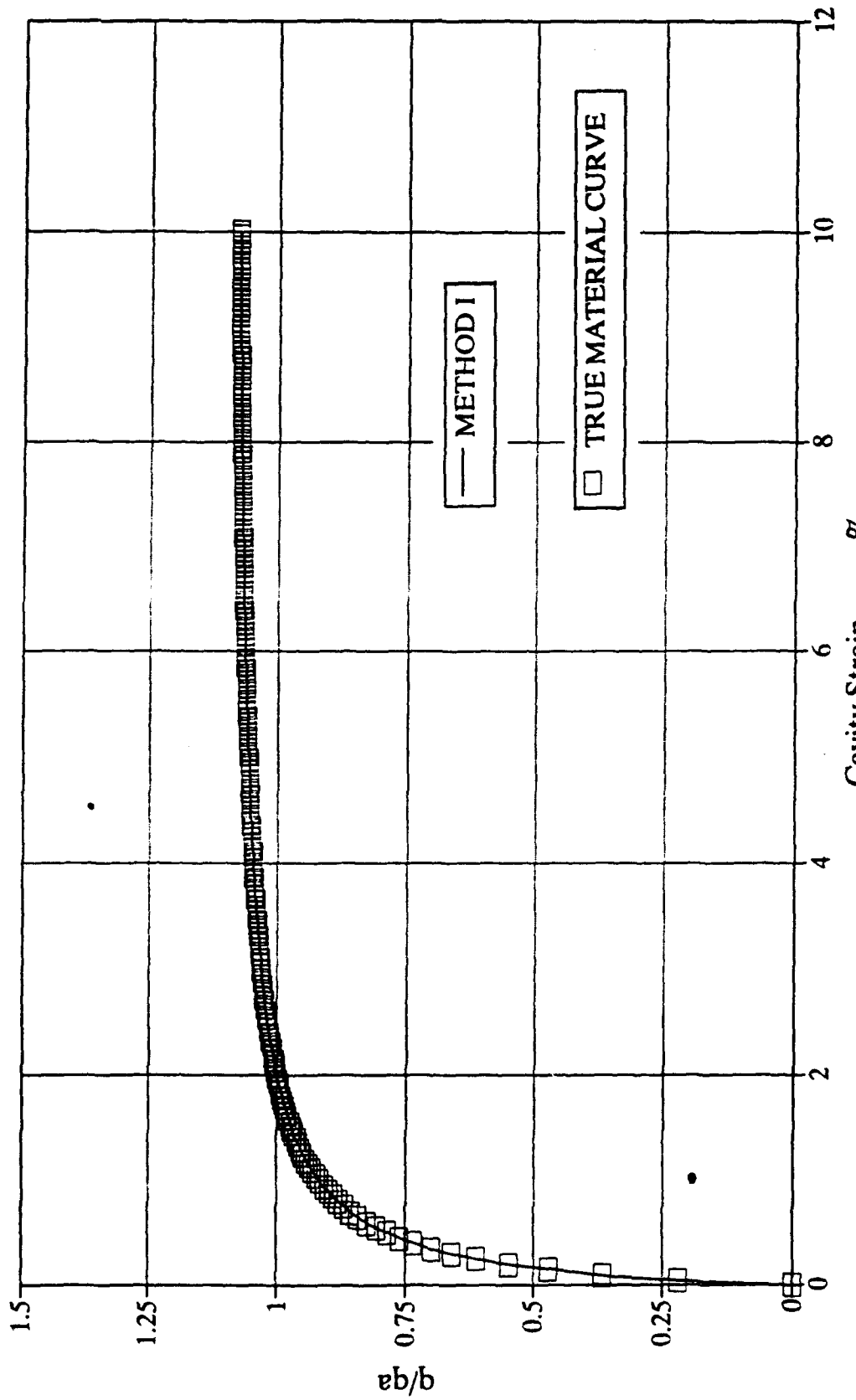

Fig. 5.12 Verification of Numerical Integration to Simulate Pressuremeter Test by Method I

incremental approach, the transformed boundary conditions are not properly implemented in the numerical integration. This is an important point to be noticed when equations alone are used in the PMT interpretation without relevance to the actual physical aspects of the test.

Using Method II which is consistent with the transformation of the boundary conditions, the stress-strain curve are derived from the pressuremeter expansion curve and shown in Fig. 5.13 with the "true" material stress-strain curve. The curves shown in the figure exactly match the published results (Fig. 5.11) for the strain rate 0.1% per min.

Influence of Upper Yield

In Chapter 4, the influence of strain rate on undrained shear strength determined by triaxial tests was discussed. Bjerrum (1972) found that the shear strength was increasing about 10% for every ten fold increase of strain rate without any upper yield. But others (Vaid and Campanella (1977), and Nakase and Kamei (1986)) observed different levels of upper yield values.

To study the influence of upper yield in the derived stress-strain curves three cases were considered:

1. Upper yield at 0.001%/min (Prapaharan et al., 1989)
2. Upper yield at 0.0001%/min
3. No upper yield (Bjerrum, 1972)

The derived stress-strain curves for the above three cases are shown in Fig. 5.14. As the upper yield is decreasing the strain softening behavior is little more pronounced. In fact, even for the no upper yield case (Bjerrum, 1972), i.e. the strength approaching zero as the strain rate tends to zero which is an unrealistic behavior, the increase of strain softening is very little. Therefore, for all practical purposes it can be assumed that

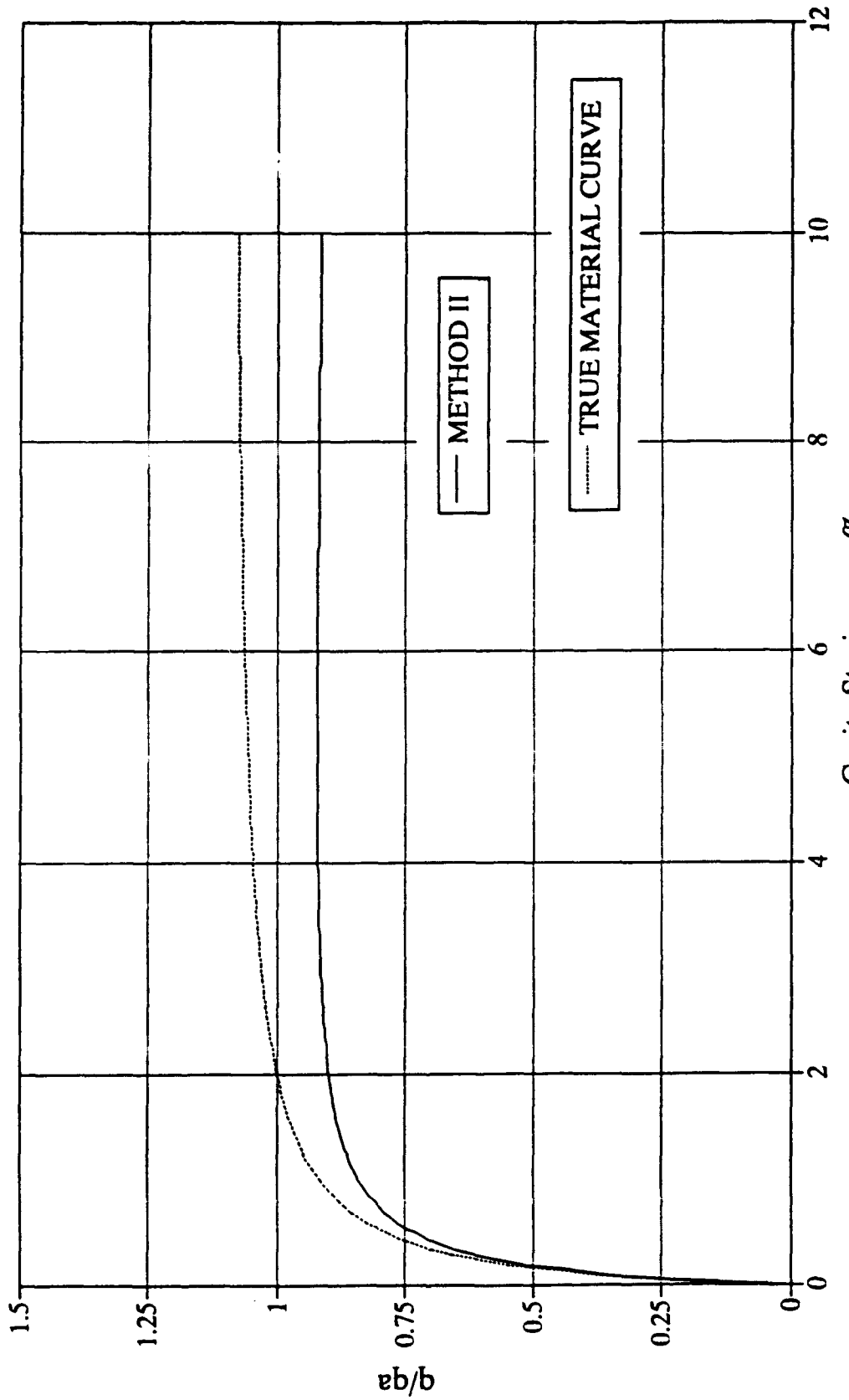

Fig. 5.13 Stress-Strain Curves Derived from Strain Hardening Model and Pressuremeter Curve Using Method II

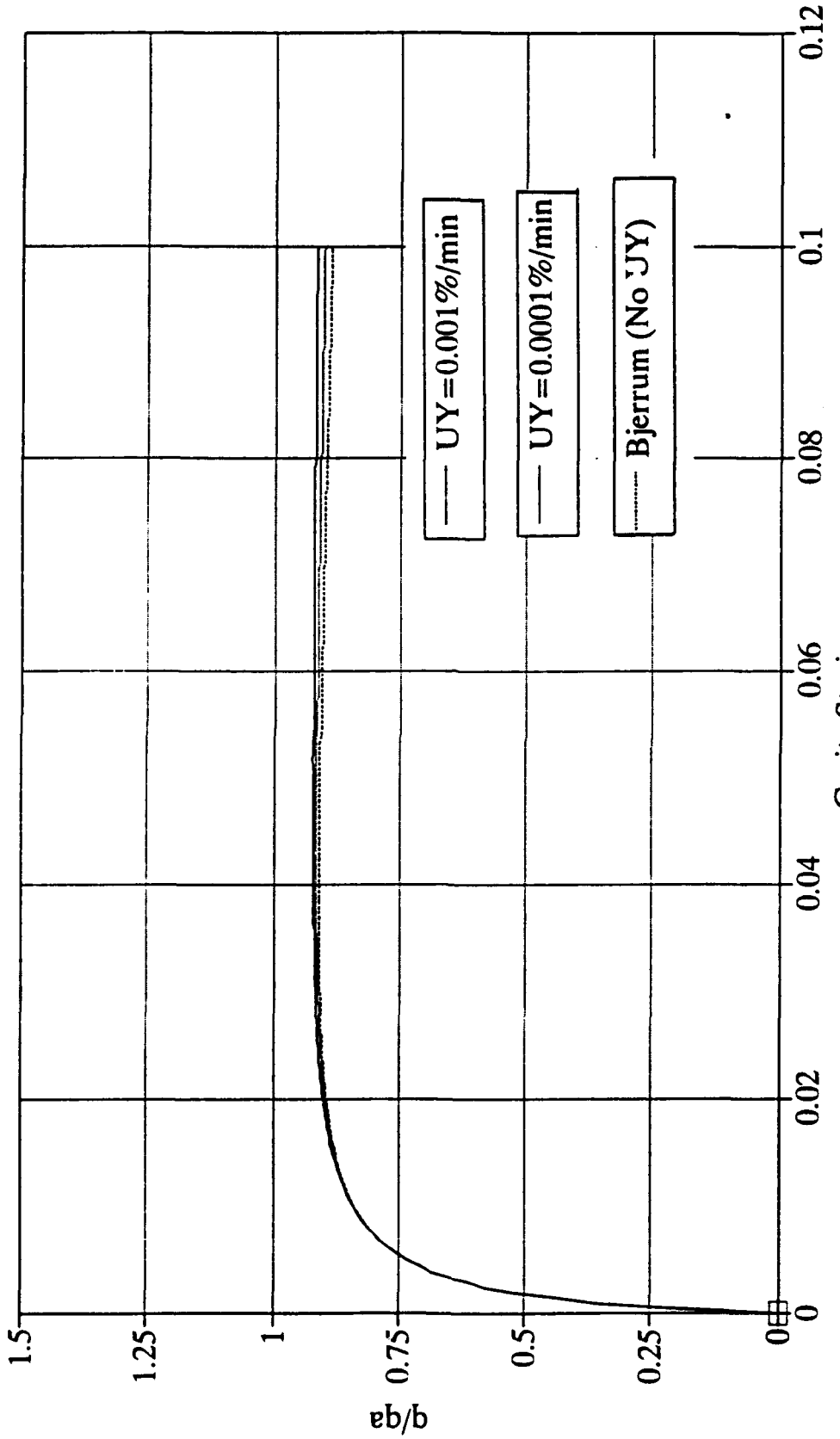

Fig. 5.14 Influence of Upper Yield on Derived Stress-Strain Curves

the level of upper yield is insignificant in the prediction of undrained shear strength from the pressuremeter test. This ascertains our previous notion that beyond a distance of about ten radius from the cavity wall the strain and strain rate effects could be neglected (Figs. 5.3 and 5.4) because the very small strain rates (0.001% per min and below) do not affect the strength predictions.

Influence of β

From Fig. 4.26, the slope of the normalized undrained shear strength versus logarithm of strain rate line, β, was determined as 0.10 for triaxial tests and 0.15 for pressuremeter tests. To study the influence of β several parametric studies were performed. Fig. 5.15 shows the normalized stress-strain curves for two strain rates 0.1%/min and 1.0%/min, D = 1/500, reference strain rate, α = 0.01%/min and β = 0.10 (the same as Fig. 5.11 of Prapaharan, et al., 1989). This plot is reproduced here in order to compare the influence of different parameters that affect the stress-strain curves. For the higher value of β = 0.15, the actual ("true" material) and the derived stress-strain curves are shown in Figs. 5.16 and 5.17 along with β = 0.10 curves for cavity expansion rate of 0.1%/min and 1%/min. The curves are basically the same at the beginning (because they have the same D) up to a cavity strain of 0.5%. Beyond this strain β has a significant influence on the actual and derived curves. For the higher value of β (PMT condition), the peak strength shows a 25% decrease, and as β increases the softening behavior also increases significantly. In fact, for β = 0.10 (triaxial condition) the actual and PMT curves are strain hardening and for β = 0.15, they are strain softening curves. As the cavity expansion rate increases from 0.1%/min to 1.0%/min, for the same β = 0.15, the softening behavior also increases, as opposed to an increase in strain hardening for β = 0.10. For a 0.1%/min cavity expansion rate, the peak strength is almost the same for β = 0.10 and 0.15, but for 1.0%/min expansion rate β = 0.15 produces slightly larger strength than β = 0.10. For the higher strain rate (1.0%/min), the PMT curve for β = 0.15 is strain softening and β = 0.10 is strain hardening type. So, they reach almost same (residual) strength at higher strains.

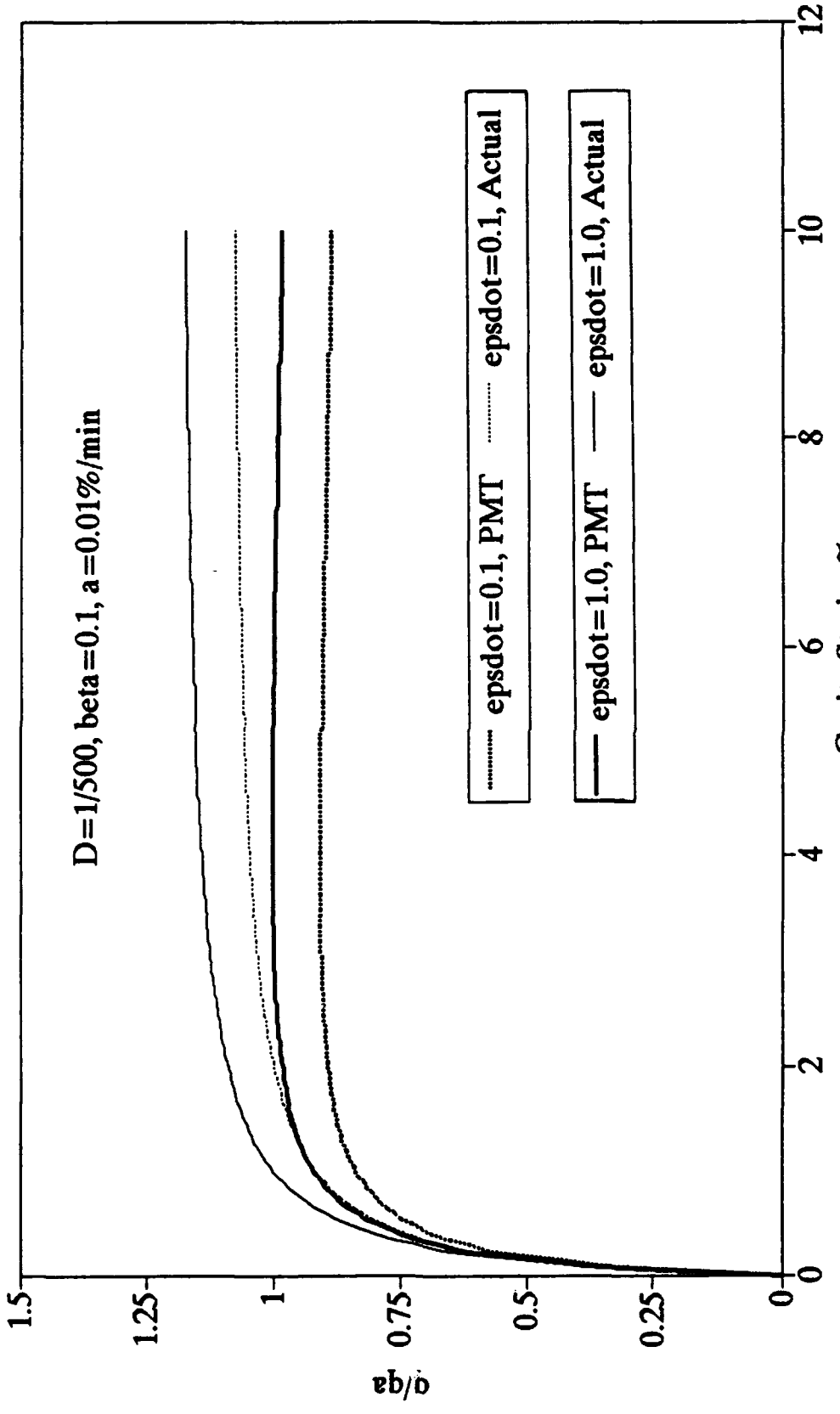

Fig. 5.15 Effect of Strain Rate on Undrained Shear Strength Derived from PMT (D = 1/500, Beta = 0.1)

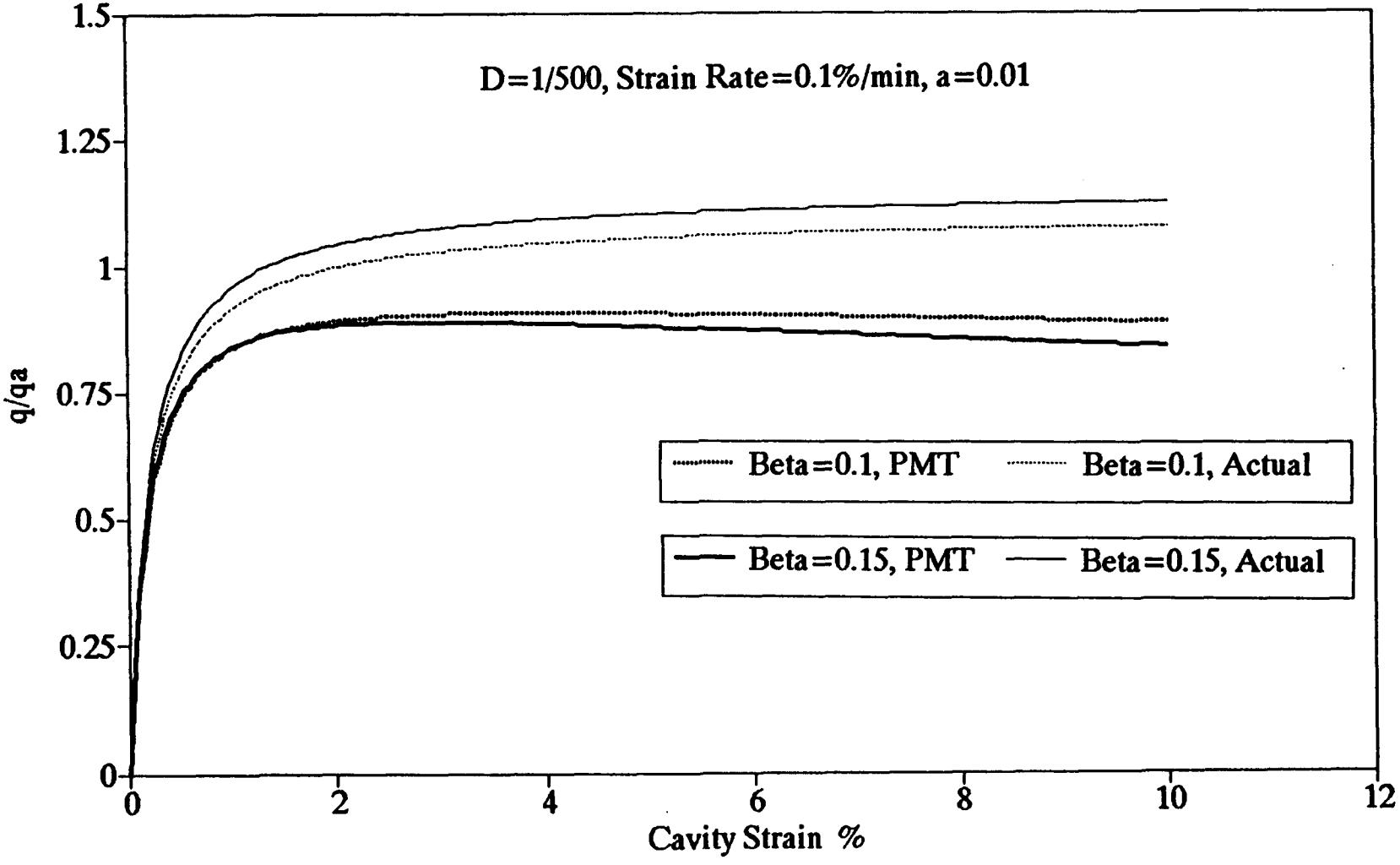

Fig. 5.16 Influence of Beta on Undrained Shear Strength Derived from PMT at Strain Rate = 0.1%/min (D = 1/500)

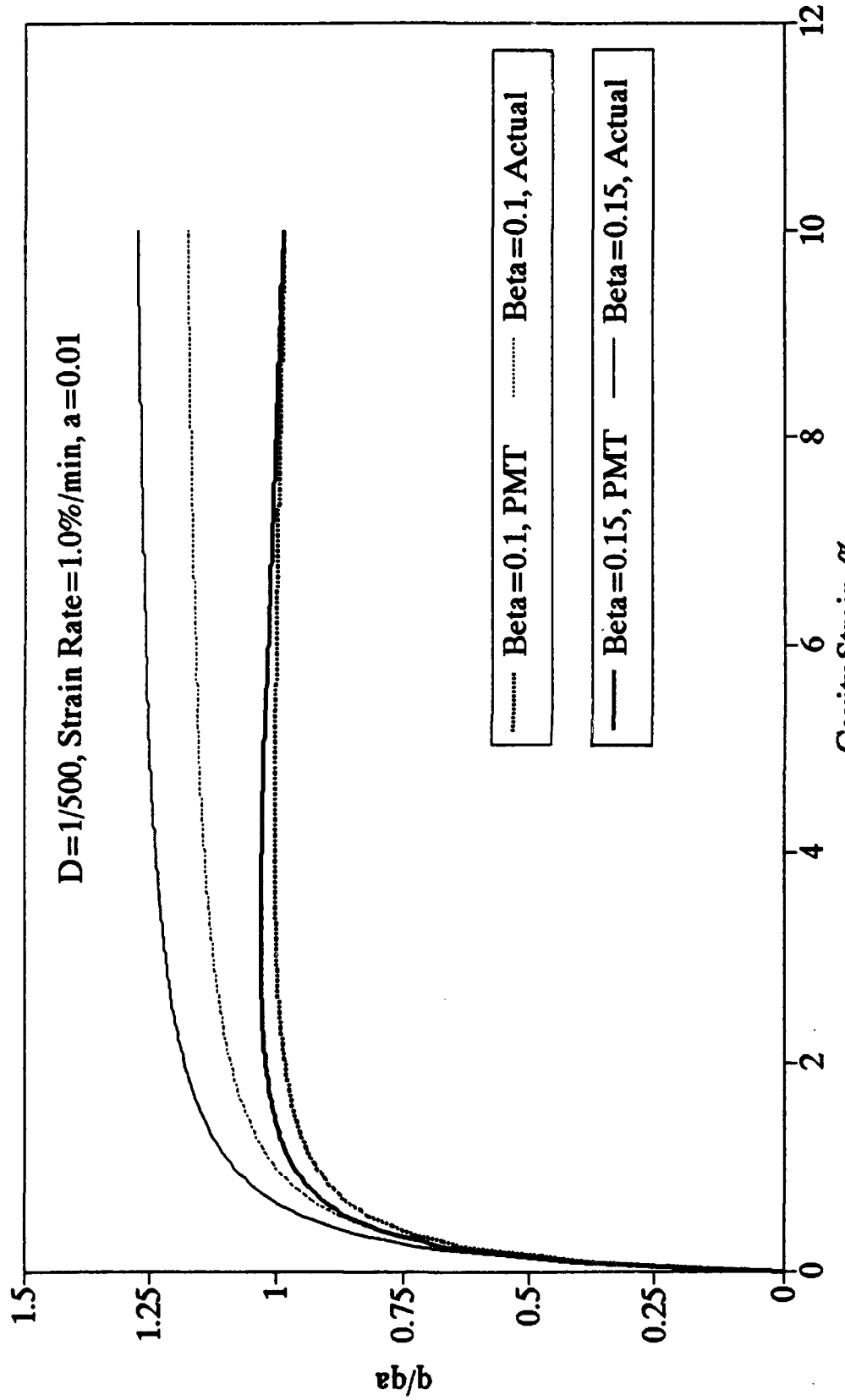

Fig. 5.17 Influence of Beta on Undrained Shear Strength Derived from PMT at Strain Rate = 1.0%/min (D = 1/500)

In general, for the PMT condition (β = 0.15), the derived curves from pressuremeter expansion curves show higher strain softening compared to the triaxial test conditions (β = 0.10), whereas the actual curves show higher strain hardening and higher strength as β increases from 0.10 to 0.15. That is, the pressuremeter test condition induces more strain softening than the triaxial test condition which very well agrees with Prevost (1976) who used a strain rate sensitive rheological model, and Jamiolkowski and Lancellota (1977) results.

Influence of D

The constant D in the hyperbolic equation which is an inverse measure of initial tangent modulus, also has a significant influence on the actual and derived (PMT) curves (Figs. 5.18-5.23). As expected, for the smaller D value (which Prapaharan et al. (1989) arbitrarily selected, D = 1/500), the actual and PMT curves have steeper slopes than for the larger D value (obtained from the CSD tests performed on kaolin-silica soil in laboratory; D = 1/160) for both cavity expansion rates. The constant D affects not only the results initially but also throughout the curve. For the larger values of D, the actual as well as derived stress-strain curves show higher strain hardening behavior irrespective of the cavity expansion rate. Even though at smaller strain levels, the larger D curves show lesser strength than the stress-strain curves with smaller D values, they reach essentially the same strength at larger strain levels (see Figs. 5.18-5.21). For both cavity expansion rate (0.1 and 1.0%/min), the derived curves from PM expansion yield exactly the same ultimate strength, irrespective of different D values. Similar to previous results, higher strain rate tests and higher β value curves give higher shear strength (Figs. 5.18-5.21).

Combined Influence of D and β

For the values obtained from triaxial tests (β = 0.10) and from the empirical correlations (D = 1/500), Prapaharan et al. (1989) studied the effect of strain rate in the

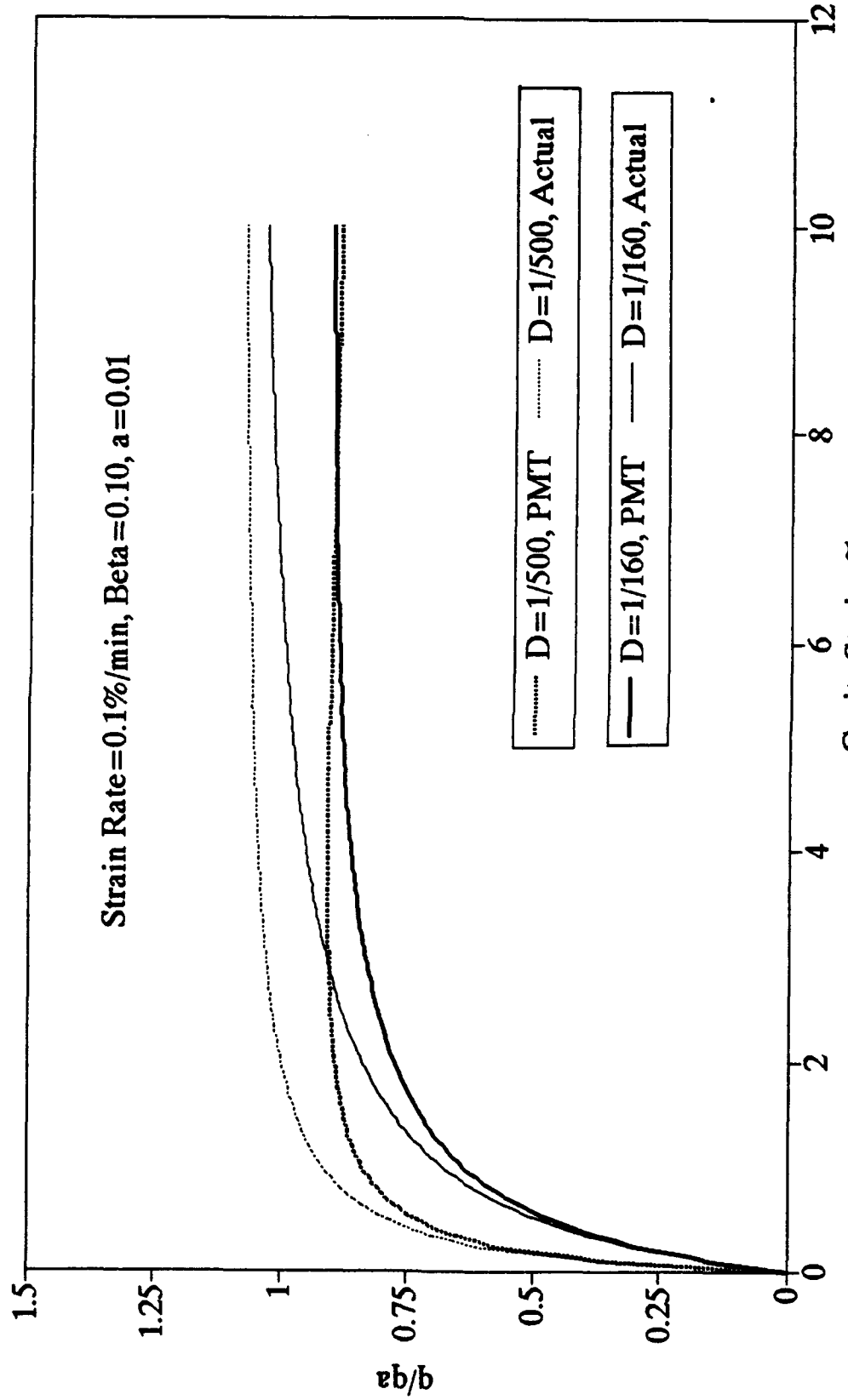

Fig. 5.18 Influence of Constant D on Undrained Shear Strength Derived from PMT at Strain Rate = 0.1%/min (Beta = 0.10)

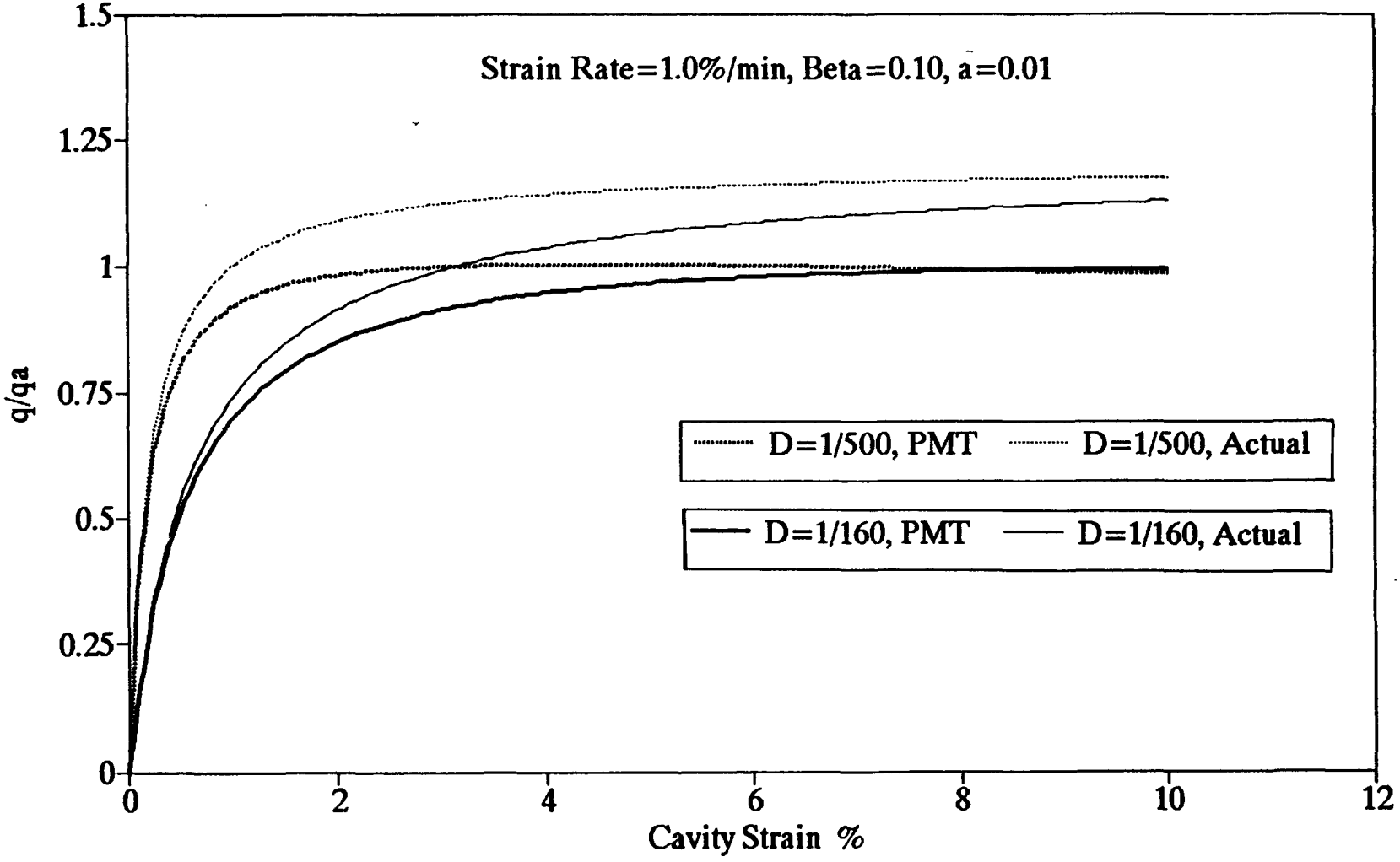

Fig. 5.19 Influence of Constant D on Undrained Shear Strength Derived from PMT at Strain Rate = 1.0%/min (Beta = 0.10)

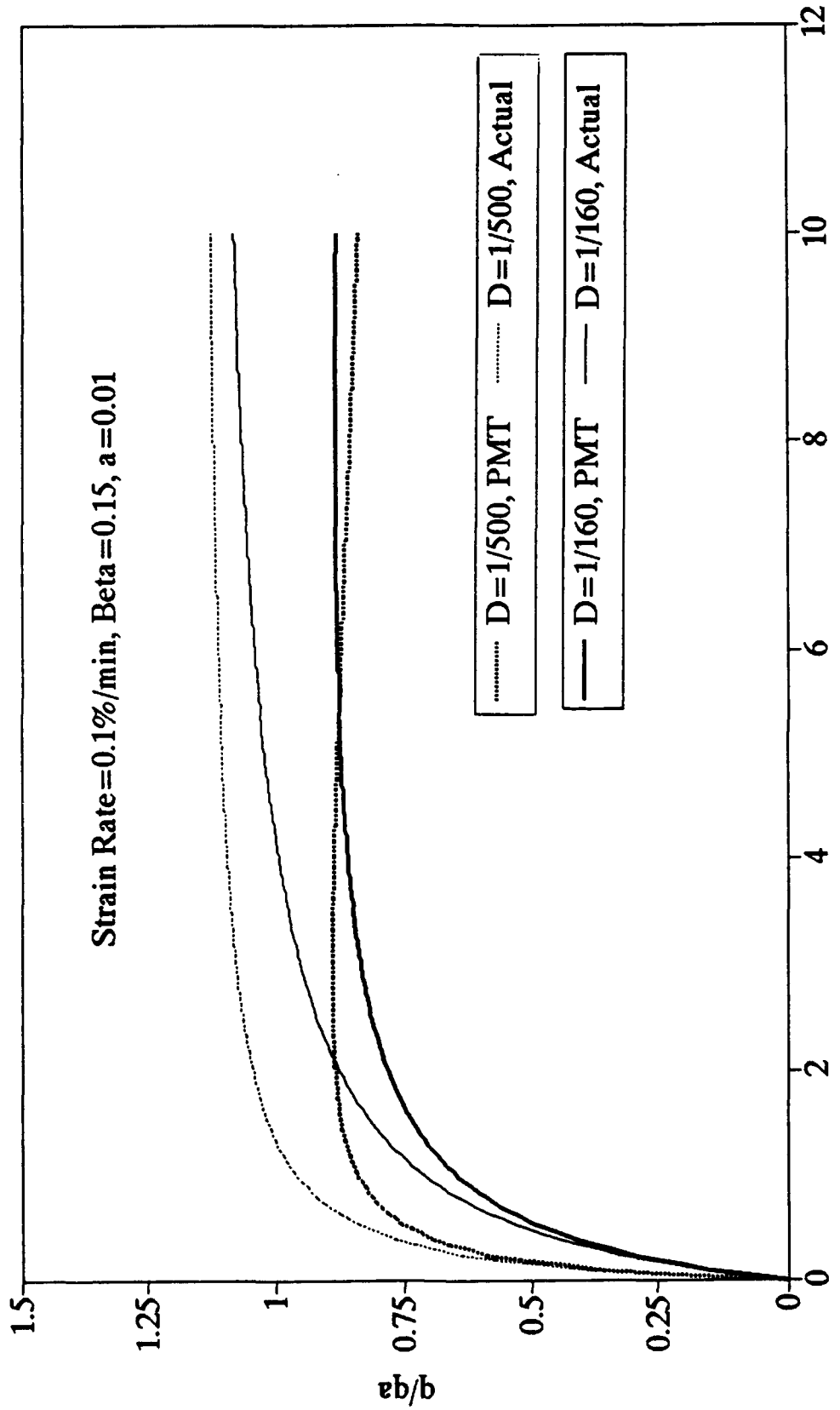

Fig. 5.20 Influence of Constant D on Undrained Shear Strength Derived from PMT at Strain Rate = 0.1%/min (Beta = 0.15)

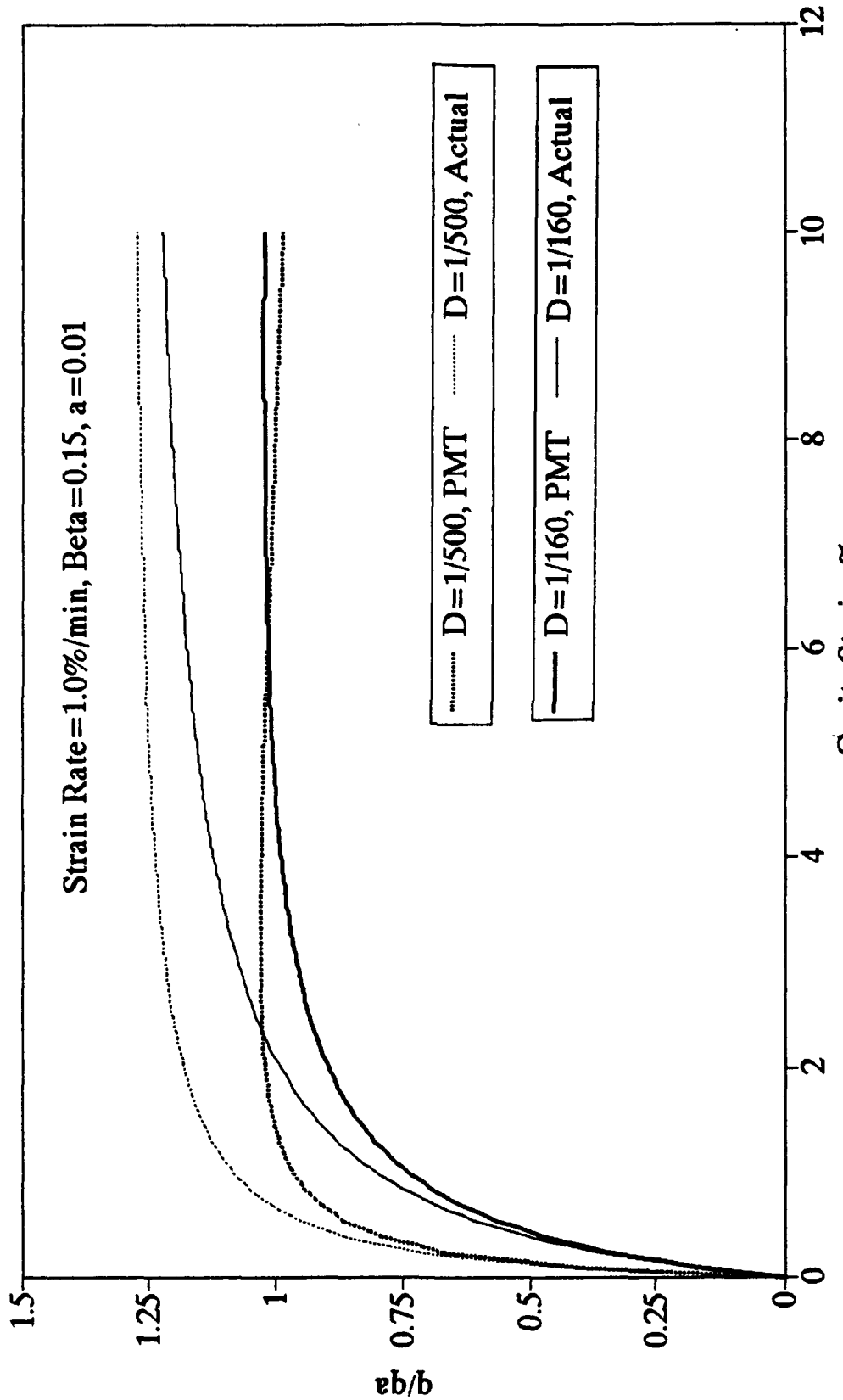

Fig. 5.21 Influence of Constant D on Undrained Shear Strength Derived from PMT at Strain Rate = 1.0%/min (Beta = 0.15)

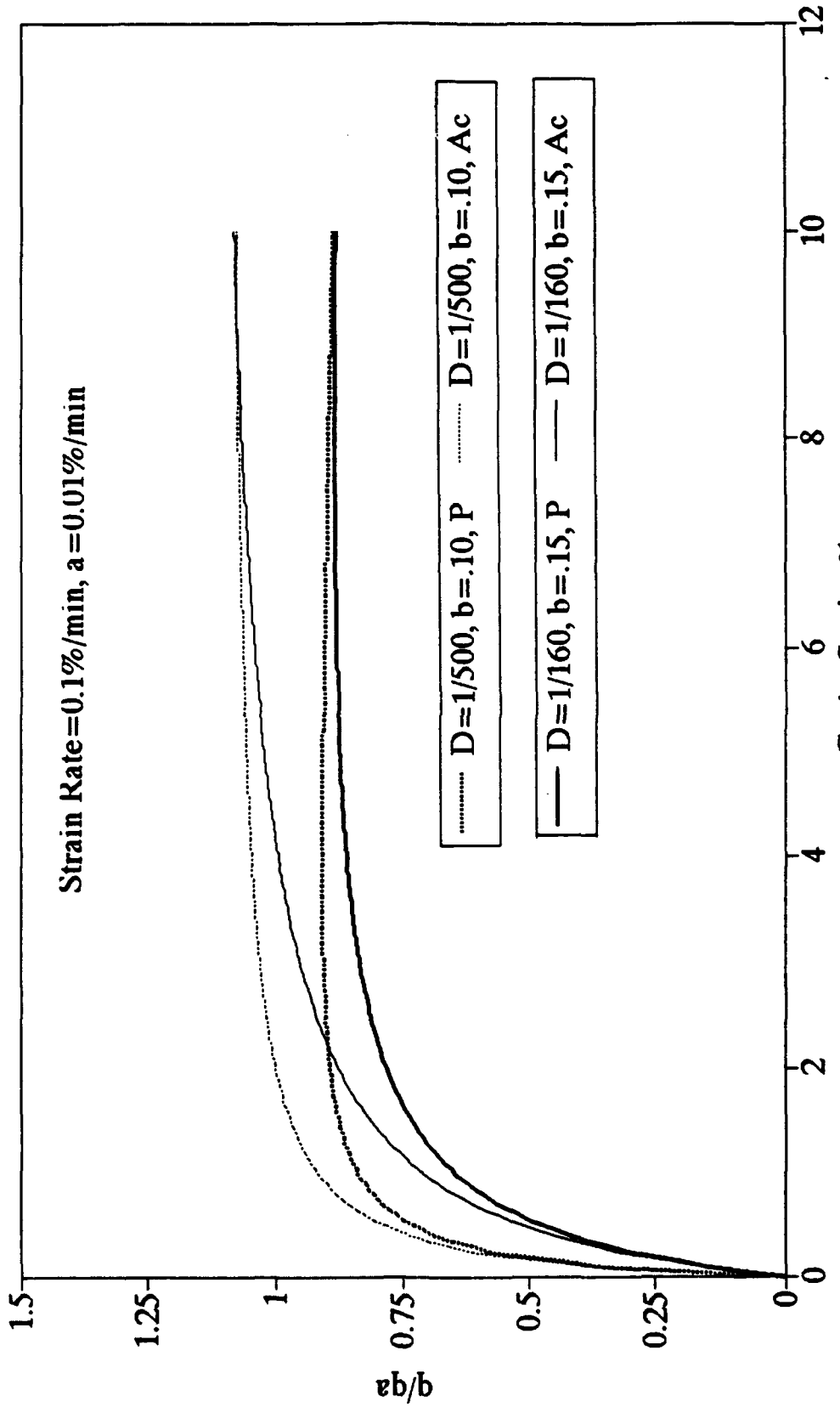

Fig. 5.22 Influence of D and Beta on Undrained Shear Strength Derived from PMT at Strain Rate = 0.1%/min

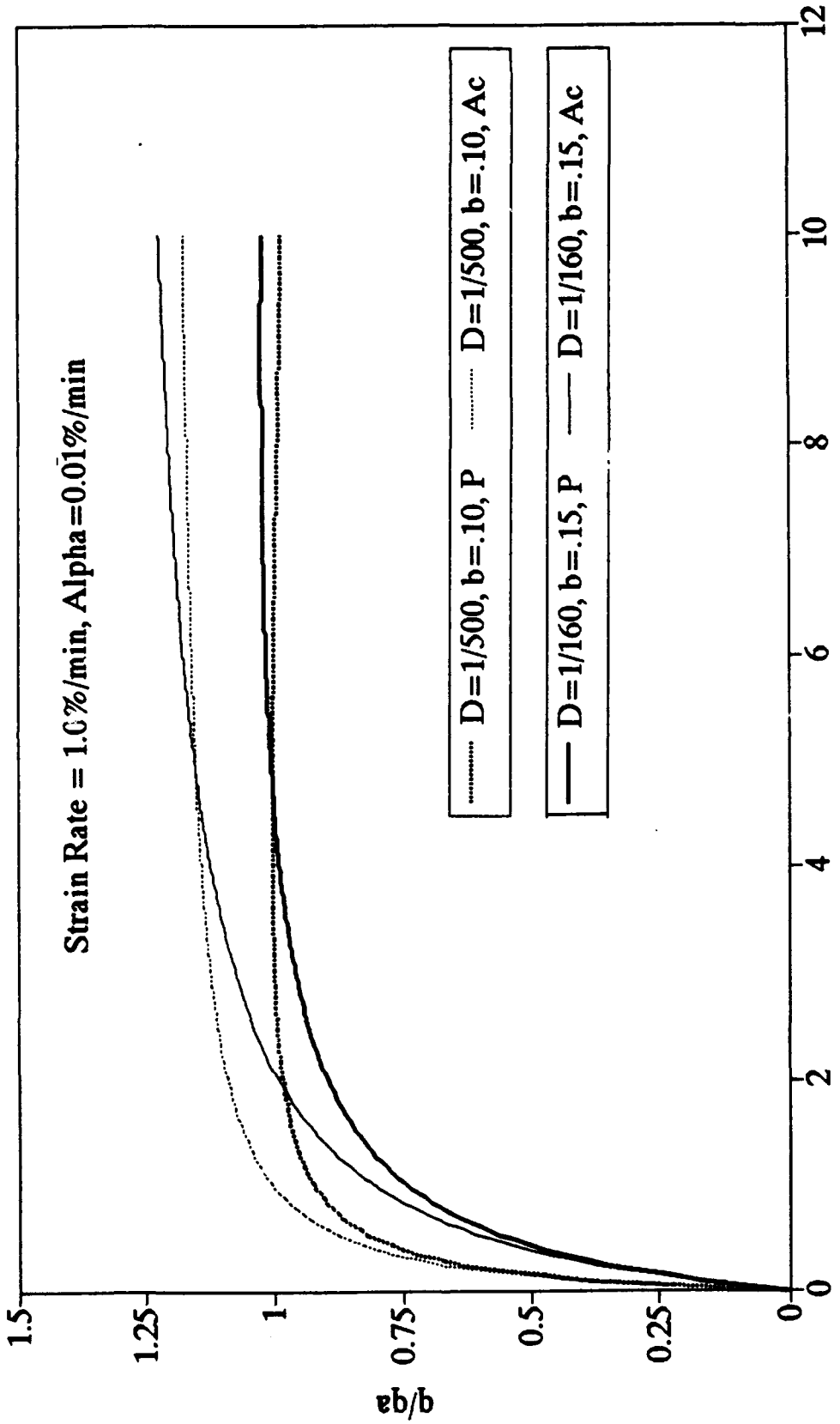

Fig. 5.23 Influence of D and Beta on Undrained Shear Strength Derived from PMT at Strain Rate = 1.0%/min

pressuremeter expansion curves and derived stress-strain curves (Figs. 5.11 and 5.15). From the laboratory tests performed on kaolin-silica soil simulating pressuremeter test condition in CSD (Chapter 4), β was found as 0.15 and D was determined as 1/160. Using these pairs of results, stress-strain curves are produced for cavity expansion rate of 0.1%/min and 1.0%/min (Figs. 5.22 and 5.23). Surprisingly, for the strain rate 0.1%/min case the ultimate strength are the same for the actual and derived curves (see Fig. 5.22). It was found earlier that increasing β values induced more strain softening, while increasing D values caused for more strain hardening. Hence, when combined in this case, the influence of β and D compensated or nullified their softening/hardening behavior and produced the same ultimate strengths (for D = 1/500, β = 0.10 and D = 1/160, β = 0.15 in both actual and PMT cases). However, in the case of larger cavity expansion rate (1%/min), the strain hardening effect is more than the softening effect, and the curves produced from the laboratory PM test data show a slight increase in the ultimate strength (Fig. 5.23). It can be concluded that the influence of D and β which cause hardening and softening, respectively, compensated their effects and the ultimate strengths were essentially the same from the triaxial tests/empirical correlations and from the PMT performed in CSD in kaolin-silica soil. Although this conclusion shed light on the reason for difference between triaxial and PMT based results, its generalization is not suggested at this stage as different soils will have different D and β values, and their effects may not always nullify each other.

5.11 Conclusions

The numerical integration performed to simulate the pressuremeter expansion curve and to derive the stress-strain curve was used to study the influences of cavity expansion (strain) rate, β and D. Furthermore, the effect of upper yield in the prediction of shear strength was also analyzed, and it was concluded that the level of upper yield has no significant influence in the derived stress-strain curve.

As the cavity expansion rate increases the shear strength also increases in both actual and PMT condition (Fig. 5.15). Furthermore, for strain hardening soils the PMT

give strain softening type stress-strain curves. As β increases (for pressuremeter test condition), even though the actual material curves show higher strength and higher hardening, the stress-strain curves derived from PM expansion curves show higher softening. This parametric study which was carried out using the results for PMT condition, confirms the findings of Prevost (1976) and Jamiolkowski and Lancellotta (1977), and demonstrates that the stress-strain curves derived from the PMT will exhibit more strain-softening characteristics under constant strain rate conditions even if the soil is strain hardening.

The studies based on the laboratory test data shown that, as D increases, although the curves have smaller initial slopes, they show strong strain hardening behavior. However, at large strains, the ultimate strength reaches the same level irrespective of the values of D. As far as the ultimate strength is concerned, the constant D does not play a major role except for the initial portion of the curve. On the other hand, the degree of strain softening slightly increases with decreasing values of D.

For the soils studied, the combined effect of β and D compensate their strain softening/hardening behavior and the ultimate strength are essentially equal for both the triaxial test and pressuremeter test values.

CHAPTER 6

STRESS RELIEF AND STRESS RELAXATION EFFECTS IN PRESSUREMETER TESTING

6.1 Introduction

The knowledge of time dependent deformation behavior of soils is important to understand the stress-strain-time effects in soils such as strain rate effect, creep, creep rupture, strength after creep, stress relaxation, strain hardening, strain softening and long term strength. The following time dependent behaviors related to pressuremeter tests will be discussed in this report: strain rate effect (already introduced in Chapters 4 and 5), stress relief, stress relaxation time (or normalizing period), creep, and stress relaxation.

In the Menard type pressuremeter or even the self-boring pressuremeter the borehole is slightly larger than the probe. Hence, before the membrane is inflated the soil around the probe tends to move inward and fill the gap. During this process of stress relief the lateral stresses are released and the in situ horizontal stress is reduced. In the SBPM, the influence of the size of cutting shoe on the stress relief is also important.

The stress relaxation time is the period usually allowed between the end of drilling and beginning of probe expansion. This time is provided to allow for dissipation of the excess pore pressure developed during the drilling operation. The relaxation time depends on the type of soil and the drilling method. In the laboratory simulation of PMT

in the CSD, relaxation tests were performed with various strain levels to study the influence of initial strains on the relaxation time.

Most material masses, when subjected to a sustained loading, deform or creep continually, i.e. their dimensions change with time. Conversely, if a material is deformed to a certain amount and then its dimensions are maintained unchanged, in general, a time-dependent decreasing stress, acting in the direction whose dimension is maintained, will be required. This phenomenon is commonly referred to as "stress relaxation". "Creep" can be defined as the deformation of a soil mass under a constant stress state and constant volume or pore pressure. Stress relaxation can be considered as the reverse of creep, i.e. stress change while keeping the same dimensions. In simple terms, creep is pressure controlled and relaxation is volume controlled.

6.2 Stress Relief in Pressuremeter Test

One of the major advantages of the in situ testing over the conventional laboratory tests is that there is an opportunity to prevent or limit sample disturbance due to stress relief. However, in the case of Menard pressuremeter test, the probe has to be inserted in a predrilled hole. During the time between drilling and probe expansion, the borehole wall is subjected to stress relief. Even in the SBPM, the cutting shoe is designed such that it makes a hole slightly larger than the membrane in order to reduce friction between the probe and wall to decrease the disturbance to the wall surface and to avoid damage to the membrane. If the borehole is larger than the probe, then a gap is created between the soil and the membrane, thus causing stress release (relief) and reduction of the in situ horizontal stress. This unloading is represented by path AB in Fig. 6.1, where point A corresponds to the in situ condition (Law and Eden, 1980). Reloading by inflating the membrane is indicated by path BC where C represents the condition when the inflated membrane diameter is exactly equal to that of the cutting shoe. That is, the clay is now pushed back to the original location before the boring. Further increasing the probe pressure leads to point D beyond which the path will be identical to the ideal test. If the

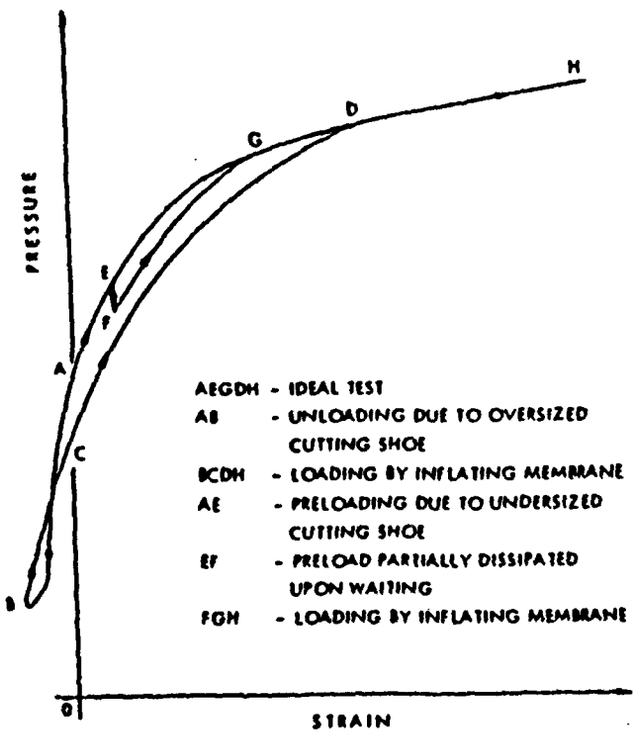

Fig. 6.1 Paths Followed by Soil Around Pressuremeter during Tests with Different Shoe Sizes (After Law and Eden, 1980)

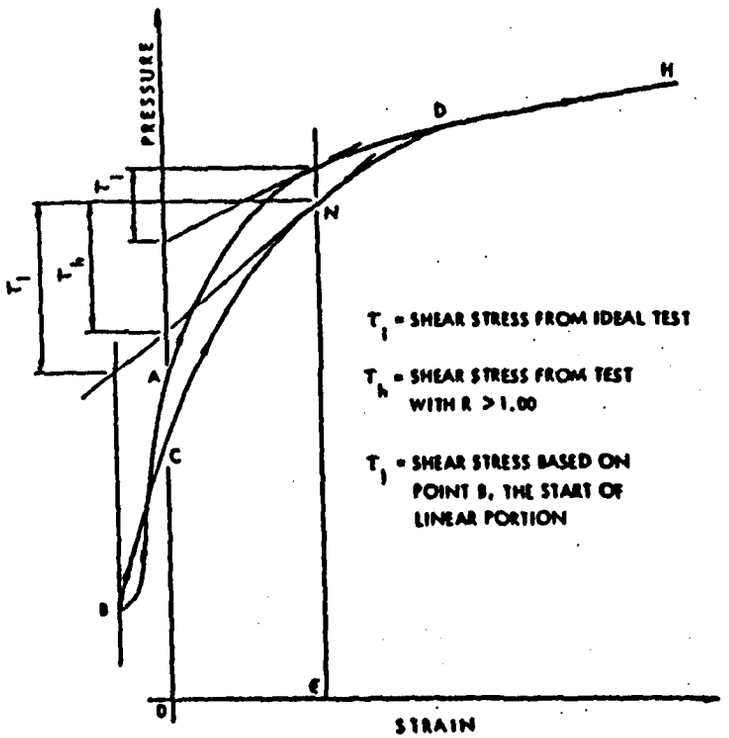

Fig. 6.2 Shear Stresses from Ideal Test and from Test with Oversized Cutting Shoe (After Law and Eden, 1980)

cutting shoe is smaller than the membrane, then the clay has to be pushed laterally to make room for the membrane, thus introducing a load on the membrane which is represented by the path AE in the figure. If the test is allowed for a stress relaxation process, the pressure will drop to F (path EF), where the inflation of the membrane begins and joins the ideal loading path at G. The corresponding interpreted shear stresses for ideal and oversized cutting shoe tests are given in Fig. 6.2. The oversized cutting shoe leads to stress relief and overestimation of the undrained shear strength. Law and Eden (1980) determined that stress relief caused by an oversized cutting shoe in a SBPM overestimated the deduced shear strength by 15 or 80% depending on the choice of the zero reference strain (point C or B in Fig. 6.1). Furthermore, the derived modulus was also overestimated by 30% due to unloading prior to shear.

Benoit and Clough (1986) conducted full scale SBPM test in soft San Francisco Bay Mud to study the effect of oversized cutting shoe on various parameters. It was observed that the lateral pressures obtained were consistently around 20% lower for the 1.1% oversized shoe than for the perfectly fitting shoe. The reason for the lower lateral pressure is obviously the stress relief caused by the oversized cutting shoe. This is supported by the data of Hughes et al. (1980), where the in situ horizontal stresses were reduced by 60 to 65% in the Coode Island silty clay when a 3% oversized cutting shoe was used. Similarly, in stiff Leda clay, Law and Eden (1980) found the lateral pressure to be underestimated by about 40-45% with a 1.1% oversized cutting shoe. Benoit and Clough (1986) also determined from the SBPM tests that the 1.1% oversized cutting shoe tests led to an overestimation of 60-100% in undrained shear strength, which is consistent with the 80% increase in shear strength reported by Law and Eden (1980).

All these results show that the stress relief occurrs in predrilled boreholes and in holes drilled by self boring pressuremeter with an oversized cutting shoe, and causes unloading of the soil around the borehole and leads to underestimation of the in situ horizontal pressure. From these experimental evidence, the importance of stress relief in PMT is evident and it should be taken care in experimental and analytical studies.

6.3 Stress Relaxation Time in Pressuremeter Test

The stress relaxation time, also called the normalization period, is the time interval between the end of self-boring and the beginning of the probe expansion. During this period, the excess pore pressure developed during the drilling operation must be allowed to dissipate, and the disturbed stress state around the probe will reach equilibrium, i.e. return to its original state. This time period is dependent upon the drilling technique used and the type of soil tested, and it varies from a few minutes to several hours.

Jamiolkowski and Lancellotta (1979) showed that for Porto Tolle clay, a relaxation time of about 100 minutes was enough to determine the proper total in-situ horizontal stress. For two Norwegian clays, Lacasse et al. (1981) reported a relaxation time between 2 and 22 hours. Lacasse and Lunne (1982) indicated that for a relaxation period varying from 90 to 1300 minutes for Drummen clay there was little effect on the total in-situ lateral stress determination. Denby (1978) showed that higher lift-off pressures were obtained when a test was performed with a relaxation time of 30 minutes compared to results from tests using a period of 120 minutes or more. However, he obtained identical shear strengths, irrespective of the different relaxation times used. Denby used a normalization period of at least 120 minutes in the San Francisco Bay Mud tests. In a Tokyo Bay soft clay, Mori (1981) indicated that a 120 minute period was necessary to bring down the excess pore pressures to less than 0.75 psi. The SBPM tests carried out in Boston Blue clay after permitting only a ten to thirty minute equilibrium period (Ladd et al., 1980) led to inconsistent values of lateral pressures. From the SBPM tests conducted in San Francisco Bay Mud, Benoit (1983) found that normalization periods of 90 minutes or more did not influence the results. A summary of several tests which used various relaxation times is shown in Table 6.1. From these results it can be concluded that most of the excess pore pressures induced from drilling are dissipated in about two hours for typical soft clays.

Table 6.1 Relaxation Time for Several Field Pressuremeter Tests (After Benoit, 1983)

TEST SITE OR SOIL TYPE	NORMALIZATION PERIOD (minutes)	EXPANSION RATE		REFERENCES
		psi/min	%/min	
Porto Tolle clay	15-120	---	0.83	Jamiolkowski and Lancellotta (1977)
Guasticce clay	15-120	---	0.83	
Drammen clay	90-1300	---	---	Lacasse and Lunne (1982)
Onsoy clay	90-1300	---	---	
Hamilton Air Force Base:				
Denby	180	1.0	---	Denby (1978)
Benoit	60-8460	0.24-6.9	0.04-0.99	Benoit (1983)
Boston Blue clay	generally 10-30 others 42-720	---	1.0	Ladd et al. (1980)
South Gloucester	60-1080	1.4	---	Law and Eden (1980)
Matagami	60-1080	1.4	---	
Coode Island	60-960	---	---	Hughes et al. (1980)
Tokyo Bay	120	---	---	Mori (1981)

For clays, the total horizontal stress during self-boring is higher than the in situ value. During relaxation, it decreases gradually and becomes asymptotic to the in situ horizontal stress (P_o). In the case of loose sands or silts, the lateral stress decreases and again increases to the in situ horizontal stress (Baguelin et al., 1974). Too short a relaxation time usually leads to an incorrect estimate of P_o (Denby 1978, and Jamiolkowski and Lancellotta 1979), and the effect seems to be larger as depth increases. This is confirmed by results from tests in Boston Blue clay that showed a total in-situ lateral stress which was consistently underestimated using normalization period of 10-30 minutes (Ladd et al., 1980). In other cases, the P_o values were overestimated for short normalization periods in the Porto Tolle clay and for long normalization periods in the Onsoy clay (Jamiolkowski and Lancellotta 1977, and Lacasse and Lunne 1982). Benoit (1983) observed relaxation periods varying from 1 to 22 hours with Bay Mud with a larger cutting shoe having no effect on the measured lateral pressure.

Selection of P_o, the datum, has significant influence on the stress-strain curve and the undrained strength derived from the pressuremeter tests (Ladd et al., 1980). Therefore, a sufficient relaxation time should be allowed for the correct determination of P_o. Baguelin et al. (1978) recommend that the test be started if the change in pressure over a period of 10 minutes is less than 0.15 psi (1 kPa).

6.4 Pressuremeter Creep Test

Many soils - clays, silts, and all frozen soils - have rheological properties, i.e., the ability to develop creep deformations and reduce strength under sustained stresses. The time-dependent deformation behavior of clays under continued loading depends upon several variables such as soil type, soil structure, stress history, effective stress, temperature, etc.

There has been extensive research performed to characterize the creep and relaxation behavior of clays using rheological models composed of linear springs in

combination with linear or nonlinear dashpots. Singh and Mitchell (1968) using a rate process theory and published experimental results, formulated a stress-strain-time relationship in which the creep rate varied exponentially with stress level, and decreased nonlinearly with time. Haefeli (1965) assumed a creep law for snow, ice, rock and soil in which the creep rate varied nonlinearly with stress but did not vary with time or strain. Prevost (1976) developed a phenomenological equation to describe the stress-strain-time behavior of normally consolidated clays loaded under undrained conditions.

Most of the above research is based on triaxial tests. Very few investigators used pressuremeters to study the creep behavior of soil. Ladanyi (1982) and his collaborators (for example, Ladanyi and Johnston, 1978) have used the pressuremeter to study the creep potential of frozen soils. The volume of the pressuremeter cell is a limitation of pressuremeter creep tests. Therefore, PM creep test is feasible only for short creep times and a medium range of stress. To obtain the long-term creep parameters, Ladanyi et al. (1991) used borehole relaxation tests as the alternative. The main advantage of the relaxation test is that the strain is controlled and the stress variation is observed so that there is no danger of exceeding the volume capacity of the PM cell. As a consequence, borehole relaxation tests can cover easily the whole range of stresses and long periods of time.

Ladanyi (1982) derived the following expressions to determine creep parameters from Menard PMT. The total strain attained after a given time under constant stress is:

$$\epsilon_e = \epsilon^i_e + \epsilon^c_e \qquad 6.1$$

where ϵ^i_e is the instantaneous, not necessarily elastic, portion of the total strain, and ϵ^c_e is the creep strain given by:

$$\epsilon^c_e = (\dot{\epsilon}_c/b)^b(\sigma_e/\sigma_c)^n\, t^b \qquad 6.2$$

where the subscript e denotes the von Mises equivalent stress and strain, σ_c is the creep modulus corresponding to an arbitrary strain rate $\dot{\epsilon}_c$, t is the time, and b and n are creep exponents.

When Eq. 6.2 is applied to the problem of an expanding cylindrical cavity in an infinite medium, originally acted upon by an isotropic lateral stress p_o, the radial creep strain rate under a constant stress $p_i > p_o$ can be derived as:

$$dr_i/dt = r_i F b t^{b-1} \qquad 6.3$$

where F is a function of (p_i-p_o), given by:

$$F = (M/2)[(p_i-p_o)/\sigma_c]^n \qquad 6.4$$

and

$$M = 2(\sqrt{3}/2)^{n+1} (\dot{\epsilon}_c/b)^b (2/n)^n \qquad 6.5$$

In a stage-loaded creep test, if p_i is the stress applied in the borehole during the stage k, following a smaller stress in the previous stage (k-1), the resulting radius increase with time is given by:

$$\ln(r_i/r_{i,k-1}) = Ft^b \qquad 6.6$$

or, in terms of the borehole volume:

$$\ln (V/V_{k-1}) = 2 Ft^b \qquad 6.7$$

where $V = \pi r_i^2 L$ is the current volume of the cavity of length L.

Finally, the value of creep modulus σ_c is given by:

$$\sigma_c = (p_i\text{-}p_o)_N \, [M/(2F)_N]^{1/n} \qquad 6.8$$

where M is given by Eq. 6.5 and $(2F)_N$ denotes the value of (2F) at an arbitrary point $(p_i\text{-}p_o)_N$, located on a (2F) versus $(p_i\text{-}p_o)$ straightline segment in a log-log plot (Fig. 6.3).

In section 6.6 this approach will be combined to relaxation tests to determine creep parameters.

6.5 Stress Relaxation Parameters from Triaxial Tests

The creep behavior of soils has been studied primarily from the point of view of deformation. There are, however, problems in which the deformations are negligible, and the prediction of the stresses acting on a structure due to interaction with a soil mass (for example a retaining wall) is of primary interest. This type of test, which studies the variation of stresses while the deformation is kept constant is called stress relaxation test.

Relatively few researchers have studied stress relaxation in soils. Murayama and Shibata (1961) that the decay of deviator stress with the logarithm of time was linear, up to a certain limit, and then remained constant. Vialov and Skibitsky (1961) also noticed the linear decrease of stress with logarithm of time but they did not find the existence of a final relaxed level of stress. Probably their relaxation time was not sufficient as the tests lasted only 4 hours. Saada (1962) obtained a linear decay stress with logarithm of time, up to about 50 days, and then the deviatoric stress abruptly fell to zero. From the stress relaxation tests carried out on undisturbed Sault St. Marie clay, Christensen and Wu (1964) also obtained linear relation between stresses and logarithm of time. Murayama et al. (1974) and Akai et al. (1975) presented similar experimental results.

Lacerda and Houston (1973) and Lacerda (1976) have thoroughly studied the stress relaxation and creep effects on soil deformation by performing several tests on undisturbed San Francisco Bay soft clay, remolded kaolinite, clean quartz sand and

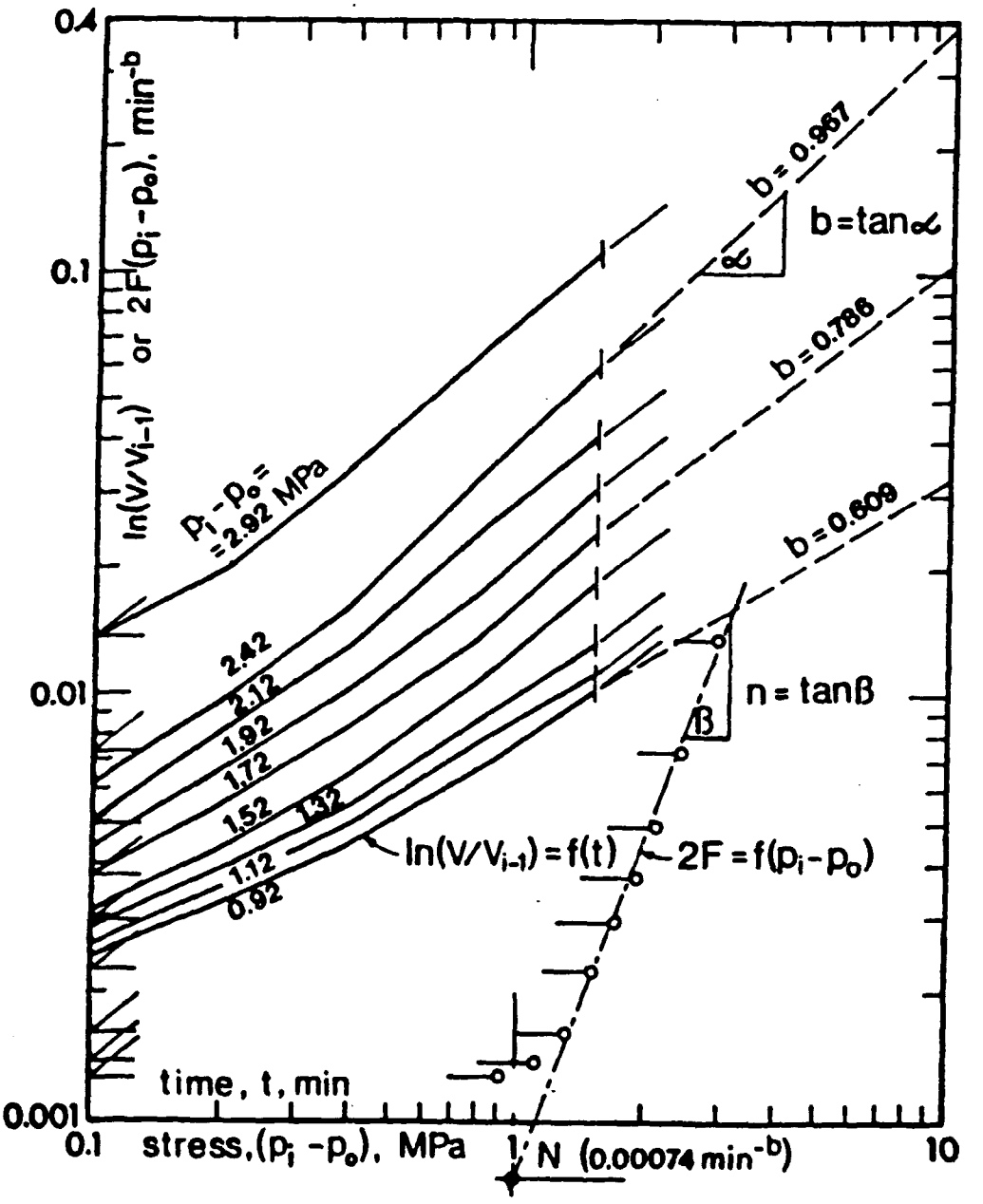

Fig. 6.3 Creep Parameter Determination from Stage-Loaded Pressuremeter Test (After Ladanyi, 1982)

compacted clay. A summary of the stress relaxation tests on various soils is shown in Fig. 6.4. These results show that when the stress relaxation process is started by confining the deformations, the shear stress starts to relax significantly after a finite time elapses and the stress relaxation is solely dependent on the strain rate and the initial stress level. Consistently with previous data, the stress relaxation was found to have an inverse linear dependence with the logarithm of time. The ratio of the deviator stress at any time to the stress at the beginning of stress relaxation is linear with the logarithm of time, and the slope is independent of the confining pressure, strain, and strain rate but dependent on initial stress level. It is observed that the variation of pore pressure was very small in the undrained stress relaxation tests. Similarly, the volume change during relaxation in the drained tests was also negligible. Furthermore, there was no difference between the stress relaxation of anisotropically and isotropically consolidated soils.

Lacerda (1976) derived the following equation for stress relaxation from Singh-Mitchell's creep equation (1968):

$$q = \frac{D}{D_o} = \frac{\bar{D}}{\bar{D}_o} = 1 - s \log(\frac{t}{t_o}), \quad for\ t > t_o \qquad 6.9$$

where s = slope of stress relaxation curve = $\phi/\bar{D}_o$ (shown in Fig. 6.5), and ϕ is defined as:

$$\phi = \frac{2.3(1-m)}{\bar{\alpha}} \qquad 6.10$$

D = deviator stress

$\bar{D}$ = deviator stress level = D/D_{max}

D_o = deviator stress at time t_o

$\bar{D}_o$ = deviator stress level at time t_o = $D_o/D_{o\,max}$

t_o = time at beginning of stress relaxation

The value of t_o is obtained from the intercept of the straight line portion of the

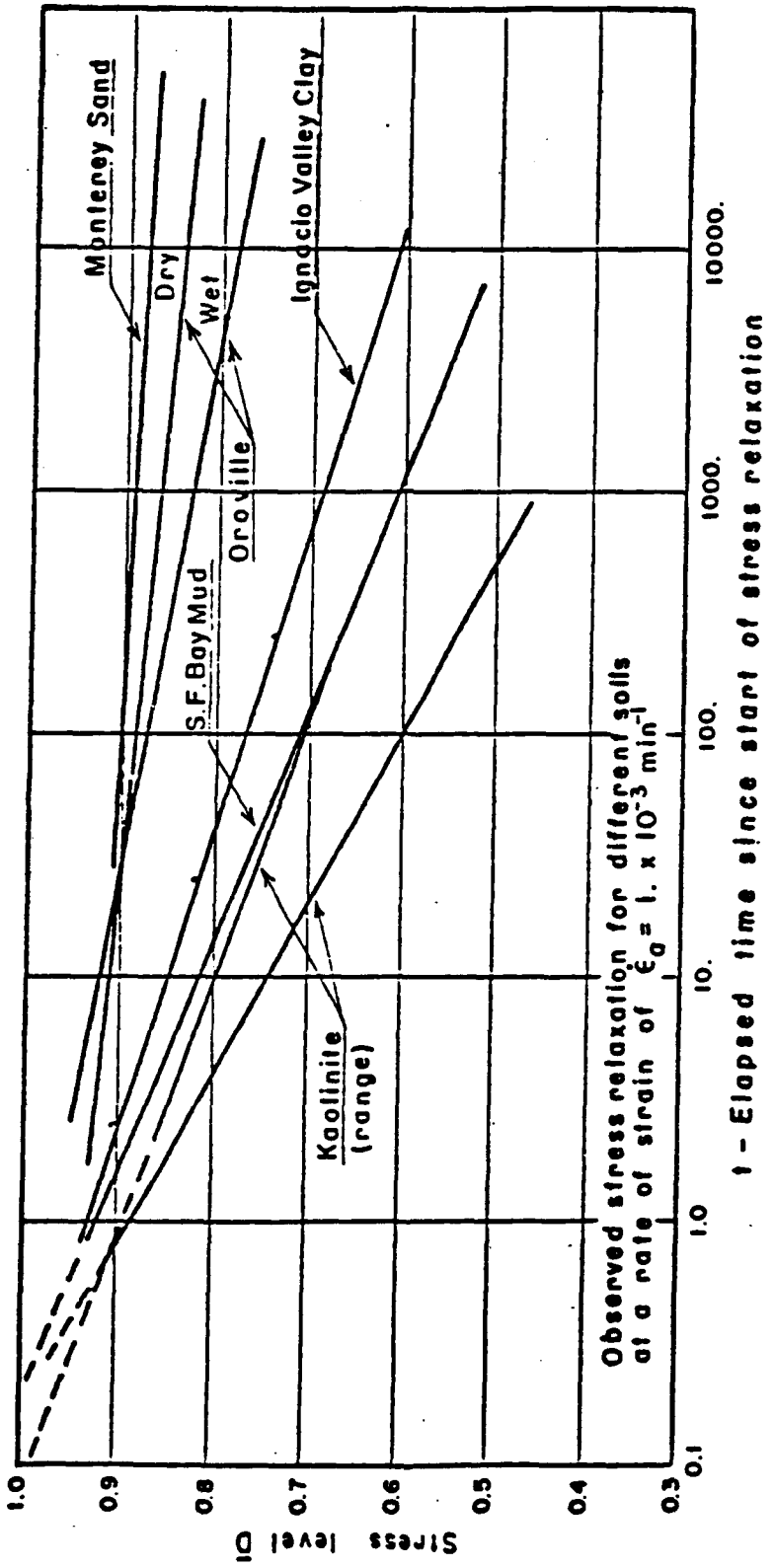

Fig. 6.4 Results of Stress Relaxation Test on Various Soils (After Lacerda, 1976)

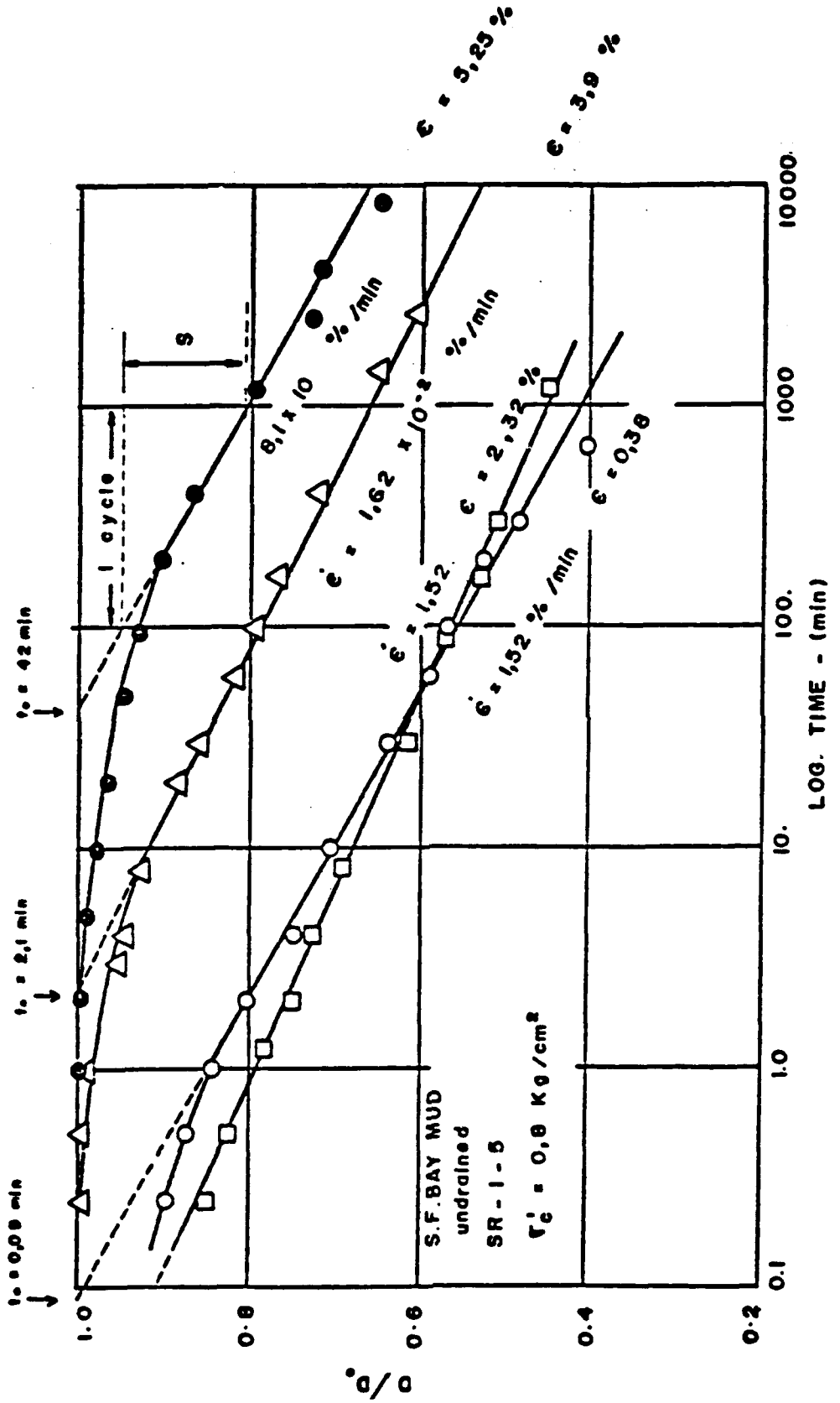

Fig. 6.5 Stress Relaxation Curves for San Francisco Bay Mud (After Lacerda, 1976)

relaxation curve on the time axis of the stress level-log time plot. It is dependent exclusively on soil type and strain rate prior to the relaxation test. The higher the strain rate, the smaller is the value of t_o.

The above equations are valid for $m < 1$ and they express the relationship between q, the relaxed stress relative to the initial stress, and time, t, which may be derived by inverting Singh and Mitchell's (1968) creep equation:

$$\dot{\epsilon} = A \exp(\bar{\alpha}\bar{D}) \ (t_1/t)^m \qquad 6.11$$

where $\dot{\epsilon}$ = strain rate (%/min), $\bar{D} = D/D_{max}$ (stress level), α = slope of the linear portion of the logarithm strain rate versus deviator stress plot obtained from creep test (in units 1/pressure), $\bar{\alpha} = \alpha D_{max}$ (dimensionless parameter), m = absolute value of the slope of the straight line relationship between the logarithm of strain rate and the logarithm of time, t_1 = unit time, e.g., 1 minute, and A = extrapolated value of strain rate for zero stress level in the linear plot of log strain rate versus deviator stress, for time t_1, in %/min.

In Eq. 6.9 t_o can be related to strain rate by:

$$t_o = h_o/\dot{\epsilon} \qquad 6.12$$

where h_o is the numerical value of the strain rate (in units of strain) necessary to yield a "delay time" of t_o before stresses begin to relax (shown in Fig. 6.6). The values of s, the slopes of the stress relaxation curves, were found to be independent of confining or consolidation pressure and of initial relative density of sand.

The relationship between A (creep) and h_o (relaxation) was derived from Eq. 6.11:

$$h_o = 13.2 \ A^{1.1} \qquad 6.13$$

From several published and his own experimental data, Lacerda (1976) obtained

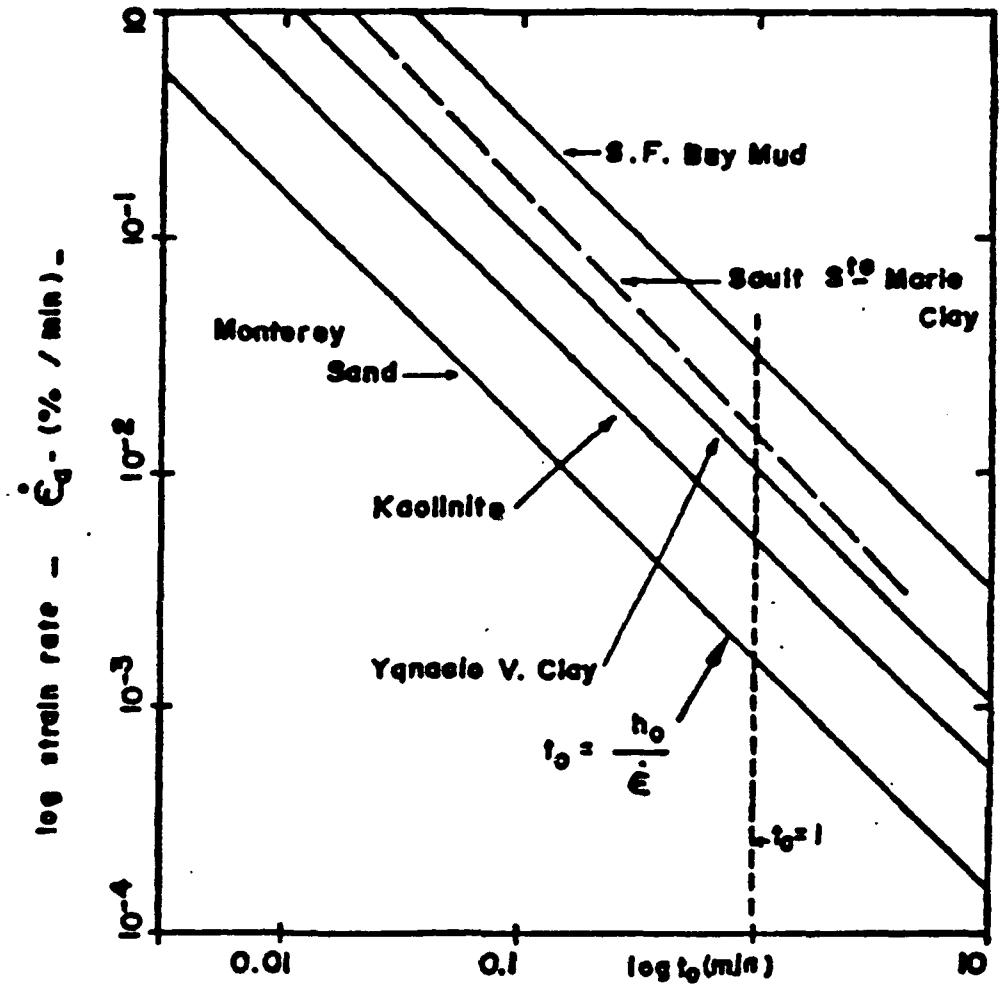

Fig. 6.6 Log Strain Rate Versus Log Time Plot (After Lacerda and Houston, 1973)

the following correlations between the stress relaxation parameters and plasticity index (PI):

$$\phi = \frac{PI}{4.4\ PI+280} + 0.022 \qquad 6.14$$

where PI is in %, and

$$\log h_o = 0.0285\ (PI) - 2.82 \qquad 6.15$$

These results can be used to obtain the stress relaxation and creep parameters and incorporated in the time dependent plasticity models to predict the stress-strain-time behavior of soils.

6.6 Pressuremeter Stress Relaxation Test

Unlike the stress relaxation studies carried out by many researchers using the triaxial apparatus, only Ladanyi and his collaborators (Ladanyi et al., 1991) have used the pressuremeter to obtain relaxation/creep parameters. Because of the volume limitations of the pressuremeter cell, borehole relaxation tests are performed as an alternative to borehole creep test to obtain the long-term creep information. In related experiments, Ladanyi (1982) used the dilatometer to perform stress relaxation tests, and Ladanyi and Huneault (1989) obtained creep parameters of frozen soil with the cone penetrometer.

Using the aging (time hardening) theory of creep, which assumes that there is a unique and continuous surface in space relating stress with strain and time, Ladanyi (1982) derived expressions for stress relaxation from which creep parameters could be inferred. In the aging theory, it is assumed that creep and relaxation are closely related, so that a relaxation curve is nothing else but a creep curve under a continuously decaying stress, resulting in a constant value of strain. In other words, according to this assumption, any constitutive creep relation can be directly transformed into a relaxation

relation by making the creep strain constant and equal to the applied initial strain.

According to the aging creep theory and using an approximate method, Ladanyi (1982) presented the equation for a family of borehole relaxation curves in an expanding cylindrical cavity problem:

$$(p_i - p_o) = \sigma_c \left[\frac{\ln(V/V_o)}{M(t'+t)^b}\right]^{1/n} \qquad 6.16$$

where M is given by Eq. 6.5, p_i is the internal pressure applied in the borehole, p_o is the total lateral ground stress around the borehole, and t' is a very short time interval. If t' is neglected, and the relaxation curves are plotted in a log (p_i-p_o) versus log t plot (Fig. 6.7), with the strain ln (V/V_o) as the parameter, then their slope at the end of interval gives the ratio:

$$\frac{b}{n} = -\frac{\Delta\log(p_i - p_o)}{\Delta\log t} = \frac{v}{h} \qquad 6.17$$

with v and h given in Fig. 6.7. For the same time interval (for the same relaxation period), where $t = t_i$ = constant, from the log $[\ln(V/V_o)]$ versus log (p_i-p_o) plot, the slope of the curve is:

$$n = \frac{\Delta\log[\ln(V/V_o)]}{\Delta\log(p_i - p_o)} = \frac{h_1}{v_1} \qquad 6.18$$

with v_1 and h_1 shown in Fig. 6.5

When b and n are known, the value of the creep modulus σ_c for a given $\dot{\epsilon}_c$ can be calculated for any point k on the line ln (V/V_o) versus (p_i-p_o) by using Eq. 6.16:

$$\sigma_c = (p_i - p_o)_k \left[\frac{M\, t_i^{\,b}}{\ln(V/V_o)_k}\right]^{1/n} \qquad 6.19$$

When Eq. 6.16 is applied to two consecutive points in a relaxation line with

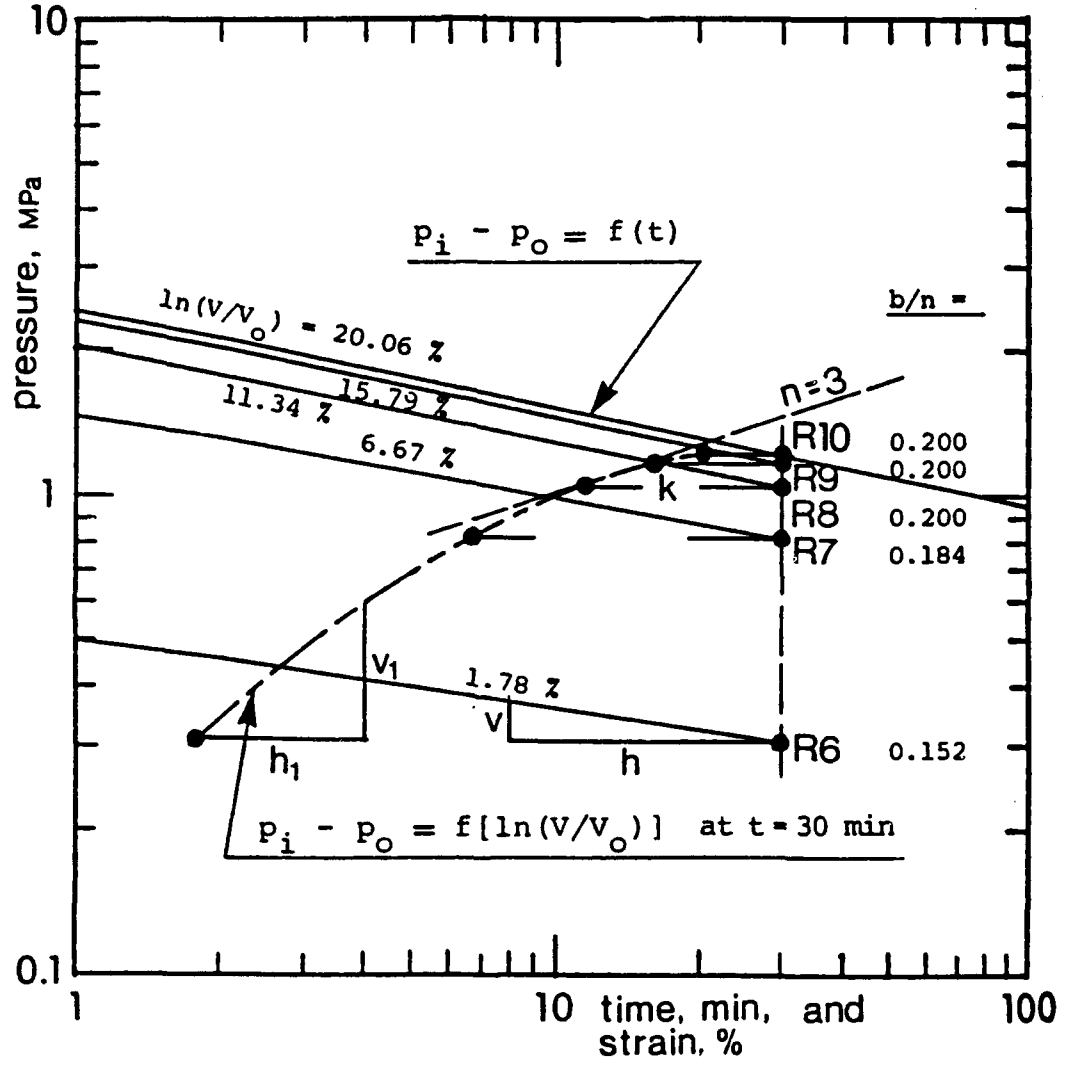

Fig. 6.7 Pressuremeter Stress Relaxation Curves for Stage-Strained Tests (After Ladanyi et al., 1991)

coordinates (t_1, p_{it1}) and (t_2, p_{it2}), the value of in situ horizontal pressure p_o can be determined from:

$$p_o = \frac{(t'+t_2)^{b/n}p_{it2}-(t'+t_1)^{b/n}p_{it1}}{(t'+t_2)^{b/n}-(t'+t_1)^{b/n}} \qquad 6.20$$

$$\approx \frac{(t_2/t_1)^{b/n}p_{it2}-p_{it1}}{(t_2/t_1)^{b/n}-1} \qquad 6.21$$

It is possible to perform the stress relaxation tests with the model pressuremeter in Calibration Chamber and can obtain the creep parameters. The in situ horizontal stress could be computed using the Eq. 6.21 and be compared with the p_o obtained from the pressuremeter expansion curve.

6.7 Pressuremeter Stress Relaxation Test in CSD

To the author's knowledge there has not been any systematic studies (field tests or laboratory simulations) conducted to evaluate the relaxation effects (relaxation time and stress relaxation) in pressuremeter testing. So far, only Ladanyi et al. (1991) performed field pressuremeter stress relaxation tests to determine creep parameters of frozen soils.

The effect of stress relief due to oversize cutting shoe on in situ horizontal stress and undrained shear strength prediction was already discussed in section 6.2. From the field SBPM tests, it was estimated that lateral pressures were 20-45% lower and undrained shear strengths 60-100% higher for a 1.1% oversized borehole (Law and Eden 1980, and Benoit and Clough 1986), and 60-65% lower in situ horizontal stress was predicted for a 3% oversized borehole (Hughes et al., 1980). However, there was no attempt made to correlate the stress relief (reduction of in situ horizontal stress) and the stress relaxation or relaxation time (normalizing period). Table 6.1 gave the relaxation

times adopted by various researchers but they were not correlated to the initial strain or to the initial strain rate which can be approximated to the cutting rate.

Therefore, a laboratory simulation study was undertaken to attempt to correlate the stress relief, stress relaxation time and stress relaxation with the initial amount of strain and strain rate in a pressuremeter test. The simulation of pressuremeter test in the cuboidal shear device has been already described in Chapter 4. Samples were prepared from artificially sedimented kaolin clay as described in Chapter 3. All the specimens were prepared and one dimensionally consolidated in exactly the same way as for the strain rate tests.

Pressuremeter stress relaxation tests were simulated in the cuboidal shear device as follows: After the one-dimensional consolidation, the drainage valve was closed and σ_x was increased such that the specimen is deformed at the specified strain rate, varying from 0.005%/min to 0.1%/min - depending on the test, up to the required amount of strain. The strain rates and strains before relaxation are tabulated in Table 6.2. Since the sample was undergoing a pressuremeter stress/strain path, σ_z was adjusted such that no vertical deformation was permitted (plane strain condition in vertical direction). The value of σ_y was adjusted such that $\epsilon_x = -\epsilon_y$, to assume no volume change (undrained condition). Having achieved the required amount of strain, the sample was permitted to relax. The relaxation condition was imposed on the specimen by adjusting all three pressures to maintain zero deformation in all three directions. A tolerance of 0.0001" was permitted in the computer control.

In actual practice, when the soil around the PM probe is relaxing there is a possibility for drainage because the soil is permitted to relax for a normalization period of 120 min to several hours. Therefore, during the relaxation period the drainage condition is neither fully undrained nor fully drained. In order to cover both extremes, relaxation tests were performed in both undrained and drained conditions.

Table 6.2 Relaxation Time for Different Strain Levels in Pressuremeter Test

Test No.	Strain Rate (% per min.)	Strain Before Relaxation (%)	Relaxation Time (min.)
87-U	0.1	1.0	200
89-U	0.1	1.0	200
90-U	0.1	1.0	250
93-U	0.05	0.5	250
94-U	0.05	0.5	200
95-U	0.05	0.5	200
88-U	0.01	0.1	225
91-U	0.01	0.1	200
99-D	0.01	0.1	250
100-D	0.005	0.1	200

U - Undrained Test D - Drained Test

6.8 Results and Discussion

Typical plots of effective stresses versus time are shown in Figs. 6.8-6.11, for each strain level of 1.0, 0.5, 0.1%, and for undrained condition and drained conditions. Other plots are presented in Appendix C. Table 6.2 summarizes the relaxation times obtained from all the relaxation tests reported herein and in Appendix C.

Irrespective of the initial strain level, the strain rate, or the drainage condition, the relaxation time needed to take the stresses to their initial (steady) state is in between 200 and 250 minutes. The relaxation time may depend on the type of soil and the type of drilling technique used because the pore pressure dissipation time depends on the permeability of the soil and the disturbance/pore pressure generation depends on the type of drilling equipment used. However, for kaolin clay, the relaxation time is about four hours regardless of cutting shoe size or the rate of cutting.

From the relaxation curves, the coefficient of lateral earth pressure (K_o) was estimated before and after relaxation, and the percent of change in K_o was also calculated and tabulated in Table 6.3. Again, the ΔK_o is more or less constant (varies between 6.3% and 6.5%) within the range of strain tested (0.1% to 1.0% strain and 0.005%/min to 0.1%/min strain rate). Therefore, it can be concluded that for an oversize boring of 0.1% to 1.0% the stress relief causes an underprediction of lateral earth pressure by 6.4% only.

6.9 Conclusion

There are several time related factors which influence the measurement and prediction of pressuremeter tests. Most importantly, the following time dependent behaviors are of concern such as loading rate or strain rate, stress relief, creep, stress relaxation, strain hardening and strain softening. The strain rate effect in pressuremeter testing was found to be about 50% more than the effect in triaxial testing.

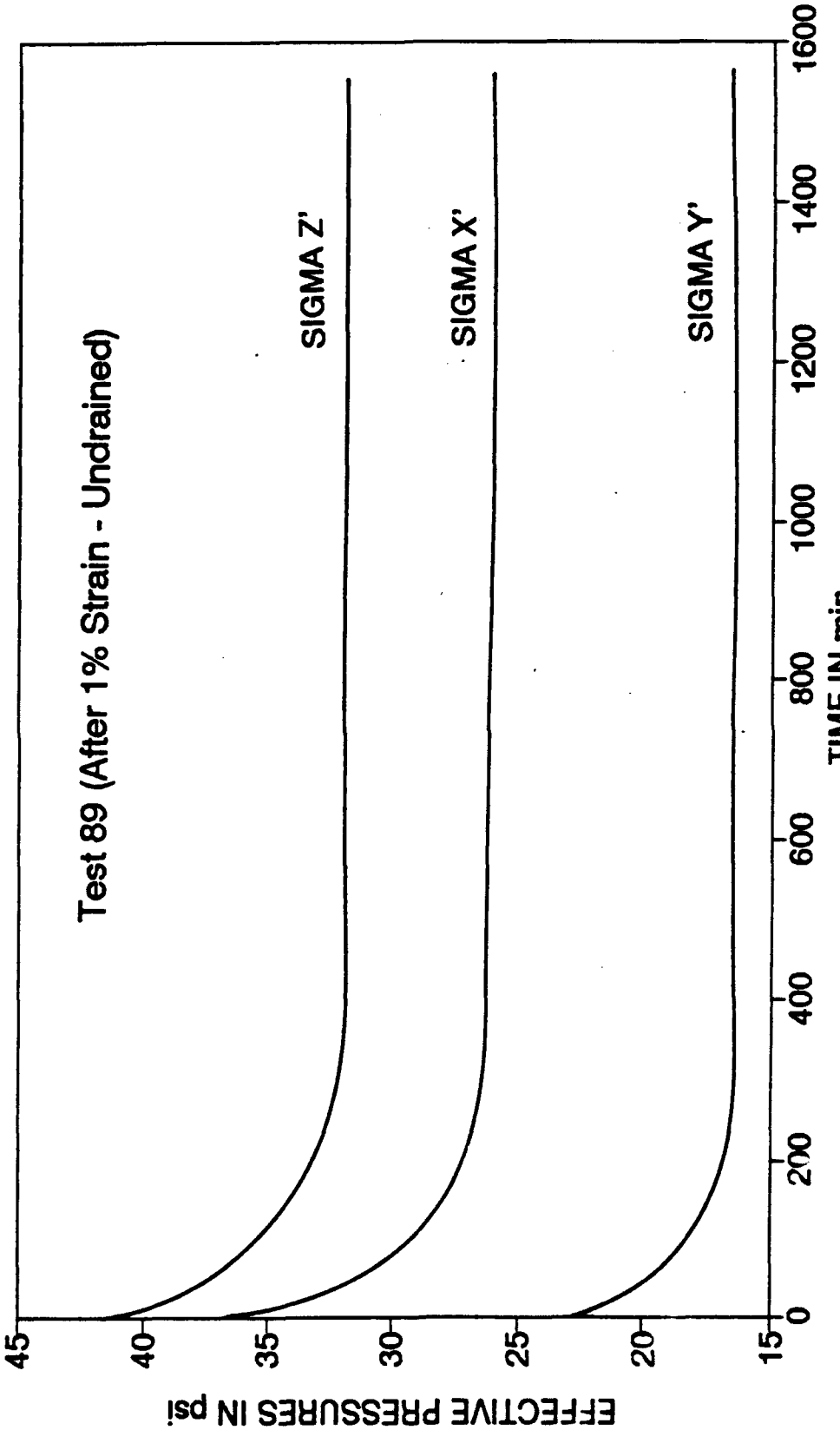

Fig. 6.8 Relaxation Curves for Kaolin After 1.0% Strain-Undrained Test (No. 89)

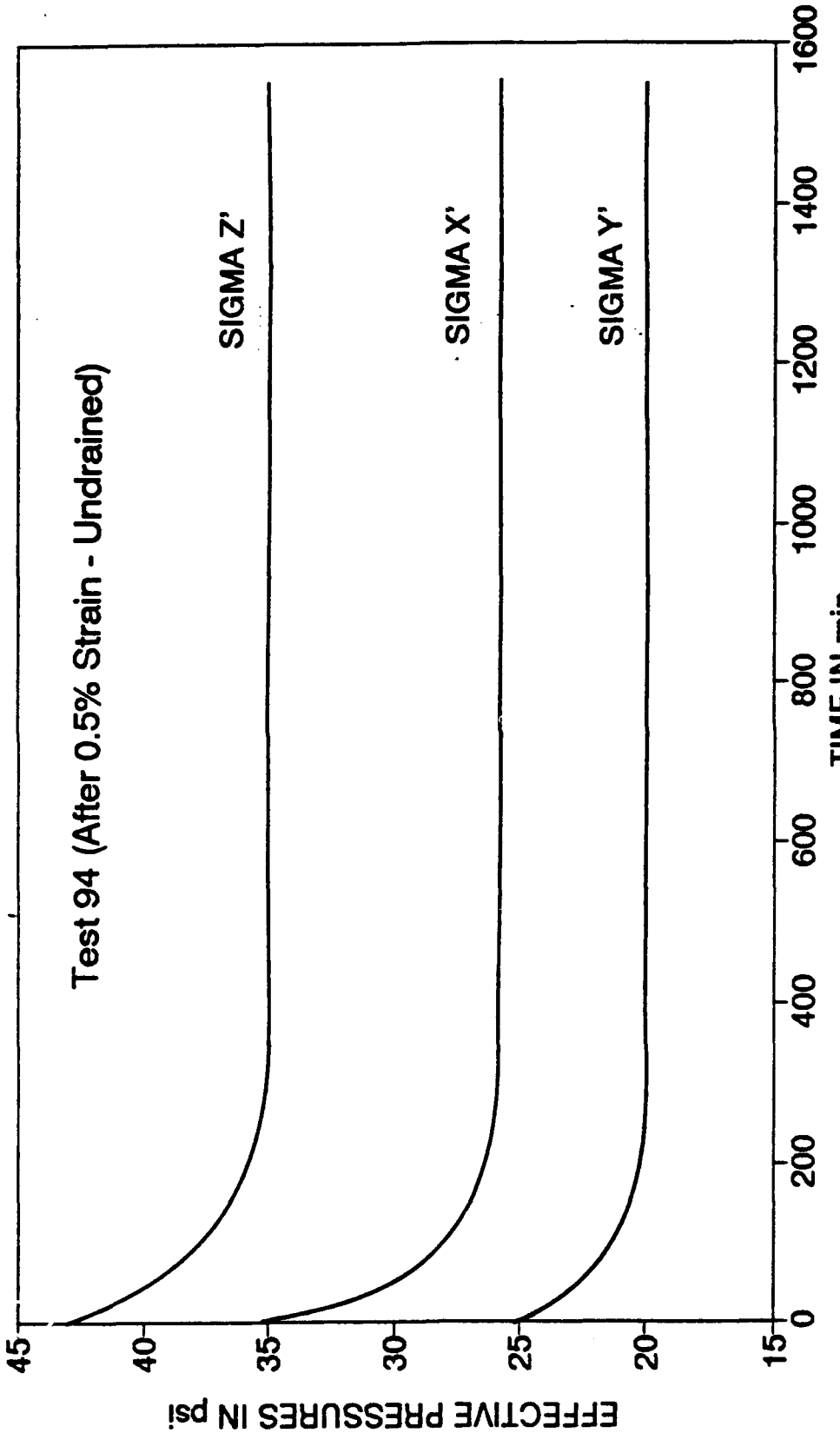

Fig. 6.9 Relaxation Curves for Kaolin After 0.5% Strain-Undrained Test (No. 94)

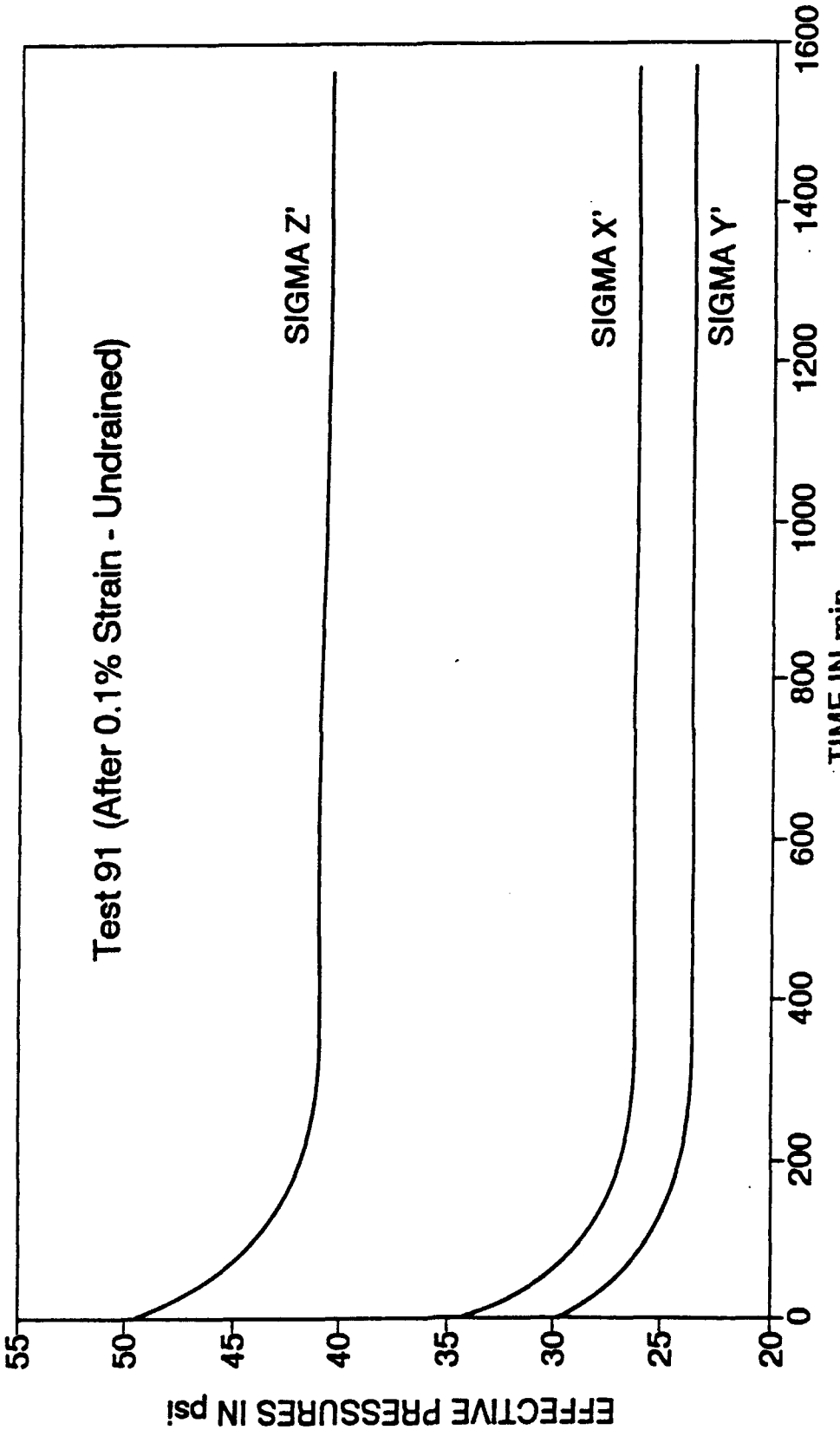

Fig. 6.10 Relaxation Curves for Kaolin After 0.1% Strain-Undrained Test (No. 91)

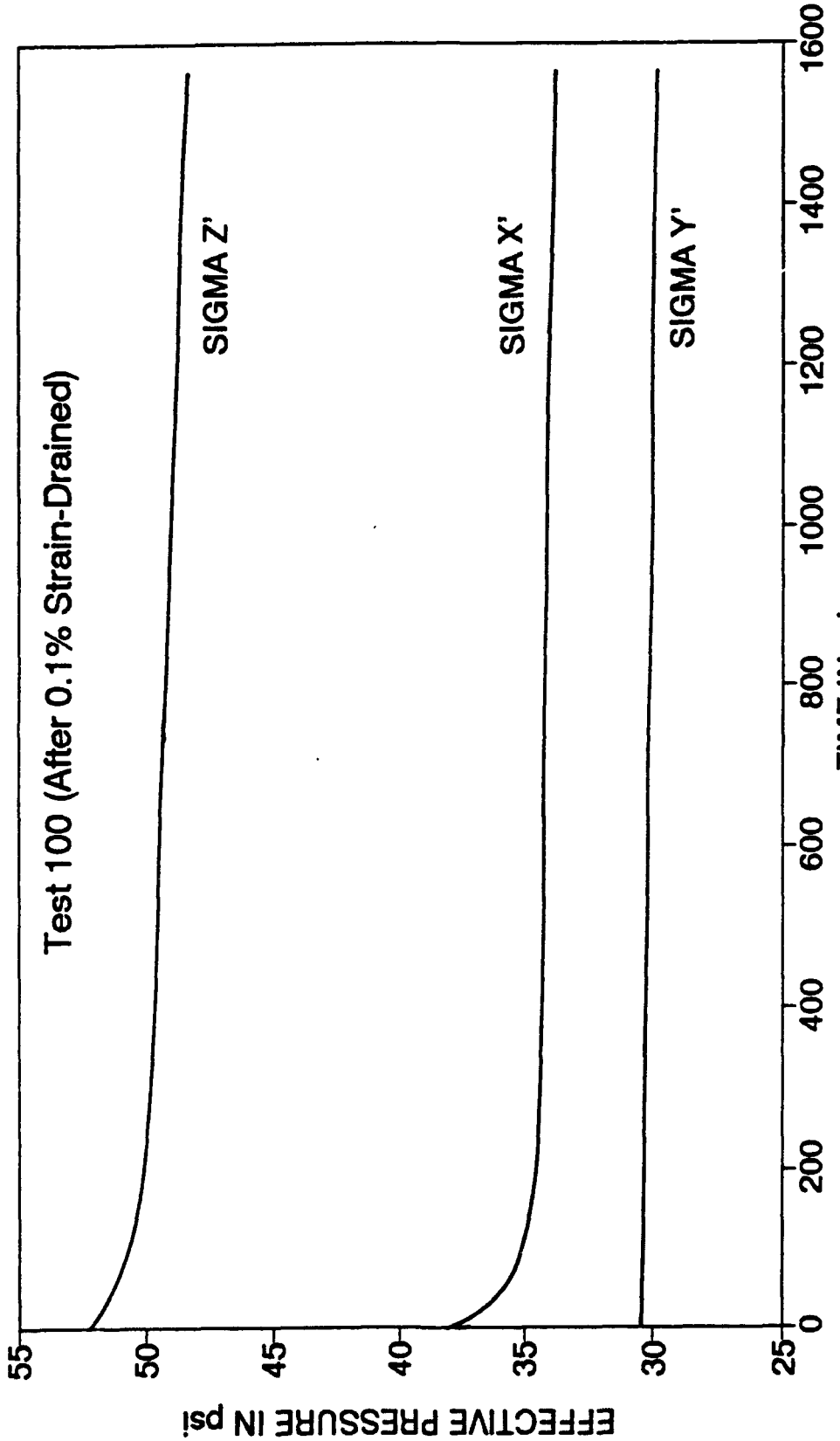

Fig. 6.11 Relaxation Curves for Kaolin After 0.1% Strain-Drained Test (No. 100)

Table 6.3 Change in Coefficient of Lateral Pressure During Relaxation

Test No.	Strain Rate (%/min)	Strain Before Relax-ation (%)	Stress Before Relaxation		Stress After Relaxation		K_o		ΔK_o (%)
			Horizontal (psi)	Vertical (psi)	Horizontal (psi)	Vertical (psi)	Before Relaxation	After Relaxation	
87	0.1	1.0	29.65	42.00	23.26	35.26	0.706	0.660	6.51
89	0.1	1.0	29.58	41.17	21.57	32.09	0.718	0.672	6.47
93	0.05	0.5	31.45	47.28	22.29	35.79	0.665	0.623	6.34
94	0.05	0.5	30.00	42.87	22.96	35.00	0.700	0.656	6.29
88	0.01	0.1	32.22	47.22	24.63	39.87	0.661	0.618	6.51
91	0.01	0.1	31.92	49.26	25.19	41.52	0.648	0.607	6.33

Stress relief and stress relaxation in PMT are important at least when compared to triaxial testing. It is commonly expected that the larger the size of overcut larger the amount of stress relief. However, the pressuremeter stress paths simulated in the cuboidal shear device revealed that the change in the coefficient of lateral earth pressure was not affected by the amount of strain (i.e., size of over cut). The change in K_o was found to be constant, about 6.4% for 0.1%, 0.5% and 1.0% strain.

Usually the stress relaxation time and the probe expansion rate are rarely quantified in the literature. But these are important parameters and little knowledge is available to guide the practitioner as to the proper value. Commonly they are referred to in a descriptive manner such as the stress relaxation time must be long enough to permit the excess pore pressure to dissipate, and the probe expansion rate fast enough to prevent drainage. Unfortunately, these parameters are not only soil dependent but also drilling technique and operator dependent. To shed more light into this qualitative nature of defining stress relaxation time, pressuremeter tests were simulated in the cuboidal shear device and the influence of strain and strain rate on the stress relaxation was studied. For kaolin clay, in the limited strain range of 0.1% to 1.0% of strain (which reflects the amount of overcutting) and for the strain rate of 0.005%/min to 0.1%/min (which is a measure of drilling rate), the relaxation time was about 200 to 250 minutes.

CHAPTER 7

CONCLUSIONS

This chapter summarizes the main conclusions drawn from this investigation. Other results and conclusions are presented at the end of each chapter.

1. The automated flexible wall calibration chamber model pressuremeter tests performed on two soils, kaolin and kaolin-silica mixture, show a satisfactory performance of the improved pressure control system (electro-pneumatic control) and the data acquisition system. The newly designed piezometer also performed very well. It was a major problem in previous studies.

2. The systematic procedure adopted in sample preparation yielded a very consistent uniform samples. The cuboidal shear device is a very versatile equipment which can simulate any kind of stress path with the proper servo-controlled hardware and software. The mechanical solenoid valves hindered the speed of the experiment, otherwise all components of the simulation system worked satisfactorily.

3. Pressuremeter tests were simulated in the cuboidal shear device by applying a shear load on a one dimensionally consolidated sample such that no deformation was allowed in the vertical direction (plane strain condition) and allowing the expansion in y- direction to be equal to the compression in the x-direction (no volume change in the undrained condition). Three or more tests were performed at strain rates of 0.01%, 0.05%, 0.10%, 0.50%, 1.00%, and 5.00% per min. Excellent agreement was observed for the tests performed at the same strain rate. It was found from the experiments that

the normalized shear strength (with respect to 0.01%/min) increases linearly with the logarithm of strain rate. The increase in undrained shear strength in the pressuremeter stress path is about 14.3% per log cycle for the kaolin clay and 15.3% for the kaolin-silica mixture. The undrained shear strength in the conventional triaxial test was found to increase about 8 to 10% for a tenfold increase in strain rate. Therefore, it can be concluded that the undrained shear strength increases about 40-50% more in pressuremeter stress path tests than in the triaxial stress path.

From the numerical studies, the influence of consolidation and creep were studied. Consolidation tends to increase the strength around the probe for slower strain rate cases, however, creep tends to decrease the strength. The creep effect is more than the consolidation influence, and the combined effect of consolidation and creep gives lesser shear strength at smaller strain rates and higher strength at higher strain rates.

4. The model developed based on cavity expansion theory is able to incorporate the influence of decreasing strain rate along the surrounding soil mass. The findings from the strain rate test for the pressuremeter was used in the model to estimate the difference in the interpretation of the undrained shear strength. The influence of the other parameters also studied parametrically. The level of upper yield did not affect the strength prediction. The slope of normalized shear strength versus logarithmic strain rate line, β was found as 0.15 and 0.10 for pressuremeter tests and triaxial tests, respectively. For the higher values of β (PMT condition), the peak strength shows about a 25% decrease, and the strain softening is also higher than for the triaxial case. In fact, for $\beta = 0.10$, the actual material curve and the PMT interpreted curves are of strain hardening type, and the $\beta = 0.15$ curves are strain softening. Thus, the different test condition influences the type of results obtained. The important conclusions from this study are that the PMT condition induces more strain softening than the triaxial test condition, which agrees well with previous studies, and higher strain rate tests (PMT) show higher shear strength.

5. The stress relief causes unloading of the soil around the borehole and leads to underestimation of the in situ horizontal pressure which in turn influences the interpreted shear strength from the pressuremeter expansion curve. It was found from the full scale tests that 1.1% oversized cutting shoe tests led to an overestimation of 60-100% in undrained shear strength.

The relaxation time or normalization period is the time period which should be allowed to dissipate the excess pore pressure developed during the drilling operation. This period is dependent upon the drilling technique used, the operator and the type of soil tested. In the literature, the relaxation time reported varies from a few minutes to several hours. The pressuremeter test was simulated in CSD and the specimen was strained to different level of strains using different strain rates and the relaxation time was monitored. Irrespective of the initial strain level, for kaolin clay the relaxation time was about 200 to 250 minutes in all cases.

Ladanyi (1982) developed equations to obtain creep parameters from the pressuremeter test in a borehole. Lacerda (1976) proposed several correlations to obtain relaxation parameters from Singh-Mitchell creep equation and empirically from plasticity index. Using the aging theory of creep, Ladanyi et al. (1991) derived expressions for stress relaxation from which creep parameters could be inferred. These creep/relaxation parameters are required to predict the time dependent behavior of soil.

LIST OF REFERENCES

Akai, K., Adachi, T., and Ando, N. (1975). "Existence of a Unique Stress-Strain-Time Relation of Clays," Soils and Foundations, 15(1), 1-16.

Anderson, W.F. and Pyrah, I.C. (1986). "Undrained Strength and Deformation Parameters from Pressuremeter Test Results," The Pressuremeter and Its Marine Applications, STP 950, ASTM, 324-338.

Anderson, W.F. and Pyrah, I.C. (1989). "Consolidation and Creep Effects in the PMT in Clay," Proc. 12th ICSMFE, Vol. 1, 153-156.

Anderson, W.F., Pyrah, I.C., and Haji-Ali, F. (1987). "Rate Effects in Pressuremeter Tests in Clays," J. Geotech. Engrg., ASCE, 113(11), 1344-1358.

Baguelin, F., Jezequel, J.F., Le Mee, E., and Le Mehaute, A. (1972). "Expansion of Cylindrical Probes in Cohesive Soils," J. Soil Mech. Found., ASCE, 98(11), 1129-1142.

Baguelin, F., Jezequel, J-F., and Le Mehaute, A. (1974). "Self-Boring Placement Method of Soil Characteristics Measurements," Proc. ASCE Spec. Conf. on Subsurface Exploration for Underground Excavation and Heavy Construction, Henniker, NH, 312-332.

Baguelin, F., Jezequel, J-F., and Shields, D.H. (1978). The Pressuremeter and Foundation Engineering, Trans Tech Publications, Rockport, MA.

Bellotti, R., Ghionna, V., Jamiolkowski, M., Robertson, P.K., and Peterson, R.W. (1989). "Interpretation of Moduli from Self-Boring Pressuremeter Tests in Sand," Geotechnique, 39(2), 269-292.

Benoit, J. (1983). "Analysis of Self-Boring Pressuremeter Tests in Soft Clay," Ph.D. Thesis, Stanford Univ., CA.

Benoit, J. and Clough, G.W. (1986). "Self-Boring Pressuremeter Tests in Soft Clay," J. Geotech. Engrg., ASCE, 112(1), 60-78.

Bjerrum, L. (1972). "Embankments on Soft Ground," Proc. ASCE Specialty Conf. on Performance of Earth and Earth Supported Structures, Purdue Univ., West Lafayette, IN, Vol. 2, 1-54.

Briaud, J-L., Tucker, L.M., and Makarim, C.A. (1986). "Pressuremeter Standard and Pressuremeter Parameters," The Pressuremeter and Its Marine Applications: 2nd Int. Symp., ASTM STP 950, 303-323.

Brucy, F. and LeTirant, P. (1986). "Use of PAM and Pressuremeters in Offshore Foundation Design," The Pressuremeter and Its Marine Applications, 2nd Int. Symp., ASTM STP 950, 5-21.

Campanella, R.G., and Vaid, V.P. (1972). "A Simple K_o Triaxial Cell", Canadian Geotechnical Journal, Vol. 9, pp. 249.

Carter, J.P. (1978). "CAMFE - A Computer Program for the Analysis of a Cylindrical Cavity Expansion in Soil," Report CUED/SOILS/TR52, Univ. of Cambridge, England.

Carter, J.P., Randolph, M.F., and Wroth, C.P. (1979). "Stress and Pore Pressure Changes in Clay During and After the Expansion of a Cylindrical Cavity," Int. J. Num. & Anal. Mtds in Geomech., Vol. 3, 305-322.

Casagrande, A. and Wilson, S.D. (1951). "Effect of Rate of Loading on the Strength of Clays and Shales at Constant Water Content," Geotechnique, Vol. 2, 251-263.

Chameau, J.L., Penumadu, D., Skandarajah, A., and Thevanayagam, S. (1990). "Anisotropic Behavior of Soils and Pressuremeter Test: Annual Report," AFOSR, Bolling, AFB.

Chapman, G. (1974). "A Calibration Chamber for Field Testing Equipment", Proceedings of the European Symposium on Penetration Testing, Stockholm, pp. 59-65.

Christensen, R.W. and Wu, T.H. (1964). "Analysis of Clay Deformation as a Rate Process," J. Soil Mech. Found., ASCE, 90(6), 125-157.

Crawford, C.B. (1959). "The Influence of Rate of Strain on Effective Stresses in Sensitive Clay," ASTM STP 254, 36-48.

Denby, G.M. (1978). "Self-Boring Pressuremeter Study on San Francisco Bay Mud," Ph.D. Thesis, Stanford Univ., CA.

Denby, G.M. and Clough, G.W. (1980). "Self-Boring Pressuremeter Test in Clay," J. Geotech. Engrg., ASCE, 106(12), 1369-1387.

Deschamps, R.J. (1991). Personal Communication.

Fyffe, S., Reid, W.M., and Summers, J.B. (1986). "Thr Push-In Pressuremeter: 5 Years Offshore Experience," ASTM STP 950, 22-37.

Gangopadhyay, C.R. and Nasr, A.N. (1986). "Interpretation of Pressuremeter Tests Using Laboratory Simulated Tests," The Pressuremeter and Its Marine Applications: 2nd Int. Symp., ASTM STP 950, 214-231.

Gibson, R.E. and Anderson, W.F. (1961). "In Situ Measurement of Soil Properties with the Pressuremeter," Civil Engrg. & Public Works Review, 56(658), 615-618.

Green, G.E. (1971). "Strength and Deformation of Sand Measured in an Independent Stress Controll Cell," Stress-Strain Behavior of Soils, Proc. Roscoe Memorial Symp., Foulis and Co., England, 285-323.

Haefeli, R. (1965). "Creep and Progressive Failure in Snow, Soil, Rock and Ice," Proc. 6th ICSMFE, Montreal, Vol. III, 134-147.

Hambly, E.C. (1969). "A New True Triaxial Apparatus," Geotechnique, 19(2), 307-309.

Hill, R. (1950). The Mathematical Theory of Plasticity. Oxford University Press.

Huang, A.B. (1986). "Laboratory Pressuremeter Experiments in Clay Soils," Ph.D. Thesis, Purdue Univ., IN.

Huang, A.B., Holtz, R.D., and Chameau, J-L. (1988). "A Calibration Chamber for Cohesive Soils," Geotech. Testing J., 11(1), 30-35.

Huang, A.B., Holtz, R.D., and Chameau, J-L. (1991). "Laboratory Study of Pressuremeter Tests in Clays," J. Geotech. Engrg., ASCE, 117(10), 1549-1567.

Hughes, J.M.O. and Robertson, P.K. (1985). "Full-Displacement Pressuremeter Testing in Sand," Can. Geotech. J., Vol. 22, 298-307.

Hughes, J.M.O., et al. (1980). "Determination of the Engineering Properties of the Coode Island Silts Using a Self-Boring Pressuremeter," Proc., 3rd Australian-New Zealand Conf. on Geomech., Wellington, 249-254.

Jacobson, B. (1957). "Some Fundamental Properties of Sand," Proc. 4th ICSMFE, London, UK, Vol. 1, 167-171.

Jain, S.K. (1985). "Analysis of the Pressuremeter by FEM Formulation with Elasto-Plastic Consolidation," Ph.D. Thesis, VPI, Blacksburg, VA.

Jamiolkowski, M. and Lancellotta, R. (1977). "Remarks on the Use of Self-Boring Pressuremeter in Three Italian Clays," Rivista Italiana di Geotecnica, Luglio, Vol. XI, No. 3, 153-171.

Jamiolkowski, M. and Lancellotta, R. (1979). "Session 4 - Design Parameters for Stiff Clays," 7th European Conf. of Soil Mech. Found. Engrg., Brighton.

Jewell, R.J., Fahey, M., and Wroth, C.P. (1980). "Laboratory Study of the Pressuremeter Test in Sand", Geotechnique, Vol. 30, pp. 507-531.

Jezequel, J.F. (1982). "The Selfboring Pressuremeter," Symp. on the Pressuremeter and Its Marine Applications, Editions Technip, Paris.

Kjellman, W. (1936). "Report on an Apparatus for Consummate Investigation of the Mechanical Properties of Soils," Proc. 1st ICSMFE, Cambridge, MA, Vol. 2, 16-20.

Ko, H.Y. and Scott, R.F. (1967). "A New Soil Testing Apparatus," Geotechnique, 17(1), 40-57.

Lacasse, S., Jamiolkowski, M., Lancellotta, R., and Lunne, T. (1981). "In Situ Characteristics of Two Norwegian Clays," 10th ICSMFE, Stockholm, Vol. 2, 507-511.

Lacasse, S. and Lunne, T. (1982). "In-Situ Horizontal Stress from Pressuremeter Tests," Norges Geotekniske Institutt.

Lacerda, W.A. (1976). "Stress-Relaxation and Creep Effects on Soil Deformation," Ph.D. Thesis, Univ. of California, Berkeley.

Lacerda, W.A. and Houston, W.N. (1973). "Stress Relaxation in Soils," Proc. 8th ICSMFE, Moscow, Vol. 1, 221-227.

Ladanyi, B. (1963). "Expansion of a Cavity in a Saturated Clay Medium," J. Soil Mech. Found., ASCE, 89(4), 127-161.

Ladanyi, B. (1972). "In-Situ Determination of Undrained Stress-Strain Behavior of Sensitive Clays with the Pressuremeter," Can. Geotech. J., 9(3), 313-319.

Ladanyi, B. (1982). "Borehole Creep and Relaxation Tests in Ice-Rich Permafrost," Proc. 4th Canad. Permafrost Conf., Calgary, NRCC-ACGR, Ottawa, 406-415.

Ladanyi, B. and Huneault, P. (1989). "Cone Penetrometer Tests in Permafrost - The Fox Tunnel, Alaska," Proc. Int. Symp. on Mining in the Arctic, Fairbanks, AK, 75-82.

Ladanyi, B. and Johnston, G.H. (1978). "Field Investigations in Frozen Ground," Chap. 9 in "Geotech. Engrg. for Cold Regions," Andersland, O.B. and Anderson, D.M. (Eds.), McGraw-Hill, 459-504.

Ladanyi, B., Touileb, B., and Huneault, P. (1991). "Pressuremeter Stress Relaxation Testing in a Permafrost Tunnel," Geotech. Engrg. Congress, Geotech. Special Pub. No. 27, Boulder, CO, 213-224.

Ladd, C.C., Germaine, J.T., Baligh, M.M., and Lacasse, S.M. (1980). "Evaluation of Self-Boring Pressuremeter Tests in Boston Blue Clay," Federal Highway Administration, Report No. FHWA/RD-80/052, Washington, D.C.

Law, K.T. and Eden, W.J. (1980). "Influence of Cutting Shoe in Self-Boring Pressuremeter Tests in Sensitive Clays," Can. Geotech. J., 17(2), 165-173.

Mori, H. (1981). "Study on the Properties of Soils in the Northern Coast of Tokyo Bay Using a Self-Boring Pressuremeter," Soils and Foundations, 21(3), 83-98.

Murayama, S., Sekiguchi, H., and Ueda, T. (1974). "A Study of the Stress-Strain-Time Behavior of Saturated Clays Based on a Theory of Nonlinear Viscoelasticity," Soils and Foundations, 14(2), 19-33.

Murayama, S. and Shibata, T. (1961). " Rheological Properties of Clays," Proc. 5th ICSMFE, Paris, 269-273.

Nadarajah, V. (1973). "Stress-Strain Properties of Lightly Over-Consolidated Clays," Ph.D. Thesis, Cambridge Univ., England.

Nakase, A. and Kamei, T. (1986). "Influence of Strain Rate on Undrained Shear Characteristics of K_o-Consolidated Cohesive Soils," Soils and Foundations, 26(1), 85-95.

Nasr, A.N. and Gangopadhyay, C.R. (1988). "Study of S_u Predicted by Pressuremeter Test," J. Geotech. Engrg., ASCE, 114(11), 1209-1226.

Palmer, A.C. (1972). "Undrained Plane Strain Expansion of a Cylindrical Cavity: A Simple Interpretation of the Pressuremeter Test," Geotechnique, 22(3), 451-457.

Pearce, J.A. (1971). "A New True Triaxial Apparatus," Stress-Strain Behavior of Soils, Proc. Roscoe Memorial Symp., 330-339.

Perloff, W.H. and Osterberg, J.O. (1963). "The Effect of Strain Rate on the Undrained Shear Strength of Cohesive Soils," Proc. 2nd Pan Am. Conf. Soil Mech. and Found., Vol. 2, 103-128.

Prapaharan, S. (1987). "Effects of Disturbance, Strain Rate, and Partial Drainage on Pressuremeter Test Results in Clay," Ph.D. Thesis, Purdue University, West Lafayette, IN.

Prapaharan, S., Chameau, J-L., and Holtz, R.D. (1989). "Effect of Strain Rate on Undrained Strength Derived from Pressuremeter Tests," Geotechnique, 39(4), 615-624.

Prevost, J-H. (1976). "Undrained Stress-Strain-Time Behavior," J. Geotech. Engrg., ASCE, 102(12), 1245-1259.

Prevost, J.H. (1979). "Undrained Shear Tests on Clays," J. Geotech. Engrg., ASCE, 105(1), 49-64.

Prevost, J-H. and Hoeg, K. (1975). "Analysis of Pressuremeter in Strain Softening Soil," J. Geotech. Engrg., ASCE, 101(8), 717-731.

Pyrah, I.C., Anderson, W.F., and Haji-Ali, F. (1985). "The Interpretation of Pressuremeter Tests - Time Effects for Fine Grained Soils, Proc. 5th Int. Conf. on Num. Mtds. in Geomech., Nagoya, 1629-1636.

Pyrah, I.C., Anderson, W.F., and Pang, L.S. (1988). "Effects of Test Procedure on Constant Rate of Strain Pressuremeter Tests in Clay," Proc. 6th Int. Conf. on Num. Mtds. in Geomech., A.A. Balkema, Rotterdam, 647-652.

Richardson, A.M. and Whitman, R.V. (1963). "Effect of Strain-Rate Upon Undrained Shear Resistence of a Saturated Remoulded Fat Clay," Geotechnique, 13(4), 310-324.

Saada, A.S. (1962). "A Rheological Analysis of Shear and Consolidation of Saturated Clays," HRB Bulletin 342, 52-75.

Sayed, S.M. and Hamed, M.A. (1987). "Expansion of Cavities in Layered Elastic System," Int. J. for Num. & Anal. Mtds in Geomech., Vol. 11. 203-213.

Sheeran, D.E. and Krizek, R.J. (1971). "Preparation of Homogeneous Soil Samples by Slurry Consolidation," J. of Materials, JMLSA, 6(2), 356-373.

Singh, A. and Mitchell, J.K. (1968). "General Stress-Strain-Time Function for Soils," J. Soil Mech. Found., ASCE, 94(1), 21-46.

Sivakugan, N. (1987). "Anisotropy and Stress Path Effects in Clays," Ph.D. Thesis, Purdue University, IN.

Sivakugan, N, Chameau, J-L., Holtz, R.D., and Altschaeffl, A.G. (1988). "Servo-Controlled Cuboidal Shear Device," Geotech. Testing J., ASTM, 11(2), 119-124.

Skandarajah, A., Penumadu, P., and Chameau, J-L. (1991). "Strain Rate Effects on Pressuremeter Testing," 8th ASCE Engrg. Mech. Conf., Columbus, OH. (Mechanics Computing in 1990s and Beyond, Adeli, H. and Sierakowski, S. (Eds.), ASCE, Vol. 2, 1141-1145.)

Sketchley, C.J. (1973). "The Behavior of Kaolin in Plane Strain," Ph.D. Thesis, Cambridge Univ., England.

Soulie, M., Ladanyi, B., and Degenne, P. (1986). "Expansion of a Cylindrical Cavity in a Very Deformable Medium," 2nd Int. Symp. Pressuremeter and Its Marine Applications, ASTM, STP 950, 232-244.

Sture, S. and Desai, C.S. (1979). "Fluid Cushion Truly Triaxial or Multiaxial Testing Device," Geotech. Testing J., 2(1), 20-33.

Suyama, K., Imai, T., and Ohya, S. (1982). "Lateral Load Tester (LLT). Its Method and Accuracy", Symposium on the Pressuremeter and Its Marine Applications, Paris.

Vaid, Y.P. and Campanella, R.G. (1977). "Time Dependent Behavior of Undisturbed Clay," J. Geotech. Engrg., ASCE, 103(7), 693-709.

Vesic, A.S. (1971). "Breakout Resistance of Objects Embedded in Ocean Bottom," J. Soil Mech. Found., ASCE, 97(9), 1183-1205.

Vesic, A.S. (1972). "Expansion of Cavities in an Infinite Soil Mass," J. Soil Mech. Found., ASCE, 98(3), 265-290.

Vesic, A.S. (1977). "Design of Pile Foundations," Synthesis of Highway Practice No. 42, TRB, Washington, D.C.

Vialov, S.S. and Skibitsky, A.M. (1961). " Problems of the Rheology of Soils," Proc. 5th ICSMFE, Paris, 387-392.

Winter, E. (1982). "Suggested Practice for Pressuremeter Testing in Soils," Geotech. Testing J., ASTM, 5(3/4), 85-88.

Withers, N.J., Schaap, L.H.J., and Dalton, C.P. (1986). "The Development of a Full Displacement Pressuremeter," The Pressuremeter and Its Marine Applications: 2nd Int. Symp., ASTM STP 950, 38-56.

Withers, N.J., Howie, J., Huges, J.M.O., and Robertson, P.K. (1989). "Performance and Analysis of Cone Pressuremeter Tests in Sands," Geotechnique, 39(3), 433-454.

Wood, D.M. and Wroth, C.P. (1977). "Some Laboratory Experiments Related to the Results of Pressuremeter Tests," Geotechnique, 27(2), 181-201.

Wroth, C.P. (1975). "In Situ Measurement of Initial Stresses and Deformation Characteristics," Proc. Conf. In Situ Measurement of Soil Properties, Raliegh, N.C., Vol. 2, 181-230.

Wroth, C.P. (1984). "The Interpretation of In Situ Soil Tests," Geotechnique, 34(4), 449-489.

Wroth, C.P. and Hughes, J. (1973). "An Instrument for the In Situ Measurement of the Properties of Soft Clays," Proc. 8th ICSMFE, Moscow, Vol. 1.2, 487-494.

APPENDIX A

LIST OF PUBLICATIONS

Two Ph.D. students were supported by the research project. One Ph.D. dissertation is in the completion stage:

> Skandarajah, A., "A Study of Strain Rate and Stress Relaxation Effects on Pressuremeter Test in Clays Using a Cuboidal Shear Device," Ph. D. Thesis, April 1992.

The other thesis is under preparation:

> Penumadu, D., "Calibration Chamber Testing and Stress-Strain Behavior with Neural Networks," Ph.D. Dissertation, Georgia Institute of Technology, (Fall 1992).

Two papers were presented in the following conferences:

> Skandarajah, A., Penumadu, D., and Chameau, J-L., "Strain Rate Effects on Pressuremeter Testing," Eighth ASCE Engineering Mechanics Specialty Conference, Columbus, Ohio, May 1991. (Mechanics Computing 1990's and Beyond, ASCE, Vol. 2, Eds. Adeli, H. and Sierakowski, R.L., pp. 1141-1145.)

> Penumadu, D., Skandarajah, A., and Chameau, J-L., "Model Pressuremeter Testing in an Automated Flexible Wall Calibration Chamber," The First International Symposium on Calibration Chamber Testing, Potsdam, NY, June 1991. (ISOCCT1, Editor Huang, A.B., Elsevier Publication, pp. 303-313.)

The following papers and discussion are submitted for publication or in preparation which will provide enough dissemination of the findings of the research supported by the U.S. AFOSR:

> Thevanayagam, S. and Chameau, J-L., "Modelling Anisotropy of Clays at Critical State," Accepted for Publication in the ASCE J. of Engrg. Mechanics.

Thevanayagam, S., Chameau, J-L., and Altschaeffl, A.G. "Some Aspects of Pressuremeter Testing," Submitted for Publication in the ASCE Geotech. Engrg. J., in Review.

Penumadu, D., Agrawal, G., and Chameau, J-L., Discussion on "Knowledge-Based Modelling of Material Behavior with Neural Networks," by Ghaboussi, J., Garrett, J.H. Jr., and Wu, X., J. of Engrg. Mech., ASCE, Vol. 117, No.1, Jan. 1991, Accepted for Publication, 1992.

Skandarajah, A., Penumadu, D. and Chameau, J-L., "An Experimental Study of Strain Rate Effects on Pressuremeter Test Using Cuboidal Shear Device," Technical Paper to be Submitted to Geotechnique.

Skandarajah, A., Penumadu, D., and Chameau, J-L., "Error in Pressuremeter Test Interpretation due to Strain Rate Effect," Technical Paper to be Submitted to J. Geotech. Engrg, ASCE.

Skandarajah, A., Chameau, J-L., and Penumadu, D. "Stress Relaxation Effects in Pressuremeter Testing," Technical Note in Preparation to be Submitted to J. Geotech. Engrg., ASCE.

Penumadu, D., Chameau, J-L., and Skandarajah, A., "Incorporating Strain Rate Effects Using Artificial Neural Networks," In Preparation.

Other Related Publications:

Huang, A.B., Holtz, R.D., and Chameau, J.L. (1991). "A Laboratory Study of Pressuremeter Tests in Clays," J. Geotech. Engrg., ASCE, 117(10), 1549-1567.

Sivakugan, N., Chameau, J-L., and Holtz, R.D. (1991). "An Inexpensive Automatic Control System for Soil Testing," Geotech. Special Pub. No. 27, Geotech. Engrg. Congress - 1991, Boulder, CO., Vol. 2, 574-581.

Sivakugan, N., Holtz, R.D., and Chameau, J.L. (1992). "Cam Clay Modeling of Plane Strain Compression Loading in Normally Consolidated Clays," 3rd Int. Conf. on Computational Plasticity Fundamentals and Applications, Barcelona, Spain, April.

We also plan to deliver the research results through presentations at technical meetings, and interaction with our geotechnical colleagues.

APPENDIX B

STRESS-STRAIN PLOTS FOR PMT STRAIN RATE TESTS

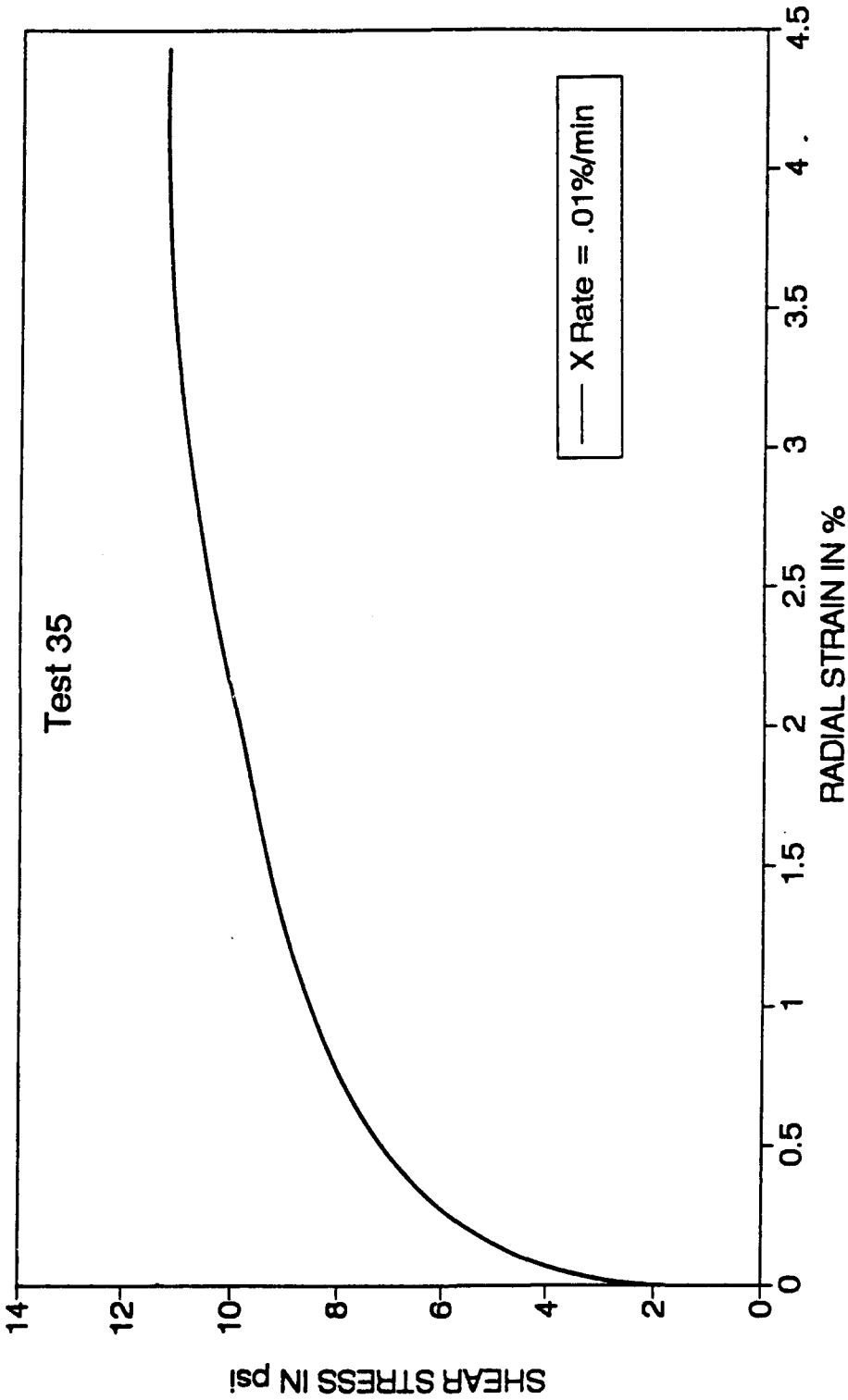

Fig. B.1 Shear Stress Vs Radial Strain for Kaolin Clay
(Test No. 35, Radial Strain Rate = 0.01%/min)

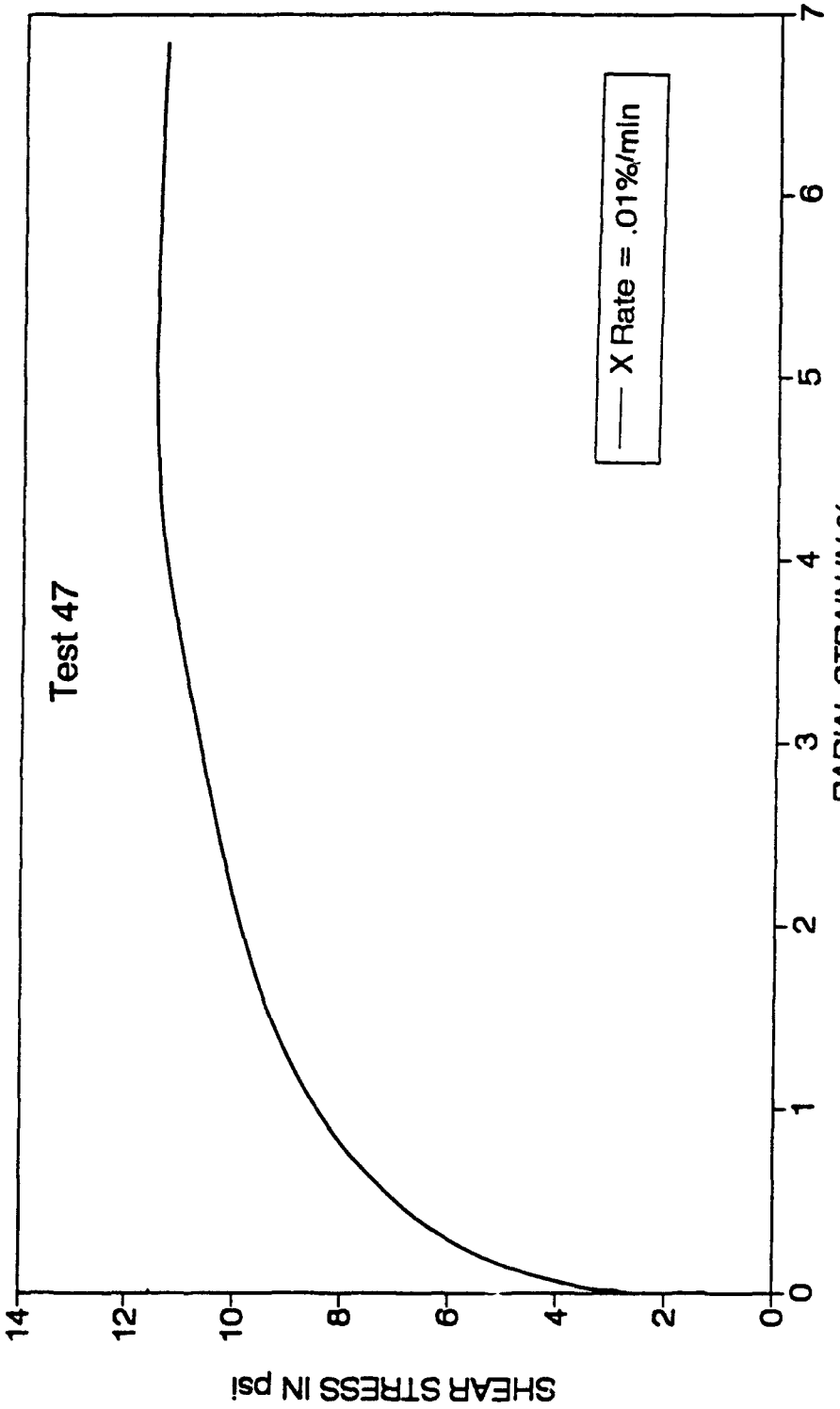

Fig. B.2 Shear Stress Vs Radial Strain for Kaolin Clay
(Test No. 47, Radial Strain Rate = 0.01%/min)

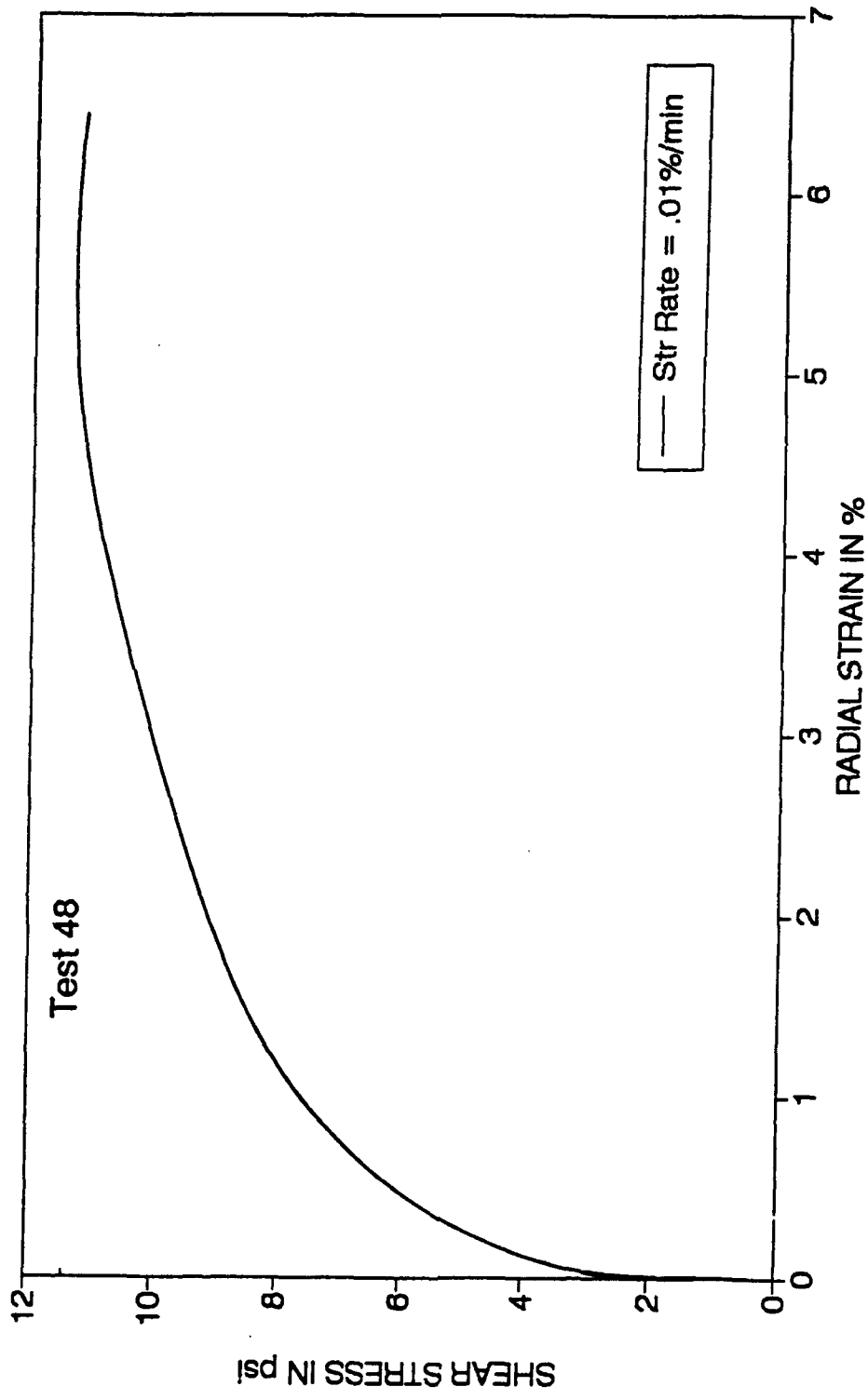

Fig. B.3 Shear Stress Vs Radial Strain for Kaolin Clay
(Test No. 48, Radial Strain Rate = 0.01%/min)

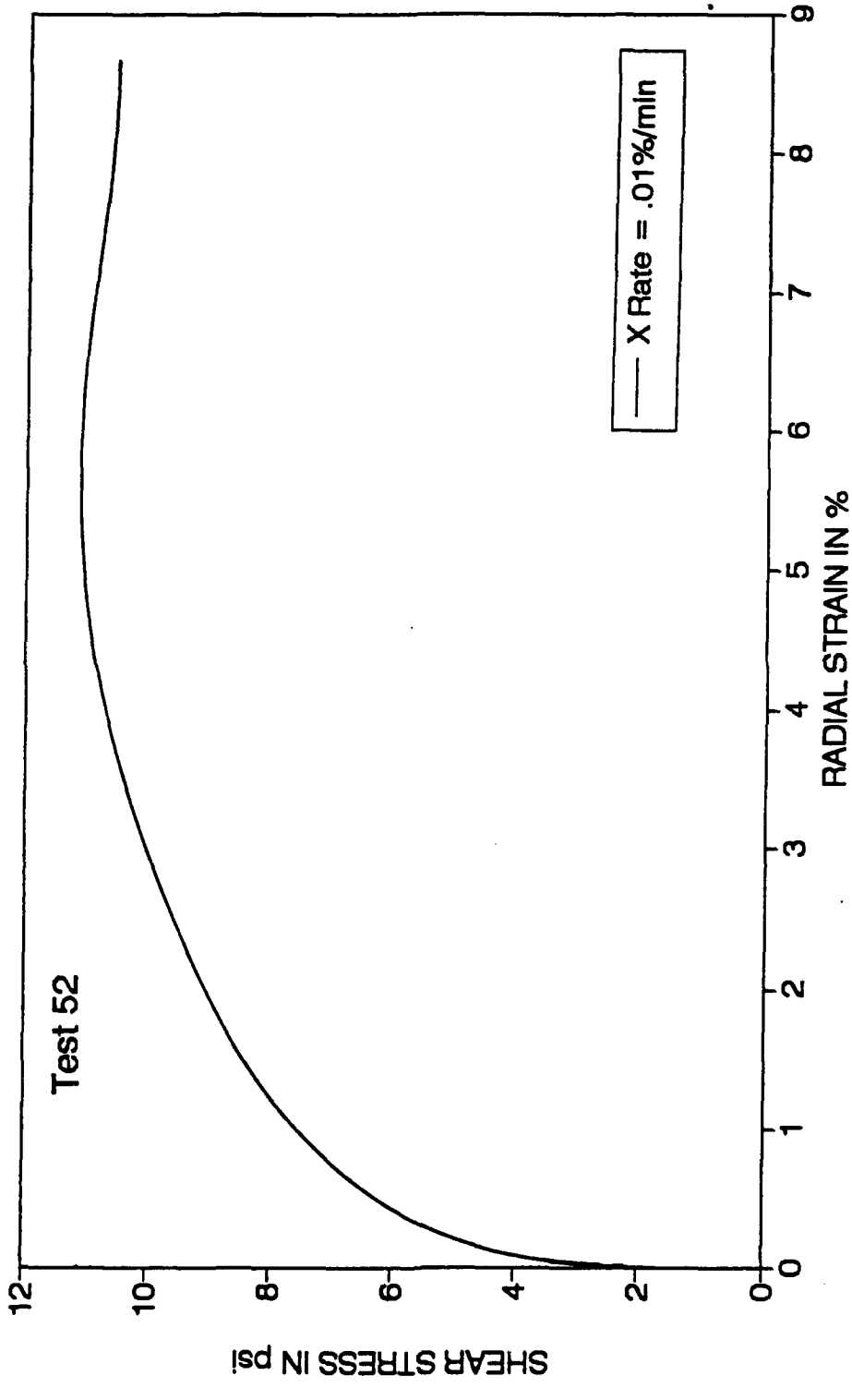

Fig. B.4 Shear Stress Vs Radial Strain for Kaolin Clay
(Test No. 52, Radial Strain Rate = 0.01%/min)

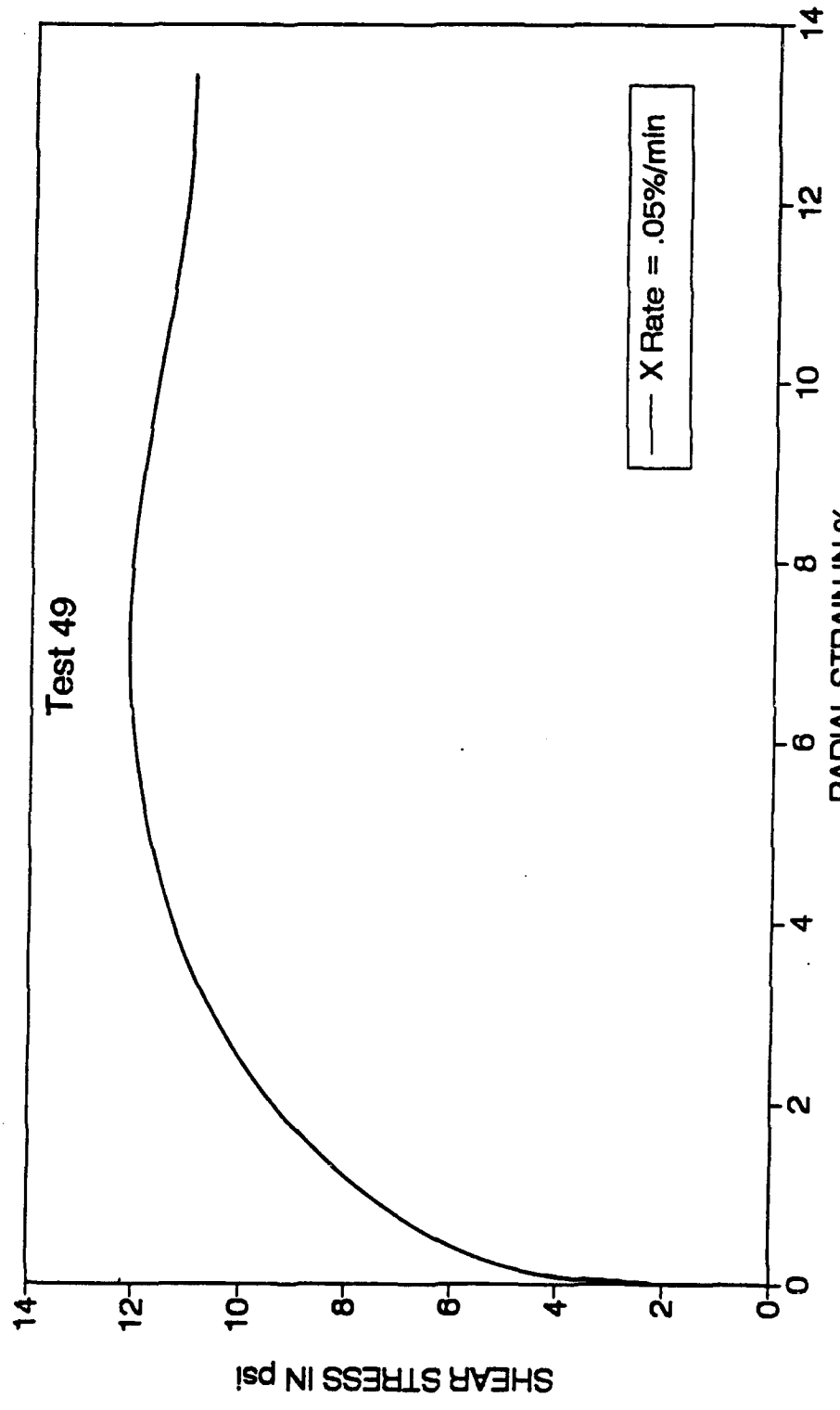

Fig. B.5 Shear Stress Vs Radial Strain for Kaolin Clay
(Test No. 49, Radial Strain Rate = 0.05%/min)

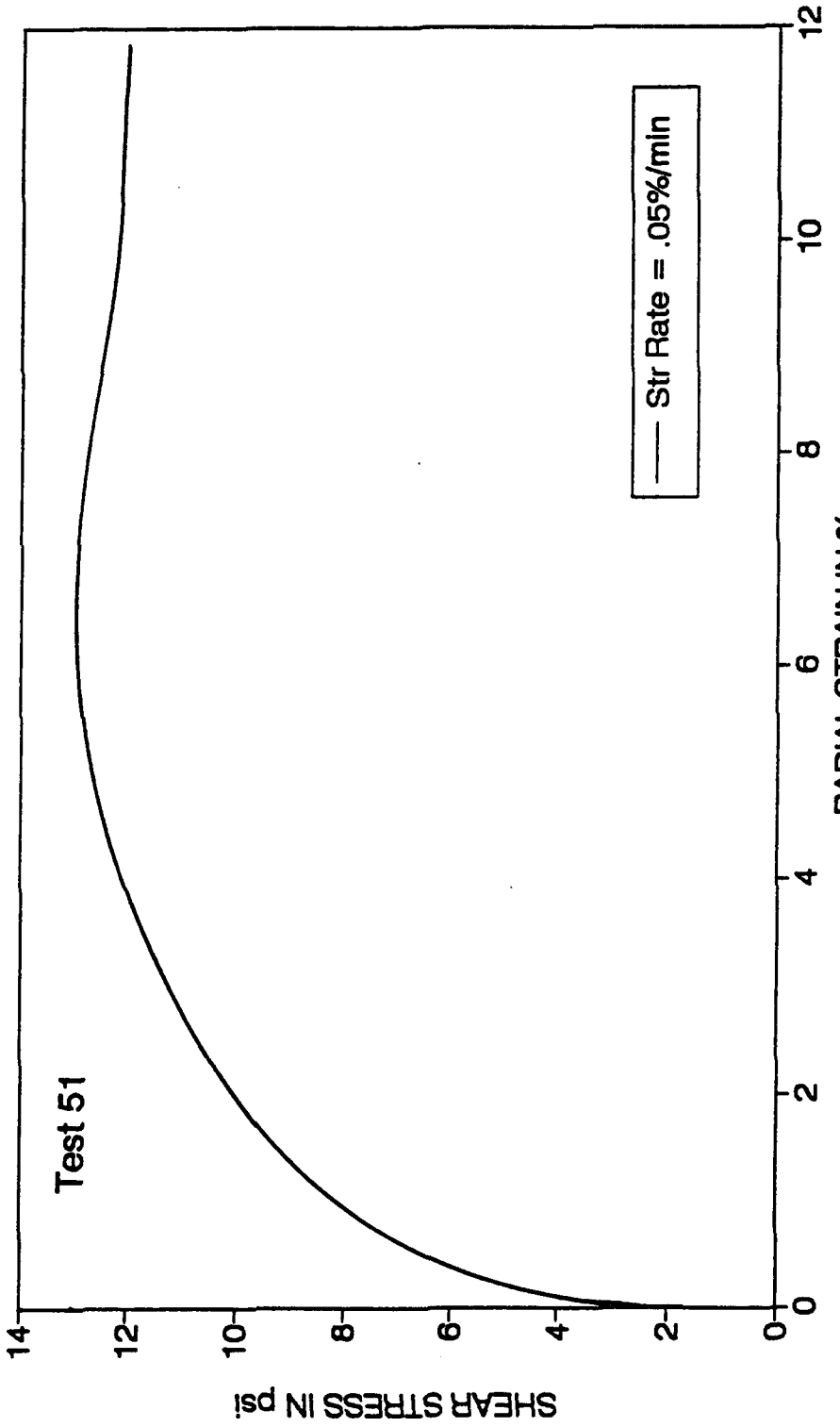

Fig. B.6 Shear Stress Vs Radial Strain for Kaolin Clay
(Test No. 51, Radial Strain Rate = 0.05%/min)

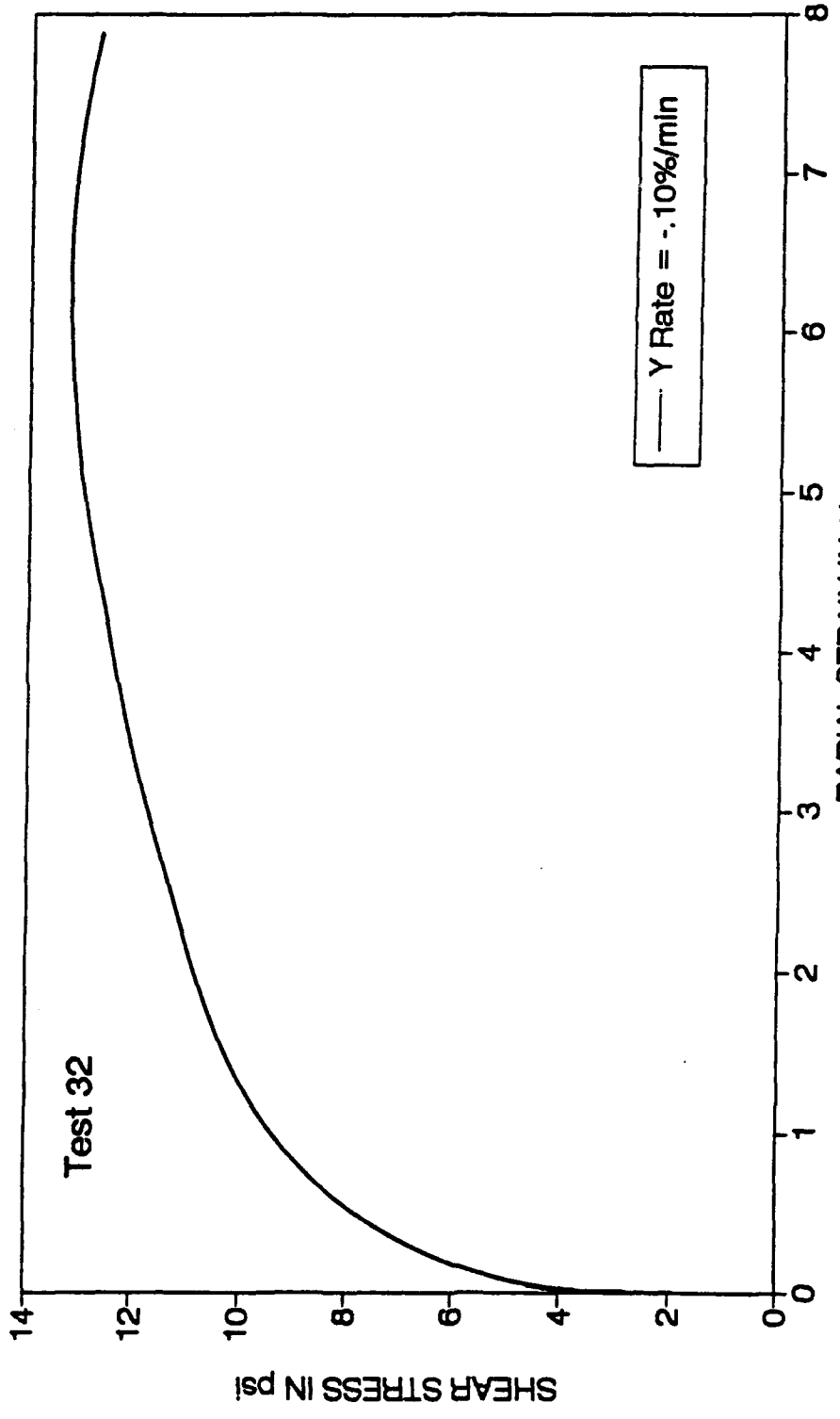

Fig. B.7 Shear Stress Vs Radial Strain for Kaolin Clay
(Test No. 32, Radial Strain Rate = 0.10%/min)

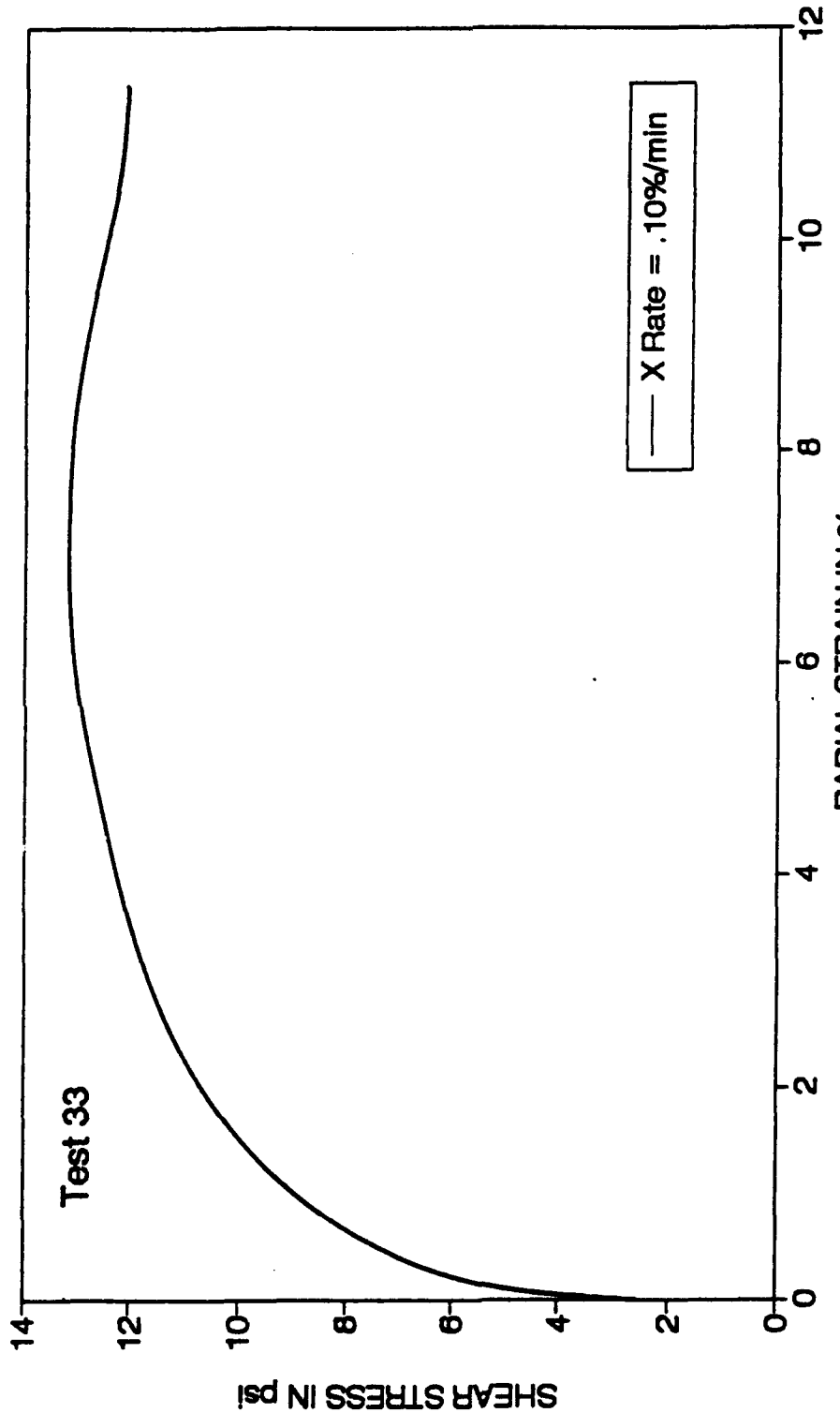

Fig. B.8 Shear Stress Vs Radial Strain for Kaolin Clay
(Test No. 33, Radial Strain Rate = 0.10%/min)

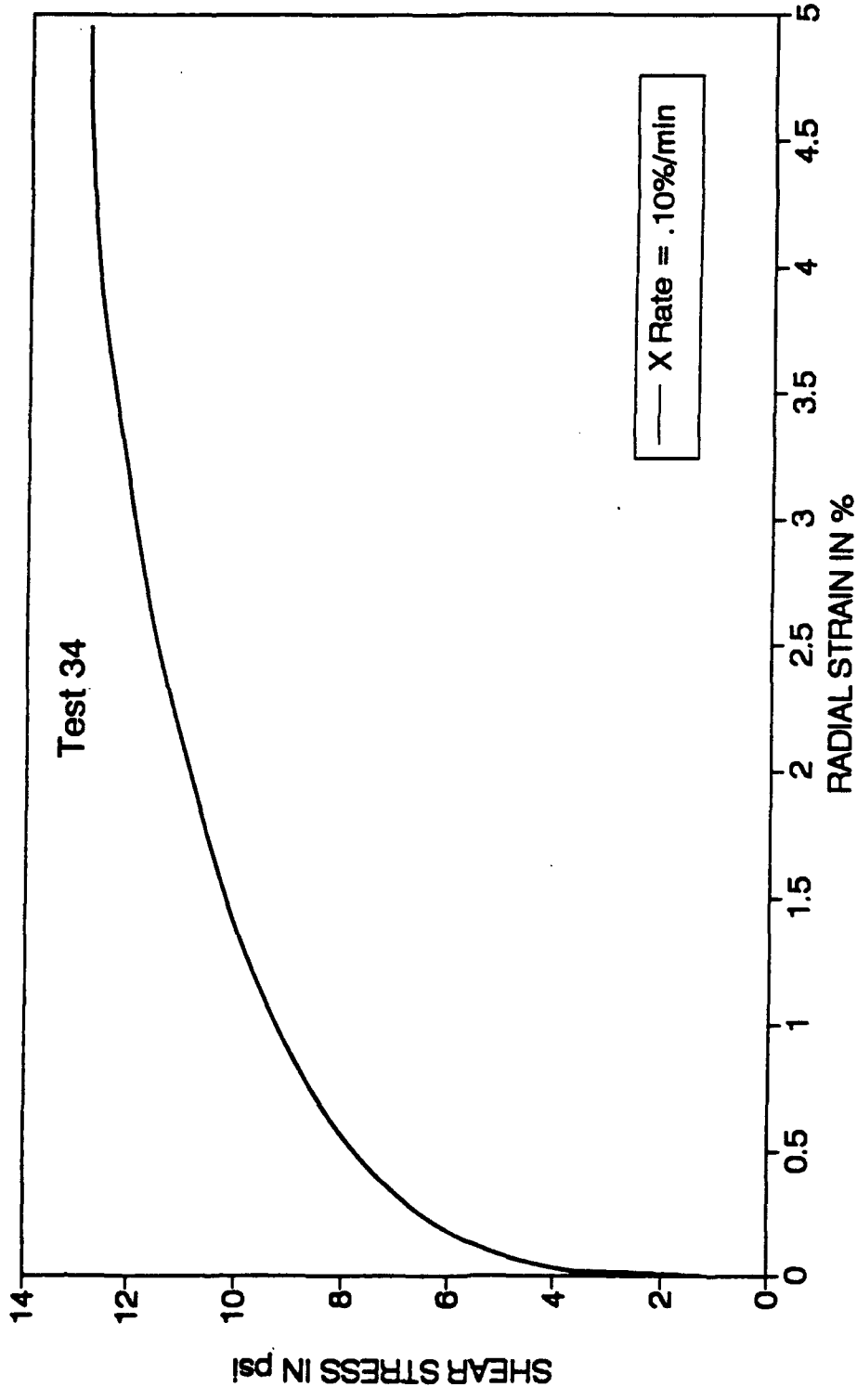

Fig. B.9 Shear Stress Vs Radial Strain for Kaolin Clay
(Test No. 34, Radial Strain Rate = 0.10%/min)

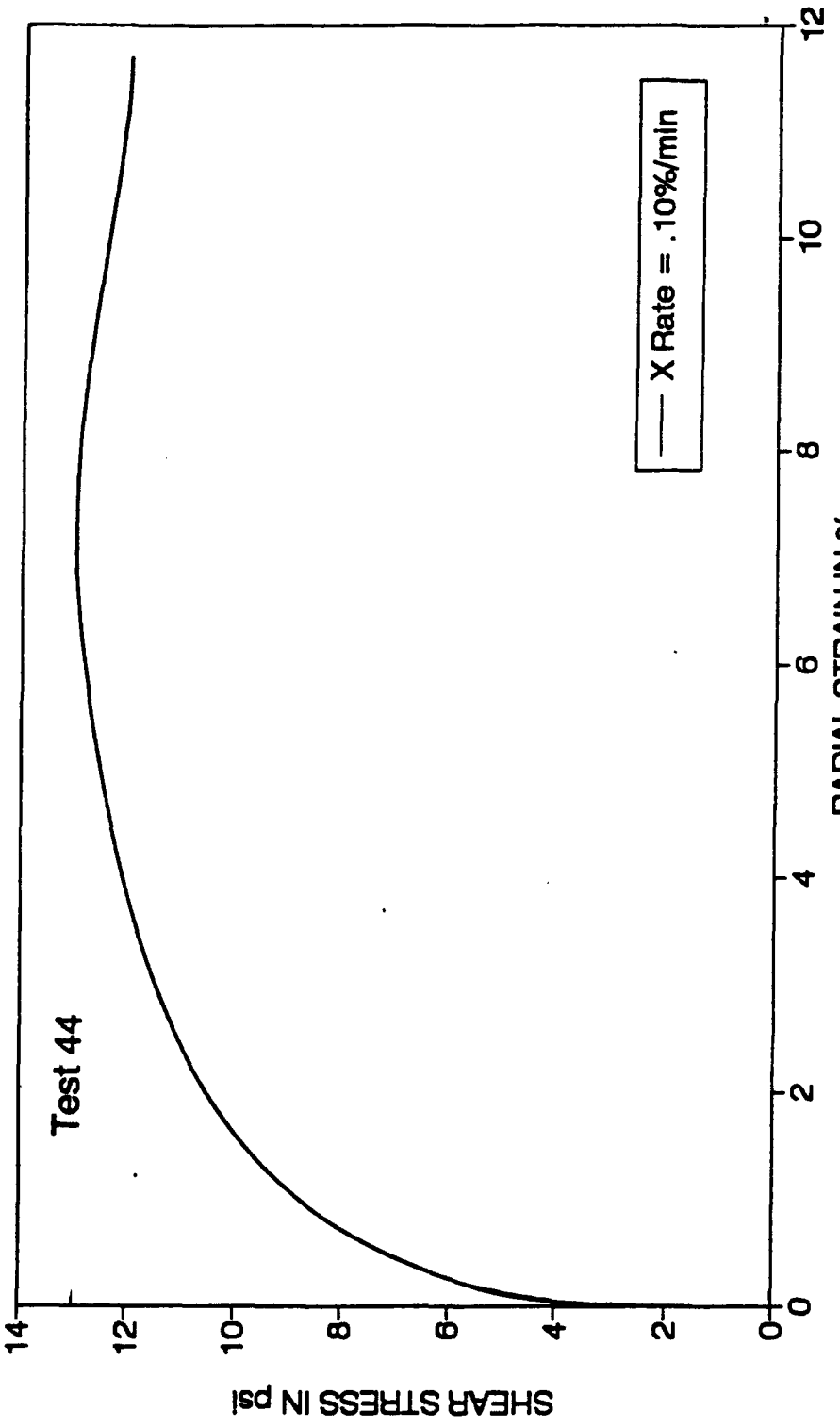

Fig. B.10 Shear Stress Vs Radial Strain for Kaolin Clay
(Test No. 44, Radial Strain Rate = 0.10%/min)

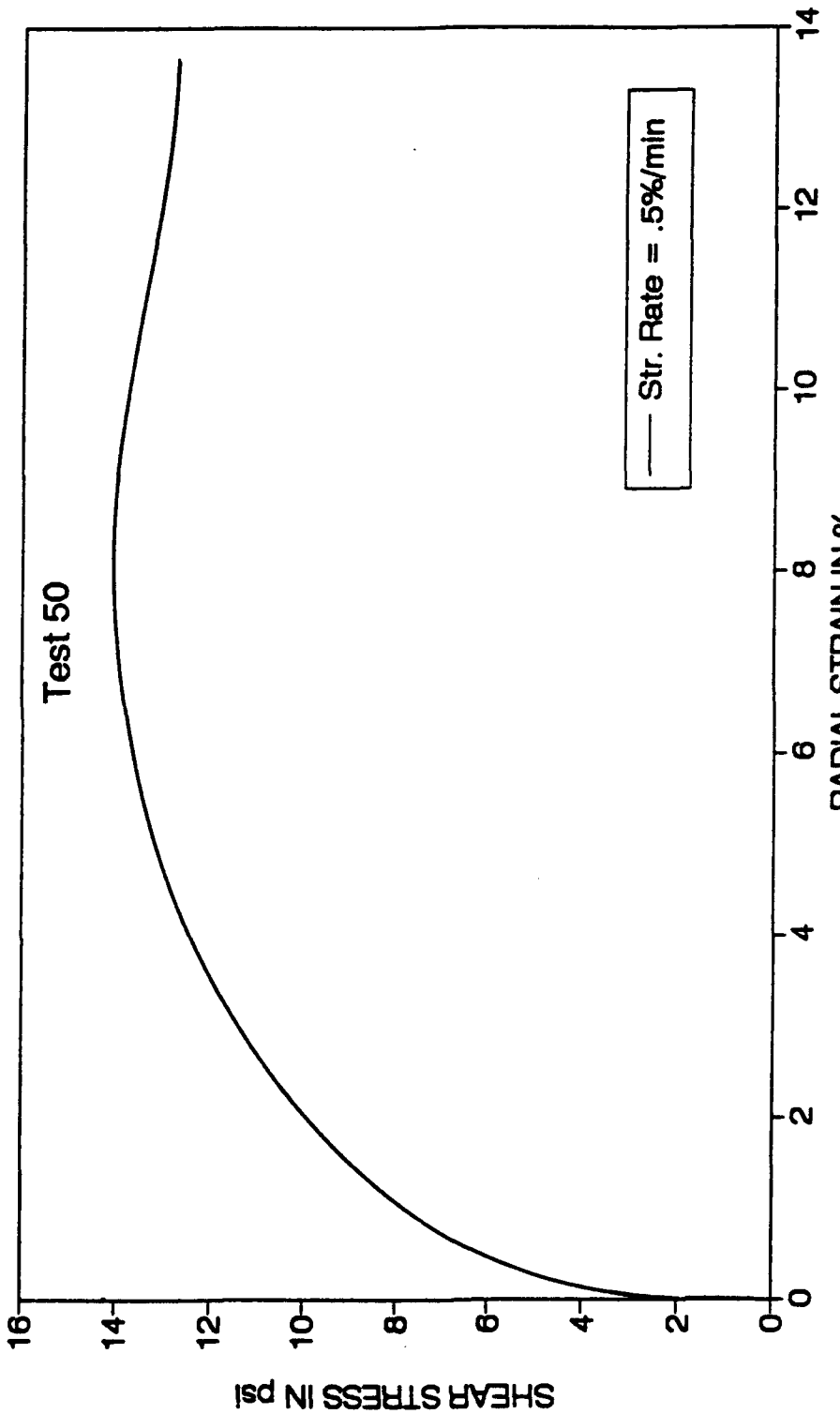

Fig. B.11 Shear Stress Vs Radial Strain for Kaolin Clay
(Test No. 50, Radial Strain Rate = 0.50%/min)

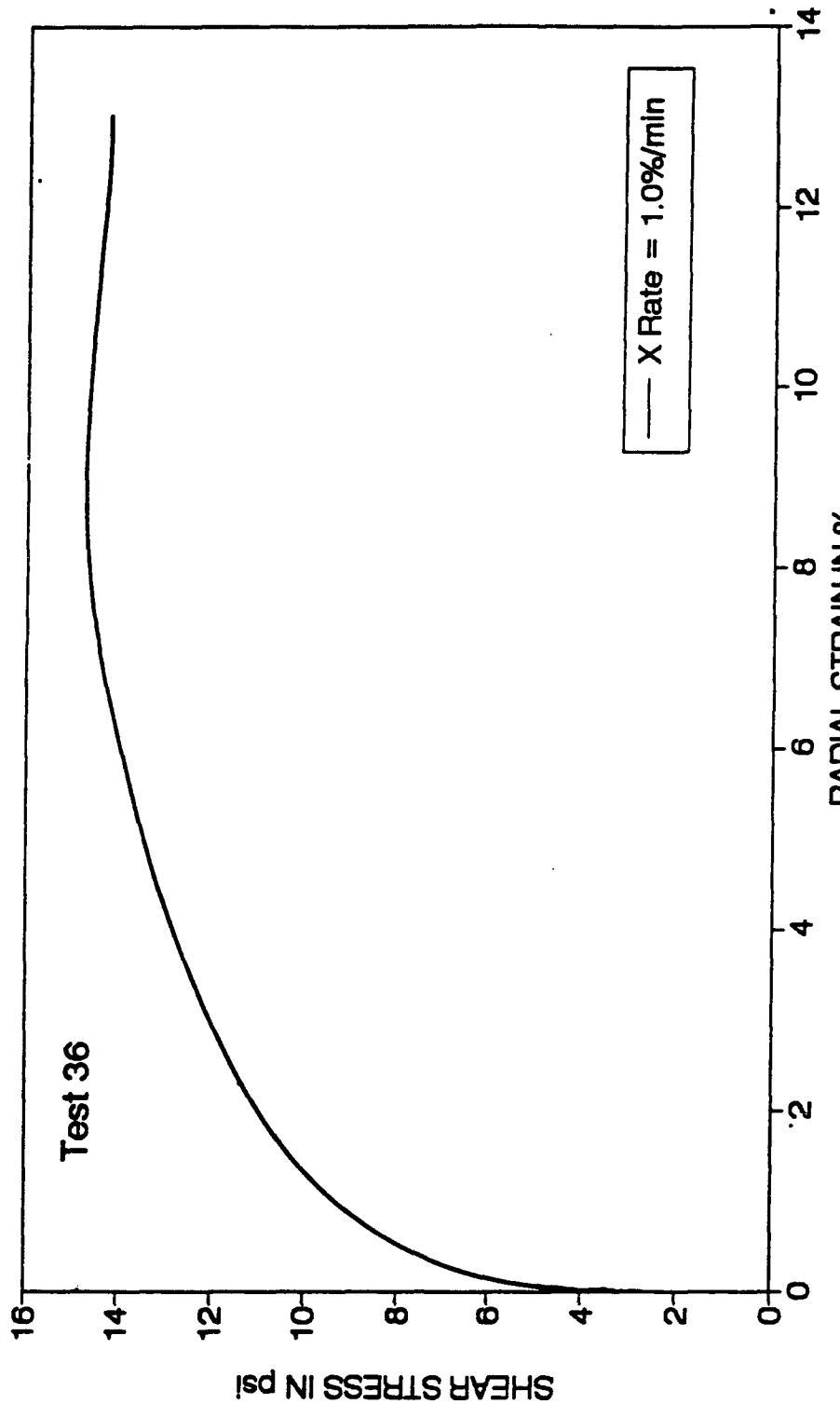

Fig. B.12 Shear Stress Vs Radial Strain for Kaolin Clay
(Test No. 36, Radial Strain Rate = 1.00%/min)

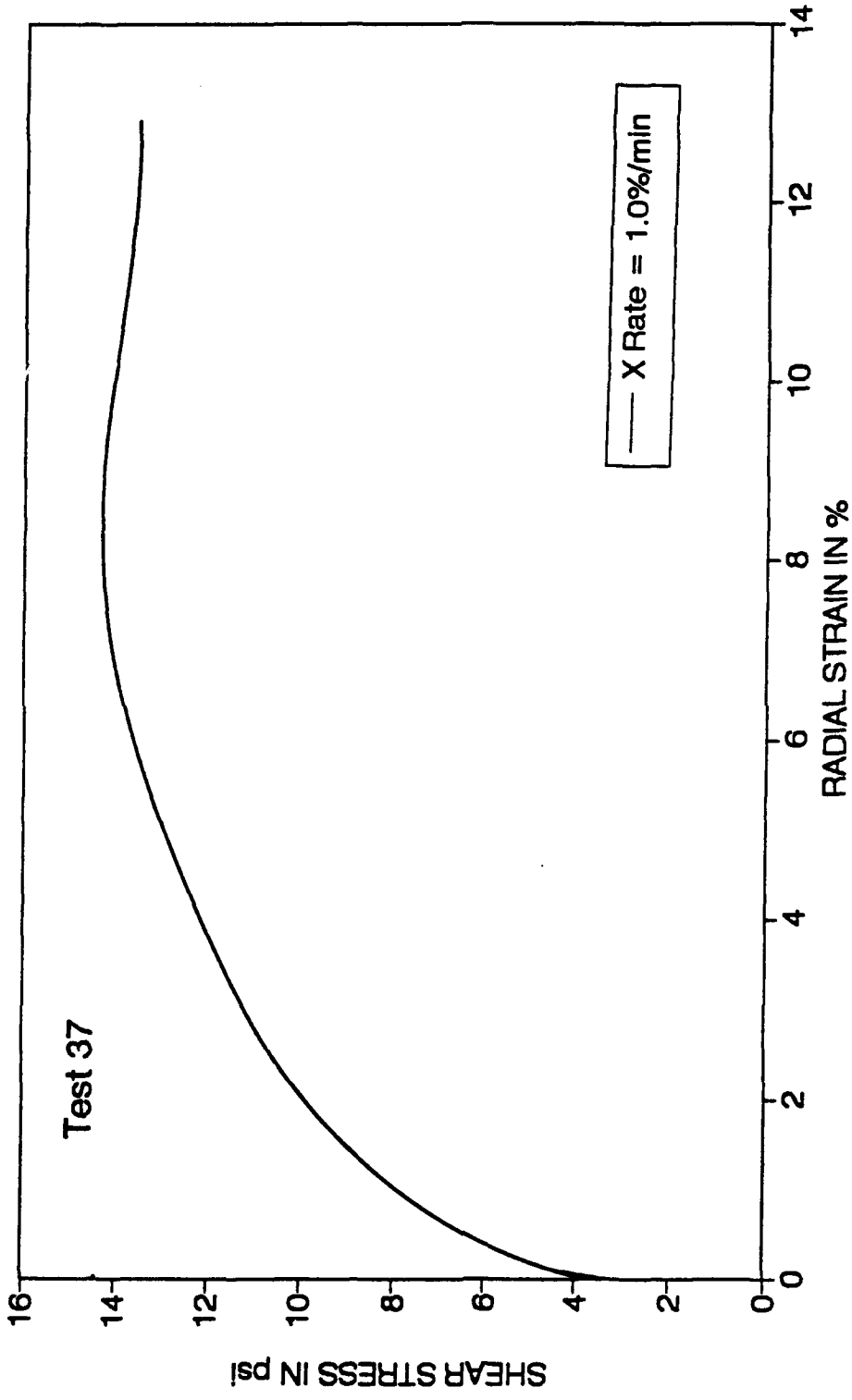

Fig. B.13 Shear Stress Vs Radial Strain for Kaolin Clay
(Test No. 37, Radial Strain Rate = 1.00%/min)

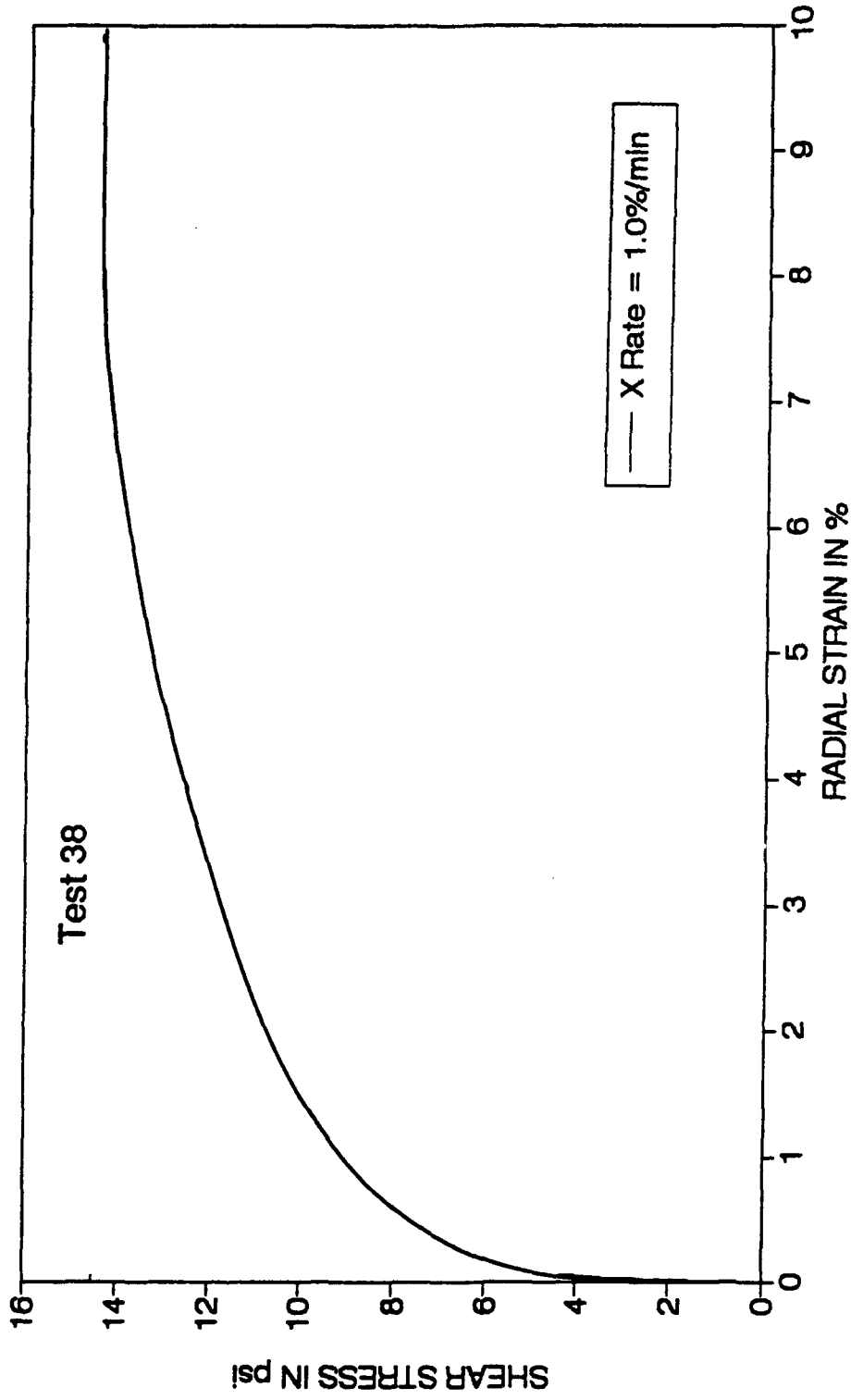

Fig. B.14 Shear Stress Vs Radial Strain for Kaolin Clay
(Test No. 38, Radial Strain Rate = 1.00%/min)

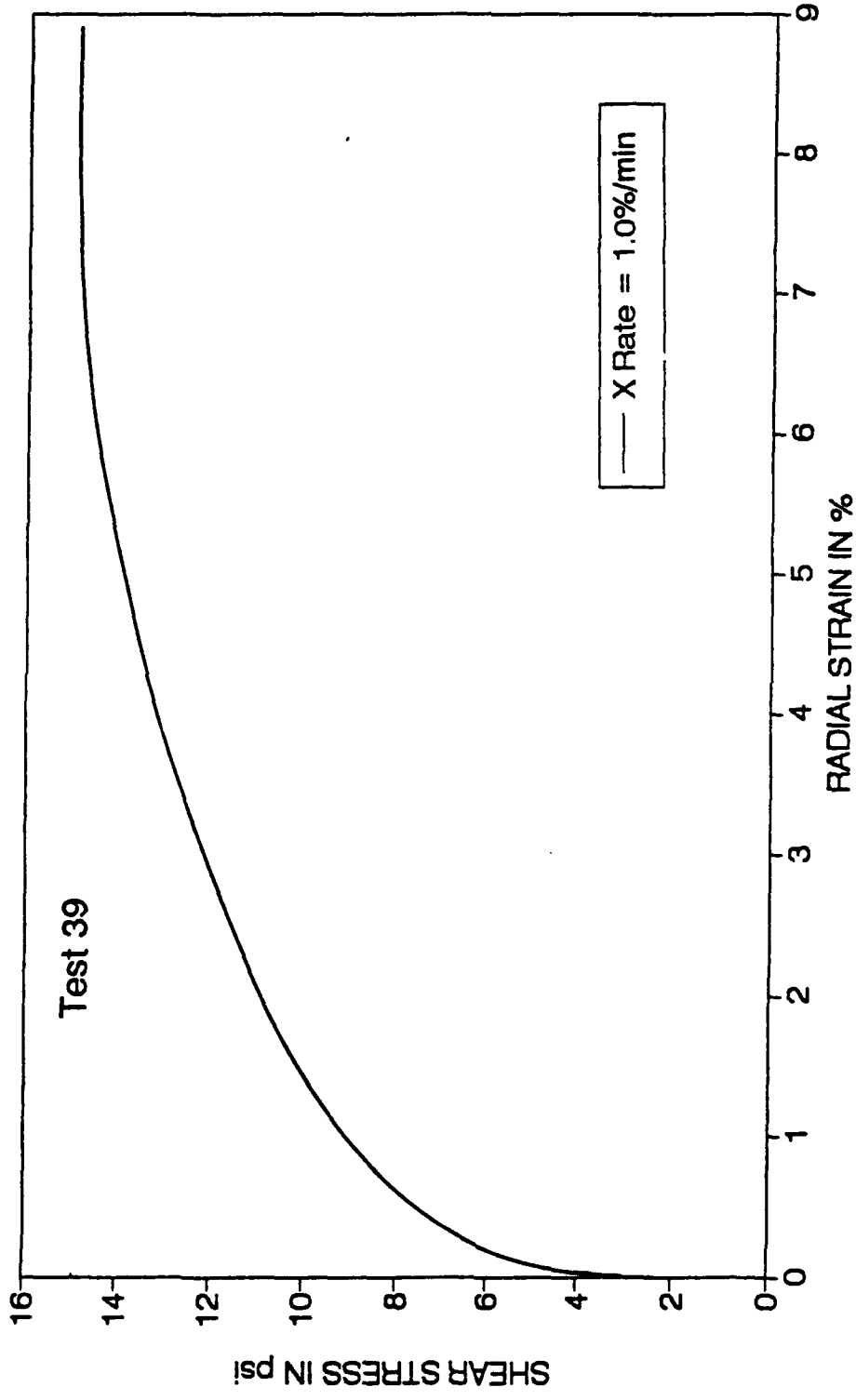

Fig. B.15 Shear Stress Vs Radial Strain for Kaolin Clay
(Test No. 39, Radial Strain Rate = 1.00%/min)

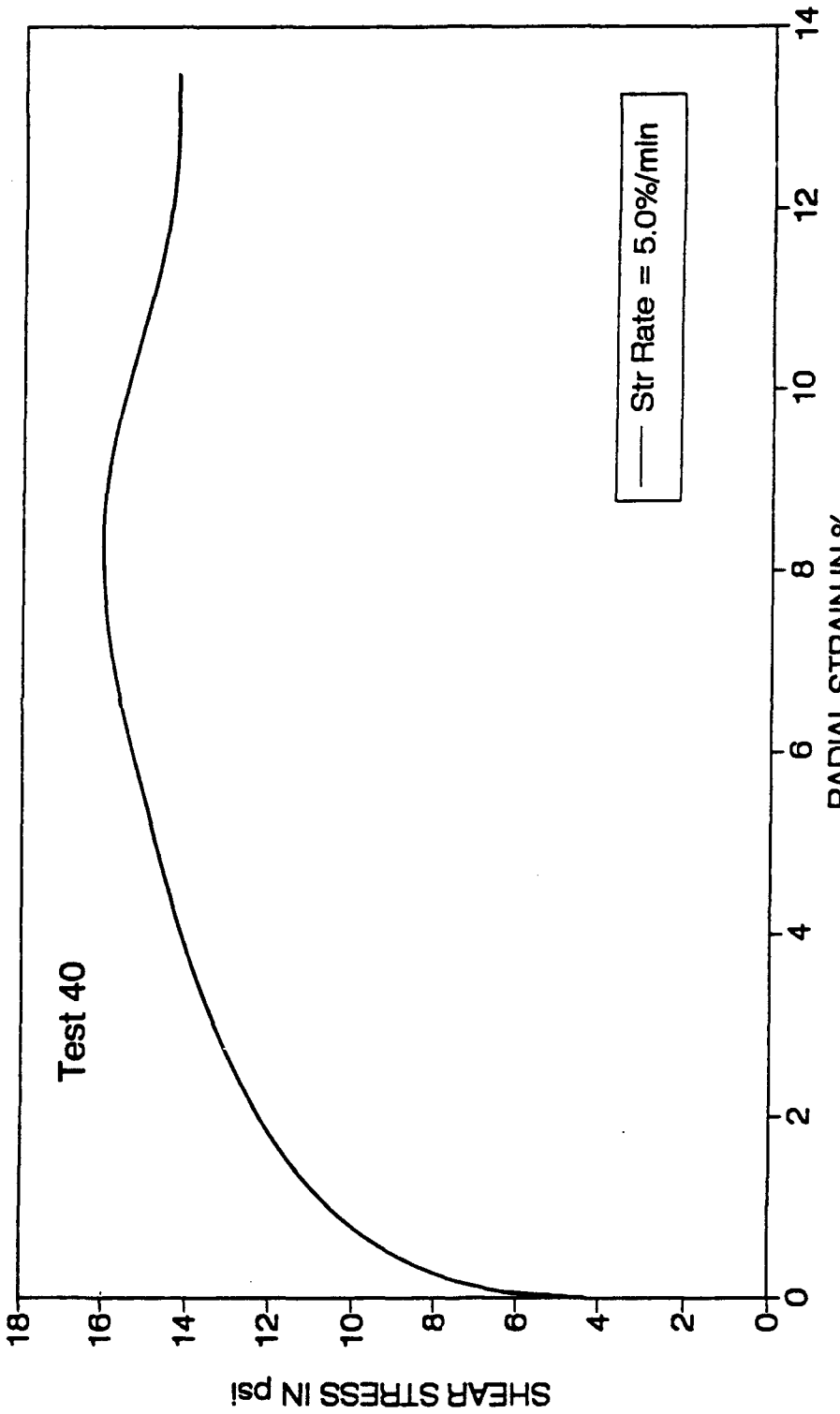

Fig. B.16 Shear Stress Vs Radial Strain for Kaolin Clay
(Test No. 40, Radial Strain Rate = 5.00%/min)

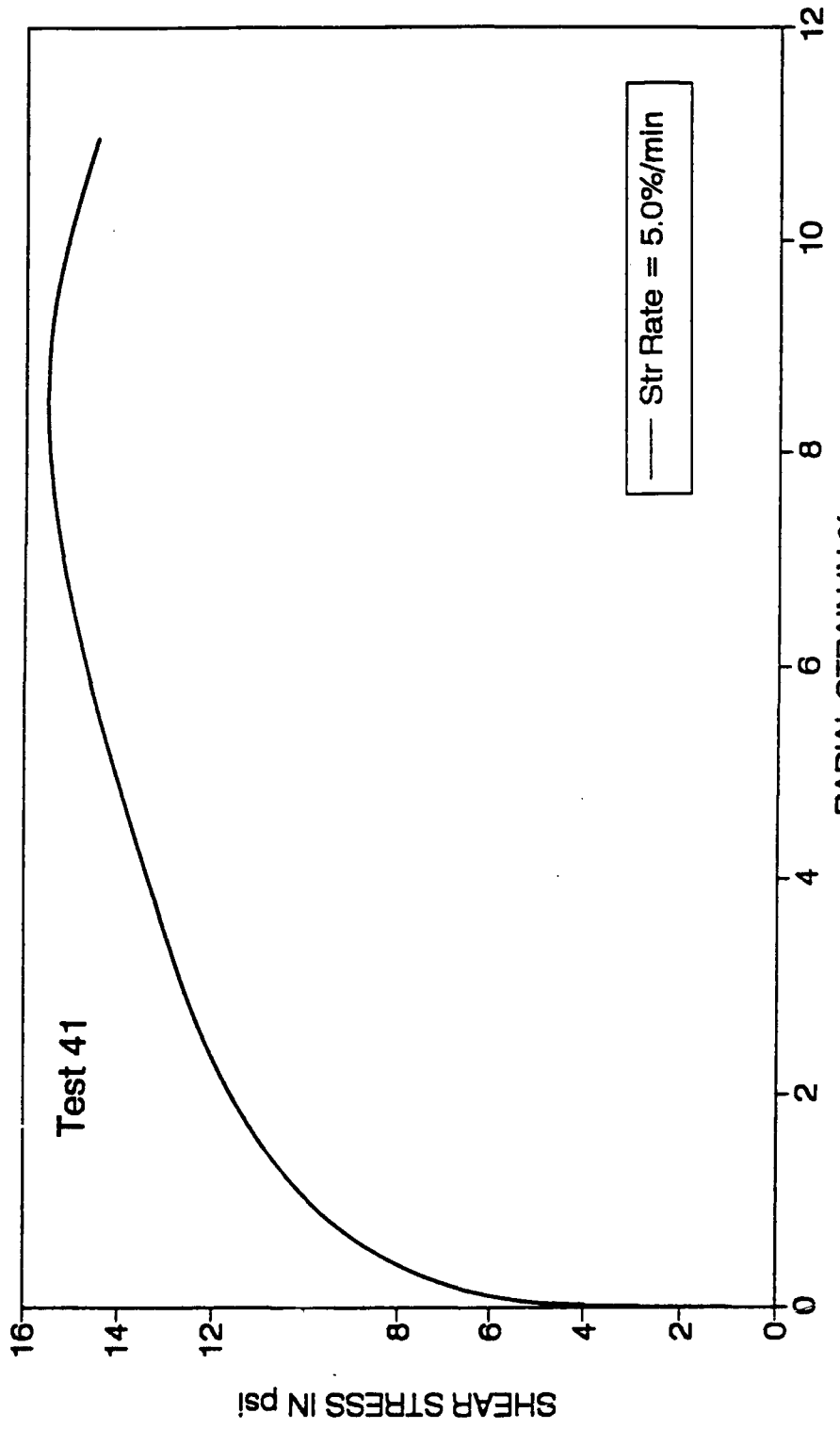

Fig. B.17 Shear Stress Vs Radial Strain for Kaolin Clay
(Test No. 41, Radial Strain Rate = 5.00%/min)

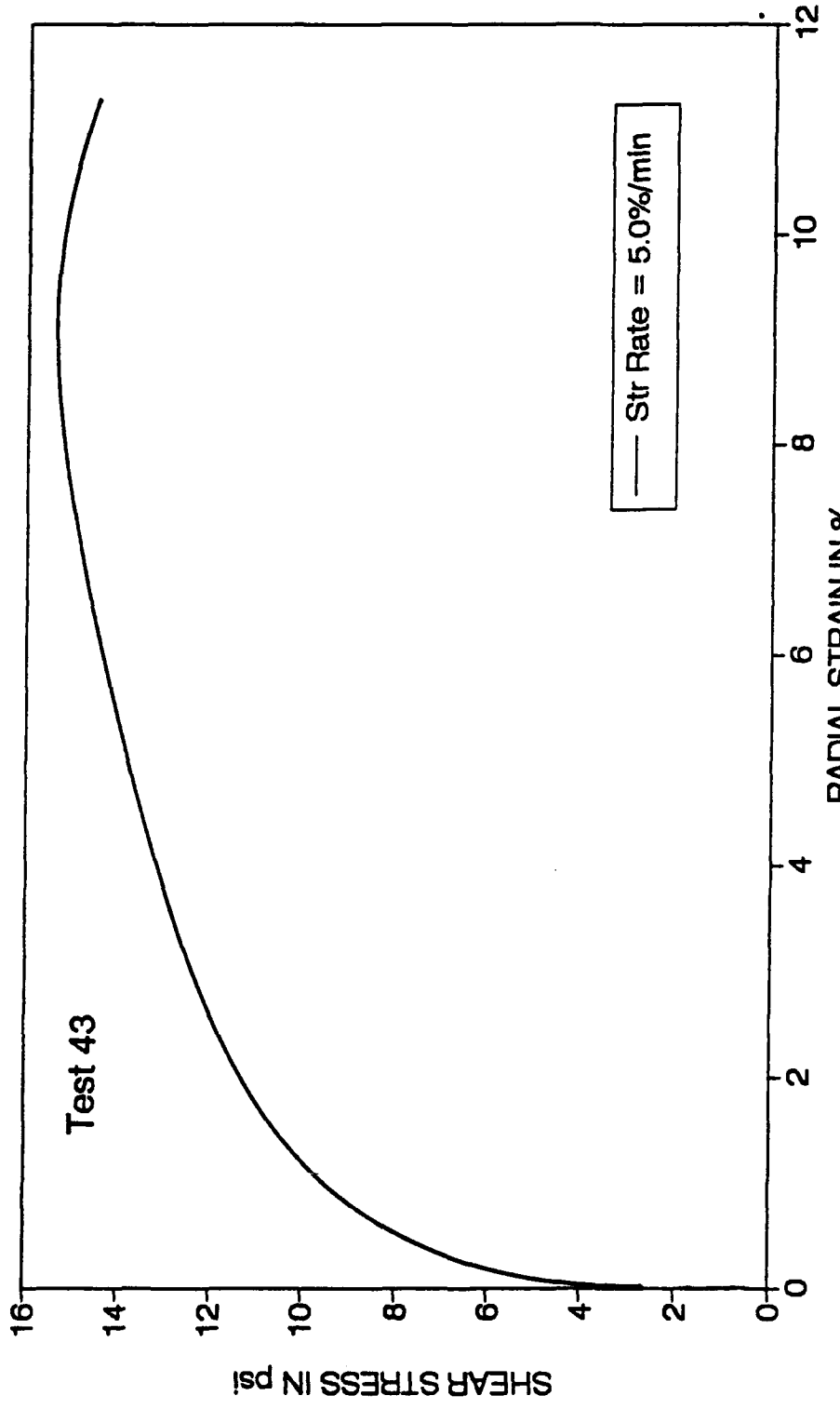

Fig. B.18 Shear Stress Vs Radial Strain for Kaolin Clay
(Test No. 43, Radial Strain Rate = 5.00%/min)

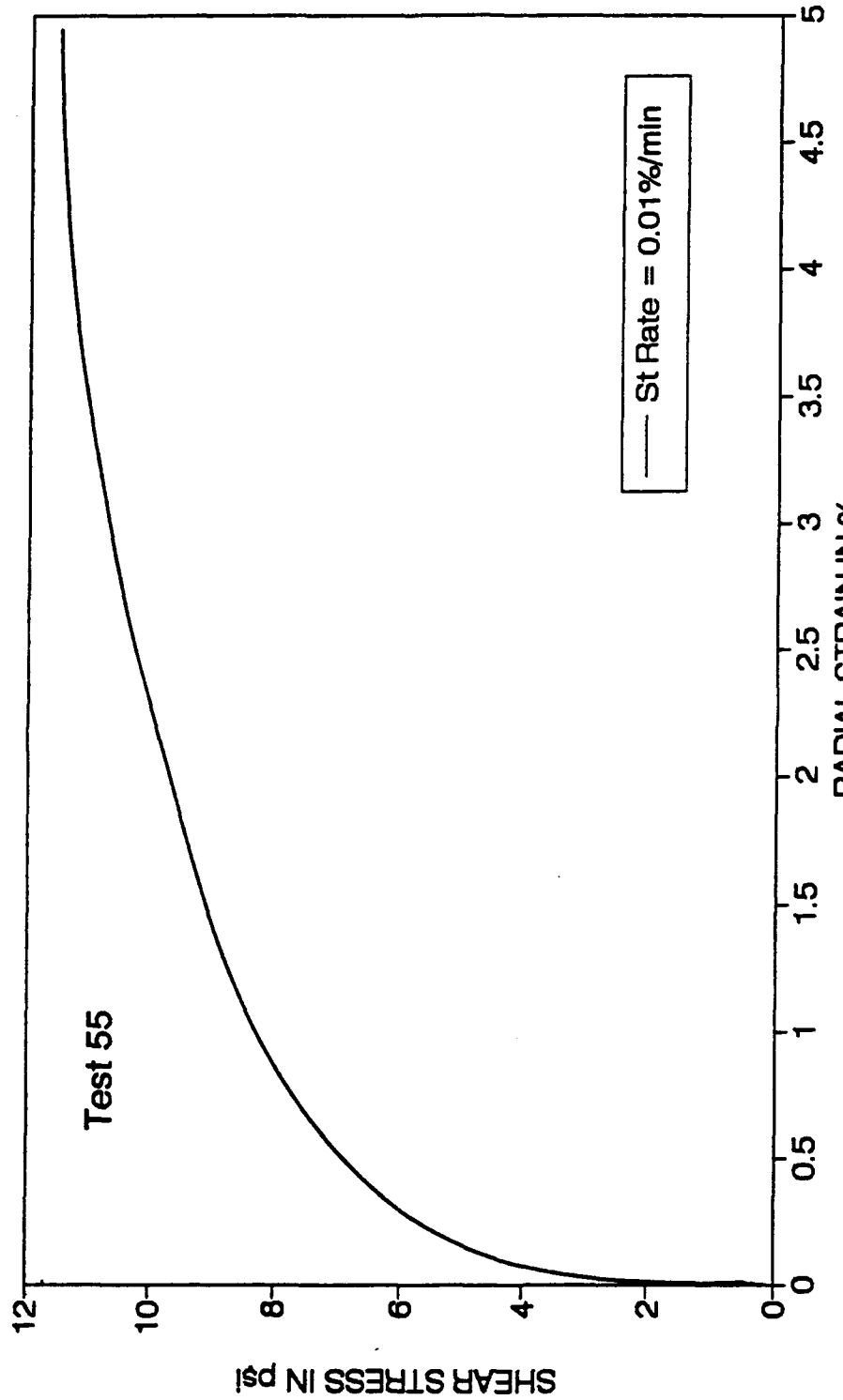

Fig. B.19 Shear Stress Vs Radial Strain for Kaolin - Silica Mix
(Test No. 55, Radial Strain Rate = 0.01%/min)

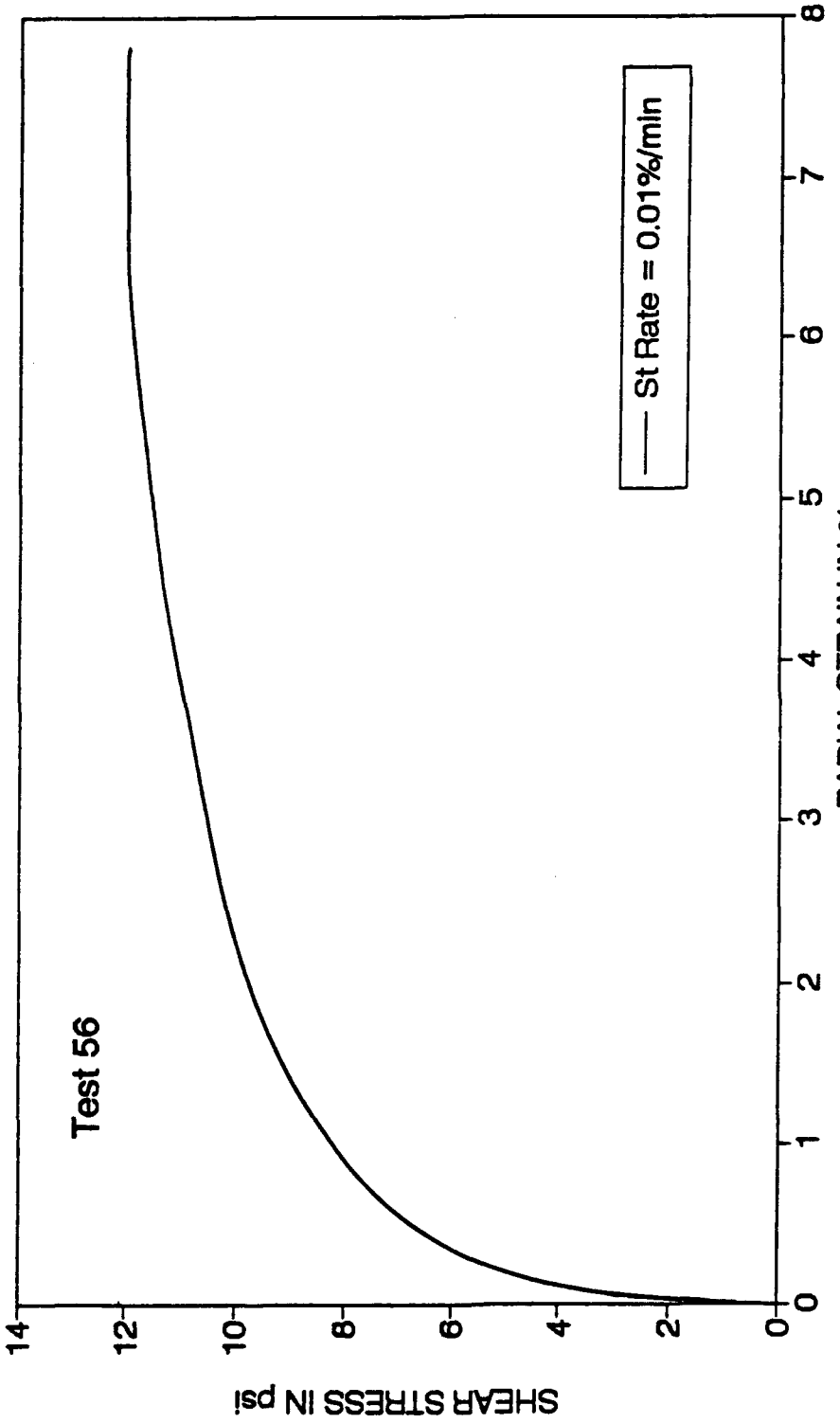

Fig. B.20 Shear Stress Vs Radial Strain for Kaolin - Silica Mix
(Test No. 56, Radial Strain Rate = 0.01%/min)

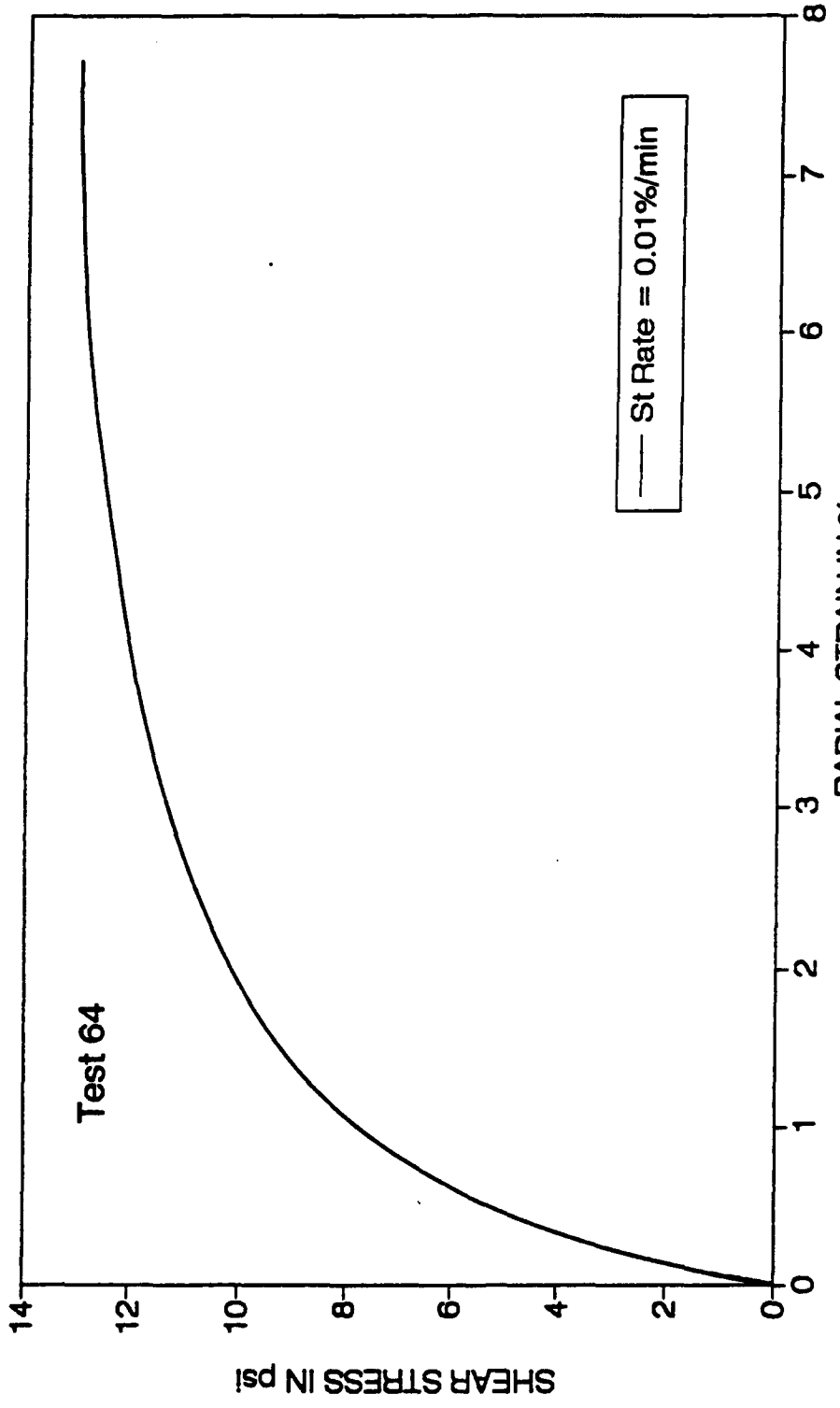

Fig. B.21 Shear Stress Vs Radial Strain for Kaolin - Silica Mix
(Test No. 64, Radial Strain Rate = 0.01%/min)

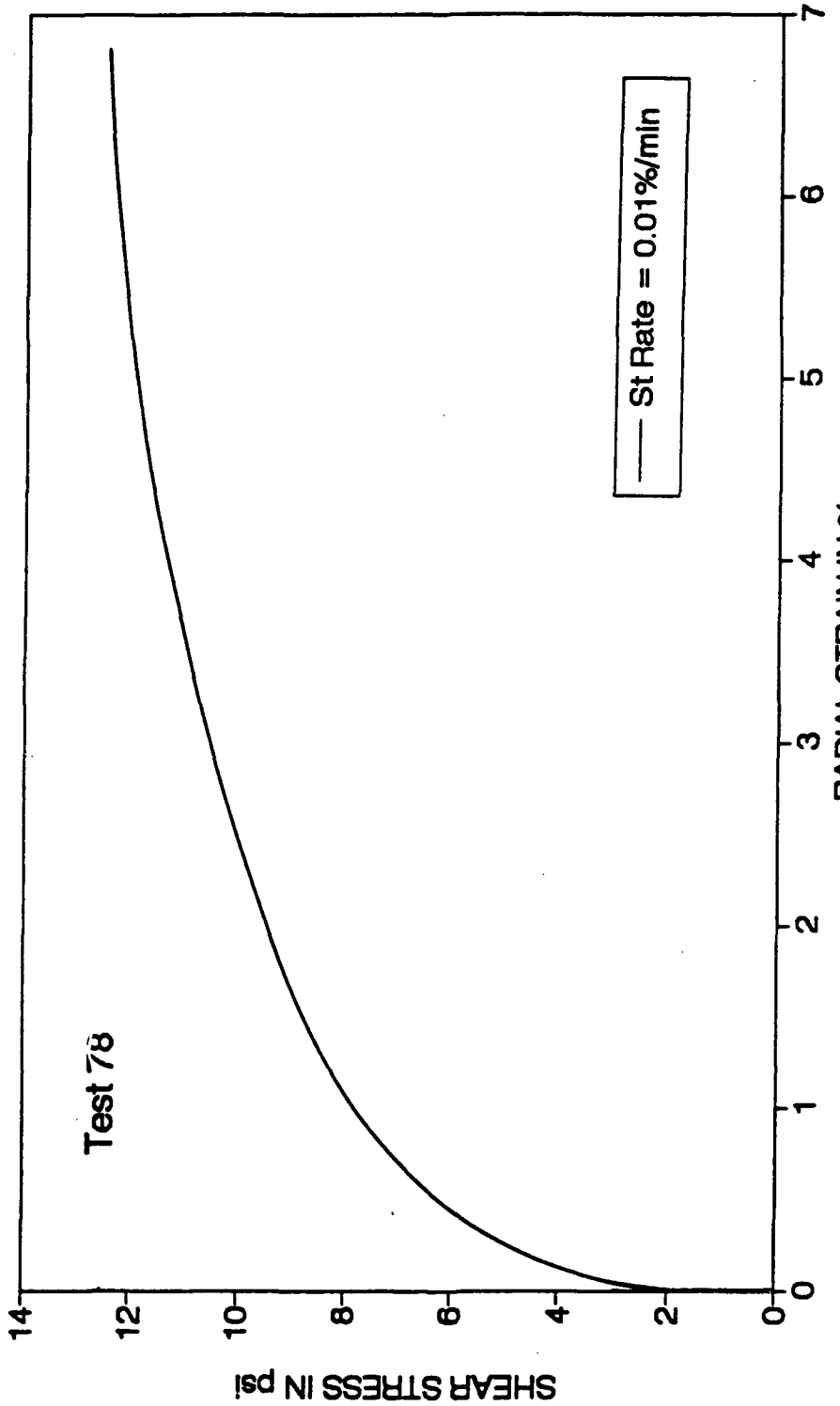

Fig. B.22 Shear Stress Vs Radial Strain for Kaolin - Silica Mix
(Test No. 78, Radial Strain Rate = 0.01%/min)

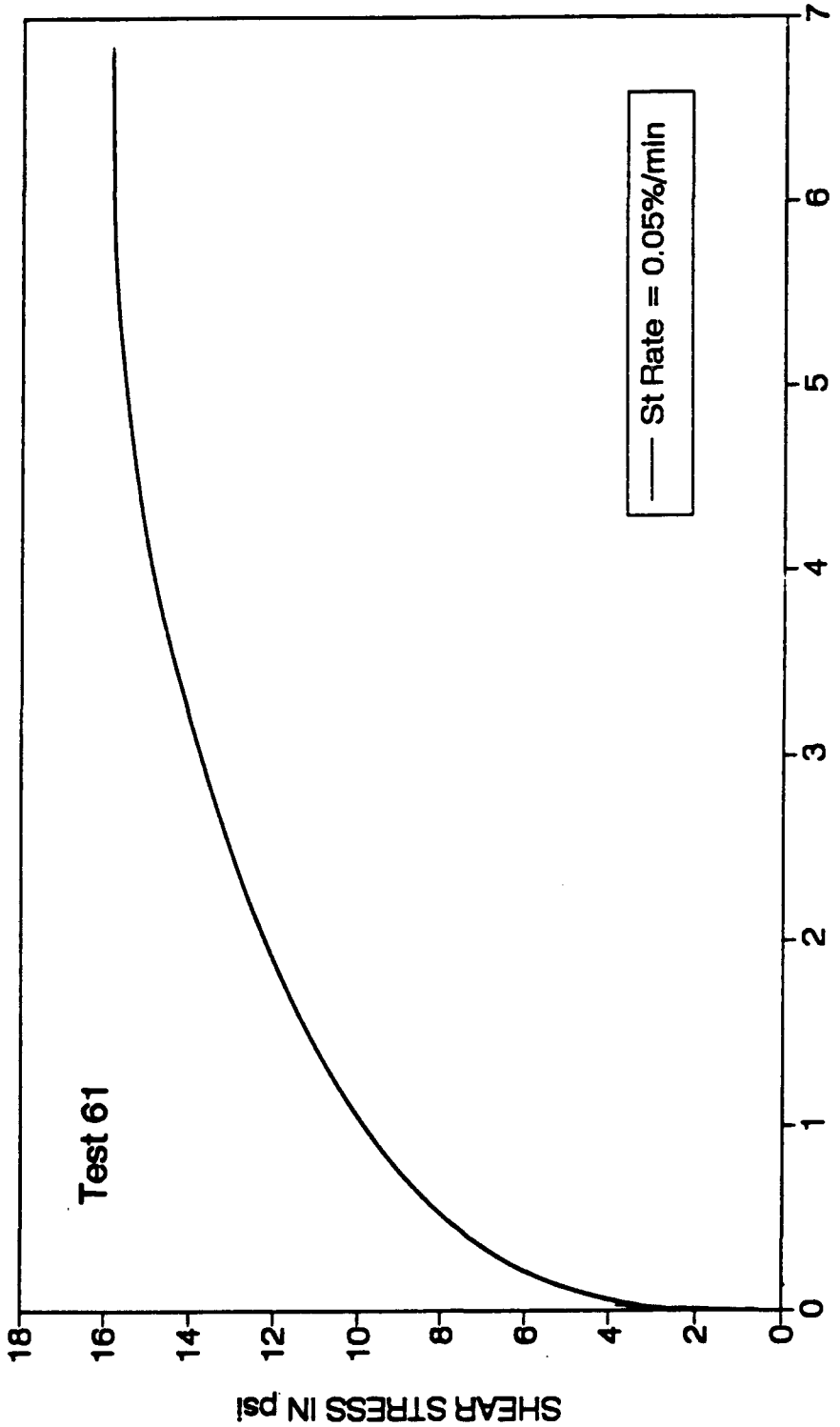

Fig. B.23 Shear Stress Vs Radial Strain for Kaolin - Silica Mix
(Test No. 61, Radial Strain Rate = 0.05%/min)

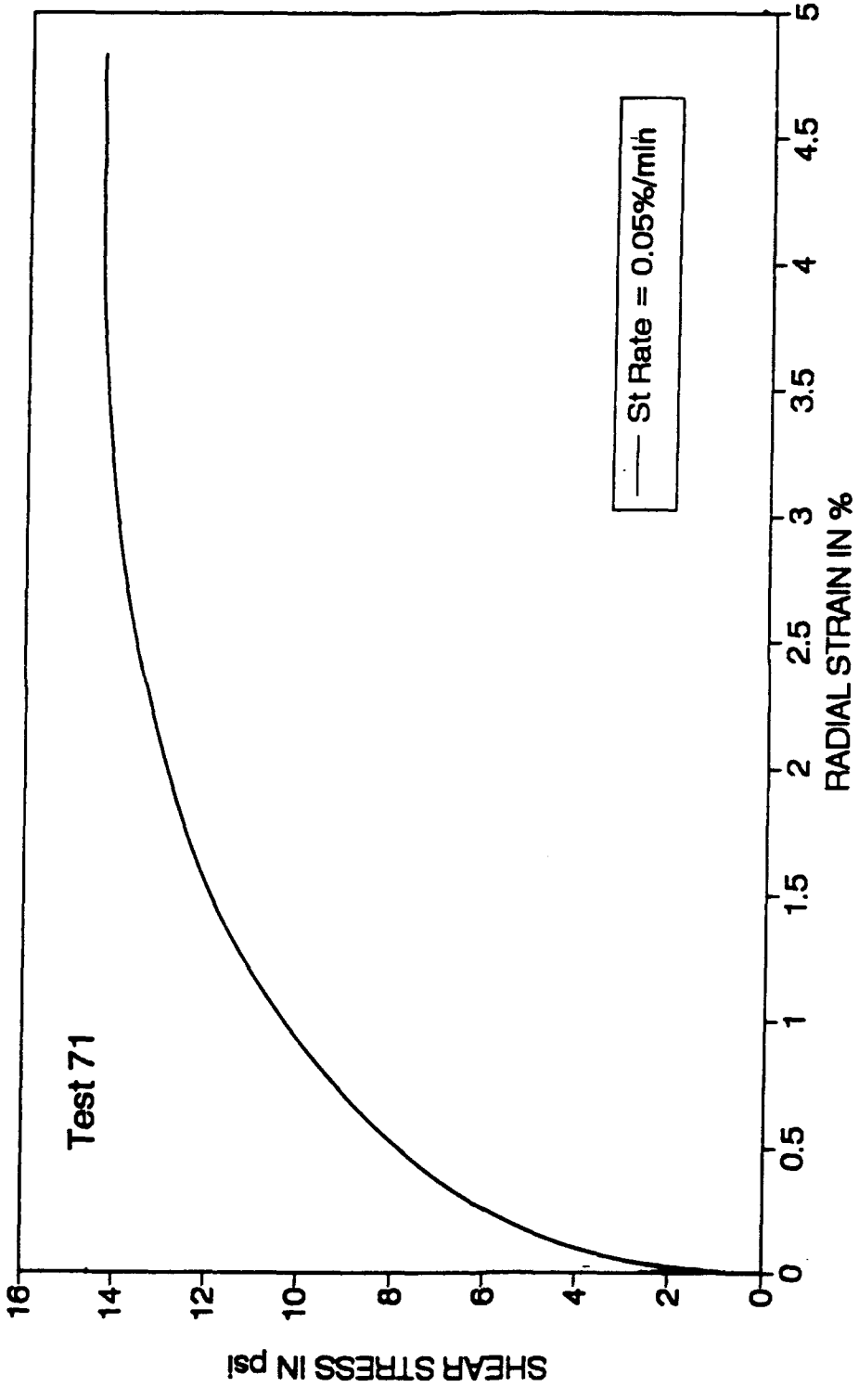

Fig. B.24 Shear Stress Vs Radial Strain for Kaolin - Silica Mix
(Test No. 71, Radial Strain Rate = 0.05%/min)

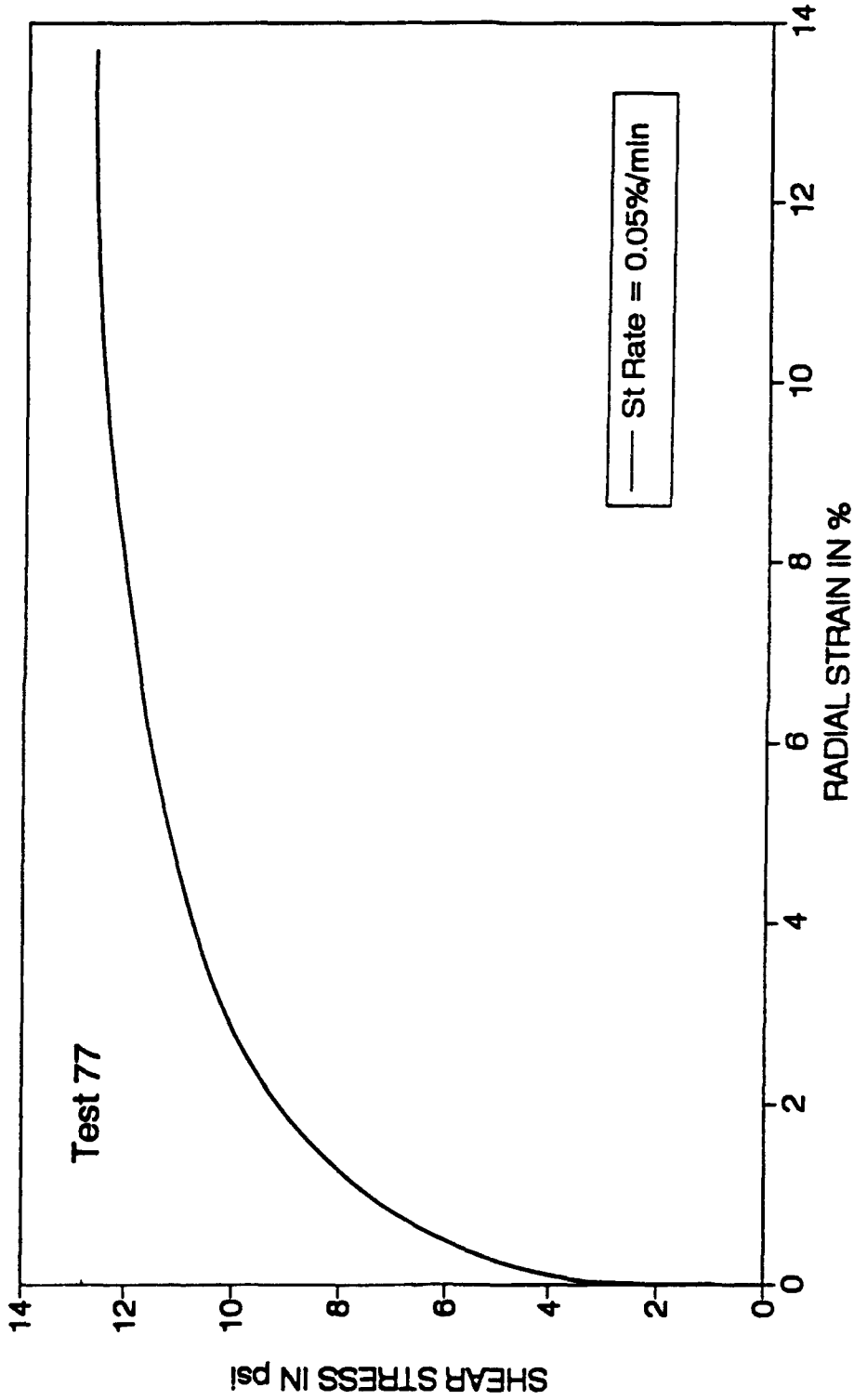

Fig. B.25 Shear Stress Vs Radial Strain for Kaolin - Silica Mix
(Test No. 77, Radial Strain Rate = 0.05%/min)

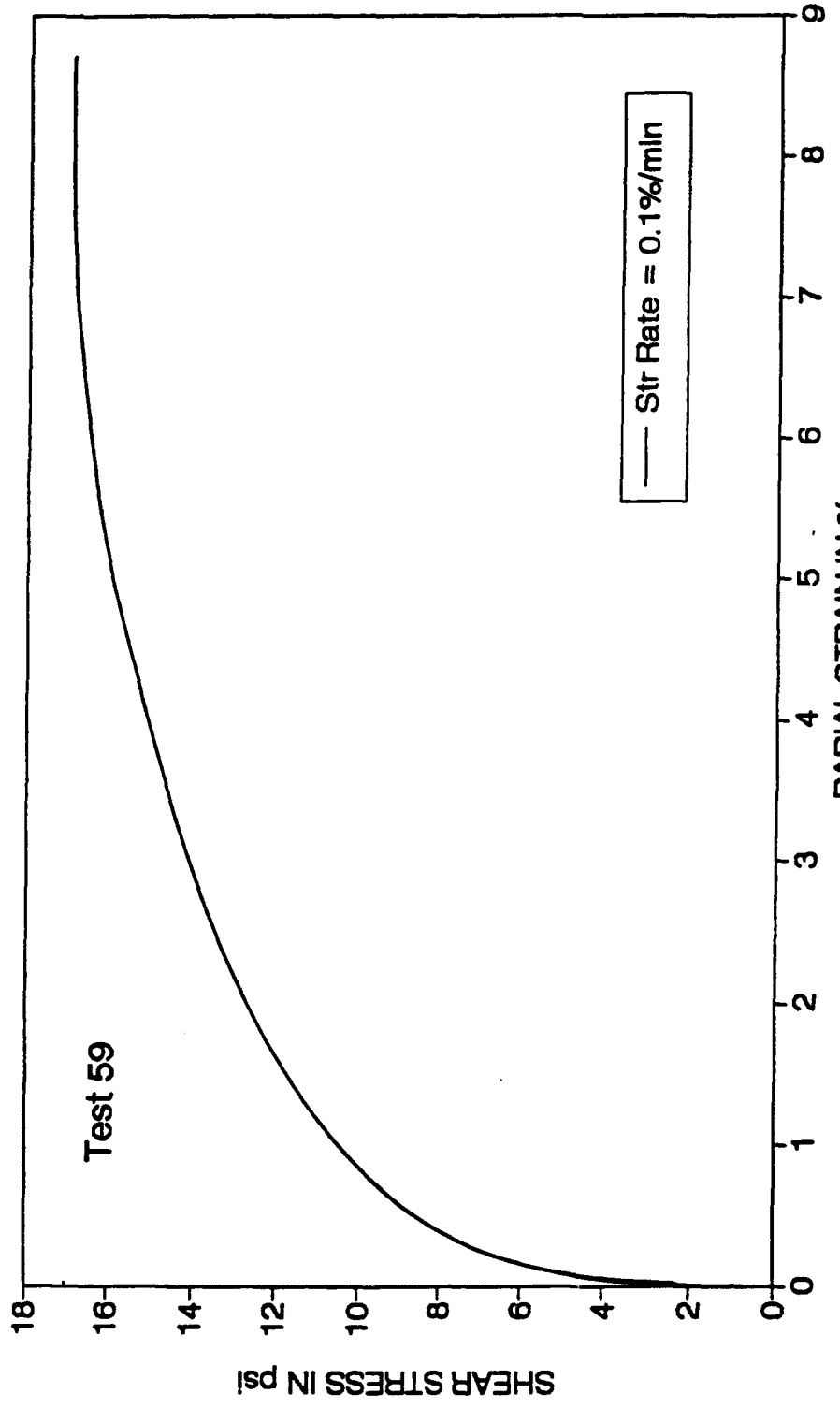

Fig. B.26 Shear Stress Vs Radial Strain for Kaolin - Silica Mix
(Test No. 59, Radial Strain Rate = 0.10%/min)

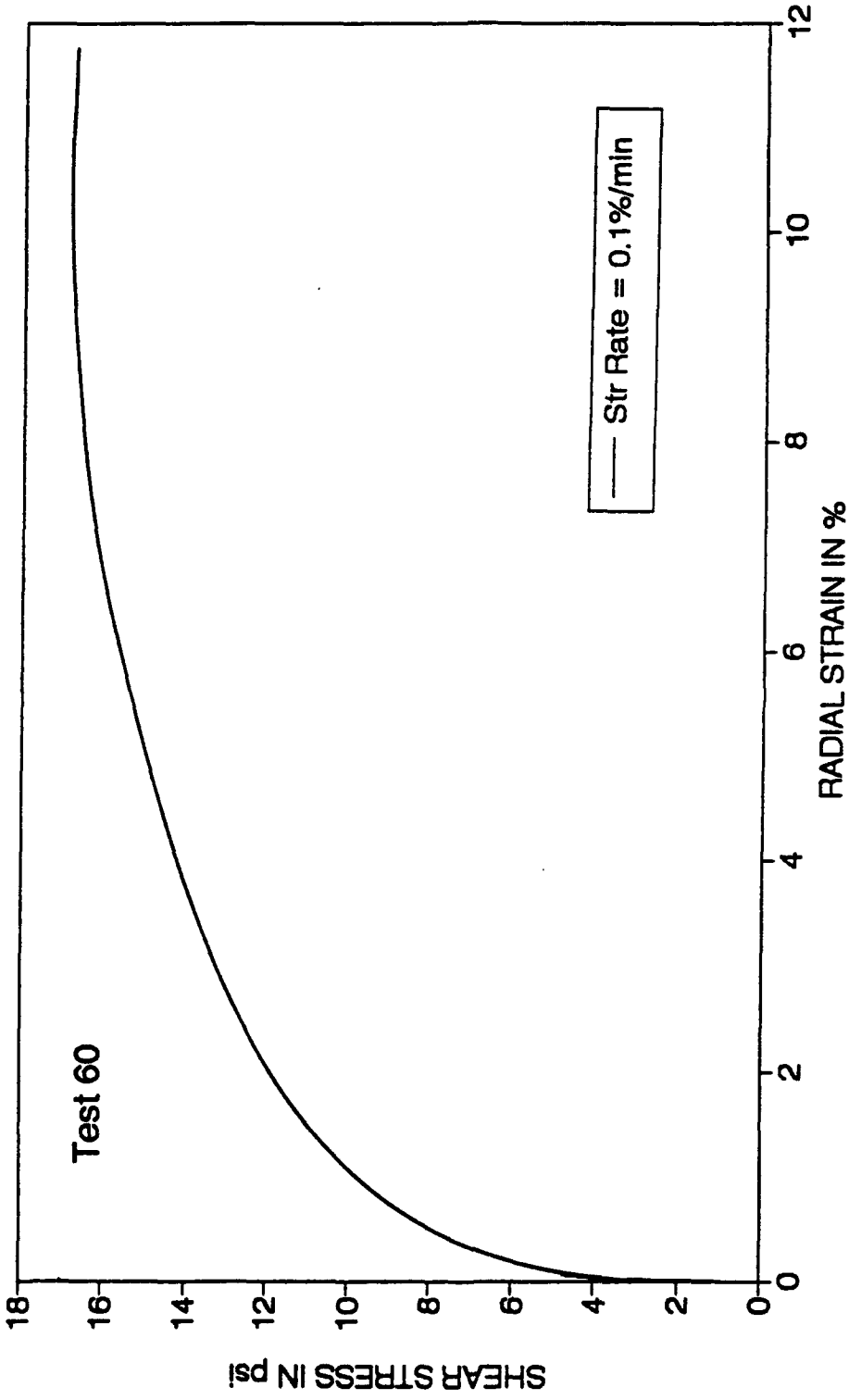

Fig. B.27 Shear Stress Vs Radial Strain for Kaolin - Silica Mix
(Test No. 60, Radial Strain Rate = 0.10%/min)

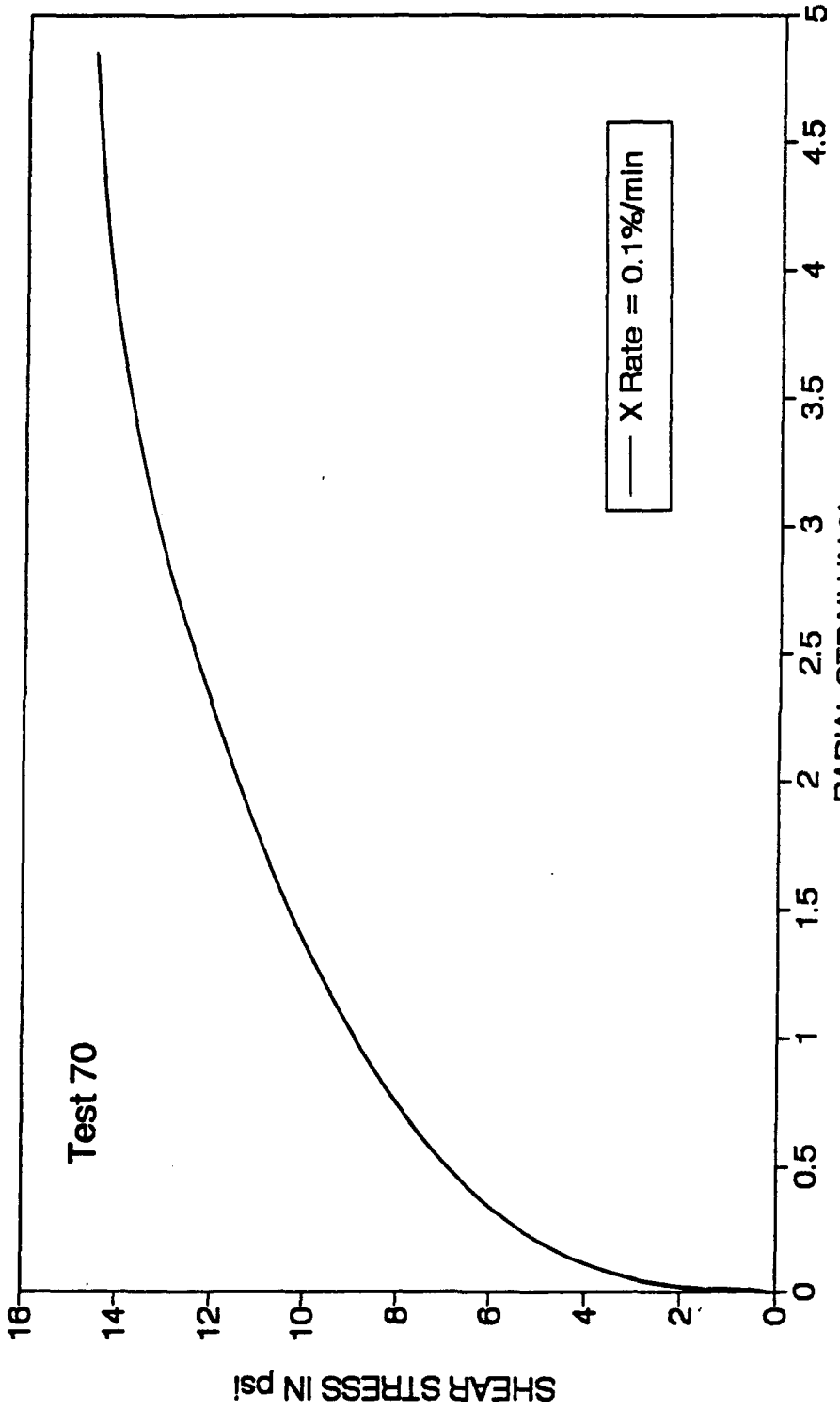

Fig. B.28 Shear Stress Vs Radial Strain for Kaolin - Silica Mix
(Test No. 70, Radial Strain Rate = 0.10%/min)

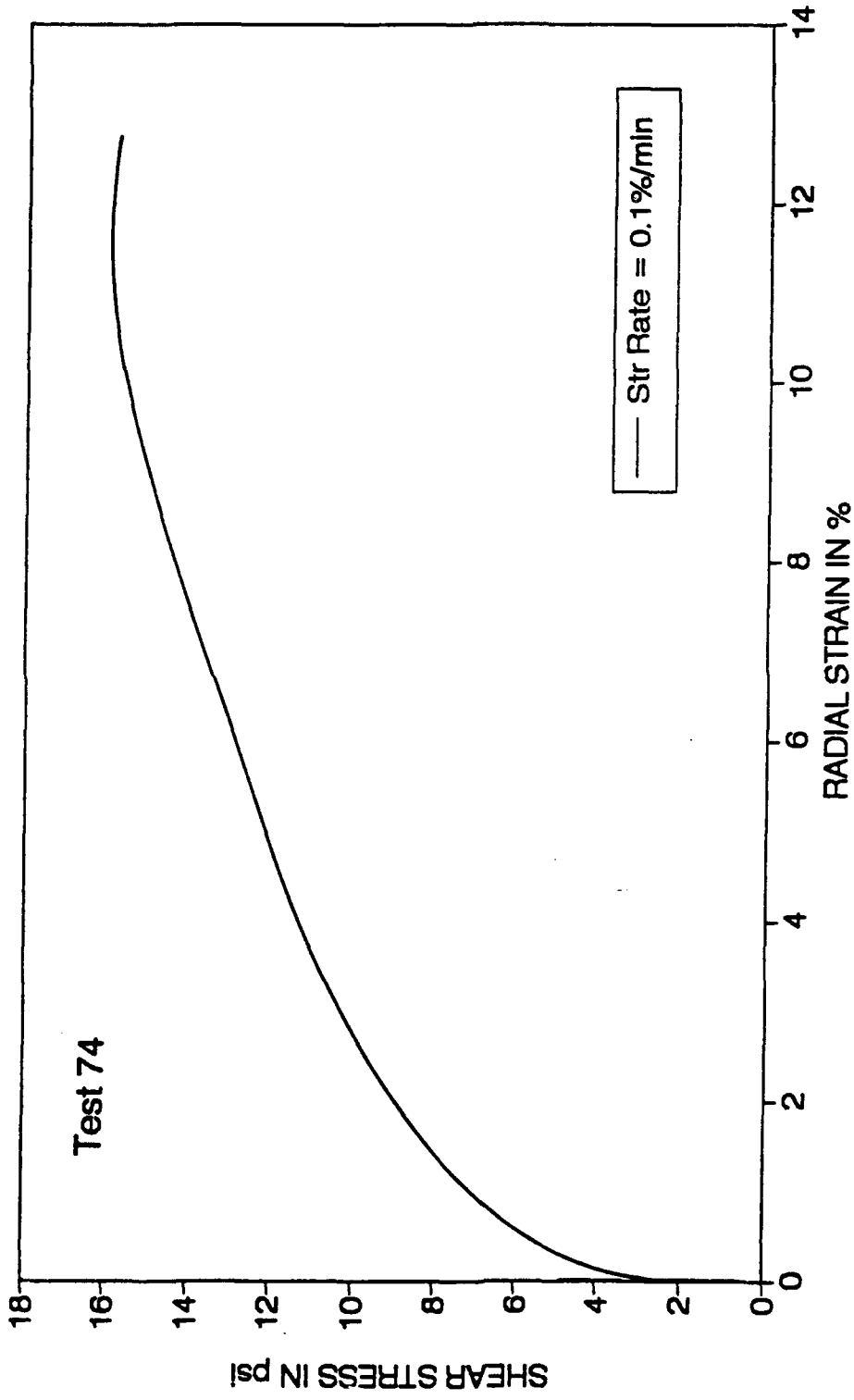

Fig. B.29 Shear Stress Vs Radial Strain for Kaolin - Silica Mix (Test No. 74, Radial Strain Rate = 0.10%/min)

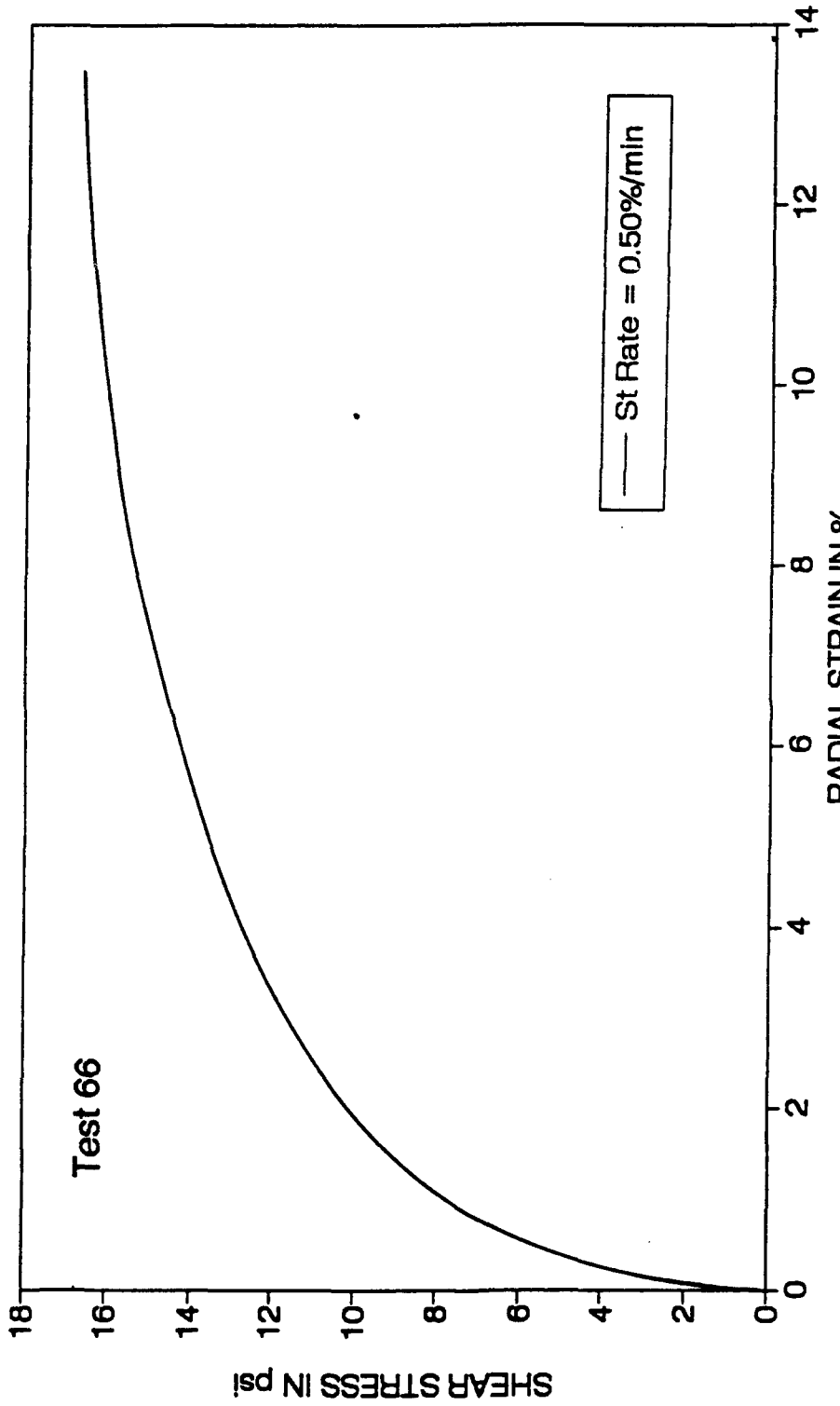

Fig. B.30 Shear Stress Vs Radial Strain for Kaolin - Silica Mix
(Test No. 66, Radial Strain Rate = 0.50%/min)

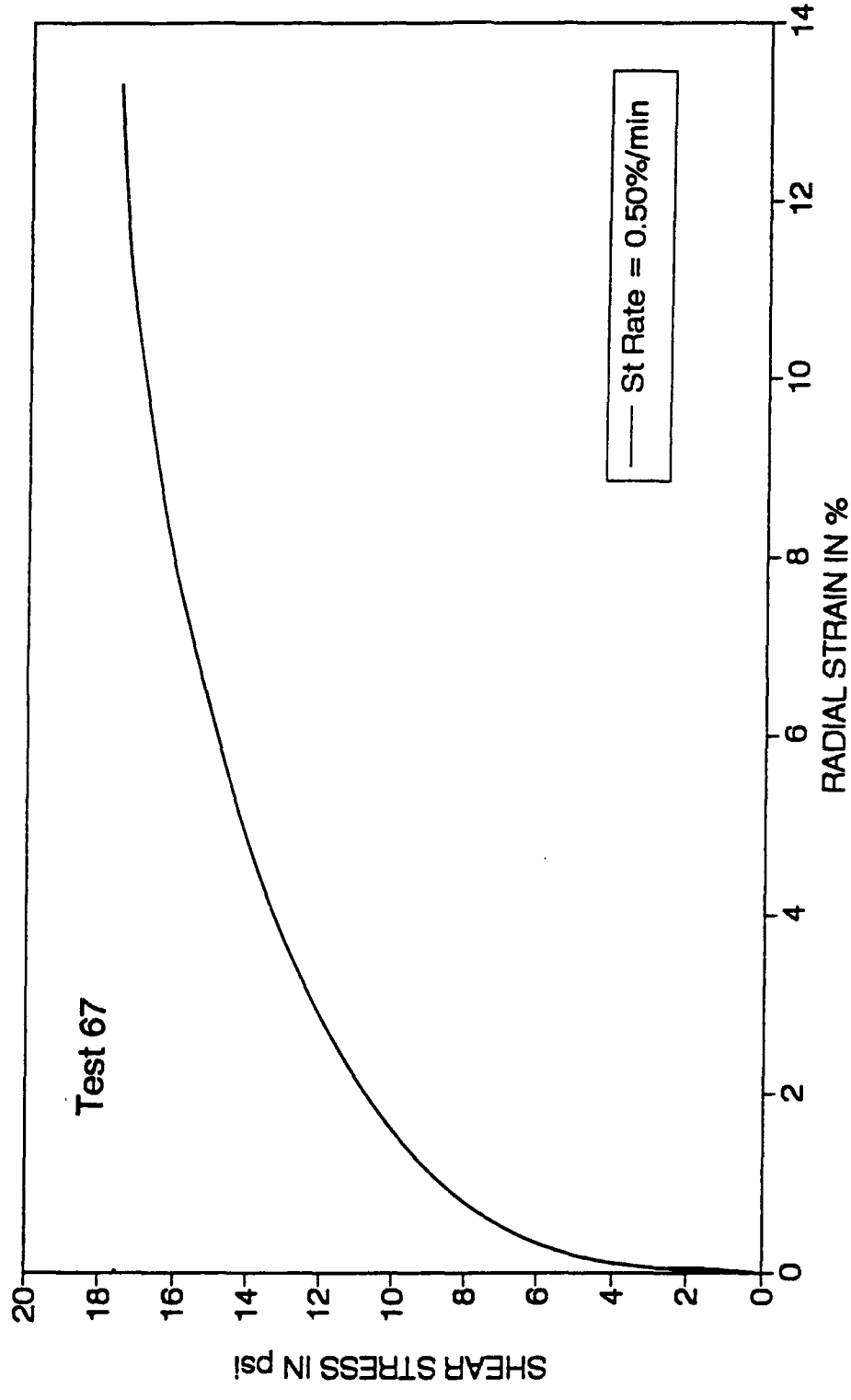

Fig. B.31 Shear Stress Vs Radial Strain for Kaolin - Silica Mix (Test No. 67, Radial Strain Rate = 0.50%/min)

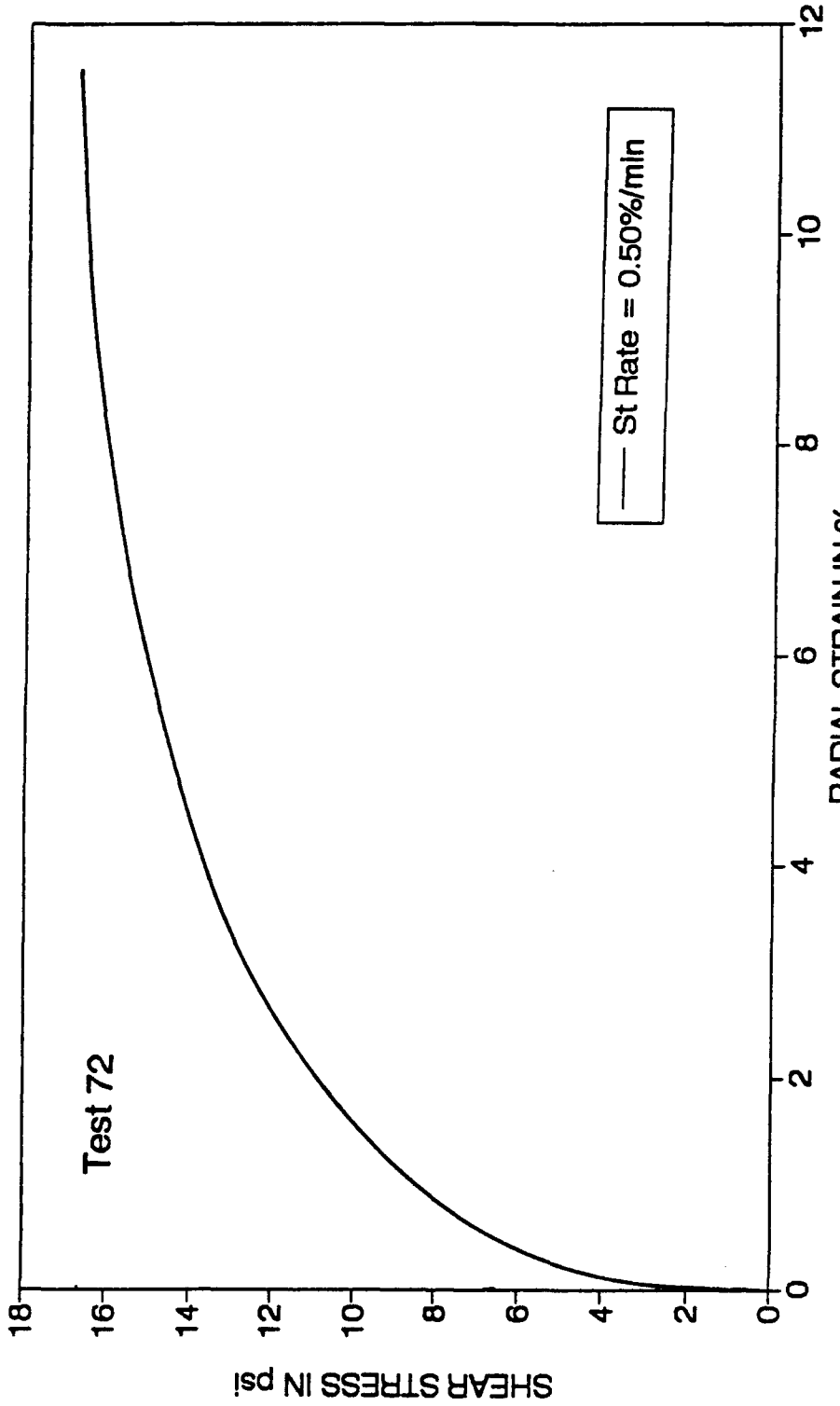

Fig. B.32 Shear Stress Vs Radial Strain for Kaolin - Silica Mix
(Test No. 72, Radial Strain Rate = 0.50%/min)

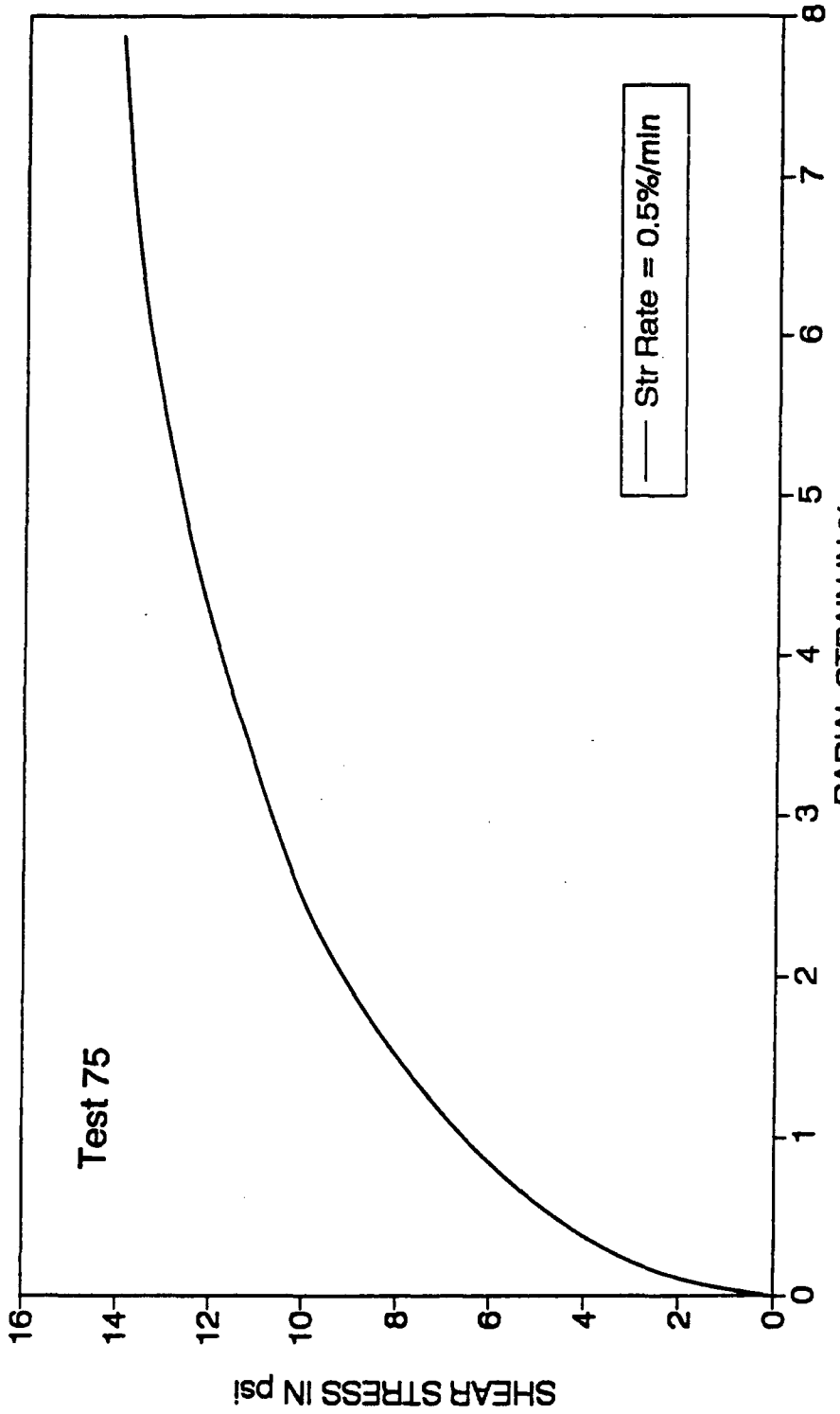

Fig. B.33 Shear Stress Vs Radial Strain for Kaolin - Silica Mix
(Test No. 75, Radial Strain Rate = 0.50%/min)

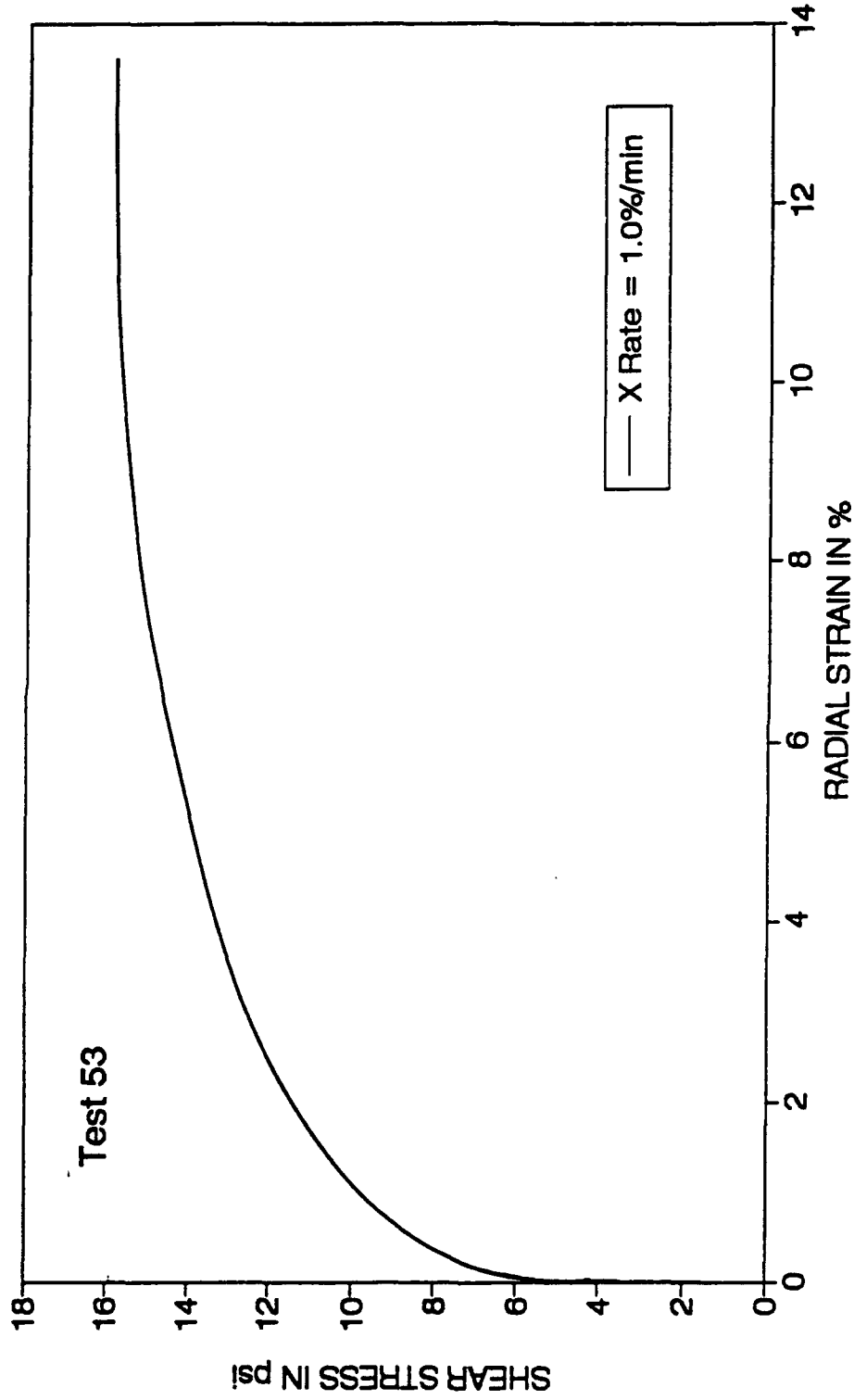

Fig. B.34 Shear Stress Vs Radial Strain for Kaolin - Silica Mix
(Test No. 53, Radial Strain Rate = 1.00%/min)

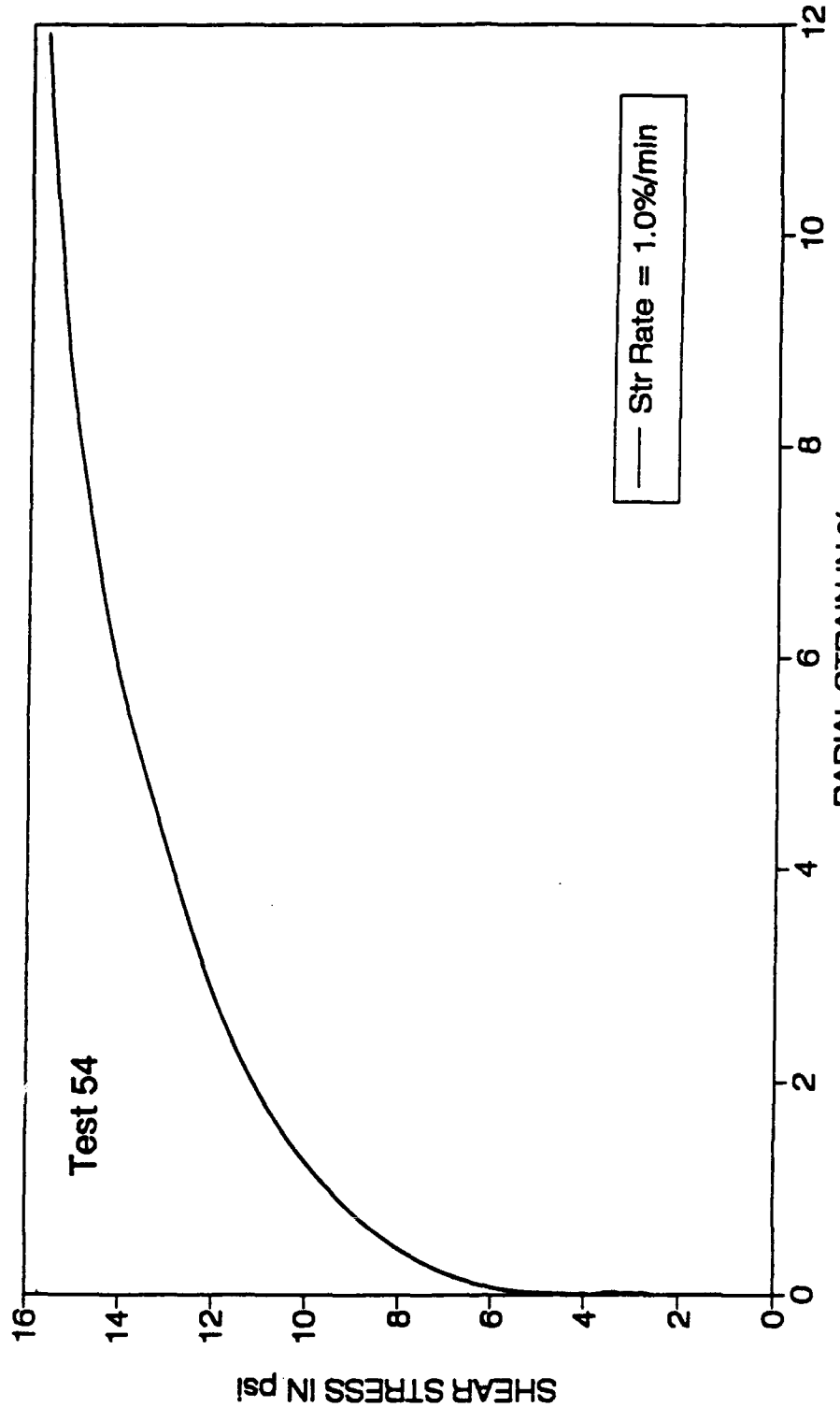

Fig. B.35 Shear Stress Vs Radial Strain for Kaolin - Silica Mix
(Test No. 54, Radial Strain Rate = 1.00%/min)

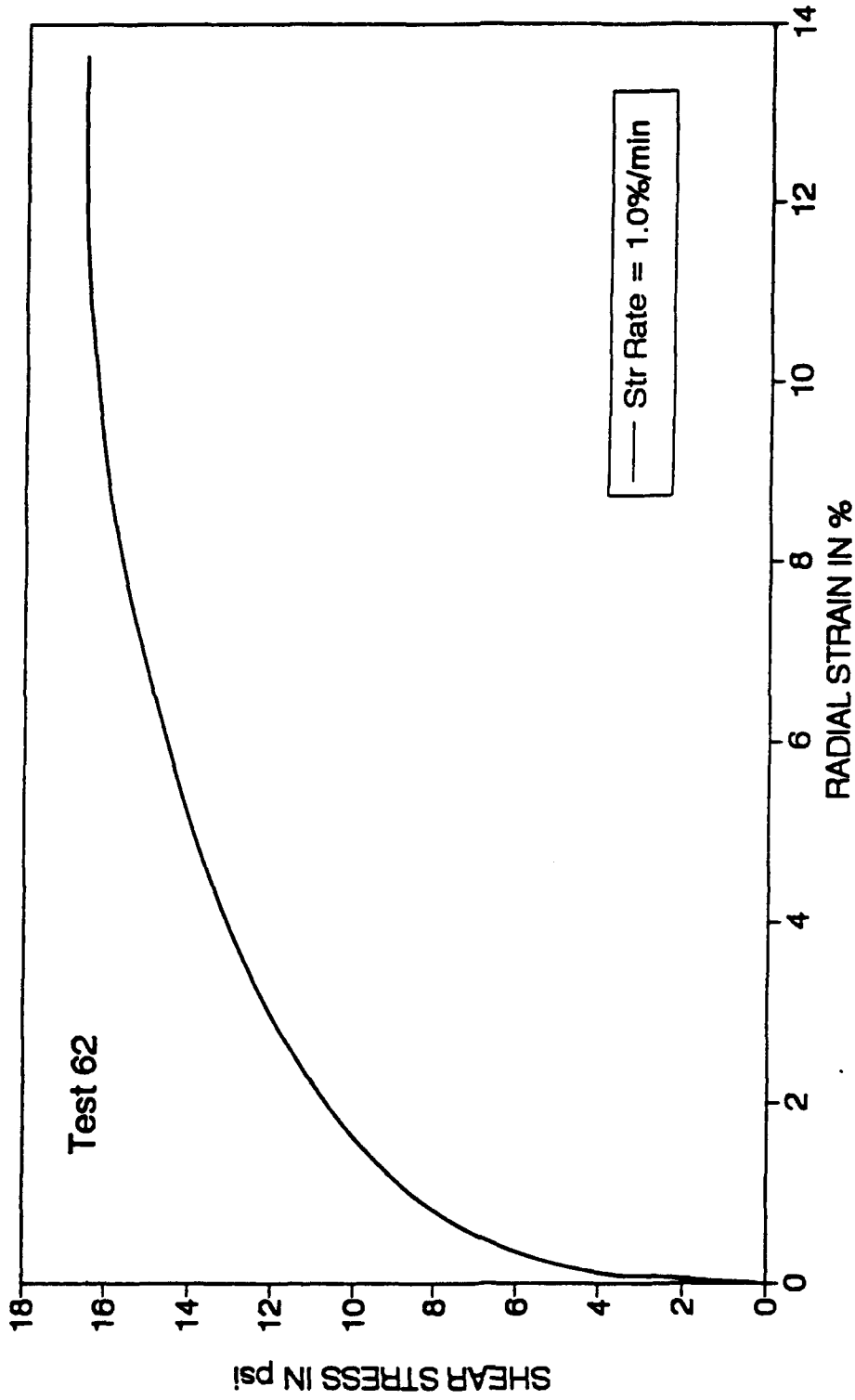

Fig. B.36 Shear Stress Vs Radial Strain for Kaolin - Silica Mix
(Test No. 62, Radial Strain Rate = 1.00%/min)

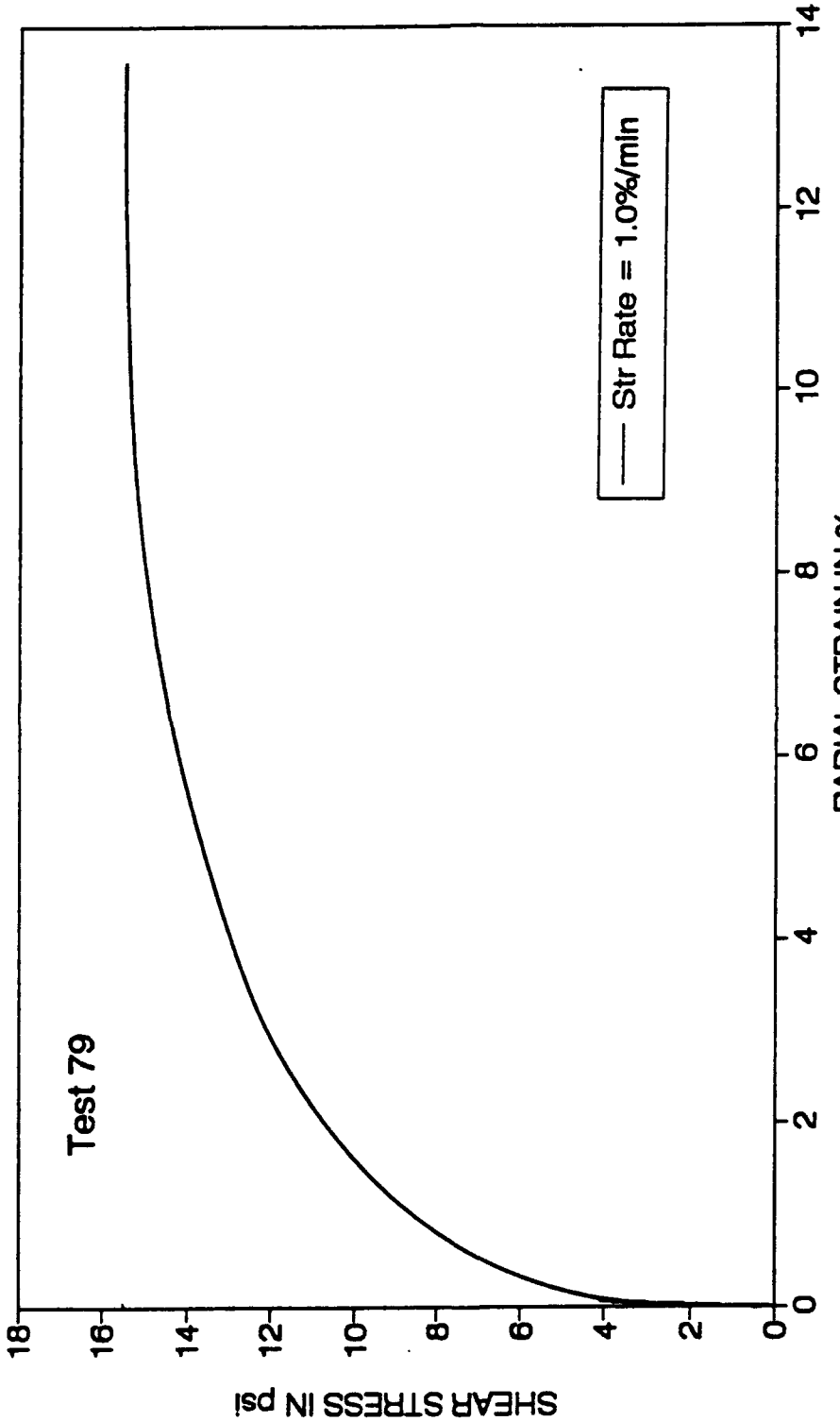

Fig. B.37 Shear Stress Vs Radial Strain for Kaolin - Silica Mix
(Test No. 79, Radial Strain Rate = 1.00%/min)

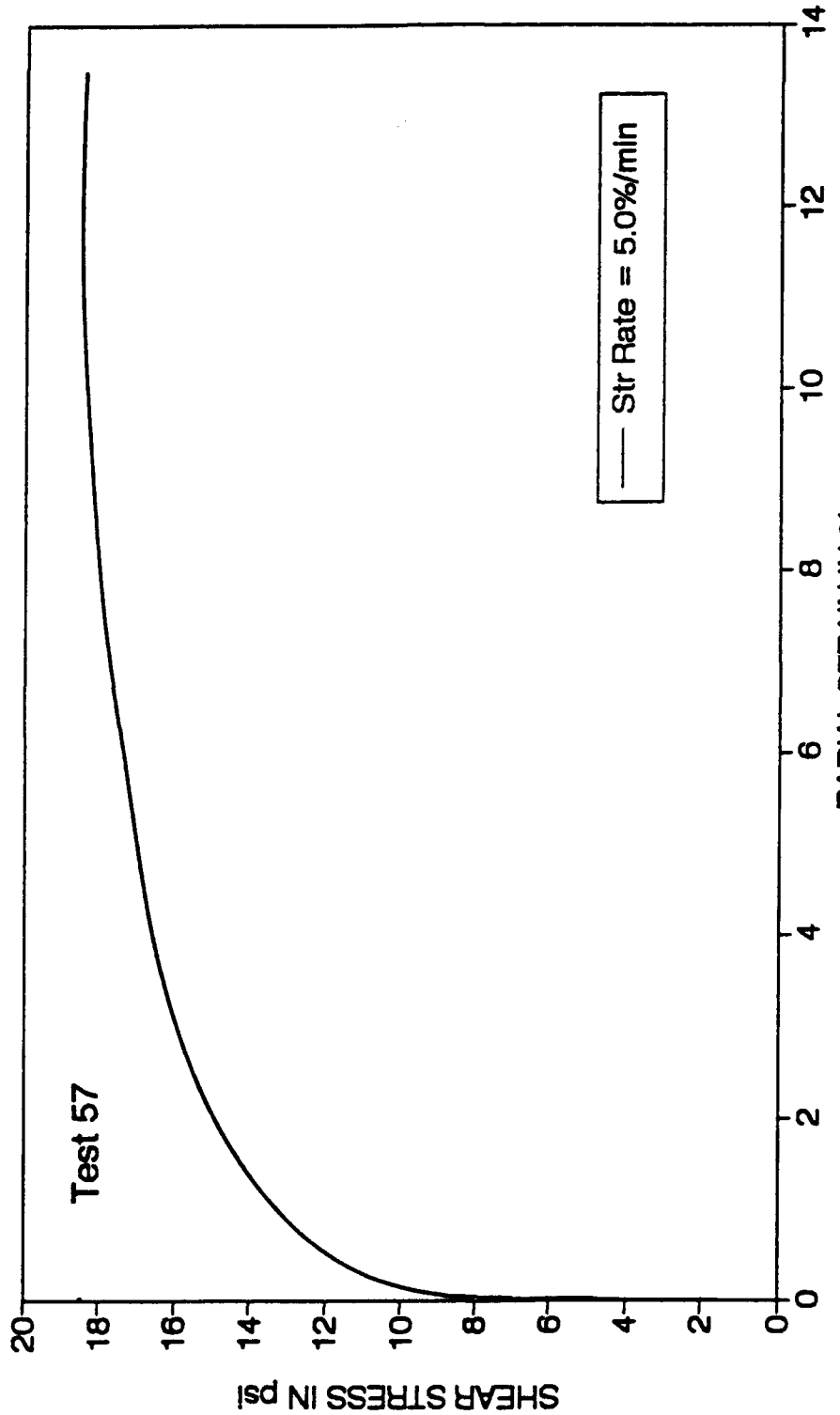

Fig. B.38 Shear Stress Vs Radial Strain for Kaolin - Silica Mix
(Test No. 57, Radial Strain Rate = 5.00%/min)

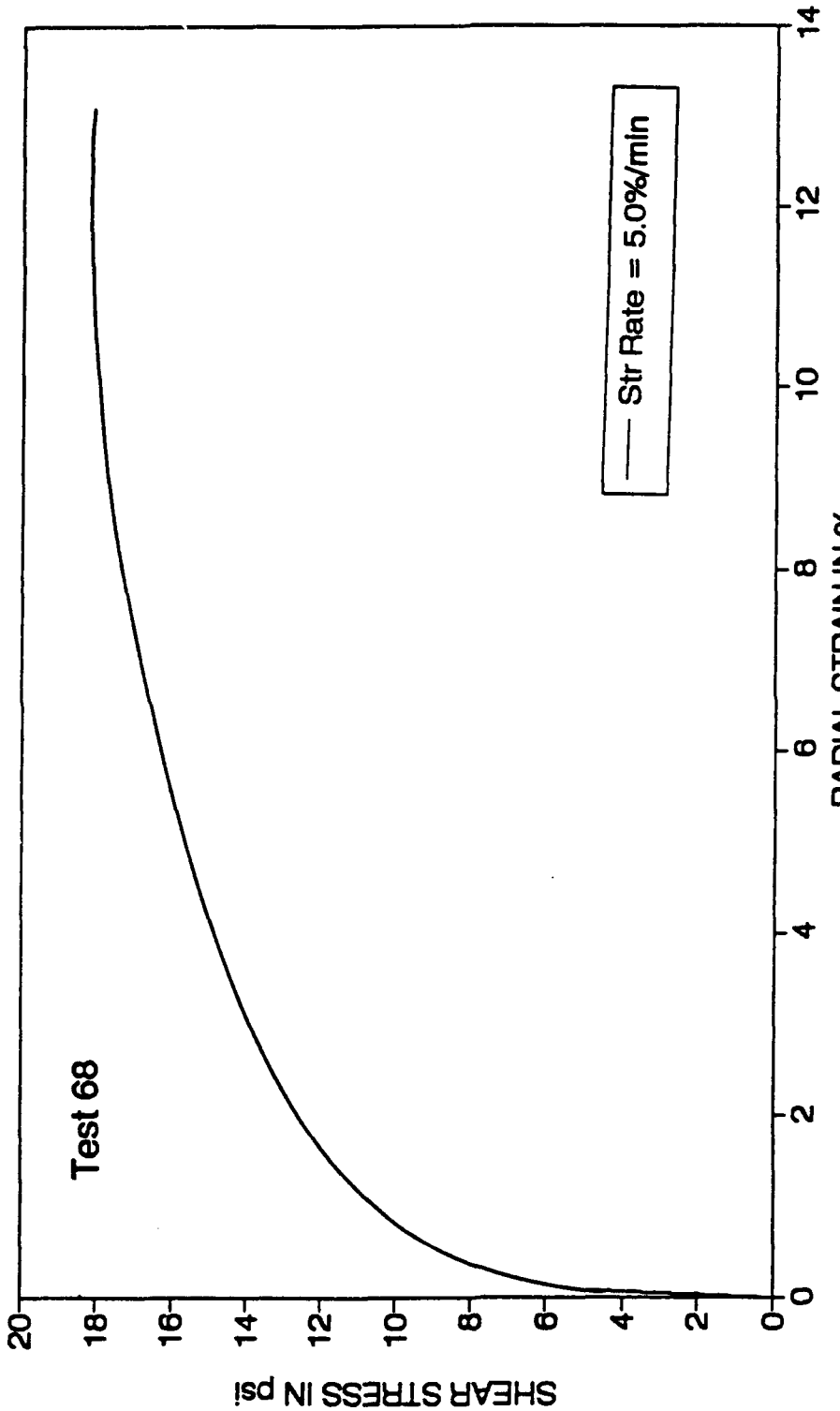

Fig. B.39 Shear Stress Vs Radial Strain for Kaolin - Silica Mix
(Test No. 68, Radial Strain Rate = 5.00%/min)

APPENDIX C

STRESS RELAXATION PLOTS FOR PMT

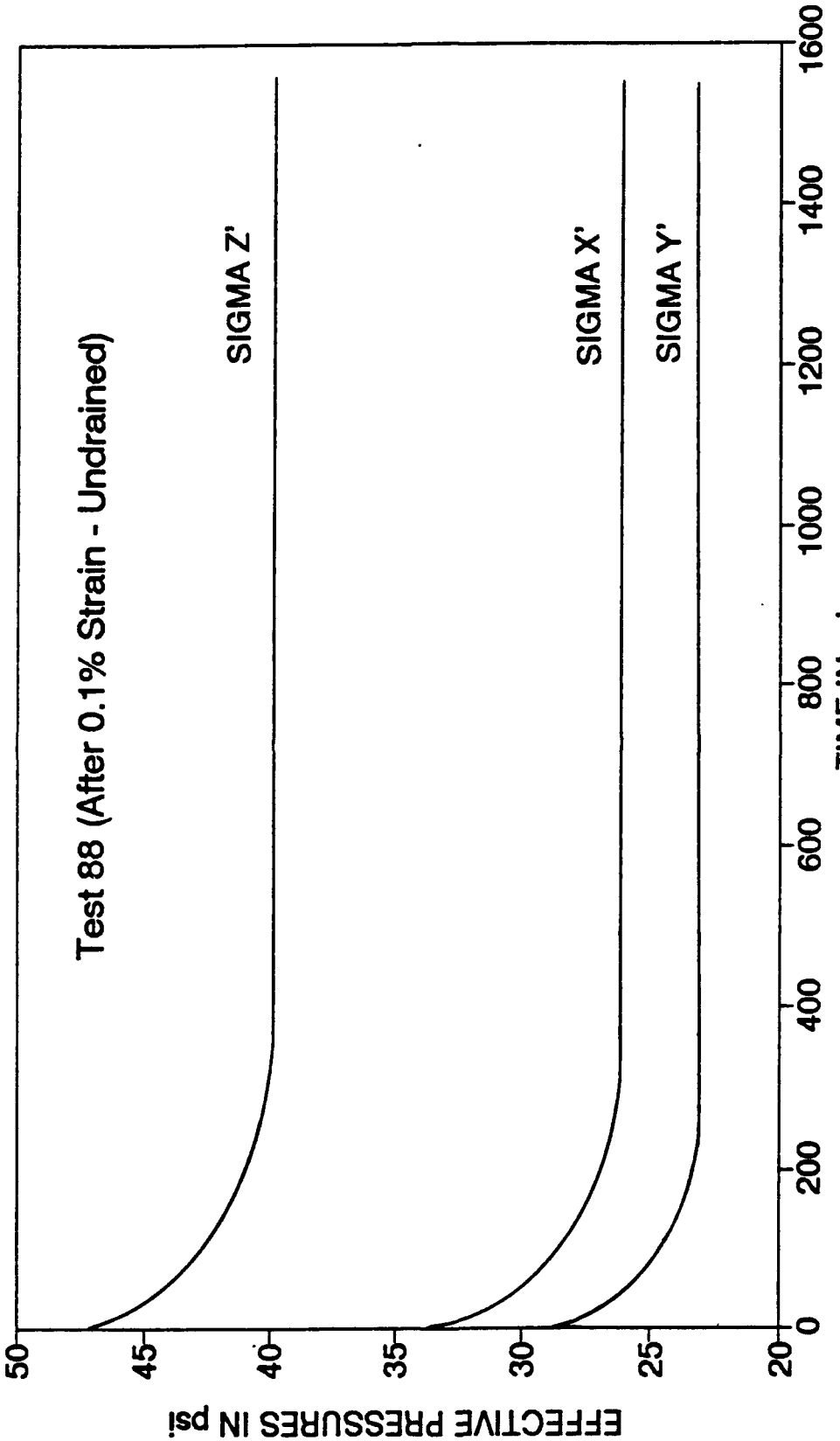

Fig. C.1 Stress Relaxation Curves After 0.1% Strain (Undrained - Test 88)

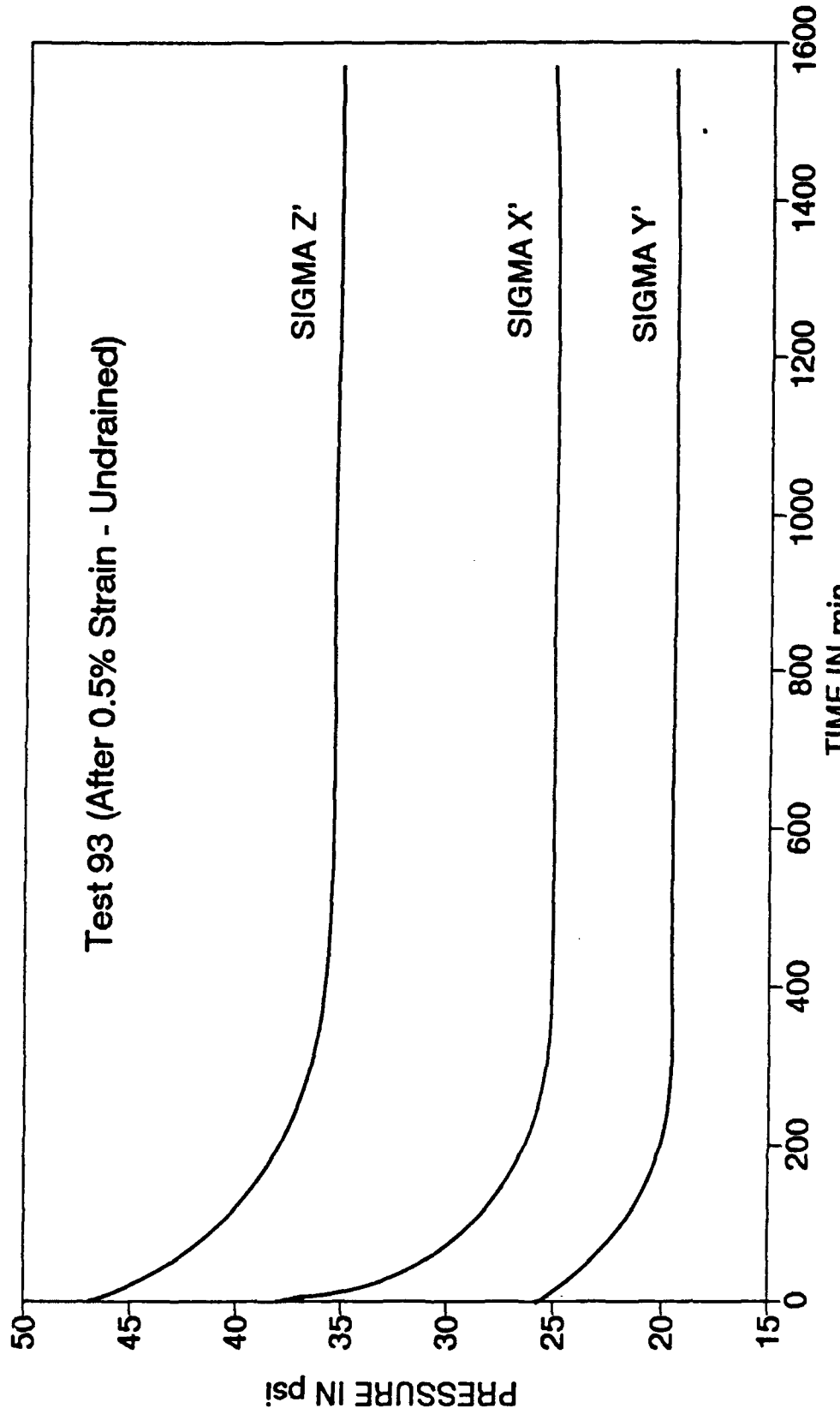

Fig. C.2 Stress Relaxation Curves After 0.5% Strain (Undrained - Test 93)

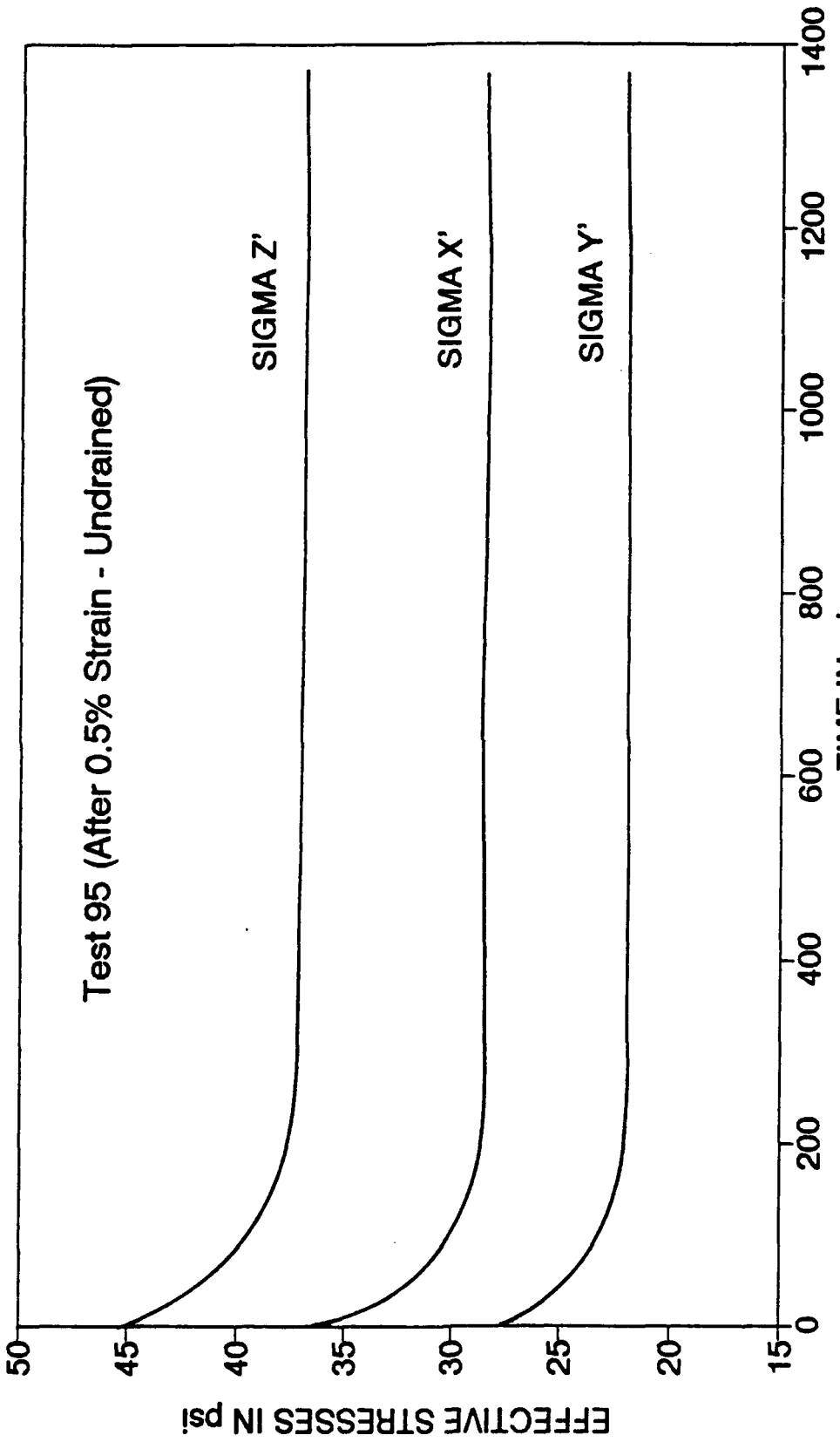

Fig. C.3 Stress Relaxation Curves After 0.5% Strain (Undrained - Test 95)

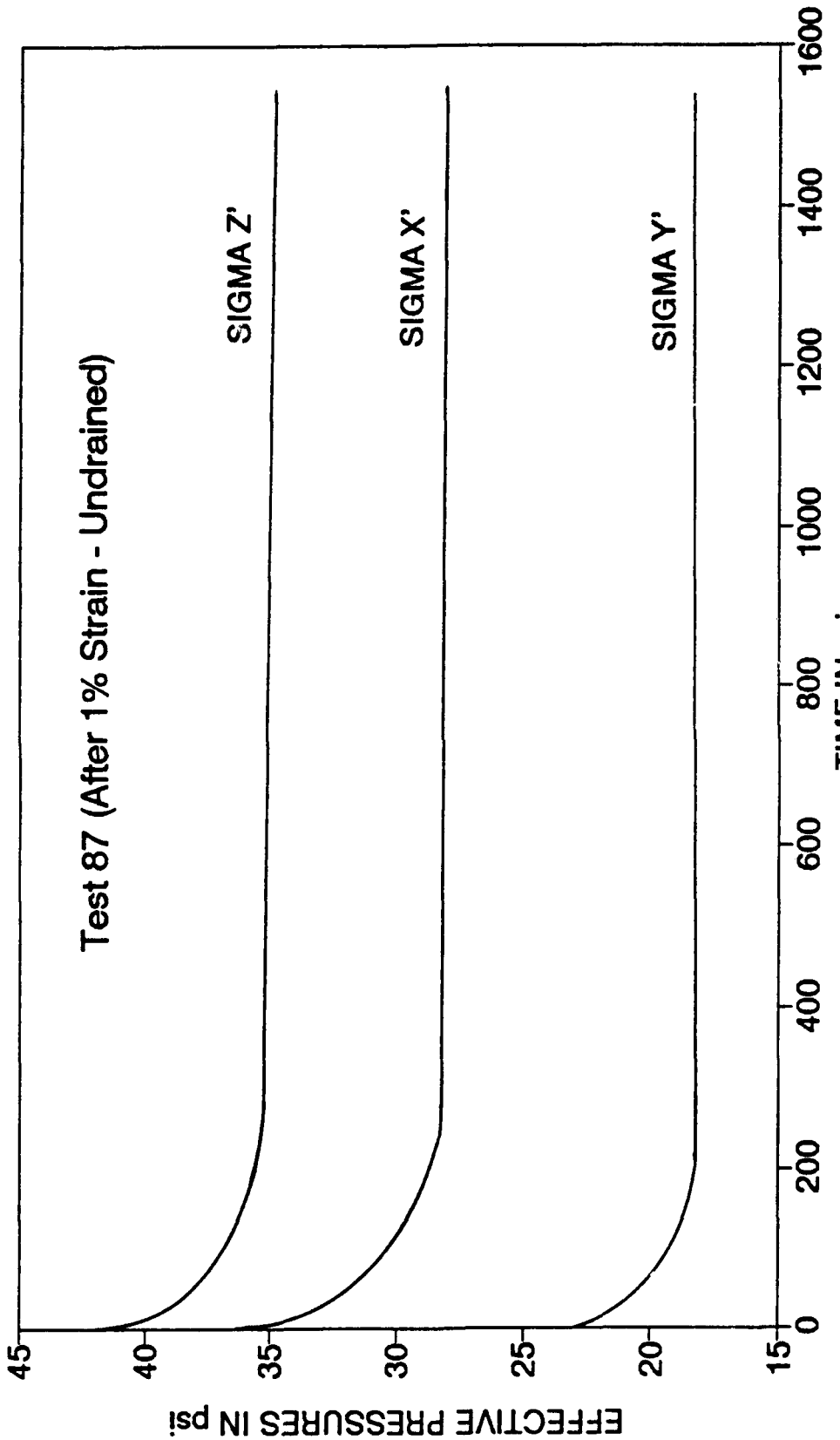

Fig. C.4 Stress Relaxation Curves After 1.0% Strain (Undrained - Test 87)

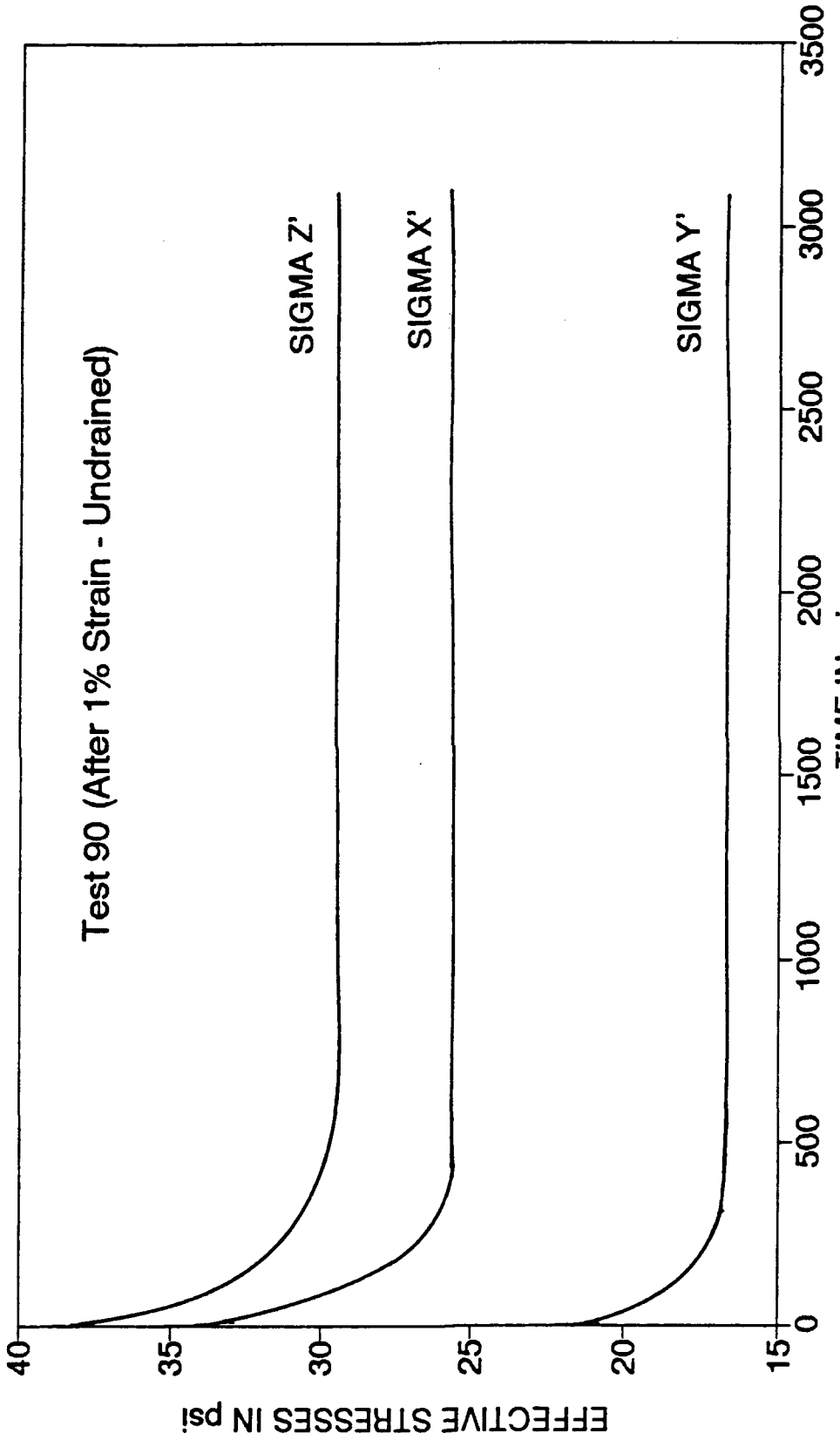

Fig. C.5 Stress Relaxation Curves After 1.0% Strain (Undrained - Test 90)

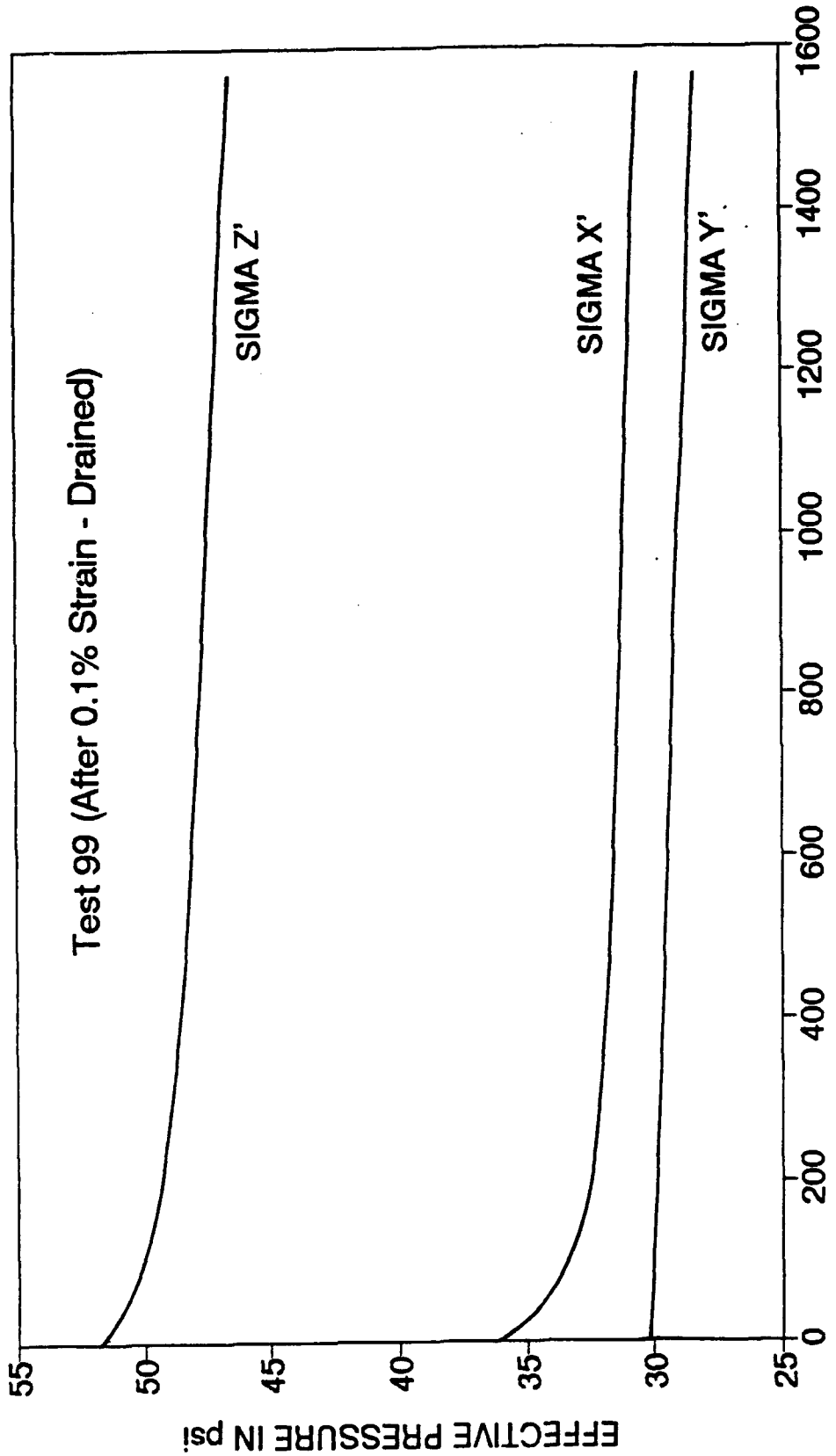

Fig. C.6 Stress Relaxation Curves After 0.1% Strain (Drained - Test 99)

APPENDIX D

CHARACTERISTICS OF KAOLINITE AND GROUND SILICA

APPENDIX D

Characteristics of Kaolinite

Trade Name	AKROCHEM SC-25 Clay
Chemical Name	Kaolin or Kaolinite
Chemical Family	Aluminum Silicate
Molecular Formula	Al_2O_3, $2SiO_2$, $2H_20$
Color	Light Cream
Fineness (thru 325 Mesh)	99.7%
Free Moisture	1% Max.
Particle Size	
Less than 2 Microns	61%
Greater than 5 Microns	20%
Alumina - %	38.5-39.5
Ignition Loss - 5%	13.6-14.0
Manganese in deleterious form	Nil
Silica - %	43.2-44.5
GE Brightness	79
Producer	Akrochem Corporation
Address	255 Fountain Street
	Akron, Ohio 44304
Phone	(216) 535-2108 (800) 321-2260
Fax	(216) 535-8947

Characteristics of Ground Silica

Trade Name	Sil-Co-Sil #270
Chemical Name	Silica
Chemical Family	Silicate
Molecular Formula	SiO_2
Mine	Ottawa, IL
Sieve Analysis (ASTM C 371-56)	
Cum. % + 100 Mesh	11.0
Cum. % + 200 Mesh	35.4
Cum. % + 325 Mesh	50.1
Particle Size	
Median (μ) (ASTM C-958)	45.0
Average (μ) (ASTM B-330)	10.2
Specific Surface Area (cm^2/g) (ASTM B-330)	2226
Oil Absorption (lbs/100 lbs) (ASTM D-1483)	15.0
Moisture (Max)	0.5%
Bulking value gal/lb	0.4536
lbs/gal	22.05
Refractive Index	1.54
GE Brightness	76.3
Yellowness	0.040
pH Value, 37.5% solids	8.1
Hardness (Moh's scale)	7
Chemical Analysis (%)	(ASTM C-146-72)

SiO_2	99.8	TiO_2	0.013	Al_2O_3	0.047		
Fl_2O_3	0.015	CaO	<0.01	Mg0	<0.01	LOI	0.09

APPENDIX E

COMPUTER PROGRAMS

```
10 '*****************************************************************************
20 '*
30 '*                    STRESS.BAS  - To Read and Record Data (Pressures and Displacements) And
40 '*                                  To Perform 1-D Consolidation
45 '*
50 '*****************************************************************************
55 'DECLARE SUB DASH8
60 CLS:KEY OFF
65 DIM DISPINIT(10),DISP(10),CALLVDT(10),TEMP%(110),PINITIAL(5),P(5)
66 DIM CALTRANS(5), TRAN%(1), DIO%(1), LT%(1)
70 KEY(1) ON: ON KEY(1) GOSUB 1550
80 KEY(2) ON: ON KEY(2) GOSUB 1590
90 KEY(3) ON: ON KEY(3) GOSUB 1650
100 KEY(4) ON:ON KEY(4) GOSUB 2250
110 KEY(5) ON:ON KEY(5) GOSUB 2350
120 KEY(6) ON:ON KEY(6) GOSUB 2380
130 KEY(7) ON:ON KEY(7) GOSUB 3180
140 OPEN "b:data1" AS #2 LEN = 56
150 FIELD #2, 4 AS XF$, 4 AS YF$, 4 AS ZF$, 4 AS BF$, 4 AS X1F$, 4 AS X2F$, 4 AS Y1F$, 4 AS Y2F$, 4 AS Z1F$, 4 AS Z2F$,4
AS Y21F$, 4 AS Y22F$,8 AS TIMEF$
160 M = LOF(2)/56
180 REM A routine for loading dash8.bin outside basic work space.
190 REM May be merged at the beginning of a program.
200 'DEF SEG = &H4000 'Change this load address to suit your memory
210 REM Loads at 92k.  A zero added automatically at right of &h1700 making it
220 REM &h17000.
230 'BLOAD "dash8.bin",0
240 OPEN "dash8.adr" FOR INPUT AS #1
250 INPUT #1, BASADR%
260 CLOSE #1
270 DASH8 = 0
280 FLAG% = 0
290 MD% = 0
300 CALL DASH8 (MD%, BASADR%, FLAG%)
310 IF FLAG% <>0 THEN PRINT "installation error"
320 MD% = 10: DIO%(0) = 2: DIO%(1) = 2  'Rate generator with counter 2
330 CALL DASH8 (MD%, DIO%(0), FLAG%)
340 MD% = 11: DIO%(1) = 2000
350 CALL DASH8 (MD%, DIO%(0), FLAG%)
360 '
370 CALLVDT(0) = 41.91:CALLVDT(1) = 41.55:CALLVDT(2) = 41.24:CALLVDT(3) = 41.78:
CALLVDT(4) = 40.91:CALLVDT(5) = 41.13:CALLVDT(6) = 41.05:CALLVDT(7) = 40.87  'Calibration constants, Volts/inch
380 CALTRANS(0) = 2.027: CALTRANS(1) = 2.02: CALTRANS(2) = 2.028: CALTRANS(3) = 2.014 'Calibration Constants in PSI/m.Volt
390 '
400 '
410 LOCATE 1,1: PRINT "INITIAL READINGS OF LVDTs:": PRINT
420 LOCATE 13,1: PRINT "INITIAL READINGS OF PRESSURE TRANSDUCERS:":PRINT
430 LOCATE 15,1: PRINT "Ch. No.";TAB(10);"Initial pressure(psi)"
440 LOCATE 22,1:PRINT "Press  s  to record data"
450 LOCATE 23,1:PRINT "Press F4 to check LVDTs/Transducers"
460 LOCATE 3,1: PRINT  "Ch. No.";TAB(10);"Volts"
470 '
480 'INITIAL READINGS OF THE LVDTS
490 FOR I% = 0 TO 7
500 GOSUB 1360
510 DISPINIT(I%) = DISP(I%)          'In inches
520 LOCATE I% + 4,1: PRINT USING " ##    ###.###";I%;VOLT
530 NEXT I%
540 PRINT:PRINT
550 '
560 'INITIAL READINGS OF THE TRANSDUCERS
570 PINITIAL(0) = 3.6: PINITIAL(1) = 1.2:PINITIAL(2) = -.3:PINITIAL(3) = 11
580 FOR I% = 0 TO 3
590 GOSUB 1170
600 P(I%) = P(I%) - PINITIAL(I%)
610 LOCATE 16 + I%,1: PRINT USING " ##          ###.###";I%;P(I%)
620 NEXT I%
630 '
```

```
640 '
650 IF INKEY$ = "s" GOTO 670
660 GOTO 490
670 N = 0: L=5
680 GOSUB 720
690 GOSUB 850
700 END
710 '
720 CLS
730 LOCATE 1,1:PRINT "DISPLACEMENTS IN INCHES:"
740 LOCATE 3,1:PRINT TAB(5); "DX1"; TAB(13); "DX2"; TAB(21); "DY1"; TAB(29); "DY2"; TAB(37); "DZ1"; TAB(45); "DZ2";
TAB(53); "DY21"; TAB(61); "DY22"
750 LOCATE 9,1:PRINT "PRESSURES IN PSI:"
760 LOCATE 11,1:PRINT "SigmaX";TAB(12);"SigmaY";TAB(23);"SigmaZ";TAB(31);"Pore Pressure"
770 LOCATE 17,1:PRINT "Number of Data Recorded: "
780 LOCATE 19,1:PRINT "Press F2 to quit"
790 LOCATE 20,1 : PRINT "Press F3 to change recording rate"
800 LOCATE 21,1: PRINT "Press F5 to check malfunctioning of LVDTs/Transducers"
810 LOCATE 22,1:PRINT "Press F6 to begin 1-D consolidation with servo control"
820 LOCATE 23,1: PRINT USING "1 in ### readings are being recorded.";L
830 RETURN
840 '
850 FOR I% = 0 TO 7
860 GOSUB 1360
870 DISP(I%) = DISP(I%) - DISPINIT(I%)
880 NEXT I%
890 FOR I% = 0 TO 3
900 GOSUB 1170
910 P(I%) = P(I%) - PINITIAL(I%)
920 NEXT I%
930 LOCATE 5,1: PRINT USING " ##.####";DISP(0);DISP(1);DISP(2);DISP(3);DISP(4);DISP(5);DISP(6);DISP(7)
940 LOCATE 13,1:PRINT USING " ###.#    ";P(0);P(1);P(2);P(3)
950 N = N + 1
960 IF L = 1 GOTO 980
970 IF ( N MOD L) <>1 GOTO 850
980 LSET XF$ = MKS$(P(0))
990 LSET YF$ = MKS$(P(1))
1000 LSET ZF$ = MKS$(P(2))
1010 LSET BF$ = MKS$(P(3))
1020 LSET X1F$ = MKS$(DISP(0))
1030 LSET X2F$ = MKS$(DISP(1))
1040 LSET Y1F$ = MKS$(DISP(2))
1050 LSET Y2F$ = MKS$(DISP(3))
1060 LSET Z1F$ = MKS$(DISP(4))
1070 LSET Z2F$ = MKS$(DISP(5))
1080 LSET Y21F$ = MKS$(DISP(6))
1090 LSET Y22F$ = MKS$(DISP(7))
1100 LSET TIMEF$ = TIME$
1110 M = M + 1
1120 PUT #2,M
1130 LOCATE 17,28:PRINT M
1140 GOTO 850
1150 RETURN
1160 '
1170 'SUBROUTINE PRESSURE
1180 LT%(0) = 1: LT%(1) = 1: MD% = 1 'Locks DASH8 on channel 1
1190 CALL DASH8 (MD%, LT%(0), FLAG%)
1200 IF FLAG% <>0 THEN PRINT "Error in setting the channel": END
1210 MD% = 14
1220 CALL DASH8 (MD%, I%, FLAG%)
1230 MD% = 5
1240 TRAN%(0) = VARPTR(TEMP%(0))
1250 TRAN%(1) = 100
1260 CALL DASH8 (MD%, TRAN%(0), FLAG%)
1270 X=0 : INDEX = 0
1280 FOR J=1 TO 98
1290 IF ABS(TEMP%(J)-TEMP%(J-1)) <2 AND ABS(TEMP%(J)-TEMP%(J+1))<2 THEN X=X+TEMP%(J): INDEX = INDEX +1
1300 NEXT J
```

```
1310 VOLT = X/(INDEX*20.48)   'In m.Volt
1320 P(I%) = VOLT*CALTRANS(I%) 'In psi
1330 RETURN
1340 '
1350 '
1360 'SUBROUTINE DISPLACEMENT
1370 LT%(0)=0: LT%(1)=0: MD%=1  'Locks DASH8 on channel 0
1380 CALL DASH8 (MD%, LT%(0), FLAG%)
1390 IF FLAG% <>0 THEN PRINT "Error in setting the channel": END
1400 MD%=14
1410 CALL DASH8 (MD%, I%, FLAG%)
1420 MD%=5
1430 TRAN%(0) = VARPTR(TEMP%(0))
1440 TRAN%(1) = 100
1450 CALL DASH8 (MD%, TRAN%(0), FLAG%)
1460 X = 0: INDEX = 0
1470 FOR J=1 TO 98
1480 IF ABS(TEMP%(J) - TEMP%(J-1)) <2 AND ABS(TEMP%(J) - TEMP%(J+1)) <2 THEN X=X+TEMP%(J): INDEX = INDEX +1
1490 NEXT J
1500 VOLT = X/(204.8*INDEX)   'In Volts
1510 IF ABS(VOLT) > 15 GOTO 1370
1520 DISP(I%) = VOLT/CALLVDT(I%) 'In inches
1530 RETURN
1540 '
1550 'SUBROUTINE TO FRESHEN THE SCREEN (F1)
1560 GOSUB 720
1570 RETURN
1580 '
1590 'SUBROUTINE TO TERMINATE THE RUN (KEY F2)
1600 CLOSE #2
1610 OUT &H320,0
1620 CLS
1630 END
1640 '
1650 'SUBROUTINE TO CHANGE RECORDING RATE (KEY F3)
1660 CLS
1670 INPUT "What is the recording rate (e.g. 1 in L) L";L
1680 GOSUB 1550
1690 RETURN
1700 '
1710 'SUBROUTINE TO CHECK MALFUNCTIONING OF LVDTs and TRANSDUCERS
1720 CLS
1730 INPUT "Do you want to check LVDTs (y/n)";AX$
1740 IF LEFT$(AX$,1) = "n" GOTO 1980
1750 IF LEFT$(AX$,1) = "y" GOTO 1770
1760 PRINT:PRINT "Say either  y  or  n  only": GOTO 1730
1770 LOCATE 10,1
1780 PRINT "*****************************************************************************************"
1790 PRINT "*                                    CHECKING THE LVDTs
1800 PRINT "*
1810 PRINT "*                The voltage induced in the LVDTs and corresponding channel
1820 PRINT "*                numbers will be displayed.  A steady flow of seemingly constant
1830 PRINT "*                 numbers (with  less than +/-0.02 volt) indicates that the LVDT
1840 PRINT "*                  is functioning satisfactorily.  LVDTs are checked one at a time.
1850 PRINT "*                PRESS ANY KEY WHEN READY.  Good Luck!
1855 PRINT "*
1860 PRINT "*****************************************************************************************"
1870 IF INKEY$="" THEN 1870
1880 CLS
1890 INPUT "Which channel (0 through 7) do you want to check ";I%
1900 GOSUB 1360
1910 PRINT USING "##          ##.##";I%;VOLT
1920 IF INKEY$="" GOTO 1900
1930 INPUT "Do you want to check any other channels (y/n) ";XX$
1940 IF  LEFT$(XX$,1) = "n" GOTO 1970
1950 IF LEFT$(XX$,1) = "y" GOTO 1880
1960 PRINT:PRINT "Say either y  or  n only": GOTO 1930
1970 '
```

```
1980 CLS
1990 INPUT "Do you want to check pressure transducers (y/n)";BX$
2000 IF LEFT$(BX$,1) = "n" GOTO 2230
2010 IF LEFT$(BX$,1) = "y" GOTO 2030
2020 PRINT:PRINT "Say either y  or  n only": GOTO 1990
2030 LOCATE 10,1
2040 PRINT "*****************************************************************************************"
2050 PRINT "*                  CHECKING THE PRESSURE TRANSDUCERS                                    "
2060 PRINT "*                                                                                       "
2070 PRINT "*    The pressure and corresponding channel numbers will be displayed.                  "
2080 PRINT "*    A steady flow of seemingly constant values of pressure (with                       "
2090 PRINT "*    less than +/- 0.5 psi variation) indicates that the pressure                       "
2100 PRINT "*    transducer is functioning satisfactorily.  They are being                          "
2110 PRINT "*    checked one at a time.  PRESS ANY KEY WHEN READY.  Good Luck!                      "
2115 PRINT "*                                                                                       "
2120 PRINT "*****************************************************************************************"
2130 IF INKEY$ = "" THEN 2130
2140 CLS
2150 INPUT "Which channel do you want to check ";I%
2160 GOSUB 1170
2170 PRINT USING "##        ###.#";I%;P(I%)
2180 IF INKEY$ = "" GOTO 2160
2190 INPUT "Do you want to check other channels (y/n) ";YY$
2200 IF YY$ = "n" GOTO 2230
2210 IF YY$ = "y" GOTO 2140
2220 PRINT:PRINT "Say either y  or n only":GOTO 2190
2230 RETURN
2240 '
2250 GOSUB 1710
2260 CLS
2270 LOCATE 1,1:PRINT "INITIAL READINGS OF THE LVDTS:": PRINT
2280 LOCATE 13,1:PRINT "INITIAL READINGS OF THE PRESSURE TRANSDUCERS:": PRINT
2290 LOCATE 15,1:PRINT "Ch. No.";TAB(10);"Initial Pressure (psi)"
2300 LOCATE 22,1:PRINT "Press s to record data"
2310 LOCATE 23,1:PRINT "Press F4 to check LVDTs/Transducers"
2320 LOCATE 3,1:PRINT "Ch. No.";TAB(10);"Volts"
2330 RETURN
2340 '
2350 GOSUB 1710
2360 GOSUB 720
2370 RETURN
2380 '
2390 CLS
2400  LOCATE  9,15:PRINT "*************************************************************************************"
2410 LOCATE 10,15:PRINT "*                                                                                   "
2420 LOCATE 11,15:PRINT "*                                                                                   "
2430 LOCATE 12,15:PRINT "*   SERVO CONTROLLED ONE DIMENSIONAL CONSOLIDATION                                  "
2440 LOCATE 13,15:PRINT "*                                                                                   "
2450 LOCATE 14,15:PRINT "*                                                                                   "
2460 LOCATE 15,15:PRINT "*************************************************************************************"
2461 KEY(3) OFF
2462 KEY(3) ON: ON KEY(3) GOSUB 4000
2470 FOR I = 1 TO 50: NEXT I:BEEP:BEEP
2480 LOCATE 9,15:PRINT "*************************************************************************************"
2490 LOCATE 10,15:PRINT "*            Watching the screen for display, adjust sigmaX,                        "
2500 LOCATE 11,15:PRINT "*            sigmaY, and sigmaZ such that they are equal to the                     "
2510 LOCATE 12,15:PRINT "*            required TOTAL vertical consolidation pressure.                        "
2520 LOCATE 13,15:PRINT "*            sigmaX and sigmaY are decreased AUTOMATICALLY                          "
2530 LOCATE 14,15:PRINT "*            during 1-D consolidation, maintaining zero lateral strain.             "
2550 LOCATE 16,15:PRINT "*                                                                                   "
2560 LOCATE 17,15:PRINT "*            NOTE: All displacements should be about 0.0000.  If                    "
2570 LOCATE 18,15:PRINT "*            different, REINITIALIZE (PRESS F2).                                    "
2580 LOCATE 19,15:PRINT "*                                                                                   "
2590 LOCATE 20,15:PRINT "*            FOR MANUAL OVERRIDE DURING CONSOLIDATION PRESS F7                      "
2600 LOCATE 21,15:PRINT "*                                                                                   "
2610 LOCATE 22,15:PRINT "*            When ready open the drainage valve and press any key                   "
2620 LOCATE 23,15:PRINT "*************************************************************"
2630 LOCATE 1,1:PRINT TAB(5); "DX1"; TAB(13); "DX2"; TAB(21); "DY1"; TAB(29); "DY2"; TAB(37); "DZ1"; TAB(45); "DZ2";
```

```
TAB(53); "DY21"; TAB(61); "DY22"
2640 LOCATE 4,1:PRINT "SigmaX";TAB(12);"SigmaY";TAB(21);"SigmaZ";TAB(30);"Pore Pressure"
2650 FOR I%=0 TO 7
2660 GOSUB 1360
2670 DISP(I%) = DISP(I%) - DISPINIT(I%)
2680 NEXT I%
2690 FOR I% = 0 TO 3
2700 GOSUB 1170
2710 P(I%) = P(I%) - PINITIAL(I%)
2720 NEXT I%
2730 LOCATE 2,1: PRINT USING " ##.####";DISP(0);DISP(1);DISP(2);DISP(3);DISP(4);DISP(5);DISP(6);DISP(7)
2740 LOCATE  5,1:PRINT USING " ###.#    ";P(0);P(1);P(2);P(3)
2750 IF INKEY$ = "" GOTO 2650
2760 GOSUB 720
2770 LOCATE 22,1:PRINT "Press F7 for manual override during 1-D consolidation"
2780 OUT &H323, &H80
2790 OUT &H320,5
2800 DELDISP = .0005
2810 FOR I% = 0 TO 7
2820 GOSUB 1360
2830 DISP(I%) = DISP(I%) - DISPINIT(I%)
2840 NEXT I%
2850 DISPX = DISP(0) + DISP(1)
2860 DISPY = DISP(2) + DISP(3)
2870 IF DISPX - DELDISP >0 THEN OUT &H320,7:FOR J=1 TO 20:NEXT J:OUT &H320,5
2880 IF DISPX + DELDISP < 0 THEN OUT &H320,4:FOR J=1 TO 120:NEXT J:OUT &H320,5
2890 IF DISPY - DELDISP >0 THEN OUT &H320,13:FOR J=1 TO 20:NEXT J:OUT &H320,5
2900 IF DISPY + DELDISP <0 THEN OUT &H320,1:FOR J=1 TO 120:NEXT J:OUT &H320,5
2910 FOR I%= 0 TO 3
2920 GOSUB 1170
2930 P(I%) = P(I%) - PINITIAL(I%)
2940 NEXT I%
2950 LOCATE 5,1: PRINT USING " ##.####";DISP(0);DISP(1);DISP(2);DISP(3);DISP(4);DISP(5);DISP(6);DISP(7)
2960 LOCATE 13,1:PRINT USING " ###.#    ";P(0);P(1);P(2);P(3)
2970 N = N + 1
2980 IF L = 1 GOTO 3000
2990 IF ( N MOD L) < >1 GOTO 2810
3000 LSET XF$ = MKS$(P(0))
3010 LSET YF$ = MKS$(P(1))
3020 LSET ZF$ = MKS$(P(2))
3030 LSET BF$ = MKS$(P(3))
3040 LSET X1F$ = MKS$(DISP(0))
3050 LSET X2F$ = MKS$(DISP(1))
3060 LSET Y1F$ = MKS$(DISP(2))
3070 LSET Y2F$ = MKS$(DISP(3))
3080 LSET Z1F$ = MKS$(DISP(4))
3090 LSET Z2F$ = MKS$(DISP(5))
3100 LSET Y21F$ = MKS$(DISP(6))
3110 LSET Y22F$ = MKS$(DISP(7))
3120 LSET TIMEF$ = TIME$
3130 M = M + 1
3140 PUT #2,M
3150 LOCATE 17,28:PRINT M
3160 GOTO 2810
3170 RETURN
3180 '
3190 CLS
3200 OUT &H320,5
3210 LOCATE 10,5:PRINT "(1). Close the plug valve (green) for X, Y directions"
3220 LOCATE 12,5:PRINT "(2). Adjust sigmaX, sigmaY regulators to the readings displayed on screen"
3230 LOCATE 14,5:PRINT "Press any key when finished"
3240 LOCATE 1,1:PRINT TAB(5); "DX1"; TAB(13); "DX2"; TAB(21); "DY1"; TAB(29); "DY2"; TAB(37); "DZ1"; TAB(45); "DZ2";
TAB(53); "DY21"; TAB(61); "DY22"
3250 LOCATE 4,1:PRINT "SigmaX";TAB(12);"SigmaY";TAB(21);"SigmaZ";TAB(30);"Pore Pressure"
3260 FOR I%=0 TO 7
3270 GOSUB 1360
3280 DISP(I%) = DISP(I%) - DISPINIT(I%)
3290 NEXT I%
```

```
3300 FOR I% = 0 TO 3
3310 GOSUB 1170
3320 P(I%) = P(I%) - PINITIAL(I%)
3330 NEXT I%
3340 LOCATE 2,1: PRINT USING " ##.####";DISP(0);DISP(1);DISP(2);DISP(3);DISP(4);DISP(5);DISP(6);DISP(7)
3350 LOCATE  5,1:PRINT USING " ###.#    ";P(0);P(1);P(2);P(3)
3360 IF INKEY$ = "" GOTO 3260
3370 CLS
3380 OUT &H320,0
3390 LOCATE 10,5:PRINT "Open the plug valves for x, y directions"
3400 LOCATE 14,5:PRINT "Press any keys when the valves are opened"
3410 IF INKEY$ = "" THEN 3410
3420 GOSUB 720
3430 LOCATE 22,1:PRINT SPC(60)
3440 GOSUB 850
3450 RETURN
4000 '
4010 GOSUB 1650
4020 LOCATE 22,1:PRINT "Press F7 for Manual Override during 1-D Consolidation"
4030 RETURN
```

```
10'*****************************************************************************************
20 '*
30 '*                    PM.BAS  - To Read and Record Data (Pressures and Displacements)
40 '*                                  during Strain Controlled Loading
50 '*
60'*****************************************************************************************
70 CLS:KEY OFF
72 DIM DISPINIT(10),DISP(10),CALLVDT(10),TEMP%(110),PINITIAL(5),P(5)
73 DIM CALTRANS(5), TRAN%(1), DIO%(1), LT%(1)
80 KEY(1) ON: ON KEY(1) GOSUB 1710
90 KEY(2) ON: ON KEY(2) GOSUB 1980
100 KEY(3) ON: ON KEY(3) GOSUB 1850
110 OPEN "b:data1" AS #2 LEN = 56
120 FIELD #2, 4 AS XF$, 4 AS YF$, 4 AS ZF$, 4 AS BF$, 4 AS X1F$, 4 AS X2F$, 4 AS Y1F$, 4 AS Y2F$, 4 AS Z1F$, 4 AS Z2F$,4
AS Y21F$, 4 AS Y22F$,8 AS TIMEF$
130 M = LOF(2)/56
150 REM A routine for loading dash8.bin outside basic work space.
160 REM May be merged at the beginning of a program.
170 'DEF SEG = &H1700 'Change this load address to suit your memory
180 REM Loads at 92k.  A zero added automatically at right of &h1700 making it
190 REM &h17000.
200 'BLOAD "dash8.bin",0
210 OPEN "dash8.adr" FOR INPUT AS #1
220 INPUT #1, BASADR%
230 CLOSE #1
240 DASH8 = 0
250 FLAG% = 0
260 MD% = 0
270 CALL DASH8 (MD%, BASADR%, FLAG%)
280 IF FLAG% <>0 THEN PRINT "installation error"
290 MD% = 10: DIO%(0) = 2: DIO%(1) = 2  'Rate generator with counter 2
300 CALL DASH8 (MD%, DIO%(0), FLAG%)
310 MD% = 11: DIO%(1) = 2000
320 CALL DASH8 (MD%, DIO%(0), FLAG%)
330 '
340   CALLVDT(0) = 41.91:   CALLVDT(1) = 41.55:   CALLVDT(2) = 41.24:   CALLVDT(3) = 41.78:   CALLVDT(4) = 40.91:
CALLVDT(5) = 41.13: CALLVDT(6) = 41.05: CALLVDT(7) = 40.87  'Calibration constants, Volts/inch
350 CALTRANS(0) = 2.027: CALTRANS(1) = 2.02: CALTRANS(2) = 2.028: CALTRANS(3) = 2.014 'Calibration Constants in PSI/m.Volt
360 '
370 'INITIAL READINGS OF THE LVDTS
380 FOR I% = 0 TO 7
390 GOSUB 1520
400 DISPINIT(I%) = DISP(I%)          'In inches
410 NEXT I%
420 'INITIAL READINGS OF THE TRANSDUCERS
430 PINITIAL(0) = 3.6: PINITIAL(1) = 1.2:PINITIAL(2) = -.3:PINITIAL(3) = 11
440 N = 0: L = 5
450 '
460 'BEGIN STRAIN CONTROLLED LOADING
470 CLS
480 LOCATE 9,15:PRINT "*****************************************************************************"
490 LOCATE 10,15:PRINT "*"
500 LOCATE 11,15:PRINT "*"
510 LOCATE 12,15:PRINT "*                              STRAIN CONTROLLED LOADING
520 LOCATE 13,15:PRINT "*"
530 LOCATE 14,15:PRINT "*"
540 LOCATE 15,15:PRINT "*****************************************************************************"
550 SOUND 1000,50: SOUND 2000,50: SOUND 3000,50
560 OUT &H323, &H80
570 OUT &H320,21
580 CLS
590 LOCATE 7,10:PRINT "Increase SigmaX to a value greater than expected final (failure) value"
600 LOCATE 9,10:PRINT "Press any key to begin strain controlled loading"
610 IF INKEY$ = "" THEN 610
620 CLS
630 LOCATE 9,10:INPUT "What are the X, Y widths of the specimen after consolidation (in.)";HX,HY
640 LOCATE 12,10:INPUT "What is the desired X-strain rate (% per min.)"; RATEX
642 LOCATE 13,10:INPUT "What is the desired Y-strain rate (% per min.) (NEG.)"; RATEY
650 LOCATE 14,10:PRINT "Make sure that the drain is closed before you proceed"
```

```
660 LOCATE 16,10:INPUT "Do you wish to change the above information (y/n)";X$
670 IF LEFT$(X$,1) = "y" GOTO 680
680 IF LEFT$(X$,1) = "n" GOTO 700
690 PRINT:PRINT "Say either Y or n only": GOTO 660
700 DELX = .01*RATEX
701 DELY = .01*ABS(RATEY)
702 DELDISP = 0.0005
705 NNN = 400
710 CLS
720 GOSUB 1900  'Timing Begins
725 TIME1 = SS
730 GOSUB 1200
750 FOR I% = 0 TO 5
760 GOSUB 1520
770 DISP(I%) = DISP(I%) - DISPINIT(I%)
780 NEXT I%
782 DISPX = DISP(0) + DISP(1)
784 DISPY = DISP(2) + DISP(3)
790 DISPZ = DISP(4) + DISP(5)
792 STRAINX = (DISPX/HX)*100
794 STRAINY = (DISPY/HY)*100
802 GOSUB 1900
804 TIME2 = SS
810 TIME = (TIME2 - TIME1)/60
820 EDOTX = STRAINX/TIME
823 EDOTY = STRAINY/TIME
825 IF TIME > 15 THEN NNN = 200
830 IF EDOTX - RATEX > DELX THEN OUT &H320,23:FOR J=1 TO 5:NEXT J: OUT &H320,21
832 IF RATEX - EDOTX > DELX THEN OUT &H320,20:FOR J= 1 TO NNN:NEXT J:OUT &H320,21
834 IF EDOTY - RATEY > DELY THEN OUT &H320,29:FOR J=1 TO 5:NEXT J: OUT &H320,21
836 IF RATEY - EDOTY > DELY THEN OUT &H320,17:FOR J=1 TO NNN: NEXT J: OUT &H320,21
842 IF DISPZ -DELDISP > 0 THEN OUT &H320,53:FOR J=1 TO 20:NEXT J: OUT &H320,21
844 IF DISPZ + DELDISP < 0 THEN OUT &H320,5:FOR J = 1 TO 120: NEXT J: OUT &H320,21
850 '
860 'FOR K = 1 TO 30000: NEXT K
870 FOR I% =0 TO 7
880 GOSUB 1520
890 DISP(I%) = DISP(I%) - DISPINIT(I%)
900 NEXT I%
910 FOR I% = 0 TO 3
920 GOSUB 1320
940 NEXT I%
950 LOCATE 5,1: PRINT USING " ##.####";DISP(0);DISP(1);DISP(2);DISP(3);DISP(4);DISP(5);DISP(6);DISP(7)
960 LOCATE 13,1:PRINT USING " ###.#    ";P(0);P(1);P(2);P(3)
970 LOCATE 21,28:PRINT USING "##.####";EDOTX
975 LOCATE 22,28:PRINT USING "##.####";EDOTY
980 N = N + 1
990 IF L = 1 GOTO 1010
1000 IF ( N MOD L) <>1 GOTO 750
1010 LSET XF$ = MKS$(P(0))
1020 LSET YF$ = MKS$(P(1))
1030 LSET ZF$ = MKS$(P(2))
1040 LSET BF$ = MKS$(P(3))
1050 LSET X1F$ = MKS$(DISP(0))
1060 LSET X2F$ = MKS$(DISP(1))
1070 LSET Y1F$ = MKS$(DISP(2))
1080 LSET Y2F$ = MKS$(DISP(3))
1090 LSET Z1F$ = MKS$(DISP(4))
1100 LSET Z2F$ = MKS$(DISP(5))
1110 LSET Y21F$ = MKS$(DISP(6))
1120 LSET Y22F$ = MKS$(DISP(7))
1130 LSET TIMEF$ = TIME$
1140 M = M + 1
1150 PUT #2,M
1160 LOCATE 17,28:PRINT M
1170 GOTO 750
1180 END
1190 '
1200 CLS
```

```
1210 LOCATE 1,1:PRINT "DISPLACEMENTS IN INCHES:"
1220 LOCATE 3,1:PRINT TAB(5); "DX1"; TAB(13); "DX2"; TAB(21); "DY1"; TAB(29); "DY2"; TAB(37); "DZ1"; TAB(45); "DZ2";
TAB(53); "DY21"; TAB(61); "DY22"
1230 LOCATE 9,1:PRINT "PRESSURES IN PSI:"
1240 LOCATE 11,1:PRINT "SigmaX";TAB(12);"SigmaY";TAB(23);"SigmaZ";TAB(31);"Pore Pressure"
1250 LOCATE 17,1:PRINT "Number of Data Recorded: "
1260 LOCATE 19,1:PRINT "Press F2 to quit"
1270 LOCATE 20,1 : PRINT "Press F3 to change recording rate"
1275 LOCATE 21,1:PRINT "Current X-Strain Rate is          % per min."
1280 LOCATE 22,1:PRINT "Current Y-Strain Rate is          % per min."
1290 LOCATE 23,1: PRINT USING "1 in ### readings are being recorded.";L
1300 RETURN
1310 '
1320 'SUBROUTINE PRESSURE
1330 LT%(0)=1: LT%(1)=1: MD%=1 'Locks DASH8 on channel 1
1340 CALL DASH8 (MD%, LT%(0), FLAG%)
1350 IF FLAG%<>0 THEN PRINT "Error in setting the channel": END
1360 MD%=14
1370 CALL DASH8 (MD%, I%, FLAG%)
1380 MD%=5
1390 TRAN%(0)=VARPTR(TEMP%(0))
1400 TRAN%(1) = 40
1410 CALL DASH8 (MD%, TRAN%(0), FLAG%)
1420 X=0 : INDEX = 0
1430 FOR J=1 TO 38
1440 IF ABS(TEMP%(J)-TEMP%(J-1)) <2 AND ABS(TEMP%(J)-TEMP%(J+1))<2 THEN X=X+TEMP%(J): INDEX = INDEX +1
1450 NEXT J
1460 VOLT = X/(INDEX*20.48)  'In m.Volt
1470 P(I%) = VOLT*CALTRANS(I%) 'In psi
1480 P(I%) =P(I%) - PINITIAL(I%)
1490 RETURN
1500 '
1510 '
1520 'SUBROUTINE DISPLACEMENT
1530 LT%(0)=0: LT%(1)=0: MD%=1  'Locks DASH8 on channel 0
1540 CALL DASH8 (MD%, LT%(0), FLAG%)
1550 IF FLAG% <>0 THEN PRINT "Error in setting the channel": END
1560 MD%=14
1570 CALL DASH8 (MD%, I%, FLAG%)
1580 MD%=5
1590 TRAN%(0) = VARPTR(TEMP%(0))
1600 TRAN%(1) = 40
1610 CALL DASH8 (MD%, TRAN%(0), FLAG%)
1620 X = 0: INDEX = 0
1630 FOR J=1 TO 38
1640 IF ABS(TEMP%(J) - TEMP%(J-1)) <2 AND ABS(TEMP%(J) - TEMP%(J+1)) <2 THEN X=X+TEMP%(J): INDEX = INDEX +1
1650 NEXT J
1660 VOLT = X/(204.8*INDEX)  'In Volts
1670 IF ABS(VOLT) > 15 GOTO 1530
1680 DISP(I%) = VOLT/CALLVDT(I%) 'In inches
1690 RETURN
1700 '
1710 'SUBROUTINE TO FRESHEN THE SCREEN (F1)
1720 GOSUB 1200
1730 RETURN
1830 '
1840 '
1850 'SUBROUTINE TO CHANGE RECORDING RATE (KEY F3)
1860 CLS
1870 INPUT "What is the recording rate (e.g. 1 in L) L";L
1880 GOSUB 1710
1890 RETURN
1900 'SUBROUTINE TIMER
1910 TIM$ = TIME$
1920 SS$ = RIGHT$(TIM$,2)
1930 MM$ = MID$(TIM$,4,2)
1940 HH$ = LEFT$(TIM$,2)
1950 SS = VAL(SS$)*1 + VAL(MM$)*60 + VAL(HH$)*3600
1960 RETURN
```

```
1970 '
1980 'SUBROUTINE TO TERMINATE THE RUN (KEY F2)
1990 CLS
2000 CLOSE #2
2010 LOCATE 7,10:PRINT "Watch the gage and turn the pressure regulator to bring down SIGMAX"
2020 LOCATE 9,10:PRINT "to about SIGMAY and SIGMAZ"
2030 LOCATE 11,10:PRINT "PRESS ANY KEY WHEN FINISHED"
2040 IF INKEY$ ="" THEN 2040
2050 OUT &H320,0
2060 CLS
2070 END
```

```
10 '*****************************************************************************************
20 '*
30 '*                    RELAX.BAS - To Read and Record Data (Pressures and Displacements)
40 '*                                during Relaxation Test
50 '*
60 '*****************************************************************************************
70 CLS:KEY OFF
72 DIM DISPINIT(10),DISP(10),CALLVDT(10),TEMP%(110),PINITIAL(5),P(5)
73 DIM CALTRANS(5), TRAN%(1), DIO%(1), LT%(1)
80 KEY(1) ON: ON KEY(1) GOSUB 1710
90 KEY(2) ON: ON KEY(2) GOSUB 1980
100 KEY(3) ON: ON KEY(3) GOSUB 1850
110 OPEN "b:data1" AS #2 LEN = 56
120 FIELD #2, 4 AS XF$, 4 AS YF$, 4 AS ZF$, 4 AS BF$, 4 AS X1F$, 4 AS X2F$, 4 AS Y1F$, 4 AS Y2F$, 4 AS Z1F$, 4 AS Z2F$,4
    AS Y21F$, 4 AS Y22F$,8 AS TIMEF$
130 M = LOF(2)/56
150 REM A routine for loading dash8.bin outside basic work space.
160 REM May be merged at the beginning of a program.
170 'DEF SEG = &H1700 'Change this load address to suit your memory
180 REM Loads at 92k.  A zero added automatically at right of &h1700 making it
190 REM &h17000.
200 'BLOAD "dash8.bin",0
210 OPEN "dash8.adr" FOR INPUT AS #1
220 INPUT #1, BASADR%
230 CLOSE #1
240 DASH8 = 0
250 FLAG% = 0
260 MD% = 0
270 CALL DASH8 (MD%, BASADR%, FLAG%)
280 IF FLAG% <>0 THEN PRINT "installation error"
290 MD% = 10: DIO%(0) = 2: DIO%(1) = 2  'Rate generator with counter 2
300 CALL DASH8 (MD%, DIO%(0), FLAG%)
310 MD% = 11: DIO%(1) = 2000
320 CALL DASH8 (MD%, DIO%(0), FLAG%)
330 '
340  CALLVDT(0) = 41.91:  CALLVDT(1) = 41.55:  CALLVDT(2) = 41.24:  CALLVDT(3) = 41.78:  CALLVDT(4) = 40.91:
CALLVDT(5) = 41.13: CALLVDT(6) = 41.05: CALLVDT(7) = 40.87  'Calibration constants, Volts/inch
350 CALTRANS(0) = 2.027: CALTRANS(1) = 2.02: CALTRANS(2) = 2.028: CALTRANS(3) = 2.014 'Calibration Constants in PSI/m.Volt
360 '
370 'INITIAL READINGS OF THE LVDTS
380 FOR I% = 0 TO 7
390 GOSUB 1520
400 DISPINIT(I%) = DISP(I%)          'In inches
410 NEXT I%
420 'INITIAL READINGS OF THE TRANSDUCERS
430 PINITIAL(0) = 3.6: PINITIAL(1) = 1.2:PINITIAL(2) = -.3:PINITIAL(3) = 1!
440 N = 0: L=5
450 '
460 'BEGIN RELAXATION TESTING
470 CLS
480 LOCATE 9,15:PRINT*****************************************************************************
490 LOCATE 10,15:PRINT
500 LOCATE 11,15:PRINT
510 LOCATE 12,15:PRINT                        RELAXATION TESTING
520 LOCATE 13,15:PRINT
525 LOCATE 14,15:PRINT         (MAINTAINING NO DEFORMATION IN ALL DIRECTIONS)
526 LOCATE 15,15:PRINT
530 LOCATE 16,15:PRINT
540 LOCATE17,15:PRINT*****************************************************************************
550 SOUND 1000,50: SOUND 2000,50: SOUND 3000,50
560 OUT &H323, &H80
570 OUT &H320,21
580 CLS
600 LOCATE 7,10:PRINT "Press any key to begin Relaxation Testing"
610 IF INKEY$ = "" THEN 610
620 CLS
650 LOCATE 14,10:PRINT "Make sure that the drain is closed before you proceed"
702 DELDISP = 0.001
705 NNN = 400
```

```
730 GOSUB 1200
750 FOR I% = 0 TO 5
760 GOSUB 1520
770 DISP(I%) = DISP(I%) - DISPINIT(I%)
780 NEXT I%
782 DISPX = DISP(0) + DISP(1)
784 DISPY = DISP(2) + DISP(3)
790 DISPZ = DISP(4) + DISP(5)
830 IF DISPX - DELDISP > 0 THEN OUT &H320,23:FOR J=1 TO 5:NEXT J: OUT &H320,21
832 IF DISPX + DELDISP < 0 THEN OUT &H320,20:FOR J= 1 TO NNN:NEXT J:OUT &H320,21
834 IF DISPY - DELDISP > 0 THEN OUT &H320,29:FOR J=1 TO 5:NEXT J: OUT &H320,21
836 IF DISPY + DELDISP < 0 THEN OUT &H320,17:FOR J=1 TO NNN: NEXT J: OUT &H320,21
842 IF DISPZ - DELDISP > 0 THEN OUT &H320,53:FOR J=1 TO 20:NEXT J: OUT &H320,21
844 IF DISPZ + DELDISP < 0 THEN OUT &H320,5:FOR J = 1 TO 120: NEXT J: OUT &H320,21
850 '
860 'FOR K = 1 TO 30000: NEXT K
870 FOR I%=0 TO 7
880 GOSUB 1520
890 DISP(I%) = DISP(I%) - DISPINIT(I%)
900 NEXT I%
910 FOR I% = 0 TO 3
920 GOSUB 1320
940 NEXT I%
950 LOCATE 5,1: PRINT USING " ##.####"; DISP(0); DISP(1); DISP(2); DISP(3); DISP(4); DISP(5); DISP(6); DISP(7)
960 LOCATE 13,1:PRINT USING " ###.#    "; P(0); P(1); P(2); P(3)
980 N = N + 1
990 IF L = 1 GOTO 1010
1000 IF ( N MOD L) < >1 GOTO 750
1010 LSET XF$ = MKS$(P(0))
1020 LSET YF$ = MKS$(P(1))
1030 LSET ZF$ = MKS$(P(2))
1040 LSET BF$ = MKS$(P(3))
1050 LSET X1F$ = MKS$(DISP(0))
1060 LSET X2F$ = MKS$(DISP(1))
1070 LSET Y1F$ = MKS$(DISP(2))
1080 LSET Y2F$ = MKS$(DISP(3))
1090 LSET Z1F$ = MKS$(DISP(4))
1100 LSET Z2F$ = MKS$(DISP(5))
1110 LSET Y21F$ = MKS$(DISP(6))
1120 LSET Y22F$ = MKS$(DISP(7))
1130 LSET TIMEF$ = TIME$
1140 M = M + 1
1150 PUT #2,M
1160 LOCATE 17,28:PRINT M
1170 GOTO 750
1180 END
1190 '
1200 CLS
1210 LOCATE 1,1: PRINT "DISPLACEMENTS IN INCHES:"
1220 LOCATE 3,1: PRINT TAB(5); "DX1"; TAB(13); "DX2"; TAB(21); "DY1"; TAB(29); "DY2"; TAB(37); "DZ1"; TAB(45); "DZ2",
TAB(53); "DY21"; TAB(61); "DY22"
1230 LOCATE 9,1:PRINT "PRESSURES IN PSI:"
1240 LOCATE 11,1:PRINT "SigmaX";TAB(12);"SigmaY";TAB(23);"SigmaZ";TAB(31);"Pore Pressure"
1250 LOCATE 17,1:PRINT "Number of Data Recorded: "
1260 LOCATE 19,1:PRINT "Press F2 to quit"
1270 LOCATE 20,1 : PRINT "Press F3 to change recording rate"
1290 LOCATE 23,1: PRINT USING "1 in ### readings are being recorded.";L
1300 RETURN
1310 '
1320 'SUBROUTINE PRESSURE
1330 LT%(0)=1: LT%(1)=1: MD%=1 'Locks DASH8 on channel 1
1340 CALL DASH8 (MD%, LT%(0), FLAG%)
1350 IF FLAG% < >0 THEN PRINT "Error in setting the channel": END
1360 MD%=14
1370 CALL DASH8 (MD%, I%, FLAG%)
1380 MD%=5
1390 TRAN%(0)=VARPTR(TEMP%(0))
1400 TRAN%(1) = 40
1410 CALL DASH8 (MD%, TRAN%(0), FLAG%)
```

```
1420 X=0 : INDEX = 0
1430 FOR J=1 TO 38
1440 IF ABS(TEMP%(J)-TEMP%(J-1)) <2 AND ABS(TEMP%(J)-TEMP%(J+1))<2 THEN X=X+TEMP%(J): INDEX = INDEX +1
1450 NEXT J
1460 VOLT = X/(INDEX*20.48)  'In m.Volt
1470 P(I%) = VOLT*CALTRAN$(I%) 'In psi
1480 P(I%) =P(I%) - PINITIAL(I%)
1490 RETURN
1500 '
1510 '
1520 'SUBROUTINE DISPLACEMENT
1530 LT%(0)=0: LT%(1)=0: MD%=1  'Locks DASH8 on channel 0
1540 CALL DASH8 (MD%, LT%(0), FLAG%)
1550 IF FLAG% <>0 THEN PRINT "Error in setting the channel": END
1560 MD%=14
1570 CALL DASH8 (MD%, I%, FLAG%)
1580 MD%=5
1590 TRAN%(0) = VARPTR(TEMP%(0))
1600 TRAN%(1) = 40
1610 CALL DASH8 (MD%, TRAN%(0), FLAG%)
1620 X = 0: INDEX = 0
1630 FOR J=1 TO 38
1640 IF ABS(TEMP%(J) - TEMP%(J-1)) <2 AND ABS(TEMP%(J) - TEMP%(J+1)) <2 THEN X=X+TEMP%(J): INDEX = INDEX +1
1650 NEXT J
1660 VOLT = X/(204.8*INDEX)  'In Volts
1670 IF ABS(VOLT) > 15 GOTO 1530
1680 DISP(I%) = VOLT/CALLVDT(I%) 'In inches
1690 RETURN
1700 '
1710 'SUBROUTINE TO FRESHEN THE SCREEN (F1)
1720 GOSUB 1200
1730 RETURN
1830 '
1840 '
1850 'SUBROUTINE TO CHANGE RECORDING RATE (KEY F3)
1860 CLS
1870 INPUT "What is the recording rate (e.g. 1 in L) L";L
1880 GOSUB 1710
1890 RETURN
1980 'SUBROUTINE TO TERMINATE THE RUN (KEY F2)
1990 CLS
2000 CLOSE #2
2030 LOCATE 11,10:PRINT "PRESS ANY KEY WHEN FINISHED"
2040 IF INKEY$ ="" THEN 2040
2050 OUT &H320,0
2060 CLS
2070 END
```

M1.BAS to Perform Numerical Integration by Method I

```
DECLARE SUB integ ()
COMMON SHARED beta#, alpha#, epsodot#, D#, epso#(), con#, n#, P#(), dp#()
COMMON SHARED low#, upp#, stp#, eps#(), epsdot#(), sum#, feps#(), q#()
CALL inputdat
CALL integ



SUB inputdat
beta# = .1
alpha# = .01
epsodot# = .1
D# = (1 / 500)
sum# = 0
n# = 1000
END SUB

SUB integ
DIM epso#(201), eps#(3), epsdot#(3), feps#(3), P#(201), q#(201), dp#(201)
DIM nr#(3), dr#(3)
CLS
INPUT "Output File Name =", out$
OPEN out$ FOR OUTPUT AS #2
stp1# = (.1 - 1E-10) / 201
FOR k% = 1 TO 201
epso#(k%) = (k%) * stp1#
con# = (epsodot# * (1 + epso#(k%))) / (epso#(k%) * (2 + epso#(k%)))
low# = 1E-10
IF k% > 1 THEN
low# = epso#(k% - 1)
END IF
upp# = epso#(k%)
stp# = (upp# - low#) / n#
FOR j% = 1 TO n# / 2
FOR i% = 1 TO 3
eps#(i%) = low# + (i% - 1) * stp#
epsdot#(i%) = con# * (eps#(i%) * (2 + eps#(i%)) / (1 + eps#(i%)))
nr#(i%) = (1 + beta# * (LOG((epsdot#(i%)) / alpha#) / LOG(10)))
IF epsdot#(i%) < .001 THEN
nr#(i%) = (1 + beta# * (-1))
END IF
dr#(i%) = ((1 + eps#(i%)) * (2 + eps#(i%)) * (D# + eps#(i%)))
feps#(i%) = nr#(i%) / dr#(i%)
NEXT i%
sum# = sum# + (((eps#(3) - eps#(1)) / 6) * (feps#(1) + 4 * feps#(2) + feps#(3)))
low# = low# + 2 * stp#
NEXT j%
PRINT "low=", low#
P#(k%) = sum#
NEXT k%
```

```
'Numerical Differntiation
FOR l% = 1 TO 201 STEP 3
w# = (epso#(l% + 2) - epso#(l%))
dp#(l%) = (-3 * P#(l%) + 4 * P#((% + 1) - P#(l% + 2)) / w#
dp#(l% + 1) = (P#(l% + 2) - P#(l%)) / w#
dp#(l% + 2) = (P#(l%) - 4 * P#(l% + 1) + 3 * P#(l% + 2)) / w#
NEXT l%
FOR k% = 1 TO 201
q#(k%) = epso#(k%) * (1 + epso#(k%)) * (2 + epso#(k%)) * (dp#(k%))
NEXT k%
FOR m% = 1 TO 201
PRINT #2, epso#(m%); P#(m%); q#(m%)
CLOSE #2
END SUB
```

M2.BAS to Perform Numerical Integration by Method II

```
DECLARE SUB inputdat ()
DECLARE SUB integ ()
COMMON SHARED beta#, alpha#, epsodot#, D#, epso#(), con#, n#, P#(), dp#()
COMMON SHARED low#, upp#, stp#, eps#(), epsdot#(), sum#, feps#(), q#()
CALL inputdat
CALL integ



SUB inputdat
beta# = .1
alpha# = .01
epsodot# = .1
D# = (1 / 500)
'sum# = 0
n# = 1000
END SUB

SUB integ
DIM epso#(201), eps#(3), epsdot#(3), feps#(3), P#(201), q#(201), dp#(201)
DIM nr#(3), dr#(3)
CLS
INPUT "Output File Name =", out$
OPEN out$ FOR OUTPUT AS #2
stp1# = (.1 - 1E-10) / 201
FOR k% = 1 TO 201
'====
sum# = 0
'====
epso#(k%) = (k%) * stp1#
con# = (epsodot# * (1 + epso#(k%))) / (epso#(k%) * (2 + epso#(k%)))
low# = 1E-10
upp# = epso#(k%)
PRINT USING "low = ##.###"; low#
PRINT USING "upp = ##.###"; upp#
stp# = (upp# - low#) / n#
FOR j% = 1 TO n# / 2
FOR i% = 1 TO 3
eps#(i%) = low# + (i% - 1) * stp#
epsdot#(i%) = con# * (eps#(i%) * (2 + eps#(i%)) / (1 + eps#(i%)))
nr#(i%) = (1 + beta# * (LOG((epsdot#(i%)) / alpha#) / LOG(10)))
'IF epsdot#(i%) < .001 THEN
'nr#(i%) = (1 + beta# * (-1))
'END IF
dr#(i%) = ((1 + eps#(i%)) * (2 + eps#(i%)) * (D# + eps#(i%)))
feps#(i%) = nr#(i%) / dr#(i%)
NEXT i%
sum# = sum# + (((eps#(3) - eps#(1)) / 6) * (feps#(1) + 4 * feps#(2) + feps#(3)))
low# = low# + 2 * stp#
NEXT j%
```

```
'PRINT "low=", low#
P#(k%) = sum#
NEXT k%
'Numerical Differntiation
FOR l% = 1 TO 201 STEP 3
w# = (epso#(l% + 2) - epso#(l%))
dp#(l%) = (-3 * P#(l%) + 4 * P#(l% + 1) - P#(l% + 2)) / w#
dp#(l% + 1) = (P#(l% + 2) - P#(l%)) / w#
dp#(l% + 2) = (P#(l%) - 4 * P#(l% + 1) + 3 * P#(l% + 2)) / w#
NEXT l%
FOR k% = 1 TO 201
q#(k%) = epso#(k%) * (1 + epso#(k%)) * (2 + epso#(k%)) * (dp#(k%))
NEXT k%
FOR m% = 1 TO 201
PRINT #2, epso#(m%); P#(m%); q#(m%)
NEXT m%
CLOSE #2
END SUB
```